

PORPHYRINS AS COLORIMETRIC INDICATORS
FOR DETECTION AND IDENTIFICATION OF
CHEMICAL AND BIOLOGICAL AGENTS

By

BRANDY JEAN WHITE

Bachelor of Science
Northeastern State University
Tahlequah, Oklahoma
1998

Master of Science
Oklahoma State University
Stillwater, Oklahoma
2001

Submitted to the Faculty of the
Graduate College of the
Oklahoma State University
in partial fulfillment of
the requirements for
the Degree of
DOCTOR OF PHILOSOPHY
JULY, 2004

PORPHYRINS AS COLORIMETRIC INDICATORS
FOR DETECTION AND IDENTIFICATION OF
CHEMICAL AND BIOLOGICAL AGENTS

Thesis Approved:

H. James Harmon

Thesis Advisor

Paul A. Westhaus

James P. Wicksted

David Peakheart

Chang-An Yu

Alfred Carlozzi

Dean of the Graduate College

ACKNOWLEDGEMENTS

I would like to acknowledge the Oklahoma Center for the Advancement of Science and Technology (OCAST) and the National Memorial Institute for the Prevention of Terrorism (MIPT) for the financial support provided to my research projects. I would also like to acknowledge the support of the National Science Foundation (NSF) provided through the Integrated Graduate Education and Research Training (IGERT) program.

I have so many people to thank for their support, advice, and assistance that I hardly know where to begin. It is inevitable that I will leave out someone very important to me. A graduate degree is not something that one can earn alone. Without the support of staff, faculty, other students, and family, I would surely have failed in my attempt. I appreciate all of you and I hope that I have made that clear along the way.

Many thanks to the support staff in the physics department office Susan Cantrell, Cindi Raymond, and Karen Hopkins. Whether it is a simple order to be placed, a misdirected package needed ten minutes ago, a missing paycheck, or a cheering “Happy Friday,” these are the people with whom you need to speak. If the emergency cannot be resolved by them, it cannot be resolved. I cannot thank them enough for the assistance that they have provided throughout my time here at OSU. Warren Grider is the guy to talk to if you need a computer or your computer just ate something important. He also knows his way around Wal-mart and Lowes. More importantly he is a very nice person

and he is always willing to help. Thanks for your help and your friendship. Thanks are also in order for Mike Lucas and the machine shop team. Those guys can build anything for you better than you imagined it (definitely better than you drew it) and looking professional. I never cease to be amazed at the wonderful work that they turn out.

I would like to express my gratitude to the faculty of the Physics department for their efforts at sharing their knowledge and their willingness to offer assistance when needed. The department is filled with people who have the best interests of the students at heart; good people whom it has been a pleasure to know. My committee members deserve special thanks. Dr. Paul Westhaus and Dr. James Wicksted joined my committee in my first year of graduate study. They have offered no end of valuable counsel and assistance as well as encouragement when my resolve was flagging. These two professors are excellent mentors and role models, each of them embodying traits to be envied and emulated. Dr. David Peakheart has been an excellent source of support from my earliest days on OSU's campus. He never once let me believe that I could fail to complete my studies at OSU. Dr. Chang-An Yu recently joined my committee receiving very little notice of my upcoming qualifying defense. Many professors would have declined under such circumstances, so I owe him a great deal of thanks for his willingness to participate. Even in the short time that I have known him, I find his sense of humor and his interest in my work to be valuable assets.

My labmates. What can I say about people who influence every project, every idea, every aspect of my day to day life in the laboratory? Mufeed Awawdeh and Mahmudur Rahman have been sitting within ten feet of me for the last three years. They are not only my colleagues but my friends. They listen when I am happy, depressed, or

feeling the pressures of graduate school and they help me with everything from lost equipment to proof reading and snags in my research. The conversations that we have are invaluable to my work and I hope they find them useful as well. I wish you guys the best of luck in your careers and your lives. I will miss you.

There are several other persons associated with my research group. Dr. Tom Collins and Dr. Tim Wilson have provided interesting discourse to our group meetings and have offered me the chance to share what I know about porphyrins with an interested audience. Jason Robinson has recently added a new level of drama to the daily activities of the group and together with the technicians, Shelley Sonner, Jennifer Stellman, and Daniel Tyler everyday is guaranteed to be entertaining. Vahik Chamras and his predecessor Cory Claflin have been willing accomplices in any wild project that I have come up with and they are very tolerant about providing muscle power when a little help is needed. Thanks guys and good luck in your careers.

Dr. H. James Harmon, my advisor, is not an easy guy to thank. The contributions that he has made to my knowledge of our field, confidence level, and writing style are just the beginning of the influence that he has had in my life. He has provided me with a great number of opportunities and experiences would not normally be had by graduate students. Dr. Harmon has been a friend to me as much as a mentor and boss. He always has time to listen to what I say and he takes the time to consider my ideas and comments. My thanks will not ever be enough. Have fun with all of your toys. I hope you win.

My parents, William and Debora Johnson, are amazing. They are willing to run to Stillwater (a 2.5 hour drive) for anything: graduation, car accidents, flooded kitchens, moral support, or a stress relieving shopping trip. I have spoken to my parents a

minimum of once a week by phone during my entire residency in Stillwater. In the ten years that I have been attending universities, neither of them questioned my decisions or suggested that it was time to stop being a student. Thanks, Mom and Dad. Thank you for my interest in reading and my love of knowledge. Thank you for shopping trips with long leisurely lunches and for starts of plants accompanied by DIY tips.

Without Brad and Brett, childhood would have been boring. Climbing trees and fences, riding bikes, playing ball (any kind), video games, you name it, we found time for it. Though they decided to join the U.S. Army, they have always been in support of my decisions. My brothers are my biggest fans. They will both willingly tell you how bright I am and they accept no arguments. This hasn't changed since we were kids; they have always stood up for me. I miss you guys. I will see you soon.

For my friends who have gone on before me, I finally made it. Thank you so much for your advice along the way. Without you, all of the tricks, deadlines, and rules would have come much harder. Eduardo, thank you for letting me vent and for proof reading (I know how much you hate it). Thank you for helping me relax and teaching me how to vacation. Lorand, you taught me more than you can know about being in a lab and you have always been a friend to me. We will meet again some day. For the rest of my friends, thank you for the card games, the language lessons, the movies, and the drinks.

This work is dedicated with love to my grandparents,

Lawrence and Barbara Bowlin and June and Retha Johnson.

TABLE OF CONTENTS

Chapter	Page
1. SENSORS.....	1
1.1 BIOSENSORS.....	2
1.2 DESCRIBED SYSTEMS.....	3
2. THEORY.....	22
2.1 MOLECULAR COMPLEXES.....	22
2.2 ENZYMES.....	34
3. PORPHYRINS.....	49
3.1 WHAT ARE PORPHYRINS.....	49
3.2 PORPHYRIN ABSORBANCE SPECTRA.....	51
3.3 LIGAND INTERACTIONS.....	53
3.4 PORPHYRIN APPLICATIONS.....	56
3.5 PROJECTS.....	58
4. IMMOBILIZATION.....	72
4.1 BASIC CONSIDERATIONS: PROTEINS.....	72
4.2 DEVELOPMENT OF A METHOD.....	75
4.3 OTHER METHODS.....	81
4.4 IMMOBILIZATION PROTOCOLS.....	83
4.5 IMMOBILIZATION OF PORPHYRINS.....	86
4.6 PORPHYRIN PROTOCOLS.....	88
5. ACETYLCHOLINESTERASE.....	104
5.1 THE TARGET.....	104
5.2 MATERIALS AND METHODS.....	105
5.3 RESULTS.....	109
5.4 DISCUSSION.....	117
6. EXTENTION OF THE CHOLINESTERASE SYSTEM.....	138

6.1 INTRODUCTION.....	138
6.2 MATERIALS AND METHODS.....	140
6.3 THE BCHE SYSTEM.....	141
6.4 THE TWO ENZYME SYSTEM.....	143
6.5 DISCUSSION.....	145
7. GLUCOSE OXIDASE.....	159
7.1 STRUCTURE AND FUNCTION.....	159
7.2 MATERIALS AND METHODS.....	160
7.3 RESULTS.....	161
7.4 DISCUSSION.....	164
8. CARBONIC ANHYDRASE.....	165
8.1 STRUCTURE AND FUNCTION.....	166
8.2 MATERIALS AND METHODS.....	166
8.3 RESULTS.....	171
8.4 DISCUSSION.....	177
9. ORGANOPHOSPHOROUS HYDROLASE.....	197
9.1 STRUCTURE AND FUNCTION.....	197
9.2 MATERIALS AND METHODS.....	198
9.3 RESULTS.....	201
9.4 DISCUSSION.....	205
10. DETECTION OF DIPICOLINIC ACID	219
10.1 BIOLOGICAL TARGETS.....	219
10.2 MATERIALS AND METHODS.....	220
10.3 RESULTS.....	222
10.4 DISCUSSION.....	226
11. PORPHYRIN DETERMINATION OF SUGARS.....	240
11.1 INTRODUCTION.....	240
11.2 MATERIALS AND METHODS.....	241
11.3 TETRA(4-AMINOPHENYL) PORPHYRIN.....	244
11.4 MONOSULFONATE TETRAPHENYL PORPHYRIN.....	245
11.5 MESO-TETRA(4-BORONIC ACID) PORPHYRIN.....	246
11.6 DISCUSSION.....	247
12. DETECTION OF CYANIDE.....	263
12.1 CYANIDE.....	263

12.2 MATERIALS AND METHODS.....	265
12.3 TPPT.....	267
12.4 MYOGLOBIN.....	268
12.5 DISCUSSION.....	269
13. FINAL STATEMENTS.....	278
REFERENCES.....	281

LIST OF TABLES

TABLE	PAGE
1.1 ENZYME BASED DETECTION PROTOCOLS.....	6
3.1 ATOMS AND SMALL MOLECULES.....	59
3.2 AMINES.....	60
3.3 AMINO ACIDS.....	61
3.4 ALCOHOLS AND CARBOHYDRATES.....	62
3.5 QUINONES AND CYCLIC COMPOUNDS.....	63
3.6 PROTEINS AND DNA.....	64
3.7 VOLATILE ORGANICS AND SURFACTANTS.....	65
4.1 IMMOBILIZATION CONSIDERATIONS.....	93
4.2 PROPERTIES TO BE CONSIDERED.....	94
5.1 CHARACTERISTIC PEAK/TROUGH LOCATIONS.....	121
5.2 IC ₅₀ AND SURFACE INTERACTION.....	122
5.3 LIFETIME EXPERIMENTS.....	123
6.1 IC ₅₀ AND LOD VALUES FOR BCHE.....	149
6.2 LOD VALUES FOR MIXED IES.....	150
8.1 INTERACTION OF PORPHYRINS WITH CARBONIC ANHYDRASE....	180
10.1 INTERACTION WAVELENGTHS.....	231
10.2 LINEAR FITTING PARAMETERS.....	232
11.1 SUMMARY OF INTERACTIONS: MRP AND RHAMNOSE.....	251

11.2	SUMMARY OF INTERACTIONS: GALACTOSAMINE AND FUCOSE..	252
12.1	PEAK FITTING RESULTS FOR FIGURE.....	272

LIST OF FIGURES

Figure		Page
1.1	ENZYME BASED BIOSENSOR.....	21
2.1	PRESENTATIONS OF DATA.....	45
2.2	ENZYME ASSAY.....	46
2.3	INITIAL VELOCITY PLOT.....	47
2.4	TYPES OF INHIBITION.....	48
3.1	PORPHYRIN MACROCYCLE.....	66
3.2	NATURALLY OCCURRING PORPHYRINS.....	67
3.3	FISCHER AND IUPAC NOMENCLATURE.....	68
3.4	ABSORBANCE SPECTRA AND SOLVENT EFFECTS.....	69
3.5	ABSORBANCE SPECTRA AND STRUCTURAL EFFECTS.....	70
3.6	π - π STACKING.....	71
4.1	TYPES OF IMMOBILIZATION.....	95
4.2	IMMOBILIZATION ONTO AMINO-FUNCTIONALIZED GLASS.....	96
4.3	PAMAM DENDRIMER.....	97
4.4	PAMAM DENDRIMER IMMOBILIZATION.....	98
4.5	PAMAM DENDRIMER IMMOBILIZATION.....	99
4.6	CARBONIC ANHYDRASE.....	100
4.7	ACETYLCHOLINESTERASE.....	101
4.8	OTHER IMMOBILIZATIONS.....	102

4.9	PORPHYRIN STRUCTURES.....	103
5.1	EVANESCENT WAVE MEASUREMENT TECHNIQUE.....	124
5.2	INTERACTION OF TPPS ₁ WITH ACHE.....	125
5.3	TPPS ₁ FLUORESCENCE SPECTRA.....	126
5.4	CHANGES IN THE TPPS ₁ EXCITATION SPECTRUM.....	127
5.5	CHANGES IN THE TPPS ₁ EMISSION SPECTRUM.....	128
5.6	INHIBITION OF ACHE BY TPPS ₁	129
5.7	REVERSAL OF TPPS ₁ -ACHE COMPLEX FORMATION.....	130
5.8	ADDITION OF INHIBITORS TO THE ACHE-TPPS ₁ COMPLEX.....	131
5.9	INTERACTION OF ACHI WITH IES.....	132
5.10	INTERACTION OF TETRACAINE WITH IES.....	133
5.11	CONCENTRATION DEPENDENCE OF ABSORBANCE CHANGES.....	134
5.12	PERCENT INHIBITION CURVES.....	135
5.13	RELATIONSHIP OF ABSORBANCE CHANGE TO IC ₅₀	136
5.14	SURFACE LIFETIMES.....	137
6.1	LINEWEAVER-BURK PLOT OF BCHE ACTIVITY.....	151
6.2	BCHE/TPPS ₁ INTERACTIONS IN SOLUTION.....	152
6.3	EXPOSURE OF THE IES TO AN INHIBITOR.....	153
6.4	CONCENTRATION DEPENDENCE OF ABSORBANCE CHANGE.....	154
6.5	PERCENT INHIBITION CURVES FOR BCHE.....	155
6.6	INTERACTION OF TPPS ₁ WITH CHOLINESTERASES.....	156
6.7	ABSORBANCE SPECTRA OF DIFFERENT IES.....	157
6.8	CONCENTRATION DEPENDENCE FOR MIXED IES.....	158

7.1	IMMOBILIZED CTPP ₄ -GOD SURFACE.....	163
7.2	CONCENTRATION DEPENDENCE OF GLUCOSE RESPONSE.....	164
8.1	PORPHYRIN-METAL COMPLEX FORMATION.....	181
8.2	CU-TPPS ₁ AND TPPS ₁ WITH CARBONIC ANHYDRASE.....	182
8.3	NH ₂ TPP AND CU-NH ₂ TPP WITH CARBONIC ANHYDRASE.....	183
8.4	CTPP ₁ AND CU-CTPP ₁ WITH CARBONIC ANHYDRASE	184
8.5	TPPS ₄ AND CU-TPPS ₄ WITH CARBONIC ANHYDRASE	185
8.6	TPPB AND CU-TPPB WITH CARBONIC ANHYDRASE	186
8.7	LINEWEAVER-BURK PLOT OF CA ACTIVITY.....	187
8.8	REVERSAL OF PORPHYRIN BINDING BY INHIBITORS.....	188
8.9	EFFECT OF UNCOMPETITIVE INHIBITORS	189
8.10	EFFECT OF UNCOMPETITIVE INHIBITORS.....	190
8.11	CU-CTPP ₁ INTERACTION WITH ZN-CONTAINING ACTIVE SITE.....	191
8.12	CU-TPPS ₁ INTERACTION WITH ZN-CONTAINING ACTIVE SITE.....	192
8.13	CU-TPPS ₁ IES.....	193
8.14	EXPOSURE OF IES TO INHIBITORS IN SOLUTION.....	194
8.15	CONCENTRATION DEPENDENCE OF ABSORBANCE CHANGES.....	195
8.16	EXPOSURE OF IES TO CO ₂ AS A VAPOR.....	195
9.1	REACTION CATALYSED BY OPH.....	207
9.2	ORGANOPHOSPHATES.....	208
9.3	INTERACTION OF OPH WITH PORPHYRINS IN SOLUTION.....	209
9.4	INTERACTION OF OPH WITH CU-NH ₂ TPP IN SOLUTION.....	210
9.5	INTERACTION OF OPH WITH CU-TPPS ₁ IN SOLUTION.....	211

9.6	INTERACTION OF OPH WITH CU-CTPP ₁ IN SOLUTION.....	212
9.7	LINEWEAVER-BURK PLOT OF OPH ACTIVITY.....	213
9.8	OPH SLIDE RESPONSE TO ANALYTE EXPOSURE.....	214
9.9	CONCENTRATION DEPENDENCE OF OPH RESPONSE.....	215
9.10	OTHER OPH SUBSTRATES.....	216
9.11	OPH SLIDE LIFETIMES.....	217
9.12	PORTABLE UNIT.....	218
10.1	NH ₂ TPP IN SOLUTION.....	233
10.2	TPPS ₁ IN SOLUTION.....	234
10.3	CTPP ₄ IN SOLUTION.....	235
10.4	OTHER PORPHYRINS IN SOLUTION.....	236
10.5	NH ₂ TPP ON GLASS.....	237
10.6	NH ₂ TPP ON CELLULOSE FIBERS.....	238
10.7	TPPS ₁ ON CELLULOSE FIBERS.....	239
11.1	SUGAR STRUCTURES.....	253
11.2	PORPHYRIN STRUCTURES.....	254
11.3	SCALING OF FLUORESCENCE SPECTRA.....	255
11.4	NH ₂ TPP IN SOLUTION.....	256
11.5	IMMOBILIZED NH ₂ TPP.....	257
11.6	TPPS ₁ IN SOLUTION.....	258
11.7	IMMOBILIZED TPPS ₁	259
11.8	TPPB IN SOLUTION.....	260
11.9	IMMOBILIZED TPPB.....	261

11.10	<i>BACILLUS THURINGENSIS</i> SPORES.....	262
12.1	EXPOSURE OF TPPT TO CYANIDE.....	273
12.2	CONCENTRATION DEPENDENCE OF ABSORBANCE CHANGE.....	274
12.3	CYANIDE EXPOSURE OF MYOGLOBIN SURFACE.....	275
12.4	CYANIDE CONCENTRATION DEPENDENCE.....	276
12.5	EXPOSURE OF MYOGLOBIN SURFACE TO HCN.....	277

NOMENCLATURE

S	substrate
L	ligand
SL	substrate-ligand complex
M	medium
K	association constant
A	absorbance
ϵ	extinction coefficient
ΔA	change in absorbance
E	enzyme
P	product
ES	enzyme-substrate complex
I	inhibitor
EI	enzyme-inhibitor complex
ν	general reaction rate
k_i	reaction rate
TPPS (or TPPS ₄)	meso tetra(4-sulfonatophenyl) porphyrin
CTPP ₄	meso tetra(4-carboxyphenyl) porphyrin
TPPB	meso tetra(4-boronic acid) porphyrin

AChE	acetylcholinesterase
BChE	butyrylcholinesterase
OPH	organophosphorus hydrolase
CA	carbonic anhydrase
GOD	glucose oxidase
MW	molecular weight
D	diameter
GA	glutaraldehyde
BSA	bovine serum albumin
TPPS ₁	monosulfonate tetraphenyl porphyrin
NaPi	sodium phosphate buffer
Gly	glycine
Lys	lysine
PAMAM	PAMAM dendrimer generation 4
TPPT	Meso-tetra (4-carboxyphenyl) porphine monoethylene diamine coupled to Traut's reagent (2-iminothiolane)
NaCl	sodium chloride in aqueous solution
DMF	N,N-dimethylformamide
NH ₂ TPP	meso tetra(4-aminophenyl) porphyrin
NaOH	sodium hydroxide in aqueous solution
HCl	hydrochloric acid in aqueous solution
PBS	phosphate buffered saline solution

TPPS ₃ -(CH ₂) ₁₀ NH ₂	tri(4-sulfonatophenyl) mono(4-carboxyphenyl) porphyrin coupled to 1,10-diaminodecane
TPPS-Si(OCH ₃) ₃	meso tetra(4-sulfonatophenyl) porphyrin coupled to trimethoxysilane
AChI	acetylcholine iodide
ATC	acetylthiocholine
K _M	substrate concentration required to achieve half of V _{max}
V _{max}	maximal enzymatic rate
IC ₅₀	inhibitor concentration to achieve 50% inhibition of enzymatic activity
DTNB	dithio-bis-nitrobenzoic acid
BTC	butyrylthiocholine
IES	immobilized enzyme surface
ICCS	immobilized combination cholinesterase surface
p-NPA	p-nitrophenol acetate
DPA	dipicolinic acid
CTPP ₁	monocarboxy tetraphenyl porphyrin
PC-NH ₂	penicillamine
D-cys	D-cysteine
1,10-P	1,10-phenanthroline
Sacc	saccharin
OP	organophosphate compound
ppm	parts per million = 1x10 ⁻³ grams per liter

ppb	parts per million = 1×10^{-6} grams per liter
ppt	parts per million = 1×10^{-9} grams per liter
TPSC ₁	meso-tri(4-sulfonatophenyl) mono(4-carboxyphenyl) porphine-cytosine amide
MRP	methyl α -L-rhamnopyranoside
rhamnose	L-rhamnose monohydrate
S/N	signal to noise
NaCN	sodium cyanide
HCN	hydrogen cyanide

CHAPTER 1

SENSORS

The basic components of any sensor system are the recognition element, the transducer, and the detector. Other possible components include data analysis hardware and software. The recognition element interacts directly with the analyte to be detected. This interaction should be as specific as possible. Any ambiguities in the interaction between the recognition element and the analyte are referred as potential interferences. An interferent is any compound that results in a false positive or false negative from the system or changes the degree of responsiveness of the system to the intended analyte. The transducer converts the interaction of the analyte with the recognition element into a signal measurable by the detector. The detector may be sensitive to almost any physical parameter: impedance, current, potential, mass, viscosity, temperature, intensity or phase of electromagnetic radiation.

Sensors can be divided into categories based on the transducer used and further subdivided based on recognition element and analyte to be detected. The major types of transduction are optical, electrochemical, acoustic, and thermometric. Optical techniques include using absorbance (most often in the UV, visible, and infrared regions), fluorescence, luminescence, polarization, and refractive index (commonly by surface plasmon resonance, SPR). Electrochemical sensors may be amperometric, potentiometric, or conductimetric. Amperometric detection is based on the current generated at fixed potential when a compound is oxidized or reduced at the electrode. Potentiometric detection is based on the change in potential resulting from accumulation

of charge on the sample electrode at zero (or fixed) current as compared to a reference electrode. Conductimetric detection is based on the change in conductance of a medium between two electrodes. This may result from selective binding to one electrode or from a change in the concentration of an analyte due to a catalyzed reaction. Finally, acoustic sensors include those based on piezoelectric transducers such as the quartz crystal microbalance and surface acoustic wave devices (SAWs). A piezoelectric device is brought into resonance by an external alternating field. A change in the mass of the crystal due to interaction with an analyte changes the frequency of oscillation. A SAW monitors wave velocity and attenuation of the surface, changes in these parameters indicate an analyte interaction. An excellent review of sensor basics as well as all of these transduction mechanisms is given in Enzyme and Microbial Biosensors [1].

1.1 BIOSENSORS

Though there has been some discussion about the definition, a biosensor is a sensor system that incorporates a bioelement (enzyme, antibody, or microorganism) as the recognition element. In an enzyme based sensor, the binding specificity of the enzyme for its substrate or an inhibitor is utilized. The signal transduction may be by any of the above mentioned methods, but the product of the enzymatic reaction is the most commonly detected compound (Figure 1.1).

An enzyme is a protein that catalyses a chemical reaction. An analyte (substrate) is recognized like a key to a lock. The analyte is bound to the enzyme, the reaction is catalyzed, and a new compound (product) is released. The product can be detected optical techniques if it absorbs light or fluoresces (etc). The product may be detected due

to interaction with another analyte whose optical characteristics change as a result of the interaction. The product may be detected amperometrically by oxidation or reduction. If the catalyzed reaction also produces H_2O_2 or consumes oxygen, this can be detected amperometrically. If ions are produced (Cl^- , Na^+ , etc) or the pH of the medium is changed due to the reaction, this can be detected by potentiometric techniques.

Often, detection of the substrate of an enzyme is not the actual goal since enzymes are frequently used for detection of their inhibitors. An inhibitor is a molecule that binds an enzyme influencing the rate of the catalyzed reaction or the binding of substrate molecules. For acoustic devices the application is obvious. The inhibitor is bound by the enzyme, while other compounds will not be held on the surface. Binding of the inhibitor changes the characteristics of the surface. In the case of optical and electrochemical detection methods, the application of enzymes traditionally involves two steps. First, the rate of change in product concentration is measured for fixed enzyme and initial substrate concentrations. Second, once this background rate is known, the rate of change in product concentration is measured for the same enzyme and initial substrate concentrations in the presence of the inhibitor. The difference in the two rates can be used to quantify the inhibitor present in the case of a known inhibitor. If the inhibitor is unknown, it is often necessary to observe its effect on different enzyme concentrations or on an array of different enzymes in order to identify it. In some cases other methods are necessary for absolute identification. This point is important; these measurements require time and are subject to fluctuations if the enzymatic activity fluctuates for reasons not related to the inhibitor (changes in pH, temperature, etc). The measurements also require

addition of substrate material, a feature not desirable when designing a field use unit.

Table 1.1 lists several of the enzyme based detection systems found in the literature.

1.2 DESCRIBED SYSTEMS

In this document a novel type of optical enzyme based sensor is described.

Unlike the traditional enzyme based systems, the system does not rely on a measurement of the enzymatic rate in the absence/presence of inhibitor. Instead it utilizes

measurement of the binding of the inhibitor (or substrate) to the enzyme using a

porphyrin as a colorimetric indicator. This novel technique has been applied to several enzymes for a variety of applications. Acetylcholinesterase (AChE) and

butyrylcholinesterase (BChE) are used for the quantification of cholinesterase inhibitors

including pesticides and some drugs. A system for the determination of glucose is

described using glucose oxidase. Carbonic anhydrase is used in a system for

determination of CO₂ and inhibitors of the enzyme. Organophosphorous hydrolase

(OPH) is used for detection of organophosphate compounds including several pesticides.

In addition to the enzyme based sensors described in Chapters 5 through 9, there are three systems described using porphyrins for both the recognition element and the transducer.

These systems comprise Chapters 10 through 12 and demonstrate the flexibility of the porphyrins for application in detection protocols.

The systems using AChE, BChE, and OPH as recognition elements share a common goal. The surfaces were designed for the detection of organophosphate compounds such as pesticides and nerve agents that threaten the health of first responders and military personnel. The system was designed in the hope that it could be made

compact and inexpensive allowing it to be used by a wide range of persons. The detection of cyanide has similar applications; cyanide can be used as a chemical warfare agent and it is a waste product of some industrial processes.

The motivation for detection of bacterial endospore components comes from recent concerns over anthrax spores discovered by the U.S. Postal System. Currently available detection protocols are unreliable and/or time consuming. A system capable of giving a unique spectrophotometric signature upon interaction with the endospore could save the lives of anyone responding to an “unknown white powder” situation.

Carbonic anhydrase was originally studied as a model for OPH as they are both zinc metalloenzymes. It was hoped that through the use of carbonic anhydrase (which is cheaply and easily obtained) the possibilities for porphyrin indicators for use in the OPH system could be limited to one or two. An enzyme base system has also been developed using carbonic anhydrase for the detection of gaseous CO₂. CO₂ levels exceeding 2,500 ppm in buildings can have adverse effects on health including burning eyes, headaches and tiredness. There is interest in monitoring CO₂ levels in buildings, on board shuttle missions, on the International Space Station and for environmental applications.

The detection of glucose has application both for testing of blood samples (diabetics) and for testing of glucose levels in foods. There is a great deal of discussion about the reason for the high incidence of obesity in the United States. Recent studies have implicated the consumption of foods with a high glycemic index. Methods for determination of glucose as well as carbohydrate content of foods are desired. Further applications exist in quality control for packaged foods.

ENZYME BASED DETECTION PROTOCOLS

Enzyme	Analyte	LOD	Technique	Detected Product/ Addend	Reference
OPAA	diisopropyl fluorophosphate	20 μ M	potentiometric - pH-FET	pH	[2]
	paraoxon	---			
	demeton-S	---			
OPH	paraoxon	20 nM	amperometric	p-nitrophenol	[3]
	methyl parathion	20 nM			
OPH	paraoxon	90 nM	amperometric	p-nitrophenol	[4]
	Methyl parathion	90 nM			
Parathion hydrolase	parathion	500 nM	amperometric	p-nitrophenol	[5]
OPH	paraoxon/parathion	---	absorbance	p-nitrophenol	[6]
OPH	paraoxon	---	absorbance	p-nitrophenol	[7]
OPH	paraoxon	~10 μ M	Amperometric/potentiometric	p-nitrophenol/ pH / F ⁻	[8]
	dichlorvos				
	diazinon				
	parathion				
OPH	paraoxon	~1 μ M	amperometric	p-nitrophenol	[9]
	parathion				
OPH	diisopropyl fluorophosphate	25 μ M	potentiometric	F ⁻	[10]
OPH	paraoxon	1 μ M	potentiometric - pH-FET	pH	[11]
OPH	paraoxon	~2 μ M	potentiometric	pH	[12]
	ethyl parathion				
	methyl parathion				
	diazinon				
OPH	paraoxon	8 μ M	fluorescence	pH	[13]
	ethyl parathion	12 μ M			
	methyl parathion	20 μ M			
	dursban	10 μ M			
	fensulfothion	40 μ M			
	crotxyphos	50 μ M			
	diazinon	15 μ M			
	mevinphos	15 μ M			
	dichlorvos	25 μ M			
	coumaphos	8 μ M			

Table 1.1 Detection protocols using enzymes as the recognition element.

ENZYME BASED DETECTION PROTOCOLS

Enzyme	Analyte	LOD	Technique	Detected Product/Addend	Reference
cholesterol esterase/cholesterol oxidase	cholesterol in serum	---	amperometric	H ₂ O ₂	[14]
cholesterol esterase/cholesterol oxidase/peroxidase	cholesterol	50 mg/dl	optical	H ₂ O ₂	[15]
cholesterol esterase/cholesterol oxidase/peroxidase	cholesterol	---	amperometric	H ₂ O ₂	[16]
cholesterol esterase/cholesterol oxidase	cholesterol	5.1 mM	optical	H ₂ O ₂	[17]
cholesterol esterase/cholesterol oxidase/peroxidase	cholesterol	0.5 mM			
cholesterol esterase/cholesterol oxidase	cholesterol in fish plasma	15 mg/dl	amperometric	O ₂	[18]
cholesterol esterase/cholesterol oxidase/peroxidase	cholesterol in serum	---	chemiluminescence	H ₂ O ₂	[19]
cholesterol esterase/cholesterol oxidase/HRP	cholesterol in whole blood	---	amperometric	H ₂ O ₂	[20]
cholesterol esterase/cholesterol oxidase/catalase	cholesterol in serum or bile	---	thermistor	---	[21]
cholesterol esterase/cholesterol oxidase	cholesterol in serum	---	amperometric/cyclic voltammetry	H ₂ O ₂	[22]
cholesterol oxidase/peroxidase	cholesterol	1 μM	optical	H ₂ O ₂	[23]
cholesterol oxidase	cholesterol	50 mM	fluorescence	O ₂	[24]
Cholesterol oxidase	cholesterol	2 mM	Amperometric	H ₂ O ₂	[25]
cholesterol oxidase	cholesterol	1.5 mM	amperometric	H ₂ O ₂	[26]
Cholesterol oxidase	cholesterol	---	potentiometric	H ₂ O ₂	[27]
Cholesterol oxidase/esterase w/ peroxidase	cholesterol in foods	0.1 mg/ml	absorbance at 500 nm	electron transfer	[28]
cholesterol oxidase/HRP	free cholesterol	40 μM	amperometric/potentiometric	electron transfer	[29]
Cholesterol Oxidase	cholesterol	---	amperometric	H ₂ O ₂	[30]
Cholesterol oxidase	Cholesterol	600 pmol	Chemiluminescence	H ₂ O ₂	[31]
cholesterol oxidase	cholesterol	25 μM	amperometric	O ₂ or H ₂ O ₂	[32]

Table 1.1 Detection protocols using enzymes as the recognition element.

ENZYME BASED DETECTION PROTOCOLS

Enzyme	Analyte	LOD	Technique	Detected Product/Addend	Reference
ACHE	ACH-Cl	0.07 mM	Conductometric	---	[33]
BCHE	BCH-Cl	0.05 mM	Conductometric	---	[33]
ChE and BChE	butyrylcholine	50 μ M	amperometric	H ₂ O ₂	[34]
BCHE	pesticides	---	potentiometric	pH change	[35]
Choline oxidase	choline	4 μ M	potentiometric	Electron transfer	[36]
ACHE and choline oxidase	choline/acetylcholine	2 μ M	amperometric	H ₂ O ₂	[37]
ACHE/BCHE	trichlorofon	150 nM	potentiometric	pH change	[38]
	coumaphos	5 nM			
	methiocarb	800 nM			
	aldicarb	200 nM			
ACHE and choline oxidase	aldicarb	12 ppb	amperometric	O ₂	[39]
ACHE and choline oxidase	choline/acetylcholine	1.2/2.7 nM	amperometric	H ₂ O ₂	[40]
	choline oxidase	choline			
BCHE	butyrylthiocholine iodide	---	amperometric	Thiol	[41]
BCHE	pesticides	---	amperometric	O ₂	[42]
	2,4-dichlorophenoxyacetic zolone				
	thiodan				
	trichlorometaphos				
	glyphosate				
ACHE (electric eel)	paraoxon	1.8 ppb	Optical abs.	Thiocholine	[43]
	Propoxur	21 ppb			
	Carbofuran	10 ppb			
	triazophos	390 ppb			
	oxydemeton-methyl	890 ppb			
	diazinon	1300 ppb			
ACHE (bovine)	paraoxon	2.3 ppb			
	Propoxur	30 ppb			
	Carbofuran	14 ppb			
	triazophos	450 ppb			
	oxydemeton-methyl	1000 ppb			
	diazinon	2100 ppb			
ACHE (human)	paraoxon	6.8 ppb			
	Propoxur	40 ppb			
	Carbofuran	17 ppb			
	triazophos	770 ppb			
	oxydemeton-methyl	4000 ppb			
BCHE (horse)	paraoxon	7.5 ppb			
	Propoxur	150 ppb			
	Carbofuran	210 ppb			
	triazophos	1000 ppb			
	oxydemeton-methyl	17 ppm			

Table 1.1 Detection protocols using enzymes as the recognition element.

ENZYME BASED DETECTION PROTOCOLS

Enzyme	Analyte	LOD	Technique	Detected Product/ Addend	Reference
ACHE	dichlorvos	500 nM	amperometric	thiocholine	[44]
	fenthion	100 nM			
	diazinon	800 nM			
Choline oxidase	choline	100 nM	amperometric	H ₂ O ₂	[45]
ACHE and choline oxidase	acetylcholine	2.5 fM	Amperometric/ Potentiometric - cyclic voltammetry	H ₂ O ₂	[46]
	choline	2.3 fM			
GOD	glucose	---			
AChE and choline oxidase	choline	30 fM	chemiluminescence	H ₂ O ₂	[47]
	acetylcholine	1.2 pM			
BCHE	2,4-dichlorophenoxyacetic acid	5 pM	amperometric	O ₂	[48]
ACHE and choline oxidase	acetylcholine	10 μM	amperometric	H ₂ O ₂	[49]
BCHE and choline oxidase	butyrylcholine	2 μM	amperometric	O ₂	[50]
ACHE, choline oxidase, and HRP	acetylcholine	35 μM	amperometric	H ₂ O ₂	[51]
ACHE and choline oxidase	paraoxon	200 ppt	amperometric	O ₂	[52]
ACHE, BCHE, choline oxidase	paraoxon	10 nM	amperometric	H ₂ O ₂	[53]
	carbofuran	10 nM			
	aldicarb	1 μM			
	monocrotofos	1 μM			
ACHE and choline oxidase	paraoxon	10 nM	amperometric	H ₂ O ₂	[54]
ACHE and choline oxidase	carbofuran	1 ppb	amperometric	H ₂ O ₂	[55]
	eserine	10 ppt			
	dichlorvos	1.3 ppt			
ACHE and choline oxidase	acetylcholine	---	amperometric	H ₂ O ₂	[56]
	Acetylthiocholine				
	Thicholine				
	Choline				
ACHE	paraoxon	1.7 nM	amperometric	Electron transfer	[57]
	dichlorvos	1.5 nM			
	chlorpyrifos	60 pM			
ACHE	paraoxon	2 nM	amperometric	Electron transfer	[58]
ACHE	carbofuran	---	amperometric/cyclic voltammetry	4-aminophenyl	[59]
	carbomyl	13 nM			
	benomyl	---			
	parathion	4 nM			
ACHE, BCHE, choline oxidase	Malathion	300 μM	amperometric	O ₂	[60]
	paraoxon	300 μM			
	parathion	200 μM			
	bisfluorophosphate	300 μM			
ACHE	thiocholine	----	amperometric	Electron transfer	[61]
BCHE and choline oxidase	physotigmine	50 μM	amperometric	H ₂ O ₂	[62]
	Neostigmine				
	Pyridostigmine				
	edrophonium				

Table 1.1 Detection protocols using enzymes as the recognition element.

ENZYME BASED DETECTION PROTOCOLS

Enzyme	Analyte	LOD	Technique	Detected Product/Addend	Reference
BCHE	paraoxon	20 ppb	amperometric/ potentiometric	choline	[63]
BCHE	trichlorfon	350 nM	amperometric	thiocholine	[64]
	coumaphos	150 nM			
BCHE	diazinon	80 μ M	amperometric	thiocholine	[65]
BCHE	paraoxon	9 nM	amperometric	thiocholine	[66]
BCHE	inhibitors/activators	---	amperometric/cyclic voltammetry	thiocholine	[67]
ACHE/BCHE	OP pesticides	---	amperometric	thiocholine	[68]
choline oxidase	butoxycarboxime	1 μ M	amperometric	H ₂ O ₂	[69]
	trichlorfon	0.5 μ M			
	dimethoate	0.5 μ M			
	fluoride	10 μ M			
	chinidine	0.25 μ M			
BCHE	gentamicin	1 ppb	amperometric	Thiocholine	[70]
ACHE	Parathion	~ 2 pM	potentiometric	PH	[71]
	Fenthion				
	Fenitrothion				
	Chlorpyrifuos				
	Diazinon				
	dichlofenthion				
	parathion-methyl				
	bromophos-ethyl				
	bromophos-methyl				
ACHE	Acetylcholine	---	potentiometric	PH	[72]
ACHE	Paraoxon	1.3 μ M	optical	Thiocholine	[73]
ACHE	Methamidophos	500 ppb	optical	Thiocholine	[74]
	Carbofuran	100 ppb			
ACHE	paraoxon	50 nM	optical	Thiocholine	[75]
ACHE	paraoxon	50 nM	optical/potentiometric	Choline/ electron transfer	[76]
	carbofuran	500 nM			
ACHE	paraoxon	500 nM	optical	PH	[77]
ACHE and choline oxidase	acetyl choline and choline	---	Amperometric/potentiometric	Choline	[78]
ACHE	dimethyl 2,2-dichlorovinyl	1 ng	amperometric	Electron transfer	[79]
ACHE	carbaryl	~1 μ M	potentiometric	pH	[80]
	carbofuran				
	aldicarb				
	bendiocarb				
	methomyl				
	mercaptodimethur				
	isoprocarb				
	dioxocarb				
propoxur					

Table 1.1 Detection protocols using enzymes as the recognition element.

ENZYME BASED DETECTION PROTOCOLS

Enzyme	Analyte	LOD	Technique	Detected Product/ Addend	Reference
ACHE, Choline oxidase, catalase, and HRP	acetylcholine	20 nM	amperometric	electron transfer	[81]
ACHE	paraoxon	50 nM	acoustic (QCM)	indigo pigment	[82]
	carbaryl	100 nM			
ACHE/BCHE	paraoxon	2 ppm	thermal		[83]
BCHE	carbaryl	8 ppm	optical	pH	[84]
	dichlorvos	30 ppb			
BCHE	diisopropyl fluorophosphate	10 ppt	acoustic		[85]
BCHE	diazinon	35 ppb	potentiometric	pH	[86]
	ethyl parathion	3.9 ppm			
	mevinphos	1.4 ppm			
	heptenophos	650 ppb			
	fenitrothion	21 ppm			
BCHE	trichlorfon	2 uM	potentiometric - ISFET	pH	[87]
BCHE	dimethylphosphoric acid	1 uM	potentiometric	butyric acid	[88]
		800 nM	optical	oxidized indophenol	
Cholinesterase	diisopropyl fluorophosphate	5 nM	optical	thiocholine	[89]
	tacrine	50 nM			
	proserine	2 uM			
BCHE	butyrylthiocholine	40 uM	potentiometric - FET	pH	[90]
BCHE	naled	12 ppm	fluorescence	indophenol	[91]
	methidation	57 ppm			
BCHE/Urease	butyrylcholine/urea	---	acoustic (SH-SAW)	pH	[92]
ACHE	acetylthiocholine	---	optical	thiocholine	[93]
OPH	paraoxon	---		p-nitrophenol	
GOD	glucose	---	chemiluminescence	H2O2	[94]
ACHE and choline oxidase	acetylcholine				
ACHE	paraoxon	28 nM	amperometric	thiocholine	[95]
	carbaryl	2 nM			
	carbofuran	2.2 nM			
	chlorfenvinphos	---			
BCHE	paraoxon	2.8 nM			
	carbaryl	--- nM			
	carbofuran	22 nM			
	chlorfenvinphos	3.6 nM			

Table 1.1 Detection protocols using enzymes as the recognition element.

ENZYME BASED DETECTION PROTOCOLS

Enzyme	Analyte	LOD	Technique	Detected Product/Addend	Reference
ACHE	Choline	---	amperometric	H ₂ O ₂	[96]
BCHE	Butyrylcholine				
Choline oxidase	Acetylcholine				
ACHE/BCHE	paraoxon	10 nM	amperometric	Thiocholine	[97]
	dichlorvos	10 nM			
	malathion	100 nM			
ACHE	Parathion	---	amperometric	Thiocholine	[98]
	Fonofos				
	Monocrotofor				
	Aldicarb				
	Paraoxon				
	Carbofuran				
ACHE and choline oxidase	Acetylcholine	100 µM	amperometric	H ₂ O ₂	[99]
ACHE/BCHE	paraoxon	1.5 ppb	amperometric	Thiocholine	[100]
	heptenophos	8.4 ppb			
ACHE (eel)	paraoxon	32 ppt	amperometric	Thiocholine	[101]
	propoxur	7 ppb			
	triazophos	90 ppb			
	carbofuran	3.8 ppb			
	oxydementon-methyl	200 ppb			
	ACHE (bovine)	paraoxon			
propoxur	7.9 ppb				
triazophos	150 ppb				
carbofuran	5.1 ppb				
oxydementon-methyl	250 ppb				
ACHE (human)	paraoxon	1.4 ppb	amperometric	Thiocholine	[101]
	propoxur	11 ppb			
	triazophos	270 ppb			
	carbofuran	5.5 ppb			
	oxydementon-methyl	1 ppm			
BCHE (horse)	paraoxon	1.6 ppb	amperometric	Thiocholine	[101]
	propoxur	28 ppb			
	triazophos	730 ppb			
	carbofuran	60 ppb			
	oxydementon-methyl	9.7 ppm			
	chlorpyrifos-methyl	6 nM			
	coumaphos	60 nM			
choline oxidase	choline	---	amperometric	H ₂ O ₂	[102]
ACHE and choline oxidase	acetylcholine				
ACHE	trichlorfon	500 nM	amperometric	Thiocholine	[103]
	chlorpyrifos-methyl	6 nM			
	coumaphos	60 nM			
BCHE	trichlorfon	700 nM	amperometric	Thiocholine	[103]
	chlorpyrifos-methyl	20 nM			
	coumaphos	30 nM			
Choline oxidase	choline	40 nM	chemiluminescence	H ₂ O ₂	[104]
choline oxidase and HRP	acetylcholine	10 fmol	Amperometric	H ₂ O ₂	[105]

Table 1.1 Detection protocols using enzymes as the recognition element.

ENZYME BASED DETECTION PROTOCOLS

Enzyme	Analyte	LOD	Technique	Detected Product/Add end	Reference
Glutamate Oxidase	glutamate	0.1 μ M	Optical abs.	ammonia	[106]
Aldose dehydrogenase	xylose/glucose	---	Amperometric	electron transfer	[107]
Glucose oxidase	glucose	200 μ M	Amperometric	H ₂ O ₂	[108]
GOD	glucose	0.17 mM	Conductometric	---	[33]
GOD/catalase		0.07 mM			
GOD	acetaminophen	100 nM	Potentiometric - cyclic voltammetry	---	[109]
	norepinephrine	300 nM			
GOD	glucose in oily food	---	Amperometric - flow injection	H ₂ O ₂	[110]
Lactate oxidase	lactate	0.05 mM	amperometric	O ₂	[111]
GOD	glucose	0.05 mM	amperometric/ potentiometric	O ₂	[112]
Lactate oxidase	lactate	0.1 mM		H ₂ O ₂	
GOD	glucose	1mM	amperometric	Electron transfer	[113]
GOD	glucose	1mM	amperometric	H ₂ O ₂	[114]
GOD	glucose	---	Optical abs.	H ₂ O ₂	[115]
Glutamate Oxidase	monosodium glutamate	50 nM	amperometric/ potentiometric	H ₂ O ₂	[116]
lactate dehydrogenase	lactate	100 μ M	amperometric	Latctate	[117]
lactate dehydrogenase	lactate	0.5 mM	Optical abs.	NADH	[118]
GOD	glucose	2 mM	potentiometric	Electron transfer	[119]
GOD	glucose	10 μ M	amperometric/ potentiometric	H ₂ O ₂	[120]
GOD	glucose	39 μ M	acoustic (piezoelectric)	Gluconic acid	[121]
Glutamate oxidase and HRP	glutamate in rat brain	100 μ M	potentiometric	H ₂ O ₂	[122]
GOD	glucose	---	amperometric	H ₂ O ₂	[123]
GOD	glucose	---	amperometric	H ₂ O ₂	[124]
GOD and HRP	glucose	33 mM	amperometric	H ₂ O ₂	[125]
GOD	glucose	21 μ M	amperometric	H ₂ O ₂	[126]
b-galactosidase and GOD and HRP	lactose in milk	10 mM	amperometric	H ₂ O ₂	[127]
GOD and peroxidase	glucose	10 nM	acoustic (SPR)	H ₂ O ₂	[128]
Galactose Oxidase	galactose	---	amperometric	H ₂ O ₂	[30]
Urease and Glutamate dehydrogenase	urea	---	amperometric	Electron transfer	[129]
GOD	glucose	200 μ M	potentiometric	H ₂ O ₂	[130]
glutamate oxidase	monosodium glutamate				
GOD	glucose	---	potentiometric	Electron transfer	[131]
Mutarotase and GOD	sucrose	0.01 mM	amperometric	H ₂ O ₂	[132]
Mutarotase and glucose oxidase and HRP	sucrose and glucose	---	amperometric	Electron transfer	[133]

Table 1.1 Detection protocols using enzymes as the recognition element.

ENZYME BASED DETECTION PROTOCOLS

Enzyme	Analyte	LOD	Technique	Detected Product/Add end	Reference
GOD	glucose	100 nM	amperometric	H ₂ O ₂	[134]
aminotransferase and glutamate oxidase and peroxidase	l-aspartate	5 μM	chemiluminescence	H ₂ O ₂	[135]
mutarotase and GOD	glucose	---	potentiometric	H ₂ O ₂	[136]
invertase, mutarotase, and GOD	sucrose				
GOD	glucose	1 mM	Potentiometric - cyclic voltammetry	Electron transfer	[137]
GOD and catalase	glucose	---	sulfonamide hydrogel swelling	pH	[138]
GOD and uricase and HRP	uric acid	1mM	chemiluminescence	H ₂ O ₂	[139]
	glucose	50 μM			
glutamate, uricase, and peroxidase	l-glutamate in serum	10 nM	chemiluminescence	H ₂ O ₂	[140]
glutamate, uricase, lysine oxidase and peroxidase	l-glutamate	136 μM	chemiluminescence	H ₂ O ₂	[141]
	l-lysine	105 μM			
GOD	glucose	1 mM	Potentiometric - cyclic voltammetry	H ₂ O ₂	[142]
GOD	glucose	2 M	amperometric	H ₂ O ₂	[143]
l-lactate oxidase	l-lactate	1 M			
GOD	glucose	---	amperometric	H ₂ O ₂	[144]
Glucose oxidase	glucose	5 mg/dm ³	amperometric	H ₂ O ₂	[145]
GOD	glucose in serum	20 μM	amperometric	Electron transfer	[146]
lactate dehydrogenase and lactate oxidase	lactate	100 μM	Potentiometric - cyclic voltammetry	Electron transfer	[147]
GOD	glucose	---	amperometric	H ₂ O ₂	[148]
GOD	glucose	40 μM	Potentiometric - cyclic voltammetry	Electron transfer	[149]
GOD	glucose	---	amperometric	H ₂ O ₂	[150]
GOD	glucose	---	amperometric	H ₂ O ₂	[151]
GOD	glucose	100 μM	chemiluminescence	H ₂ O ₂	[152]
GOD and HRP	glucose	---	fluorescence	H ₂ O ₂	[153]
glucose oxidase	glucose	150 pmol	chemiluminescence	H ₂ O ₂	[154]
lactate oxidase	lactate	60 pmol			
		30 pmol			
glucose oxidase	glucose	60 pmol	chemiluminescence	H ₂ O ₂	[31]
glucose oxidase	glucose	200 μM	chemiluminescence	H ₂ O ₂	[155]
lactate oxidase	lactic acid in yogurt	10 mM	chemiluminescence	H ₂ O ₂	[156]
glucose oxidase and lactate oxidase	glucose in serum	60 μM	amperometric	H ₂ O ₂	[157]
	Lactate in serum	100 μM			

Table 1.1 Detection protocols using enzymes as the recognition element.

ENZYME BASED DETECTION PROTOCOLS

Enzyme	Analyte	LOD	Technique	Detected Product/Add end	Reference
GOD	glucose	---	Amperometric	O ₂	[158]
GOD	glucose	300 μM	Amperometric/ potentiometric	H ₂ O ₂	[159]
GOD	glucose	1mM	Amperometric	H ₂ O ₂	[160]
GOD	glucose	1 mM	Amperometric	H ₂ O ₂	[161]
GOD	glucose	50 μM	Amperometric	Electron transfer	[162]
GOD and HRP	glucose	---	Fluorescence	pH change	[163]
GOD and glucose dehydrogenase	glucose	20 fM	Amperometric	electron transfer	[164]
GOD and HRP	glucose	10 nM	Amperometric/ Potentiometric	electron transfer	[165]
GOD	hemoglobin-A1c	7.8 nM	Amperometric	H ₂ O ₂	[166]
GOD	glucose	---	Acoustic		[167]
GOD	glucose	80 μM	Amperometric	Electron transfer	[168]
glactose oxidase and peroxidase	dihydroxyacetone	800 nM	Amperometric	electron transfer	[169]
GOD	glucose	---	Optical abs.	pH change	[170]
lactate oxidase and HRP	lactate in milk	5 nM	Amperometric	electron transfer	[171]
GOD	glucose in wine	1 μM	Amperometric	H ₂ O ₂	[172]
GOD	glucose	50 μM	Amperometric	H ₂ O ₂	[173]
GOD	glucose	1 μM	Chemiluminescence	H ₂ O ₂	[174]
GOD	glucose	10 μM	Amperometric	H ₂ O ₂	[175]
GOD	glucose	200 μM	Fluorescence	pH change	[176]
α-chymotrypsin and alcohol oxidase	aspartame	56 μM	Amperometric	O ₂	[177]
GOD	glucose	10 μM	Amperometric	H ₂ O ₂	[178]
GOD and xanthine oxidase	glucose	1 μM	Amperometric	H ₂ O ₂	[179]
	hypoxanthine	200 nM			
GOD	glucose	5 μM	Amperometric	H ₂ O ₂	[180]
glutamate oxidase, glutamate dehydrogenase, and saccharopine dehydrogenase	glutamate	500 nM	Amperometric	H ₂ O ₂	[181]
GOD and lactate oxidase	Glucose	100 μM	Amperometric	H ₂ O ₂	[47]
	lactate	200 μM			
GOD	glucose	30 mg/dl	Potentiometric - ENFET	Electron transfer	[182]
GOD	glucose	10 μM	Chemiluminescence	H ₂ O ₂	[183]
glutamate oxidase	glutamate	7 nM	Potentiometric	NH ³⁺	[106]
aldose dehydrogenase	xylose and glucose	---	Amperometric	Electron transfer	[107]
alcohol dehydrogenase, GOD	glucose	3 mM	Amperometric	NADH	[184]
	ethanol	2 mM			

Table 1.1 Detection protocols using enzymes as the recognition element.

ENZYME BASED DETECTION PROTOCOLS

Enzyme	Analyte	LOD	Technique	Detected Product/ Addend	Reference
GOD	Norepinephrine	300 nM	Potentiometric - cyclic voltammetry	quinones	[109]
	Acetaminophen	100 nM			
carboxylesterase and alcohol oxidase	Aspartame	50 nM	amperometric	O ₂	[185]
lipases, GOD, proteases, HRP	Glucose	---	optical abs.	H ₂ O ₂	[186]
	Methyl propionate				
	Amino acid derivatives				
GOD and glucose dehydrogenase	Glucose	---	amperometric	Electron transfer	[99]
GOD	Glucose	---	amperometric	H ₂ O ₂	[102]
GOD	Glucose	800 μM	amperometric	H ₂ O ₂	[187]
GOD	Glucose	1.5 mM	Optical abs.	H ₂ O ₂	[188]
glucose dehydrogenase, GOD, cytochrome b562	Glucose	100 μM	Potentiometric - cyclic voltammetry	Electron transfer	[189]
GOD	glucose	10μM	potentiometric	H ₂ O ₂	[190]
GOD	Glucose	1 mM	amperometric	H ₂ O ₂	[161]
GOD	Glucose	50 μM	amperometric	Electron transfer	[162]
GOD and xanthine oxidase	Glucose	1 μM	amperometric	H ₂ O ₂	[179]
	Hypoxanthine	200 nM			
HRP and glucose-6-phosphate dehydrogenase	glucose-6-phosphate	---	optical abs.	NADH	[191]
lactate oxidase and HRP	lactate in milk	5 nM	amperometric	Electron transfer	[171]
glycolate oxidase and catylase	glycolic acid in cosmetics, coffee, and urine	<200 μM	amperometric	O ₂ /H ₂ O ₂	[192]
Myrosinase and GOD	Glucosinolates	4 μM	amperometric	H ₂ O ₂	[193]
Urease and catalase	Urea	50 to 100 μM	conductivity		[33]
GOD and catalase	Glucose				
BCHE and catalase	Butyrylcholine				
ACHE and catalase	Acetylcholine				

Table 1.1 Detection protocols using enzymes as the recognition element.

ENZYME BASED DETECTION PROTOCOLS

Enzyme	Analyte	LOD	Technique	Detected Product/ Addend	Reference
Alcohol dehydrogenase	ethanol	80 μ M	amperometric/ potentiometric	Electron transfer	[194]
Alcohol dehydrogenase	ethanol	1mM	Amperometric	NADH	[184]
Alcohol oxidase/catalase	n-butanol	---	amperometric	O ₂	[195]
alcohol oxidase	ethanol	0.1	amperometric/ potentiometric	H ₂ O ₂	[112]
Alcohol oxidase	methanol	3.7 mM	amperometric	Electron transfer	[196]
	ethanol	3 mM			
	n-butanol	6.2 mM			
	benzyl alcohol	5.2 mM			
alcohol oxidase	ethanol	150 ug/dm ³	amperometric	H ₂ O ₂	[145]
alcohol oxidase	ethanol	10 μ M	amperometric	H ₂ O ₂	[197]
	methanol				
	1-propanol				
	1-butanol				
alcohol oxidase and HRP	methanol	0.002%	Optical abs.	Aldehydes	[198]
alcohol oxidase and HRP	ethanol	0.0001%	Optical abs.	Quinoimine	[199]
horseradish peroxidase	H ₂ O ₂	250 nM	amperometric	Electron transfer	[120]
tobacco peroxidase/HRP	H ₂ O ₂	---	potentiometric	Electron transfer	[200]
horseradish peroxidase	peroxides	100 μ M	amperometric	Electron transfer	[201]
	t-butyl hydroperoxide				
	t-butyl peracetate				
	2-butanone peroxide				
	cumene hydroperoxide				
horseradish peroxidase	hydrogen peroxide	90 μ M	amperometric	Electron transfer	[202]
horseradish peroxidase	peroxides	280 nM	chemiluminescence	H ₂ O ₂	[203]
peroxidase	chlorophenols	10 nM	chemiluminescence	H ₂ O ₂	[154]
	4-chloro-3-methylphenol				
horseradish peroxidase	hydrogen peroxide		chemiluminescence	H ₂ O ₂	[204]
peroxidase	phenol	---	amperometric	electron transfer	[205]
HRP	H ₂ O ₂	1 μ M	amperometric	electron transfer	[206]

Table 1.1 Detection protocols using enzymes as the recognition element.

ENZYME BASED DETECTION PROTOCOLS

Enzyme	Analyte	LOD	Technique	Detected Product/ Addend	Reference
Aldehyde dehydrogenase	3,4 dihydroxybenzaldehyde	5 μM	Amperometric	NADH	[207]
aldehyde dehydrogenase	maneb	50 ppb	Amperometric	NADH	[98]
carboxypeptidase A	c-terminal amino acids	---	optical abs.	quinone	[208]
superoxide dismutase	super oxide	---	Amperometric	H ₂ O ₂	[209]
Superoxide dismutase	superoxide	nM range	Amperometric	O ₂ /H ₂ O ₂	[168]
Urease	urea	0.1 mM	Conductometric		[33]
urate oxidase/peroxidase	uric acid in urine	0.1 μM	Amperometric	O ₂	[210]
urease	Hg	50 nM	Potentiometric	pH change	[211]
	Cd, Zn, Pb, Ni, Co, Mn, Fe, Cr, Ag, Cu	1 μM			
Urease	urea	500 nM	Potentiometric	NH ³⁺	[212]
creatininase, creatinase, and sarcosine oxidase	creatinine	60 μg/dl	Amperometric	H ₂ O ₂	[213]
creatininase, creatinase, and sarcosine oxidase	creatinine	800 nM	Amperometric	H ₂ O ₂	[214]
creatininase and creatinase and sacrosine oxidase	creatinine	5 μM	Amperometric	H ₂ O ₂	[215]
xanthine oxidase and cytochrome c	superoxide dismutase	2 units/ml	Amperometric/potentiometric	Super oxide	[216]
xanthine oxidase, HRP, polyphenol oxidase, GOD	nitric oxide	---	Amperometric	Electron transfer	[217]
Xanthine oxidase	hypoxanthine	1.5 μM	Amperometric	H ₂ O ₂	[218]
xanthine oxidase and nucleoside phosphorylase	inosine-5'-monophosphate	---	Amperometric	H ₂ O ₂	[219]
	inosine				
	hypoxanthine				
xylitol oxidase	xylitol	---	Amperometric	O ₂	[220]
Pyruvate oxidase, oxaloacetate decarboxylase, and citrate lyase	pyruvate	---	Amperometric	H ₂ O ₂	[221]
	oxaloacetic acid			CO ₂	
	citric acid			CH ₃ COOH	
pyruvate oxidase	phosphate	5 μM	Amperometric	H ₂ O ₂	[222]
pyruvate oxidase, pyruvate kinase, and urea amidolase	urea	5 μM	Amperometric	O ₂	[223]
pyruvate oxidase	pyruvate	50 μM	Amperometric	H ₂ O ₂	[224]
pyruvate oxidase	alanine amino transferase	10 nM	Amperometric	H ₂ O ₂	[225]
oxalate oxidase	oxalate	2.5 μM	Potentiometric	H ₂ O ₂	[226]
oxalate oxidase	oxalate	8 mM	Amperometric	CO ₂ /pH	[227]

Table 1.1 Detection protocols using enzymes as the recognition element.

ENZYME BASED DETECTION PROTOCOLS

Enzyme	Analyte	LOD	Technique	Detected Product/ Addend	Reference
polyphenol oxidase (tyrosinase)	p-cresol		Optical abs.	quinone	[228]
polyphenol oxidase (tyrosinase)	Dopamine	500 pM	potentiometric	H ₂ O ₂	[229]
polyphenol oxidase (tyrosinase)	Dopamine	500 pM	potentiometric	H ₂ O ₂	[230]
polyphenol oxidase (tyrosinase)	Phenol	1.7 nM	amperometric	O ₂	[231]
	4-cresol	1.7 nM			
	2-cresol	760 nM			
	4-chlorophenol	1.1 nM			
polyphenol oxidase	Dopamine	200 μM	amperometric	Leucodopaminechrome	[232]
polyphenol oxidase (tyrosinase)	phenolic compounds in red wine	---	Optical abs.	Quinone product	[233]
tyrosinase	3,4-dihydroxyphenylalanine	50 μM	reflectance	Electron transfer	[234]
l-amino acid oxidase	Tryptophan	---	amperometric	H ₂ O ₂	[235]
D-amino acid oxidase	D-alanine	1.1 μM	chemiluminescence	H ₂ O ₂	[236]
amino acid oxidase	Leucine	0.08 mM	amperometric/ potentiometric	H ₂ O ₂	[112]
amino acid oxidase	amino acids	1 μM	amperometric	H ₂ O ₂	[237]
Cytochrome c	super oxide		potentiometric	Electron transfer	[238]
Cytochrome c and xanthine oxidase and ascorbate oxidase	Superoxide dismutase	50 ng/ml	potentiometric	Super oxide	[239]
monamine oxidase	Fluoxetine	100 μM	amperometric	H ₂ O ₂	[240]
Monoamine oxidase	Benzylamine	50 μM	potentiometric	H ₂ O ₂	[241]
catalase	ethanol in beer samples	0.05 mM	amperometric	O ₂	[242]
ascorbate oxidase	ascorbic acid	5 μM	chemiluminescence	H ₂ O ₂	[243]
3-hydroxybutyrate dehydrogenase, glucose dehydrogenase, NADH oxidase, and peroxidase	3-hydroxybutyrate	40 nM	chemiluminescence	H ₂ O ₂	[244]
	Glucose	100 nM			
phosphate-binding protein	Phosphate	100 μM	potentiometric		[245]
Nitroreductase	2,4,6-trinitrotoluene	2 μM	amperometric		[246]
	2,4-dinitrotoluene				
putrescine oxidase	Putrescine	50 nM Hg	amperometric	H ₂ O ₂	[247]
sulfite oxidase	sodium sulfite	500 μM	amperometric/ potentiometric	H ₂ O ₂	[271]

Table 1.1 Detection protocols using enzymes as the recognition element.

ENZYME BASED DETECTION PROTOCOLS

Enzyme	Analyte	LOD	Technique	Detected Product/ Addend	Reference
alkaline phosphatase and adenosine deaminase	Adenosine triphosphate		Amperometric	O ₂	[249]
	Adenosine diphosphate				
	Adenosine monophosphate				
	inosine monophosphate				
	Inosine				
	Hypoxanthine				
myo-inositol dehydrogenase	myo-inositol	1 mM	Fluorescence	NAD	[250]
protease and amino acid oxidase	Protein	< 0.5 mg/ml	Amperometric	H ₂ O ₂	[251]
ornithine carbamyl transferase and pyruvate oxidase	ornithine	50 μM	Amperometric	O ₂	[252]
histimine oxidase and peroxidase	histimine	100 nM	Chemiluminescence	H ₂ O ₂	[253]
lysine oxidase	Lysine	25 μM	Potentiometric	NH ³⁺	[254]
maltose phosphorylase, mutarotase, GOD	Phosphates	500 nM	Amperometric	H ₂ O ₂	[255]
	Orthophosphates				
glycerokinase and glycerol-3-phosphate oxidase	Glycerol	7 mM	Chemiluminescence	H ₂ O ₂	[256]
liver esterase and alcohol dehydrogenase	Fluoride	800 nM	Absorbance	NADH	[257]
lipoxygenase	fatty acids		Amperometric	O ₂	[258]
	α-linolenic acid	4.8 μM			
	linolenic acid	7.7 μM			
neuropathy target esterase	phenyl valerate	1 μM	Absorbance	Phenol	[259]
		800 nM	Amperometric	O ₂	
heroine ester, morphine dehydrogenase, and luciferase	Heroin	250 pmol	Luminescence	NADH	[260]
acetolactate synthase	sulfomethuron methyl	---	Optical	FAD	[98]
	thifensulfuron methyl				

Table 1.1 Detection protocols using enzymes as the recognition element.

ENZYME BASED BIOSENSOR

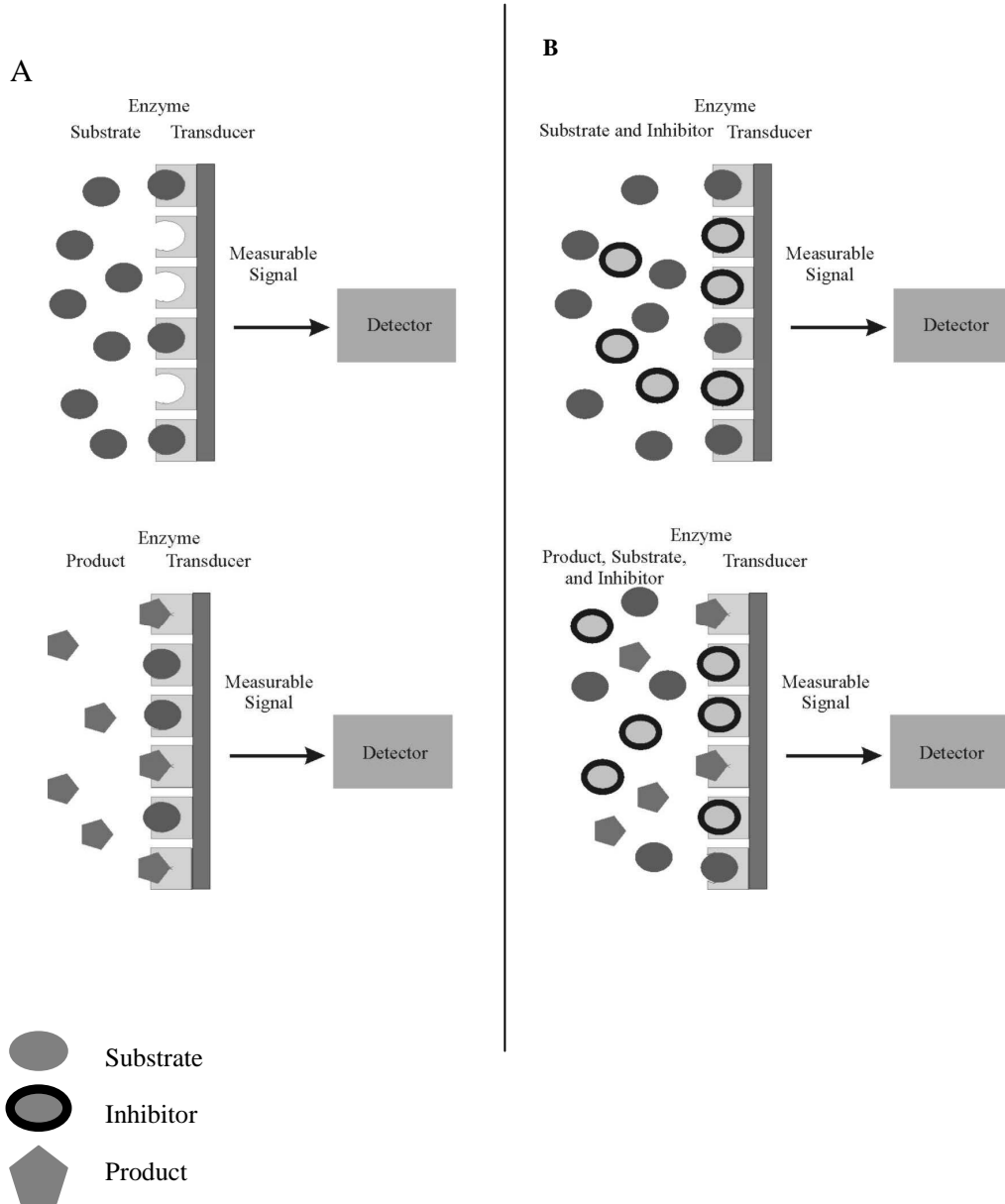


FIGURE 1.1 Enzyme based biosensors for the detection of substrate (A) or inhibitors (B) of the enzyme recognition element.

CHAPTER 2

THEORY

2.1 MOLECULAR COMPLEXES

A molecular complex is a noncovalently bound composite of substrate and ligand with a specific stoichiometry formed in an equilibrium process that is much more rapid than the rate of the measurement processes. Throughout this section substrate (S) refers to the interactant whose properties (physical or chemical) are experimentally observed and ligand (L) refers to the interactant whose concentration is the independent variable. Complex formation is recognized and investigated through changes in the observed property of the substrate as a function of ligand concentration. Stoichiometric ratios will be noted substrate:ligand so that 1:2 denotes SL_2 and 2:1 denotes S_2L . The equilibrium constant K_{11} indicates the stability of the 1:1 complex SL , and so on.

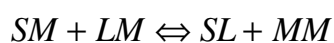
2.1.1 FORCES

Binding constants allow one to understand the forces responsible for complex formation. In a two component system (S and L) the attractive noncovalent forces between the components are of three types: electrostatic, induction, and dispersion forces. Electrostatic interactions include the interactions between the multipole moments of the molecules including charge, dipole, and quadrupole. Interaction involving dipole moments and/or quadrupole moments are orientation dependent. Charge-charge interactions are dependent only on the magnitude of the charges and the intermolecular distances. The induction (polarization) forces result from the induced charge in a

molecule resulting from the moment in an adjacent polar molecule. Dispersion force (also known as the London force) results from the instantaneous dipole moment possible even in spherical nonpolar molecules. Assuming there is an instantaneous dipole moment is present in S, this dipole moment induces a moment in L that interacts with the moment in S. This force is also referred to as the van der Waals force. As two molecules approach they are subject to long range attractive forces while repulsion results at small intermolecular distances (electron-electron repulsion).

In a chemical sense, interaction forces consist of electron-electron exchange, internuclear repulsive forces, short-range covalent bonding, and long-range noncovalent attraction. These types of interaction are related to the basic forces described in the previous paragraph. Of particular interest from these categories of interactions are charge-transfer and hydrogen bonding. The concept of charge-transfer describes the formation of a complex which has a new electronic absorption band observed in neither the substrate nor the ligand (may also be referred to as an electron donor-acceptor complex). In this type of interaction non-localized covalent bonding is possible. This means that charge transfer can occur between delocalized orbitals such as in aromatic compounds [261]. Hydrogen bonding occurs between F, O, or N and a hydrogen atom bound to one of these. It is a strong intermolecular dipole-dipole interaction [262].

It must be noted that the solvent is not a continuous medium but a molecular system and it is subject to the same intermolecular forces as the solutes. The following illustrates the necessary changes needed in order to form the SL molecular complex (M represents a molecule of the solvent).



Eq. 2.1.1

If the solvent-solute or solvent-solvent interactions are not strong, then SL complexes will dominate. If solvent-solvent and solvent-solute interactions are extensive, SL complexation will be inhibited. When MM interactions are very strong (as in polar solvents, especially water), the hydrophobic effect is observed, that is nonpolar solutes to aggregate in aqueous solution. Note that this implies that the stability of a SL complex is different depending on the solvent used.

2.1.2 ASSOCIATION CONSTANT.

The quantity K_{mn} is the binding, stability, formation, or association constant for the complex S_mL_n . The association constant has units of inverse molarity (M^{-1}). The inverse of this constant is referred to as the dissociation or instability constant. In the case where m or n is greater than 1, either the substrate m or the ligand n has more than one binding site. The simplest stoichiometry is the 1:1 SL complex with the association constant given by ([S] indicates the equilibrium molar concentration of S):

$$K_{11} = \frac{[SL]}{[S][L]} \quad \text{Eq. 2.1.2}$$

If we assume a more likely stoichiometry with three possibilities: SL, SL_2 , and S_2L , the following relations describe the formation of the complexes:

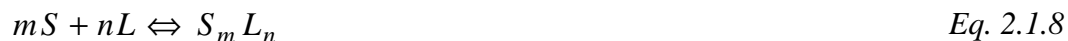


and the binding constants are:

$$K_{12} = \frac{[SL_2]}{[SL][L]} \quad \text{Eq. 2.1.6}$$

$$K_{21} = \frac{[S_2L]}{[S][SL]} \quad \text{Eq. 2.1.7}$$

The association constant for any complex can be developed in this way so that S_3L_2 would be produced from S_2L and SL , etc. It is also possible to write an overall binding constant for the formation of higher order complexes [263]:



$$\beta_{mn} = \frac{[S_m L_n]}{[S]^m [L]^n} \quad \text{Eq. 2.1.9}$$

2.1.3 STOICHIOMETRY.

Before binding constants can be evaluated, it is necessary to know the stoichiometric coefficients m and n . Several techniques exist for evaluation of these coefficients including measurement of complex molecular weight, observation of isosbestic points, continuous variation method, mole ratio method, interpretation of solubility phase diagrams, and, perhaps the most useful method, the fitting of data to assumed models [263-264]. In the data presented in the following chapters this final method has been used. However, a brief description of the other methods follows.

In the mole ratio method total substrate concentration is held constant while the ligand concentration that is varied. Discontinuities or abrupt changes in slope of the plot of the measured property of the system against the ration L_T/S_T yield information on the stoichiometric ratio [265]. In an ideal system, each addition of m moles of S and n moles of L results in exactly one mole of $S_m L_n$, so the concentration of the complex increases until $L_T/S_T = n/m$ after which all of the substrate will be reacted and more complex can not form. Unfortunately, in a real system the stability constant decreases so dissociation increases. The result is a rounded inflection point in the curve necessitating extrapolation in order to determine the exact point at which the discontinuity occurs.

The ratio n/m can also be determined using the method of continuous variations [264] where the sum of the ligand and substrate concentrations is held constant while the ratio is varied. This method is frequently employed using absorbance spectroscopy data. Here the ratio $L_T/(L_T+S_T)$ that gives the largest complex absorbance is used to calculate n/m [$n/m = X_M/(1-X_M)$]. Here again the method is more effective for strong association constants that yield sharper slope changes. This method generally assumes that only one type of complex is formed which may not be the case.

Solubility phase diagrams make use of the concept that the solubility of a substance depends on the solvent composition, though interpretation of the results can be difficult [266]. The basic premise is that formation of SL complexes increases the solubility of S. Measurements are carried out with several samples containing equal concentrations of substrate significantly higher than the normal solubility and a fixed volume of solvent containing varying concentrations of the ligand. The samples are brought to equilibrium, often requiring 1 to 2 days of shaking at constant temperature. The solution part of the sample is then analyzed, often by absorbance spectroscopy, for substrate content. For $n = 1$ a linear plot of S_T versus L_T will be observed, however a linear plot does not guarantee $n = 1$. When the slope of a linear plot is greater than 1, there is at least one complex for which m is greater than 1; however, a slope of less than 1 does not insure that only a 1:1 complex is formed. A diagram that curves upward from linearity (concave-up) indicates complexes with $n > 1$, and a diagram that curves downward from linearity (concave-down) indicates self-association effects. A plateau in the diagram can indicate that the ligand concentration has reached its saturation level or that the S_nL_m complex has reached its saturation limit.

Some authors claim that neither the presence nor absence of any isosbestic point in a solubility phase diagram is evidence of the number of states in a system [261,263]. In general, however, a system for which the overlaid spectra of different concentrations of the two states involved all intersect at a single (isosbestic) point is considered to be 1:1. This assumes that spectral characteristics are unaffected by changes in the solvent composition, etc. In general, isosbestic point analysis is combined with other data on the system to obtain an analysis appropriate to the different types of collected data.

2.1.4 BINDING ISOTHERM.

Beer's Law relates the absorbance (A) of a sample to the concentration ([S] and extinction coefficient (ϵ) of the analyte and the path length (d) of the measurement.

Beer's Law can be stated as follows (where ϵ is from the log base 10 form of the equation rather than the exponential form. This will be the standard throughout this document.):

$$A = \epsilon[S]d \quad \text{Eq. 2.1.10}$$

If all species S, L, and SL in a 1:1 complex obey Beer's Law the expressions for the association constants for a complex can be derived as follows:

For a substrate with extinction coefficient ϵ_S at total concentration $[S_T]$ (assuming a unit path length) the absorbance of the solution is:

$$A_0 = \epsilon_S[S_T] \quad \text{Eq. 2.1.11}$$

For a sample containing a ligand of total concentration $[L_T]$ and extinction coefficient ϵ_L with the same total substrate concentration the absorbance can be written:

$$A_L = \varepsilon_S[S] + \varepsilon_L[L] + \varepsilon_{11}[SL] \quad \text{Eq. 2.1.12}$$

Here ε_{11} is the extinction coefficient of the complex SL. Note that the mass balances on [S] and [L] are:

$$[S] = [S_T] - [SL] \quad \text{Eq. 2.1.13}$$

$$[L] = [L_T] - [SL] \quad \text{Eq. 2.1.14}$$

so Eq. 2.1.12 can be rewritten:

$$A_L = \varepsilon_S([S_T] - [SL]) + \varepsilon_L([L_T] - [SL]) + \varepsilon_{11}[SL] \quad \text{Eq. 2.1.15}$$

If we define $\Delta\varepsilon_{11}$ as follows:

$$\Delta\varepsilon_{11} = \varepsilon_{11} - \varepsilon_S - \varepsilon_L \quad \text{Eq. 2.1.16}$$

and take the spectrum against a reference containing $[L_T]$ or verify that the ligand has no absorbance in the region of interest, we can rewrite Eq. 2.1.15:

$$A = \varepsilon_S[S_T] + \Delta\varepsilon_{11}[SL] \quad \text{Eq. 2.1.17}$$

Now we can write the change in absorbance (ΔA) using Eqs. 2.1.11 and 2.1.17:

$$\Delta A = A - A_0 = \varepsilon_S[S_T] + \Delta\varepsilon_{11}[SL] - \varepsilon_S[S_T] = \Delta\varepsilon_{11}[SL] \quad \text{Eq. 2.1.18}$$

Recall that the stability constant for the 1:1 complex is defined as:

$$K_{11} = \frac{[SL]}{[S][L]} \quad \text{Eq. 2.1.19}$$

so that the change in absorbance is:

$$\Delta A = K_{11}\Delta\varepsilon_{11}[S][L] \quad \text{Eq. 2.1.20}$$

An important point to note here is that this equation indicates the dependence of the change in absorbance not only on the ligand concentration but also on the substrate

concentration [264]. The implication of this point for detection protocols will be demonstrated in a later chapter.

If we again use the mass balance for [S] and the expression for K_{11} , we find that [S] can be excluded from *Eq. 2.1.20*:

$$[S] = \frac{[S_T]}{K_{11}[L] + 1} \quad \text{Eq. 2.1.21}$$

So that the change in absorbance becomes:

$$\Delta A = \frac{K_{11}\Delta\epsilon_{11}[S_T][L]}{1 + K_{11}[L]} \quad \text{Eq. 2.1.22}$$

One other important relation to note is that between the total ligand concentration and the free ligand concentration ([L]). Using *Eq. 2.1.21* and the mass balance on [L] from *Eq. 2.1.14*, we can write:

$$[L_T] = [L] + \frac{S_T K_{11}[L]}{K_{11}[L] + 1} \quad \text{Eq. 2.1.23}$$

Because we are considering the very simple 1:1 binding, the free ligand concentration can be eliminated and it is now possible to solve for the desired parameters by measuring ΔA over a range of known total ligand concentrations. *Eq. 2.1.22* is one form of the binding isotherm. The 1:1 binding isotherm is useful because it directly applies to several real systems and several systems can be treated as deviations from this case. It is typical to test this model against any data before adopting a more complicated approach [263].

There are several methods for relating the total ligand concentration to the free ligand concentration, which is necessary before the parameters $\Delta\epsilon_{11}$ and K_{11} can be evaluated. For cases in which $[L_T] \gg [S_T]$ or when the binding coefficient can be assumed to be small, it is appropriate to choose $[L] = [L_T]$ [266]. In other cases an

iterative solution may be necessary where the first assumption is based on an estimate of K_{11} which is used to calculate $[L]$ from Eq. 2.1.23. The parameters $\Delta\epsilon_{11}$ and K_{11} are then solved for using the binding isotherm (Eq. 2.1.22, process described below). The process is repeated until the parameters converge. For the following discussions, we have assumed $[L]=[L_T]$.

2.1.5 PRESENTATION AND INTERPRETATION OF DATA.

A direct plot of ΔA versus $[L]$ is shown in Figure 2.1 (A) (also referred to as the binding curve). {Note: here we have set all binding isotherm parameters to 1, so that $\Delta A=[L]/(1+[L])$.} This curve is half of one branch of a rectangular hyperbola (vertex corresponds to the origin). In this type of plot it is difficult to determine the asymptotic limit of ΔA , so it is desirable to plot the data differently. There are several methods that will lead to linear plots of the data.

The semi-log plot of ΔA versus $[L]$ is known as the Bjerrum formation function (Figure 2.1 B). The advantage is that data covering several orders of magnitude can be presented. There is still difficulty in determining the maximal change in absorbance (ΔA_{\max}), but the inflection point in the curve is $\Delta A_{\max}/2$.

An A. V. Hill plot is a log-log presentation of the binding isotherm written in a different form:

$$[L] = \frac{\Delta A}{[S_T]K_{11} - K_{11}\Delta A} \Rightarrow \text{Log}\left(\frac{\Delta A}{[S_T] - \Delta A}\right) = \text{Log}[L] - \text{Log}(K_{11}) \quad \text{Eq. 2.1.24}$$

Figure 2.1 C is a plot of $\text{Log} [\Delta A/(\Delta A_{\max} - \Delta A)]$ versus $\text{Log} [L]$. At the point $\Delta A = \Delta A_{\max}$, $\Delta A/(\Delta A_{\max} - \Delta A) = 1$ ($\text{Log} 1 = 0$) allowing the K_{11} value to be determined. The

slope of this plot should be linear over the entire substrate range if there is no complicated behavior involved such as cooperative binding. The slope of this line also gives an indication of the number of independent binding sites [263,267].

For chemical binding, there are three non-logarithmic plot forms, x-reciprocal (Scatchard plot), y-reciprocal (Hanes-Woolf plot), and double reciprocal, that give linear representations of the hyperbola [263, 267-268]. The forms of the equations are as follows (respectively):

$$\frac{[L]}{\Delta A} = \frac{[L]}{[S_T]\Delta\epsilon_{11}} + \frac{1}{K_{11}[S_T]\Delta\epsilon_{11}} \quad \text{Eq. 2.1.25}$$

$$\frac{\Delta A}{[L]} = -\Delta A K_{11} + [S_T]K_{11}\Delta\epsilon_{11} \quad \text{Eq. 2.1.26}$$

$$\frac{1}{\Delta A} = \frac{1}{[S_T]K_{11}\Delta\epsilon_{11}[L]} + \frac{1}{[S_T]\Delta\epsilon_{11}} \quad \text{Eq. 2.1.27}$$

The x-reciprocal plot has the disadvantage that the independent variable (generally contains the greatest degree of error) appears on both axes (Figure 2.1 D). The advantage of this form is that it gives a closed y-axis. The slope of the line in this form gives $-K_{11}$ with y-intercept = $[S_T]K_{11}\Delta\epsilon_{11}$ and x-intercept = $[S_T]\Delta\epsilon_{11}$. So that the parameters K_{11} and $\Delta\epsilon_{11}$ can be calculated as follows:

$$K_{11} = -\text{slope} \quad \text{Eq. 2.1.28}$$

$$\Delta\epsilon_{11} = \frac{\text{x-intercept}}{[S_T]} \quad \text{Eq. 2.1.29}$$

The y-reciprocal plot maintains the spacing of the points along the x-axis and has the independent variable appearing only on the y-axis (Figure 2.1 E). Here the x-intercept is equal to $-(K_{11})^{-1}$ with y-intercept = $([S_T]K_{11}\Delta\epsilon_{11})^{-1}$ and slope = $([S_T]\Delta\epsilon_{11})^{-1}$, allowing the parameters K_{11} and $\Delta\epsilon_{11}$ to be calculated as follows:

$$K_{11} = \frac{\text{slope}}{y\text{-intercept}} \quad \text{Eq. 2.1.30}$$

$$\Delta\epsilon_{11} = \frac{1}{[S_T]\text{slope}} \quad \text{Eq. 2.1.31}$$

The most widely used version of the three is the Lineweaver-Burk or double-reciprocal plot. Here the dependent and independent variables appear on independent axes (Figure 2.1 F). The difficulty with this form is that it maximizes the error by giving the least accurately measured data (smallest data values) the most statistical weight. Since it is the most intuitive presentation of the data, it is commonly used by statistically weighting the data to correct this problem [262-263, 267-268]. The x-intercept gives $-K_{11}$ with slope = $([S_T]K_{11}\Delta\epsilon_{11})^{-1}$ and y-intercept = $([S_T]\Delta\epsilon_{11})^{-1}$, allowing K_{11} and $\Delta\epsilon_{11}$ to be calculated by the following:

$$K_{11} = \frac{y\text{-intercept}}{\text{slope}} \quad \text{Eq. 2.1.32}$$

$$\Delta\epsilon_{11} = \frac{1}{y\text{-intercept}[S_T]} \quad \text{Eq. 2.1.33}$$

2.1.6 CONCENTRATION RANGE.

It is not possible to determine if a function is a rectangular hyperbola when only narrow ranges of dependent variable are investigated. The question of the extent of investigation necessary has been addressed by several groups. One study points out that the investigation must be taken at least to the strongly curved portion of the direct binding curve in order to verify that there exists a chemical equilibrium [269]. This insures a nonlinear relationship between analytical response and ligand concentration and that the concentration of complex is approximately equal to that of the free substrate

when there is an excess of ligand. If we consider the simplest form of the binding isotherm,

$$f_{11} = \frac{\Delta A}{[S_T]\Delta\epsilon_{11}} = \frac{K_{11}[L]}{1 + K_{11}[L]} \quad \text{Eq. 2.1.34}$$

the point at which definite curvature sets in ($f_{11} = 0.1$) is given by $[L] = 0.1/K_{11}$. The range of ligand concentrations should extend beyond this point for reliable parameter calculation.

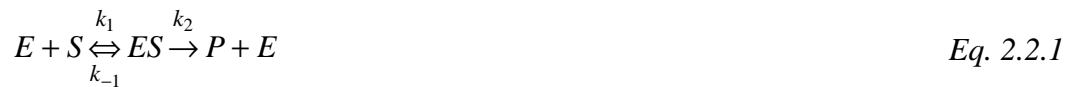
Calculations of the relative error in K_{11} (assuming negligible error in ligand concentration) determine of the appropriate ligand range to use [270-273]. This analysis points out that there is no information in the points $f_{11} = 0$ or 1 and that the error in K_{11} can be minimized by working in the area $f_{11} = 0.2$ to 0.8, the error sharply increasing at the extremes of the f_{11} range. Yet another model based on geometrical criterion indicates that 60% of the f_{11} range should be covered by experiment to achieve reliable results [263]. This range may be difficult in cases of weak association constants, poor ligand solubility, or medium effects.

2.2 ENZYMES

Enzymes mediate (catalyze) reactions such as hydrolysis, polymerization, oxidation, and reduction to name a few. We will discuss some enzymes in detail in later chapters. Here the goal is to generalize the concepts discussed for chemical complexes for application to enzyme kinetics allowing determination of reaction rates and binding affinities.

2.2.1 MICHAELIS – MENTEN EQUATION

There are two basic reaction steps for formation of a product from a substrate by an enzyme (E = enzyme, S = substrate, P = product, ES = enzyme-substrate complex):



Here k_1 , k_{-1} , and k_2 are the reaction rates, so that the general rate of this reaction is:

$$v = \frac{d[P]}{dt} = k_2[ES] \quad \text{Eq. 2.2.2}$$

Now the rate of production of [ES] depends on all three reactions so:

$$\frac{d[ES]}{dt} = k_1[E][S] - k_{-1}[ES] - k_2[ES] \quad \text{Eq. 2.2.3}$$

Two assumptions are necessary to proceed: (1) assumption of equilibrium and (2) assumption of steady state. If $k_{-1} \gg k_2$ the first step of the equation achieves an equilibrium and the dissociation constant of the first reaction can be written:

$$K_S = \frac{k_{-1}}{k_1} = \frac{[E][S]}{[ES]} \quad \text{Eq. 2.2.4}$$

Under this assumption *Eq. 2.2.3* can be integrated. The ES complex here is referred to as the Michaelis complex. This assumption was proposed by Michaelis and Menten in 1913 [274]. If the substrate is in vast excess of the enzyme, [ES] remains nearly constant until the substrate is nearly consumed. That is, the rate of formation of ES must equal its rate of consumption. The steady-state assumption proposed by Briggs and Haldane in 1925 states that the concentration of the ES complex does not change in time [275]. As in the case of the chemical discussion, [E] and [ES] are not directly measurable, so they need to be related to the total enzyme concentration:

$$[E]_T = [E] + [ES] \quad \text{Eq. 2.2.5}$$

Now, combining *Eq. 2.2.3* with the steady-state assumption and the conservation equation (*Eq. 2.2.5*) we find:

$$k_1([E]_T - [ES])[S] = (k_{-1} + k_2)[ES] \quad \text{Eq. 2.2.6}$$

or

$$[ES] = \frac{[E]_T[S]}{K_M + [S]} \quad \text{Eq. 2.2.7}$$

where K_M is the Michaelis constant:

$$K_M = \frac{k_{-1} + k_2}{k_1} \quad \text{Eq. 2.2.8}$$

Now we can express the initial velocity of the reaction in terms of the measurable variables:

$$v_0 = \left(\frac{d[P]}{dt} \right)_{t=0} = k_2[ES] = \frac{k_2[E]_T[S]}{K_M + [S]} \quad \text{Eq. 2.2.9}$$

This initial velocity is generally experimentally measured as the rate measured before consumption of 10% of the substrate (ie, when concentrations are known to a reasonable approximation)(Figure 2.2). The use of the initial rate rather than the overall rate

eliminates the need to consider factors such as the reversibility of the reaction, inhibition of the reaction by product, and progressive inactivation of the enzyme. This rate is measured as the change in the observed parameter over time (such as absorbance) and is converted to a change in substrate concentration per time using, for example, the extinction coefficient of the measured product (optical technique).

The maximal velocity ($V_{\max} = k_2[E]_T$) of a reaction occurs when the enzyme is totally saturated by substrate, that is, it is fully in the ES form ($[ES] = [E]_T$) allowing us to rewrite Eq. 2.2.9:

$$v_0 = \frac{V_{\max}[S]}{K_M + [S]} \quad \text{Eq. 2.2.10}$$

This is the basic equation of enzyme kinetics referred to as the Michaelis-Menten equation. Notice that this form is one half of one branch of a rectangular hyperbola, similar to that discussed for molecular complex formation (Figure 2.3 A).

The Michaelis constant (K_M) is the substrate concentration at which v_0 is half of V_{\max} . An enzyme with a small K_M will achieve maximum efficiency at low substrate concentrations. It should be noted that K_M may depend on temperature and pH with the degree of dependence varying between enzymes and substrates. K_M also gives an indication of the affinity of the enzyme for the substrate provided the condition $k_2 < k_{-1}$ holds [267].

$$K_M = K_S + \frac{k_2}{k_1} \quad \text{Eq. 2.2.11}$$

2.2.2 ANALYSIS OF KINETIC DATA

Because the plot of v_0 versus $[S]$ is half-hyperbolic, we can use the techniques discussed earlier in Chapter 2 for presentation and analysis of the data. The maximal

enzymatic rate (V_{\max}) is approached asymptotically making it difficult to assess from direct plots (Figure 2.3 A). Even for very high concentrations of $[S]$, measuring v_0 will result in underestimation of the actual V_{\max} ($[S] = 10K_M$ yields $v_0 = 0.91V_{\max}$). The Lineweaver-Burk plot (double reciprocal; Figure 2.1) is the most commonly used form for evaluation of enzymatic data. This plot can also give information on kinetic data when there is more than one substrate present.

The Michaelis-Menten equation can be rewritten as follows:

$$\frac{1}{v_0} = \left(\frac{K_M}{V_{\max}} \right) \frac{1}{[S]} + \frac{1}{V_{\max}} \quad \text{Eq. 2.2.12}$$

so a plot of $1/v_0$ versus $1/[S]$ has slope equal to K_M/V_{\max} and y-intercept equal to $1/V_{\max}$ (note that this also indicates x-intercept equal to $-1/K_M$; Figure 2.3 B). The disadvantages to this type of plot are that the data points may be crowded to the low end of the x-axis and measurements at low values of substrate concentration lead to large errors in the $1/v_0$ values distorting K_M and V_{\max} values. Often data is analyzed using non-linear regression techniques to avoid these problems, however, the Lineweaver-Burk plot is still a valuable presentation tool [267-268].

2.2.3 INHIBITION OF ENZYMES

A molecule that binds an enzyme decreasing the rate of the catalyzed reaction or the binding of the substrate is an inhibitor. An inhibitor can act through several mechanisms: competitive inhibition, uncompetitive inhibition, or mixed inhibition (nomenclature from Segel [267]). Competitive inhibition involves the binding of the inhibitor in such a way that it competes directly with the binding of the substrate. Typically, this type of inhibitor resembles the substrate and binds specifically to the

active site. Uncompetitive inhibition involves the binding of the inhibitor to the enzyme resulting in distortion of the active site and loss of catalytic activity. This binding of inhibitor typically takes place only after conformational changes occur upon binding of the substrate. If the inhibitor-enzyme complex is formed before substrate binding, there is no effect on substrate affinity. Mixed inhibition involves the binding of inhibitor to both enzyme and enzyme-substrate complex. A mixed inhibitor can bind either the active site or another site on the enzyme.

2.2.3A COMPETITIVE INHIBITION

The model for competitive inhibition is shown by the reaction scheme:



where I indicates inhibitor, EI indicates enzyme-inhibitor complex, and K_I is the dissociation constant for the EI complex. If this inhibitor is reversible, K_I can be written:

$$K_I = \frac{[E][I]}{[EI]}
 \qquad \text{Eq. 2.2.14}$$

The point is that the competitive inhibitor functions by reducing the effective concentration of the enzyme in the reaction, so that the rate of catalysis slows [267].

Again we need to express v_0 in terms of measurable quantities.

$$[E]_T = [E] + [EI] + [ES] \quad \text{Eq. 2.2.15}$$

If we again make the steady-state assumption that the concentration of ES doesn't change in time, we can restate Eq. 2.2.6 to give the enzyme concentration in terms of [S] and [ES]:

$$[E] = \frac{[ES]K_M}{[S]} \quad \text{Eq. 2.2.16}$$

Using Eqs. 2.2.16 and 2.2.14, we can write the concentration of the enzyme-inhibitor complex ([EI]) as a function of [I], [S], and [ES]:

$$[EI] = \frac{[E][I]}{K_I} = \frac{[I][ES]K_M}{[S]K_I} \quad \text{Eq. 2.2.17}$$

Now, if we used Eqs. 2.2.16 and 2.2.17 together with the mass balance from Eq. 2.2.15 and solve for [ES]:

$$[ES] = \frac{[E]_T[S]}{K_M \left(1 + \frac{[I]}{K_I} \right) + S} \quad \text{Eq. 2.2.18}$$

Using this equation with Eq. 2.2.9 we can now write the Michaelis-Mention equation for an enzyme in the presence of a competitive inhibitor.

$$v_0 = k_2[ES] = \frac{k_2[E]_T[S]}{K_M \left(1 + \frac{[I]}{K_I} \right) + S} = \frac{V_{\max}[S]}{\alpha K_M + [S]} \quad \text{Eq. 2.2.19}$$

Where V_{\max} is as in Eq. 2.2.10 and α is defined as:

$$\alpha = 1 + \frac{[I]}{K_I} \quad \text{Eq. 2.2.20}$$

The parameter α depends on both the concentration of the inhibitor and the dissociation constant of the enzyme-inhibitor complex. Note that in *Eq. 2.2.19* when $v_0 = V_{\max}/2$, the value of $[S]$ is αK_M . Another interesting point is that for any α as $[S]$ approaches infinity, v_0 approaches V_{\max} . Increasing the substrate concentration shifts the equilibrium toward the ES complex, so there is direct competition between the substrate and inhibitor for the enzyme binding site [268].

Again one can note that *Eq. 2.2.19* is half-hyperbolic, so if we rewrite the expression for v_0 in the double reciprocal form the curve will be linear.

$$\frac{1}{v_0} = \frac{\alpha K_M}{V_{\max} [S]} + \frac{1}{V_{\max}} \quad \text{Eq. 2.2.21}$$

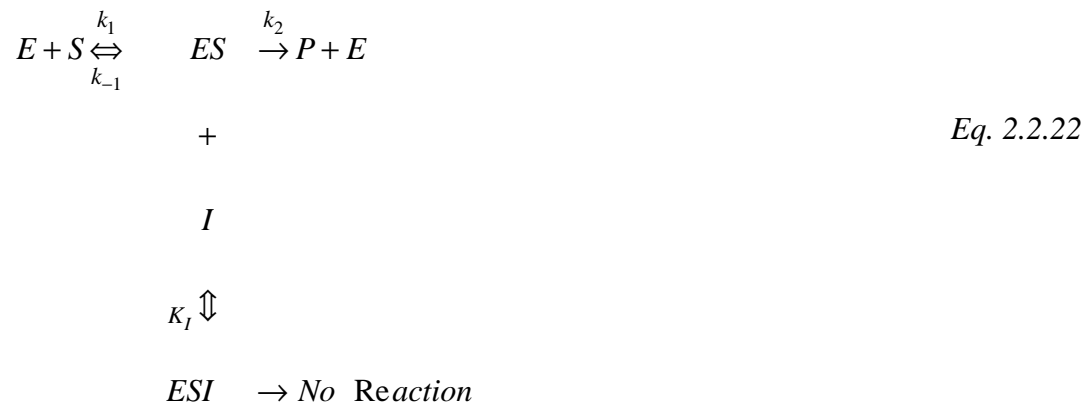
This line will have a slope equal to $\alpha K_M/V_{\max}$, an x-intercept of $-1/\alpha K_M$, and a y-intercept of $1/V_{\max}$. If we compare these results to those for *Eq. 2.2.12*, we see that while the y-intercept has not changed both the x-intercept and the slope have. These are the characteristics used to identify a competitive inhibitor (Figure 2.4 A). The activity of the enzyme shows no change in maximum enzymatic velocity (V_{\max}) in the presence/absence of a competitive inhibitor but shows a change in the substrate concentration needed to achieve half of the maximal enzymatic velocity (K_M). This is observed on the Lineweaver-Burk plot as curves that intersect at the y-axis. The K_I for a given inhibitor can be determined from the expression for α (*Eq. 2.2.20*) and the experimentally determined x-intercept [267].

In some cases a molecule may bind irreversibly to the active site of the enzyme. Such inhibitors are referred to as inactivators and this is a case of competitive inhibition as the substrate and inhibitor are competing for the active site. The concentration of active enzyme is truly reduced in the presence of an inactivator and the resulting plot of

the data is not the same as that of the reversible competitive inhibitor. The question of how to identify this type of inhibition will be addressed later in this discussion.

2.2.3B UNCOMPETITIVE INHIBITION

The following reaction scheme illustrates the mechanism for uncompetitive inhibition [268].



The dissociation constant for the inhibitor under this mechanism is written:

$$K_I' = \frac{[ES][I]}{[ESI]} \qquad \text{Eq. 2.2.23}$$

By a derivation similar to the preceding case, the Michaelis-Menten equation can be written:

$$v_0 = \frac{K_M}{V_{\max}[S]} + \frac{\alpha'}{V_{\max}} \qquad \text{Eq. 2.2.24}$$

Here α' is of the form of the previously defined α :

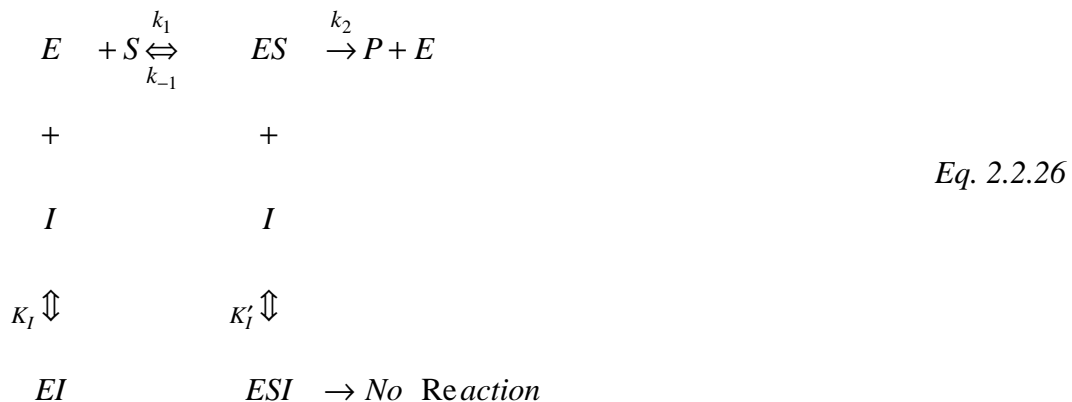
$$\alpha' = 1 + \frac{[I]}{K_I'} \qquad \text{Eq. 2.2.25}$$

For this equation as [S] increases, the value of v_0 approaches V_{\max}/α' . This indicates that the effects of an uncompetitive inhibitor are not reversed by substrate saturation. Also of interest is the fact that for small [S] ($\ll K_M$) the effect of the inhibitor becomes negligible. This behavior is opposite to that of a competitive inhibitor. In double reciprocal form, the curve for each inhibitor concentration is again linear with slope equal to K_M/V_{\max} , y-intercept equal to α'/V_{\max} , and x-intercept equal to $-\alpha'/K_M$ (Figure 2.4 B). So, in the presence of an uncompetitive inhibitor, the x- and y-intercepts (that is, K_M and V_{\max}) of the Lineweaver-Burk plot of enzymatic activity are changed while the slope of the line is unchanged.

The mechanism of uncompetitive inhibition requires the interference of the inhibitor with the catalytic function of the enzyme while leaving the substrate binding affinity unchanged. This type of inhibition is important for multi-substrate enzymes and small inhibitors such as protons and metal ions [267].

2.2.3C MIXED INHIBITION

Mixed inhibition (including noncompetitive inhibition) occurs when both the enzyme and the enzyme-substrate complex can bind the inhibitor. It can be illustrated as follows:



Notice that the two different types of inhibitor binding have unique dissociation constants (defined previously) [268]. The Michaelis-Menten equation for mixed inhibition can be written as follows:

$$v_0 = \frac{V_{\max}[S]}{\alpha K_M + \alpha'[S]} \quad \text{Eq. 2.2.27}$$

It is apparent from this equation where the name mixed inhibition originated. The denominator has the factor α operating on K_M as in competitive inhibition and the factor α' acting on $[S]$ as in uncompetitive inhibition. The implication is that a mixed inhibitor will act at both high and low concentration. The Lineweaver-Burk plot of enzyme activity at different inhibitor concentrations will give a group of lines with slope $\alpha K_M/V_{\max}$, y-intercept equal to α'/V_{\max} , and x-intercept equal to $-\alpha'/\alpha K_M$ (Figure 2.4 C). A special case of mixed inhibition referred to as noncompetitive inhibition occurs if $K_I = K_I'$; $\alpha = \alpha'$ and the lines of varying inhibitor concentration will intersect on the x-axis (Figure 2.4). This case is rarely encountered in practice [267]. A closer look at the equation indicates that the family of lines generated here will always intersect to the left of the y-axis at the point [267]:

$$\left[\frac{1 - \alpha'}{(\alpha - 1)K_M}, \frac{\alpha - \alpha'}{(\alpha - 1)V_{\max}} \right] \quad \text{Eq. 2.2.28}$$

2.2.3D INACTIVATION

Inhibition of an enzyme by an inactivator is often mistaken for mixed inhibition. The inactivator effectively reduces the presence of free enzyme. This appears as a change in both K_M and V_{\max} . The two types of inhibition can be distinguished by generating a plot of V_{\max} versus enzyme concentration ($[E]_T$) (Figure 2.4 D). A

reversible mixed inhibitor will intersect the y-axis at $[E]_T$ equal zero as will the control with no inhibitor. An inactivator will result in a curve that intersects the y-axis at a negative value [267].

PRESENTATIONS OF DATA

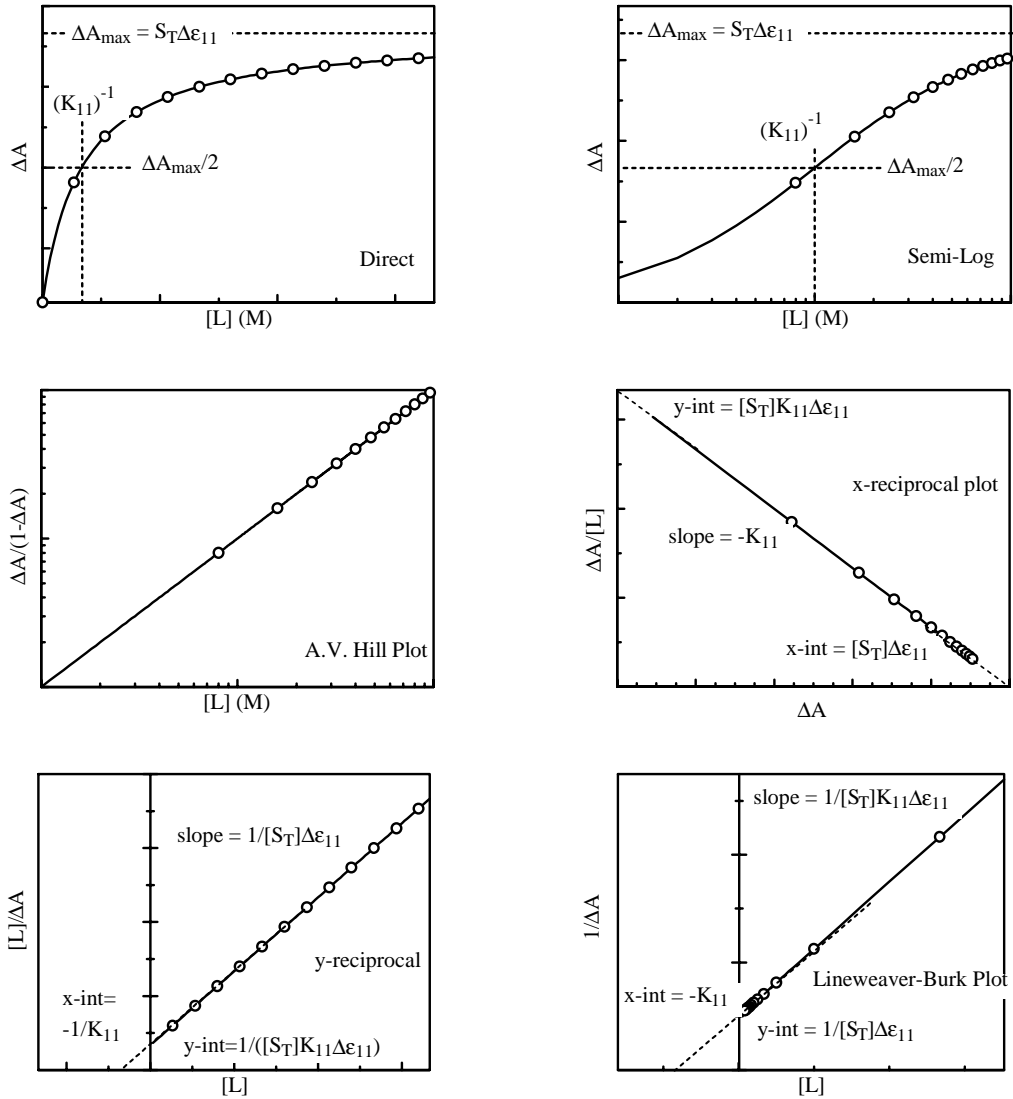


FIGURE 2.1 All graphs are generated based on a binding isotherm of the form

$$y = \frac{x}{x+1},$$

that is, all parameters $[S_T]$, K_{11} , and $\Delta\epsilon_{11}$ are assumed to be unity.

ENZYME ASSAY

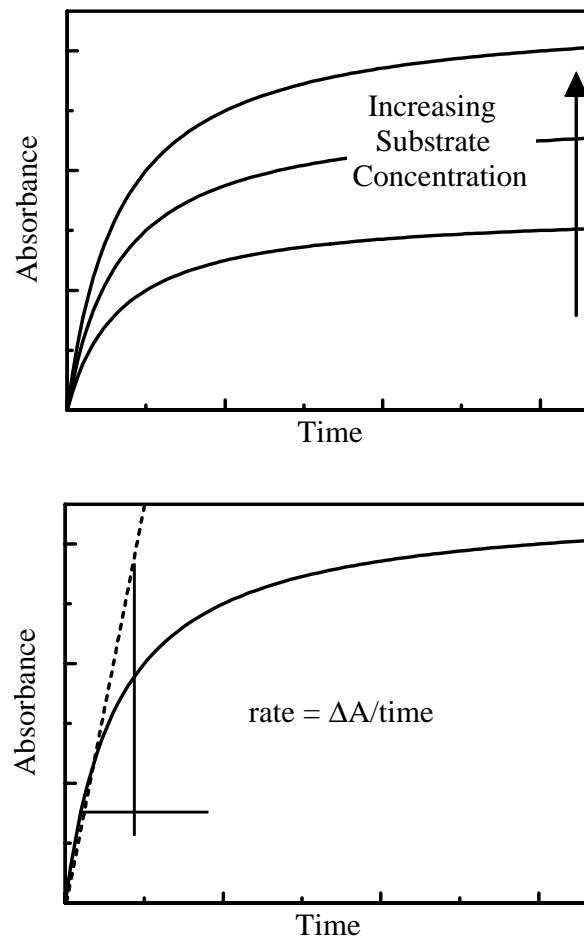


FIGURE 2.2 For fixed enzyme concentration, the initial rate for enzyme catalysis depends on the substrate concentration. The initial rate should be measured before more than 10-20% of the substrate has been consumed.

INITIAL VELOCITY PLOT

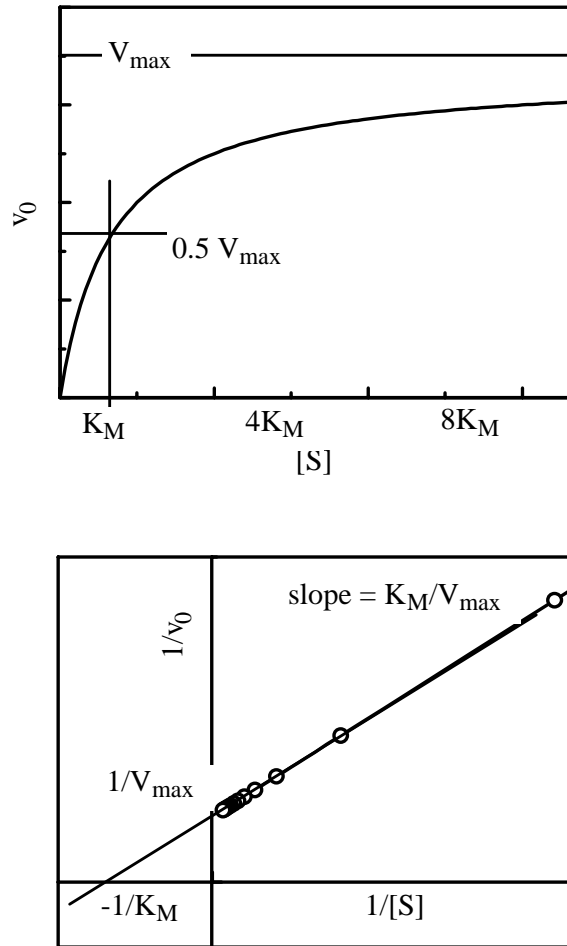


FIGURE 2.3 A. The plot of initial velocity versus substrate concentration is half-hyperbolic. B. The Lineweaver-Burk (double reciprocal) plot of the same data is linear allowing determination of the reaction parameters.

TYPES OF INHIBITION

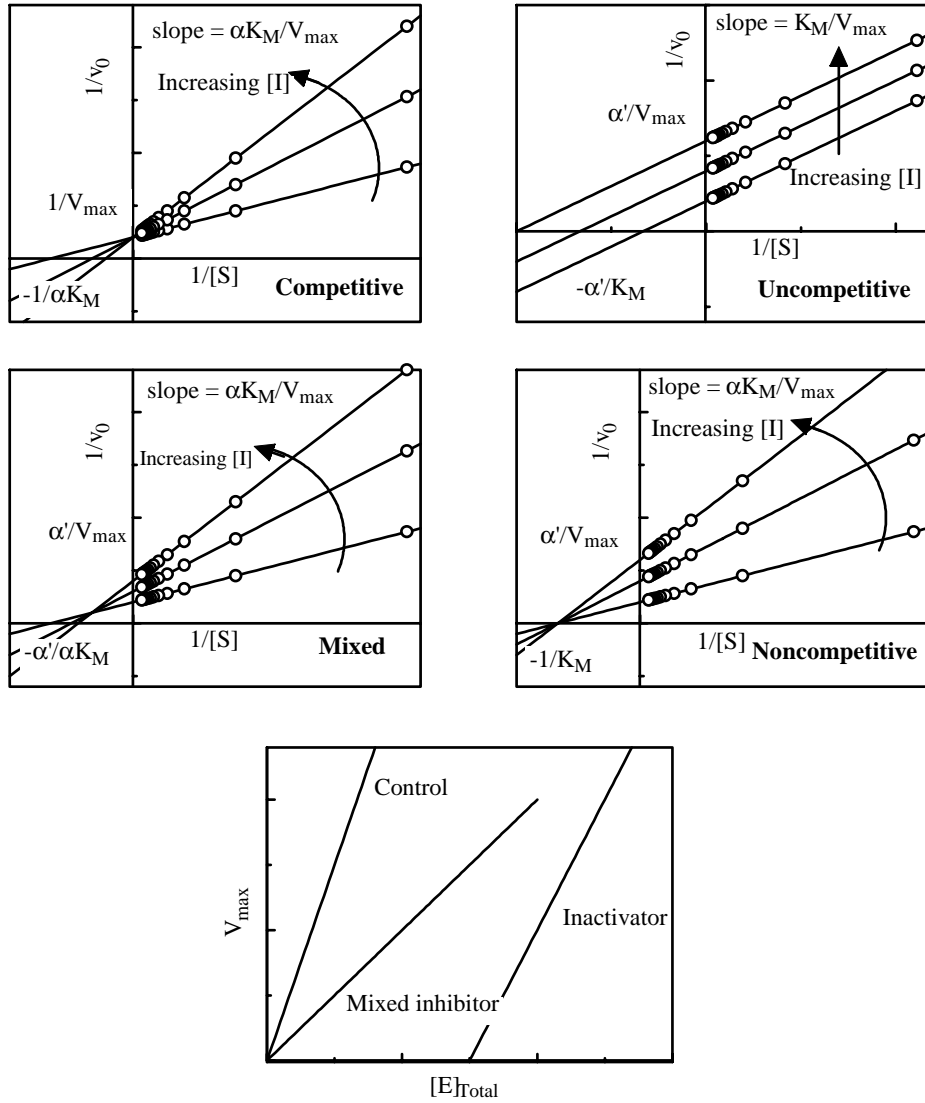


FIGURE 2.4 Lineweaver-Burk Plots showing different types of inhibition, competitive, uncompetitive, and mixed and a plot of V_{\max} versus $[E]_T$ illustrating the difference between inactivation and reversible mixed inhibition.

CHAPTER 3

PORPHYRINS

3.1 WHAT ARE PORPHYRINS

The name porphyrin has its origin in ancient Greece with the word *porphura* meaning purple. The color purple has been used throughout history to distinguish royalty or nobility. Porphyrin is the name given to a family of intensely colored molecules all sharing a macrocycle of twenty carbon atoms and four nitrogen atoms (Figure 3.1). The macrocycle is four pyrrole rings joined by methine bridges. The porphyrin is a nearly flat molecule (x-ray crystallographic data), though it may be distorted by certain ligand binding or by various substituent groups bound to the periphery [276].

The macrocycle follows Hückel's rule of aromaticity with 22 π -electrons. The ring is very stable tolerating temperatures up to 250° C [277] and highly acidic conditions (concentrated sulfuric acid) [276]. Strong bases can deprotonate the nitrogen atoms of the porphyrin resulting in a dianion or acids such as trifluoroacetic acid can be used to protonate the pyrroline nitrogen atoms. The central cavity of the porphyrin can bind metals such as Fe, Zn, Cu, Ni, Mg, Ag, Au, and Co, though binding of small atoms (Ni for example) may cause distortion of the planar conformation. The metal can be removed from the porphyrin by acidification in most cases [278].

The high degree of conjugation in the porphyrin ring results in several absorbance bands. A very intense band is observed around 400 nm with an extinction coefficient often exceeding 500 $\text{mM}^{-1}\cdot\text{cm}^{-1}$ (solvent and porphyrin dependent). This band is referred to as the Soret band. In addition to the Soret band, there are several weaker absorbance

bands (generally five) in the region from 450 nm to 700 nm, the Q-bands. Porphyrins are, in general, intensely fluorescent with emission bands in the region between 600 and 750 nm. The absorbance and fluorescence spectra of porphyrins are sensitive to binding of a metal in the central ring position, addition of substituent groups to the macrocycle, solvent conditions, and the presence of other analytes. These effects will be discussed in detail below.

A wide range of natural and synthetic porphyrins are available. Naturally occurring porphyrins include heme found in hemoglobin, myoglobin, and some peroxidases; heme *c* from cytochrome *c*; and chlorophyll used in photosynthesis (Figure 3.2). In all of these cases, the protein structure surrounding the porphyrin alters the characteristics of the porphyrin making it suitable for the given function. In hemoglobin and myoglobin the iron metalloporphyrin is responsible for the reversible binding of oxygen allowing transport or storage. The combination of the protein environment with the porphyrin ligand changes the redox potential of the iron so that the oxidation state is not irreversibly changed upon oxygen binding. Typically, in the presence of water and air, Fe(II) would be oxidized to Fe(III). Changing the protein environment changes the properties of the iron ligand, such that in cytochrome *c*, electron transfer takes place as the iron cycles between the 2⁺ and 3⁺ oxidation states. In chlorophyll, groups of porphyrins (2-300 molecules) work together as an antenna to collect large quantities of photons that produce excited electrons used as the energy source for carbohydrate production. Some other naturally occurring porphyrin systems are peroxidases, catalases, and cytochromes (such as P-450 and *b*) [279].

There are two nomenclature schemes for the porphyrins, Fischer and IUPAC [276, 280]. For simple porphyrins the Fischer scheme is straightforward, however, when two or more substituent groups are involved, it becomes unwieldy. As seen in Figure 3.1, each of the pyrrol rings was given a letter, each bridging (meso) carbon was labeled α - δ , and each of the β carbons is numbered 1-8. Under this system, a porphyrin with a phenyl ring at each of the bridging carbons is referred to as $\alpha,\beta,\gamma,\delta$ -mesotetrakisphenylporphyrin while protoporphyrin IX (heme structure without iron) is 2,4-divinyl-1,3,5,8-tetramethylporphyrin-6,7-dipropionic acid (Figure 3.3). The IUPAC system of nomenclature was introduced in 1979. This system numbers all of the carbon and nitrogen atoms in the macrocycle. As in other IUPAC systems, carbon number 1 is determined based on the substituent groups present. Under this system protoporphyrin IX becomes 8,13-diethyl-3,7,12,17-tetramethylporphyrin-2,18-dipropionic acid and $\alpha,\beta,\gamma,\delta$ -mesotetrakisphenylporphyrin becomes 5,10,15,20-tetraphenylporphyrin (Figure 3.3). Porphyrin names given in this document are based on the names given in the Frontier Scientific catalog (Logan, UT) as this was the source for all porphyrins used. These names are based on the Fischer system, though the meso labels ($\alpha,\beta,\gamma,\delta$) are often dropped.

3.2 PORPHYRIN ABSORBANCE SPECTRA

The porphyrin absorbance spectrum is sensitive to the environment of the porphyrin. Changes in acidity, hydrophobicity, ion content, etc can result in increased or decreased absorbance intensity at any or all of the bands as well as changes in the exact wavelength position of any or all of the bands. Examples of these effects are given in

Figure 3.4. The porphyrin used in all traces is iron meso tetra(4-sulfonatophenyl) porphyrin (Fe-TPPS) at 0.8 μM . In Frame A, the absorbance spectrum of Fe-TPPS is shown in 50 mM pH 7 NaPi and in 50 mM pH 7 NaPi with 50% ethanol, methanol, and DMSO. There are changes in absorbance apparent not only in the Soret region but also in the Q-band region [264]. Fe-TPPS is freely soluble in water and in several organic solvents such as DMSO. Fe-TPPS is also soluble in ethanol, though the solubility in methanol is somewhat less than that in water. The three traces shown in Frame B demonstrate the pH sensitivity of Fe-TPPS showing the blue shift of the Soret upon acidification of the medium [264]. The Q-bands are also effected by the change in pH in a similar manner. Frame C shows the effects of ion concentration on the absorbance spectrum of Fe-TPPS. The red shift of the Soret is indicative of porphyrin stacking as is the loss in intensity of the Q-bands [264].

The addition of different substituent groups also effects the absorbance spectrum of the porphyrin [281]. This can be seen when the spectrum of chlorophyll *a* is compared to chlorophyll *b*. Chlorophyll *a* has strong absorbance peaks at 420 and 660 nm while chlorophyll *b* has strong absorbance peaks at 450 and 620 nm. This change in the absorbance spectrum results from changing a substituent on a b-carbon from a methyl group (CH_3) to an aldehyde group (CHO) [262]. Figure 3.5 demonstrates this showing the difference in the absorbance spectra of meso tetra(4-carboxyphenyl) porphyrin (CTPP_4) and meso tetra(4-boronic acid) porphyrin (TPPB); structures of the porphyrins are also given. Both porphyrins have phenyl rings with acidic substituents bound to the number 4 carbon. The spectra are very different with extinction coefficients of 725 mM^{-1} (414 nm) and 380 mM^{-1} (417 nm) (one centimeter path lengths) for CTPP_4 and TPPB

absorbance peaks, respectively. The Soret of TPPB is broadened as compared to CTPP₄ and the positions of the Q-bands are shifted. Binding of a metal by the porphyrin ring also causes changes in the absorbance characteristics [282]. Figure 3.5 shows the absorbance spectra of Cu-CTPP₄ and CTPP₄. The Soret of CTPP₄ is blue shifted upon complexation with copper and the Q-bands shift both in position and in number from four to two. The extinction coefficient of Cu-CTPP₄ (540 mM⁻¹ for a one centimeter path length) is also less than that of CTPP₄.

3.3 LIGAND INTERACTIONS

The great sensitivity of the porphyrin absorbance spectrum to its environment is not limited to solvent effects but extends to the presence of other solutes in a given solvent. Three papers are central to understanding porphyrin ligand interactions Mauzerall 1965 [264], Shelnut 1983 [283], Schneider and Wang 1994 [284]. Mauzerall's paper from 1965 discusses the interaction of several organic compounds with uroporphyrin (III). The results of this study are fundamental to understanding porphyrin ligand interactions. The author discusses the formation of complexes of different stoichiometry indicating the involvement of hydrophobic effects and π - π , ionic, dispersion, dipole, and hydrogen bond interactions. The cofacial binding of cyclic compounds to the porphyrin macrocycle is determined to be the preferred binding conformation (Figure 3.6). Changes in porphyrin absorbance spectra as a result of solvent reorganization are observed. The formation of charge-transfer complexes between porphyrin and ligand is mentioned and aggregation of porphyrins is shown to quench fluorescence as well as distort the absorbance spectrum of the porphyrin.

Mauzerall demonstrates that the change in the absorbance spectrum for even very similar compounds is unique and that the magnitude of the change in absorbance upon binding of a ligand is dependent upon the concentration of the porphyrin present [264]. This means that even very similar compounds react with the porphyrin to yield a unique set of spectral changes or “fingerprint” making compound recognition possible and that the intensity of the change in absorbance can be used for quantification of the analyte.

A study by Shelnutz involved seventeen different aromatic ligands interacting with copper or nickel uroporphyrin [283]. Using shifts in the Raman spectra of the porphyrins, Shelnutz determined that the interaction of the aromatic ligands with the porphyrins is co-facial even when the compound bears a nitrogen. The nitrogen-metal interaction does not dominate as was expected. He also found evidence of a π - π charge-transfer interaction between the porphyrin and a ligand.

A key study by Schneider and Wang on porphyrin-ligand interactions demonstrates the specificity of changes in the porphyrin absorbance spectrum for several closely related aromatic compounds as well as other structurally related molecules [284]. The study used three different meso tetra(4-*x*-phenyl) porphyrins one of which was used as a free base, copper complexed, or zinc complexed. The changes in the absorbance of the Soret band were measured upon interaction with twenty three different ligands in water. The study shows that the association of the ligands with the porphyrins is dependent on ionic interactions as well as π - π interactions while under these conditions solvophobic factors do not contribute. The authors go on to point out that the changes in the absorbance spectrum, that is, the size of the wavelength shift is related to the

association energy of the complex and that the complexes formed are between a single porphyrin and a single ligand molecule.

The copper metalloporphyrin used in the study by Schneider and Wang showed similar results to the free base porphyrin. Copper (Cu^{2+}) ions are known to form a planar coordination with four nitrogen atoms. There is little ring distortion upon binding of the copper ion and ligand interactions resulted in changes in the absorbance spectra similar to those observed with the free base porphyrin. The zinc metalloporphyrin on the other hand showed smaller complex association energies and smaller wavelength shifts. The zinc ion is generally found in a five coordinate geometry: the four nitrogen atoms of the porphyrin ring plus a water molecule or the nitrogen of a ligand are involved. The authors conclude that the interactions of the ligands with the central metal are not strong enough to result in axial interaction; rather, the plane to plane stacking described by both Mauzerall [264] and Shelnutz [283] is the strongly favored conformation.

Formation of metal-porphyrin complexes has been studied since the early 1940's. Banks and Bisque were the first group to attempt the use of changes in the spectral characteristics of porphyrins for determination of metals [285]. The authors demonstrate the complexes between a porphyrin and zinc, cadmium, magnesium, beryllium, iron, yttrium, and rare earth alkali metals can be formed with each metal complex giving a distinct absorbance spectrum. In 1985 a paper was published on determination of copper, lead, cadmium and zinc [286]. This paper as well as a paper from 1957 all point out that attaining an equilibrium between porphyrin and metal requires more than 70 minutes. Several groups have described methods decrease the time needed to reach equilibrium

[278, 287-289] such as heating, use of an asymmetric porphyrin (greater ring flexibility), and use of reducing agents to increase the rate of complex formation.

A further point in the literature is that the exchange of one metal for another, especially in the case of large atoms like zinc, is much faster than the direct binding of the atom. Zinc is capable of binding several water molecules and the size of the atom decreases steric hindrance allowing fairly tight binding. This “water shell” is difficult to disperse for porphyrin binding. If a copper is bound in the porphyrin ring, the water ligands can be shared between the copper and zinc atoms facilitating the metal exchange [278, 287-289].

The papers discussed here do not begin to cover the extensive amount of information available on porphyrin chemistry. The Porphyrin Handbook is twelve volumes covering a range of topics from synthesis to sensor applications. The seven volume set The Porphyrins deals with structure and synthesis, biochemistry, and physical chemistry of porphyrins. The information given here is that which directly pertains to the topics to be covered in this document.

3.4 PORPHYRIN APPLICATIONS

Porphyrins have been used in a wide range of sensor applications. Tables 3.1-3.7 give only a sample of the literature available on porphyrin interactions. The interaction of porphyrins with many compounds has been studied including, but not limited to: metals (atoms) [278, 285, 287-291, 293-300, 302-63, 324-338, 340-352, 355, 357, 360-364, 377], small molecules [297-298, 301, 305, 312, 314, 316, 318, 320, 323, 328, 330, 333, 337, 339-342, 349-356, 358-359, 364-371], amines [292, 364, 372-373], amino

acids and amino acid derivatives [292, 299, 351, 374-376], alcohols [292], carbohydrates [292, 377-379], quinones [283-284, 373], proteins [383-400], DNA [292, 401-403], nucleobases and nucleic acids [404-405], surfactants [406-407], volatile organic compounds [351, 365, 370, 373, 408-413], and a variety of other cyclic and/or aromatic compounds [264, 293, 300, 283-284, 364-365, 372, 380-382]. The sensitivity of the porphyrin spectrum makes porphyrins ideal for use as indicators in absorbance or fluorescence spectroscopy. The peripheral substituents of the porphyrins can be modified, as can the centrally coordinated metal, to achieve binding specificity allowing for their application in amperometric or potentiometric protocols or for use with acoustical devices such as quartz crystal microbalances.

Some interesting work has been done using porphyrin arrays as electronic noses or electronic tongues [414-421]. Electronic noses are used for detection of vapors and electronic tongues are used for detection of compounds in solution. One group has demonstrated the identification and quantification of fourteen different volatile organic compounds (VOCs) using an array of eleven metalloporphyrins. They have also shown that the system can be used to classify an unknown compound that is similar to others in the library. The system used for this demonstration consisted of an HP flat-bed scanner as the spectrometer/light source and Adobe PhotoShop for data analysis [370, 379]. Several other protocols using porphyrin arrays employ quartz crystal microbalances [416, 418, 420].

Porphyrins have also been used in amperometric and potentiometric detection protocols due to their ability to catalyze oxidation/reduction reactions [293, 414]. Generally a metalloporphyrin thin film is used. Binding specificity and redox properties

can be altered by modifications to the porphyrin side chain and incorporated metal. These sensors have been employed for detection of compounds such as metal cations, nitric oxide, salicylate and nitrite [293, 367, 422-423].

3.5 PROJECTS

The porphyrin macrocycle can be used for detection in two ways. The most common use is as described above in the optical techniques where the porphyrin is involved in the recognition event and in signal transduction. The following chapters present a few detection protocols based on this use of the porphyrin. The porphyrin can also be used as only the recognition event for example in the quartz crystal microbalance protocols or less commonly as only the transducer. The other detection protocols presented in the following chapters use the porphyrin as a transducer only for indication of enzyme binding a compound. Most of the detection protocols are based on changes in the porphyrin absorbance spectra and our focus will be on the Soret region of the spectrum because very large extinction coefficient in that region allows for detection of small amounts of analyte. Aside from the chapter on porphyrin determination of sugars changes in the fluorescence spectra of the porphyrins are only briefly mentioned.

ATOMS AND SMALL MOLECULES

Platinum (Pt II) ^{293, 297-298, 328, 336-337, 348}	Lanthanum (La III) ^{307, 329, 330, 332, 355}	Cerium (Ce) ³³⁰
Palladium (Pd II) ^{293, 298, 316, 319, 336, 348}	molybdenum (Mo) ^{292, 322, 326, 337}	N ³⁻ ³⁶⁵
Nickel (Ni II) ^{292-294, 305, 314, 324, 341, 345}	Lead (Pb II) ^{292, 294, 308, 313, 314, 334, 343, 344}	Samarium (Sm III) ^{364, 330, 332}
Cobalt (Co II or Co III) ^{287-288, 290, 292-293, 299-300, 312, 324, 326, 333, 340}	Bismuth (Bi III) ^{303, 304, 330}	Terbium (Tb III) ^{364, 331, 332}
Silver (Ag I or Ag II) ^{292-294, 308}	Bromine (Br) ^{292, 304, 330, 365}	Europium (Eu III) ^{364, 307, 310, 332, 355}
Gold (Au) ^{346, 348}	Beryllium ²⁸⁵	Dysprosium (Dy III) ^{364, 332}
Copper (Cu II) ^{278, 287, 292-293, 308, 324, 342, 344, 355, 360-361}	Potassium (K) ^{293, 308, 325}	Holmium (Ho III) ^{364, 321, 332, 335}
Iron (Fe II or Fe III) ^{285, 292-293, 295, 308, 317-318}	Yttrium (Y) ^{307, 332, 335, 285, 364}	Erbium (Er III) ^{364, 306, 307, 321, 331, 332}
Zinc (Zn II) ^{278, 285, 287-289, 291-293, 298, 322, 324, 334, 345, 355, 362-363}	Tin (Sn II or Sn IV) ³⁴⁵	Thulium (Tm III) ^{321, 332, 364}
Magnesium (Mg) ^{293, 292, 308, 285}	Ruthenium (Ru) ^{292, 295}	Ytterbium (Yb III) ^{364, 321, 332, 355}
Manganese (Mn II or Mn III) ^{287, 292, 295, 314, 320, 324, 333, 392}	Rhodium (Rh) ^{292, 357}	ClO ₄ ⁻ ³⁶⁴
Cadmium (Cd II) ^{293, 292, 294, 308, 311, 313, 334, 344, 290, 288, 291, 360}	Chromium (Cr) ^{292, 351}	NO ₂ ^{368, 367, 369, 365}
Lithium (Li) ^{293, 308, 338}	Titanium (Ti) ^{292, 315}	Ozone (O ₃) ³⁶⁷
Sodium (Na) ^{293, 308, 325}	Gallium (Ga) ^{292, 295, 345}	Ammonia ^{370, 371}
Barium (Ba) ²⁹³	Vanadium (V) ^{292, 350}	Dichloromethane ³⁶⁶
Iodine (I) ^{292, 304, 330, 349}	Mercury (Hg II) ^{289, 292, 294, 308, 313, 334}	SO ₃ ²⁻ ^{364, 359}
Chlorine (Cl) ^{292, 304, 317}	Cyanide ^{293, 292, 342}	Nitrite ^{293, 312, 318}
Indium (In III) ^{295, 330, 345}	Thiocyanate ^{292, 333, 352}	Nitrate ³¹²
Gadolinium (Gd III) ^{307, 310, 331, 332, 355}	Carbon monoxide (CO) ^{292, 340}	Nitric oxide (NO) ^{314, 365}
Calcium (Ca II) ³⁴⁸	Thiourea ²⁹²	Carbon Dioxide (CO ₂) ³⁵⁴
Osmium (Os IV) ³⁰²	Nitric oxide (NO) ^{293, 341}	O ²⁻ ³⁶⁵
Neodymium (Nd III) ^{306, 307, 310, 321, 332, 364}	Fluorene (F) ^{364, 365, 338}	Salicylate ^{293, 351}
Lutetium (Lu III) ^{307, 309, 331, 332}	Oxygen (O ₂) ^{364, 367, 297, 298, 316, 328, 340, 97}	Acetylsalicylate ²⁹³
Praseodymium (Pr III) ^{307, 330, 332}	Selenium (Se ²⁻) ^{365, 347}	H ₂ O ₂ ^{302, 337, 355, 358}
Zirconium (Zr) ³¹⁵	Singlet oxygen ^{301, 339, 365}	Sulfite (SO ₂) ^{305, 359}
Arsenic (As) ³²⁰	O ₂ ²⁻ ³⁶⁵	Nitrogen (N ₂) ³¹⁶
Triiodide ^{320, 349}	NO ₃ ⁻ ^{365, 292, 304}	Chlorine (Cl ₂) ^{322, 353}
Antimony (Sb) ³³⁰	N ₃ ⁻ ³⁶⁵	Ammonium iodide ³³⁰

TABLE 3.1 Selected studies on the interaction between porphyrins and atoms or small molecules.

AMINES

N,N'-diimidazolylmethane ³⁷³	tert-butylamine ³⁷³	1,8-diaminooctane ³⁷³
1-methyl-imidazole ³⁷³	azetidine ³⁷³	pyridine ³⁷³
γ,γ' -dipyridylmethane ³⁷³	pyrrolidine ³⁷³	butylamine ³⁷³
γ -picoline ³⁷³	1,2,3,4-tetrahydroisoquinoline ³⁷³	DABCO ³⁷³
1,3-di(4-pyridyl)propane ³⁷³	diethylamine ³⁷³	Piperidine ³⁷³
1,2-di(4-pyridyl)ethane ³⁷³	dipropylamine ³⁷³	Pyrazine ³⁷³
di(4-pyridyl)-methane ³⁷³	Diisopropylamine ³⁷³	1,2-di(4- piperadiny)ethane ³⁷³
cis-1,2-di(4-pyridyl)ethene ³⁷³	isoquinoline ³⁷³	propylamine ³⁷³
trans-1,2-di(4-pyridyl)ethene ³⁷³	3-pyrroline ³⁷³	butylamine ³⁷³
3,3'-dipyridyl ³⁷³	1,2,4-triazole ³⁷³	cyclohexylamine ³⁷³
4,4'-dipyridyl ³⁷³	1,6-diaminohexane ³⁷³	1-butylamine ³⁷²
1,3-di(4-pyridyl)propane ³⁷³	1,8-diaminooctane ³⁷³	benzylamine ³⁷²
1,2-di(4-pyridyl)ethane ³⁷³	1,10-diaminododecane ³⁷³	phenethylamine ³⁷²
1,2-diaminoethane ³⁷³	1,12-diamino-dodecane ³⁷³	imidazole ^{373, 292}
1,4-diaminobutane ³⁷³	ethylenediamine ³⁷³	Acetoaminophen ³⁶⁴
1,5-diaminopentane ³⁷³	1,7-diaminoheptane ³⁷³	1,6-diaminohexane ³⁷³

TABLE 3.2 Studies on the interaction between porphyrins and amine compounds.

AMINO ACIDS

Glycine (Gly) ²⁹²	leucine tert-butyl ester ²⁹²	N-Boc-valinate ²⁹²
Leucine (Leu) ^{292, 374}	leucinol ²⁹²	N-acetyl-valinate ²⁹²
Glutamic Acid (Glu) ^{292, 374}	4-heptylamine ²⁹²	N-Cbz-norvalinate ²⁹²
Arginine (Arg) ^{292, 391, 374}	isoleucine methyl ester ²⁹²	N-Cbz-leucinate ²⁹²
Phenylalanine (Phe) ^{292, 374, 375}	proline methyl ester ²⁹²	N-Cbz-norleucinate ²⁹²
Tryptophane (Trp) ^{292, 391, 374, 375}	serine benzyl ester ²⁹²	N-Cbz-prolinate ²⁹²
Valine (Val) ^{292, 391, 374}	1-phenyl-ethylamine ²⁹²	N-Cbz-methionate ²⁹²
Isoleucine (Ile) ^{292, 374}	aminoethanol ²⁹²	N-Cbz-serinate ²⁹²
Aspartic Acid (Asp) ^{292, 391, 374}	L-DOPA-OMe ²⁹²	N-Cbz-phenylglucinate ²⁹²
Tyrosine (Tyr) ^{292, 391, 374, 375}	D-DOPA-OMe ²⁹²	N-(3,5-dinitrobenzoyl)-phenylglycinate ²⁹²
Valine methyl ester ²⁹²	3-amino-2,4-dimethylpentane ²⁹²	N-Cbz-phenylalaninate ²⁹²
n-Pr ₂ CHNH ₂ ²⁹²	phenylglycine methyl ester ²⁹²	N-Cbz-tryptophanate ²⁹²
glycine ^{292, 391, 374}	cystein methyl ester ²⁹²	Poly(glutamic acid) ²⁹²
methyl ester ²⁹²	methionine methyl ester ²⁹²	Histidine methyl ester ²⁹²
alanine methyl ester ²⁹²	L-histidine benzyl ester ²⁹²	Histidine benzyl ester ²⁹²
leucine methyl ester ²⁹²	L-lysine benzyl ester ²⁹²	Octyl α -glucopyranoside ²⁹²
phenylalanine methyl ester ²⁹²	Leucine benzyl ester ²⁹²	(Glu) ₄ Tyr ¹¹⁷
tyrptophan methylester ²⁹²	N-Cbz-alaninate ²⁹²	(Glu) ₄ Trp ¹¹⁷
aspartic acid dimethylester ²⁹²	N-Cbz-N-methylalaninate ²⁹²	alanine ^{391, 374, 375}
glutamic acid dimethylester ²⁹²	N-Cbz-valinate ²⁹²	serine ^{391, 374}
histidine ^{391, 374, 375}	proline ^{374, 375}	lysine ^{391, 374}
threonine ³⁷⁴	asparagine ³⁷⁴	methionine ^{391, 374, 375}
glutamine ³⁷⁴	cysteine ^{374, 375}	

TABLE 3.3 Selected studies on the interaction between porphyrins and amino acids or amino acid derivatives.

ALCOHOLS AND CARBOHYDRATES

Octyl- β -D-mannoside ²⁹²	1,3-cyclohexanediol ²⁹²	D-galactose ³⁷⁹
Octyl- α -D-mannoside ²⁹²	octyl α -D-2 <i>O</i> -methylmannoside ²⁹²	Methyl- α -D-glucoside ³⁷⁹
Octyl- β -D-glucoside ²⁹²	octyl β -D-6 <i>O</i> -acetylglucoside ²⁹²	Methyl- β -D-glucoside ³⁷⁹
Octyl- α -D-glucoside ²⁹²	octyl β -D-6 <i>O</i> -benzylglucoside ²⁹²	octyl- α -D-glucoside ³⁷⁹
Octyl- α -L-glucoside ²⁹²	cyclohexanol ²⁹²	D-trehalose ³⁷⁹
Octyl- β -D-galactoside ²⁹²	tetrahydropyran ²⁹²	D-lactose ³⁷⁹
Octyl- α -D-galactoside ²⁹²	2-hydroxymethyl tetrahydropyran ²⁹²	Maltotriose ³⁷⁹
Methanol ²⁹²	cyclohexanemethanol ²⁹²	Octyl- α -D-glucopyranoside ³⁷⁸
1-propanol ²⁹²	<i>cis</i> -1,2-cyclohexanediol ²⁹²	Octyl- β -D-glucopyranoside ³⁷⁸
MeO(CH ₂) ₂ OH ²⁹²	<i>trans</i> -2-hydroxymethylcyclohexanol ²⁹²	Methyl- β -D-glucopyranoside ³⁷⁸
MeO(CH ₂) ₂ Ome ²⁹²	<i>cis</i> -2-hydroxymethylcyclohexanol ²⁹²	Methyl- α -D-glucopyranoside ³⁷⁸
Diethyl ether ²⁹²	2-hydroxymethyltetrahydropyran ²⁹²	D-galactose ³⁷⁸
Tetrahydrofuran (THF) ²⁹²	dimethyl L-tartrate ²⁹²	α -D-glucose ³⁷⁸
1,2-ethanediol ²⁹²	diethyl L-tartrate ²⁹²	D-fructose ³⁷⁸
1,3-propanediol ²⁹²	diisopropyl L-tartrate ²⁹²	D-ribose ³⁷⁸
1,4-butanediol ²⁹²	di- <i>sec</i> -butyl L-tartrate ²⁹²	D-trehalose ³⁷⁸
1,5-pentanediol ²⁹²	di- <i>tert</i> -butyl L-tartrate ²⁹²	α -D-lactose ³⁷⁸
1,8-octanediol ²⁹²	diethyl meso-tartrate ²⁹²	β -D-lactose ³⁷⁸
1,2-propanediol ²⁹²	diethyl 2-hydroxysuccinate ²⁹²	maltotriose ³⁷⁸
<i>trans</i> -1,2-cyclohexanediol ²⁹²	(2 <i>R</i> ,3)-dihydroxybutane ²⁹²	D-glucose ³⁷⁷
	Maltotriose ³⁷⁷	Maltose ³⁷⁷
	Maltotetraose ³⁷⁷	
	Maltopentaose ³⁷⁷	
	Maltohexaose ³⁷⁷	
	Maltoheptaose ³⁷⁷	

TABLE 3.4 Selected studies on the interaction between porphyrins and alcohols or carbohydrates.

QUINONES AND CYCLIC COMPOUNDS

Quinones	pyrazine ²⁸⁴	1,3-benzenediol ³⁸⁰
2,3,5,6-tetramethoxy-p-benzoquinone ³⁷³	2,6-dimethoxybenzoate ²⁸⁴	3,5-benzoic acid hexyl ester diol ³⁸⁰
2,3-dimethoxy-p-benzoquinone ³⁷³	benzoic acid ²⁸⁴	4,4'-dipyridyl-1,1'-methyl ³⁸⁰
p-benzoquinone ³⁷³	3,5-dimethylbenzoate ²⁸⁴	4,4'-dipyridyl-1,1'-ethanol ³⁸⁰
2-methoxy-p-benzoquinone ³⁷³	1,2,3,4-tetrahydro-2-naphthalene carboxylate ²⁸⁴	butane dicarboxylic acid ²⁸⁴
2,6-dimethoxy-benzoquinone ³⁷³	1,4-bezenedicarboxylic acid ²⁸⁴	ethene dicarboxylic acid ²⁸⁴
2,3,6-trimethoxy-p-benzoquinone ³⁷³	p-nitrobenzoate ²⁸⁴	triethylenediamine ²⁸⁴
2,3-dimethoxy-6-methyl-p-benzoquinone ³⁷³	3,5-dinitrobenzoate ²⁸⁴	pyridine ²⁸⁴
2,3,5,6-tetrafluoro-p-benzoquinone ³⁷³	cinoline ²⁸⁴	α,α' -Dipyridyl ²⁶⁴
2,3,5,6-tetrachloro-p-benzoquinone ³⁷³	1,2,4,5-benzentetracarboxylic acid ²⁸⁴	γ,γ' -Dipyridyl ²⁶⁴
quinoline ²⁸⁴	2-naphthalene sulfonic acid ²⁸⁴	γ,γ' -Dipyridyl ²⁶⁴
1,5-disulfonatoanthraquinone ²⁸⁴	1,5-naphthalene disulfonic acid ²⁸⁴	<i>o</i> -phenanthroline ²⁶⁴
2,2'-diquinoline-4,4'-dicarboxylic acid ²⁸⁴	2,6-naphthalene disulfonic acid ²⁸⁴	methyl viologen ²⁶⁴
8-chloroquinoline ²⁸³	2,6-naphthalene dicarboxylic acid ²⁸⁴	Phenol ³⁶⁴
	1,1'-biphenyl-4,4'-dicarboxylic acid ²⁸⁴	Dopamine ³⁶⁴
	<i>o</i> -phenanthroline ²⁸⁴	2-Hydroxybenzyhydroxamate ³⁴
Other cyclic compounds	cinchophen ²⁸⁴	1,2-bis(4-pyridyl)ethane ³⁶⁵
Acetaminophen ³⁸²	pyridine ³⁸⁰	1-methylpiperazine ³⁷²
Guaiacol ³⁸²	4-pyridol ³⁸⁰	piperidine ^{372, 366}
1,4-dicarboxylate cyclohexane ²⁸⁴	3-pyridol ³⁸⁰	pyrrolidine ³⁶⁶
4,4'-bipyrene ²⁸³	1,7-phenanthroline ²⁸³	4-dimethylamino pyridine ³⁶⁵
5-nitro-1,10-phenanthroline ²⁸³	4,7-dimethyl-1,10-phenanthroline ²⁸³	Caffeine ²⁶⁴
phenol ³⁶⁵	1-ethoxy imidazole ³⁶⁵	3-amino pyridine ³⁶⁵
3-cyano pyridine ³⁶⁵	3-methyl pyridine ³⁶⁵	Berberine ³⁸¹
2-cyano pyridine ³⁶⁵	3-chloro pyridine ³⁶⁵	1,2-methyl imidazole ³⁶⁵
pyrazole ³⁶⁵	3-pyridol ³⁶⁵	3,5-dichloropyridine ³⁶⁵
quinine ³⁶⁵	3-methoxy pyridine ³⁶⁵	3-bromo pyridine ³⁶⁵
2-methyl imidazole ³⁶⁵	3-ethoxy pyridine ³⁶⁵	3,4-methyl pyridine ³⁶⁵
5,6-dimethyl-1,10-phenanthroline ²⁸³	1,10-phenanthroline-4,7-diol ²⁸³	2,6-lutidine ²⁸³
5-phenyl-1,10-phenanthroline ²⁸³	4-amino pyridine ³⁶⁵	4-piperidol ³⁶⁵
5-methyl-1,10-phenanthroline ²⁸³	4-cyano pyridine ³⁶⁵	4-methyl pyridine ³⁶⁵
4-methyl-1,10-phenanthroline ²⁸³	4-methyl imidazole ³⁶⁵	4-phenyl pyridine ³⁶⁵
5-chloro-1,10-phenanthroline ²⁸³	4,4'-dipyridine ³⁶⁵	4-phenyl imidazole ³⁶⁵
1,10-phenanthroline-5,6-dione ²⁸³	3,5-lutidine ²⁸³	Tetramethylbenzidine ³⁸²
1-methyl imidazole ³⁶⁵	Hexadecyltrimethylammonium bromide ²⁶⁴	1-(2-hydroxyethyl)pyridinium chloride ²⁶⁴
4-methoxy pyridine ³⁶⁵	1-Hexadecylpyridinium bromide ²⁶⁴	Adenine ²⁶⁴
4-ethoxy pyridine ³⁶⁵	Nicotinamide ²⁶⁴	pyrrole ³⁶⁵
1-Carbamidomethyl-3-carbamylpyridinium chloride ²⁶⁴	1-Carbamidomethyl-pyridinium-3-carboxylate betaine ²⁶⁴	1-(2-Hydroxyethyl)-3-carbamylpyridinium chloride ²⁶⁴
1-Carboxymethylpyridinium-3-carboxylate, sodium ²⁶⁴	(2-Hydroxyethyl)-trimethylammonium chloride ²⁶⁴	4,7-phenanthroline ²⁸³

TABLE 3.5 Selected studies on the interaction between porphyrins and quinones or other cyclic compounds.

PROTEINS AND DNA

Proteins	Nucleobases and Nucleosides
Telomerase ³⁸³	Adenine ^{404, 405}
Serum Albumin ^{384, 385}	Cytosine ^{404, 405}
Cosynthetase ³⁸⁶	Thymine ^{404, 405}
HIV-1 Protease ³⁸⁷	Uracil ⁴⁰⁴
Acetylcholinesterase ³⁸⁸⁻³⁹⁵	Adenosine ⁴⁰⁴
Organophosphorus Hydrolase ³⁹⁶	Cytidine ⁴⁰⁴
Butyrylcholinesterase ^{393, 395, 397}	Uridine ⁴⁰⁴
Glucose Oxidase ³⁹⁸	Thymidine ⁴⁰⁴
Carbonic Anhydrase ³⁹⁹	
Antibodies ⁴⁰⁰	
DNA	
DNA ^{292, 401-402}	
DNA major groove ⁴⁰³	

TABLE 3.6 Selected studies on the interaction between porphyrins and proteins, DNA, nucleosides, or nucleobases.

VOLATILE ORGANICS AND SURFACTANTS

Surfactants	THF ³⁷⁰	CHCl ₃ ³⁵¹
CTAC ⁴⁰⁷	Methylene chloride ³⁷⁰	P(OC ₂ H ₅) ₃ ³⁵¹
HPS ⁴⁰⁷	Chloroform ³⁷⁰	P(C ₄ H ₉) ₃ ³⁵¹
Triton X-100 ⁴⁰⁷	Dipropylsulfide ³⁷⁰	C ₆ H ₃ SH ³⁵¹
Brij-35 ⁴⁰⁷	Benzene ³⁷⁰	(C ₃ H ₇)S ³⁵¹
Tween-60 ⁴⁰⁶	Toluene ^{370, 408}	benzene ³⁵¹
	Ethylbenzene ⁴⁰⁸	n-octylamine ³⁵¹
Volatile organics	Cumene ⁴⁰⁸	Tributylphosphine ³⁷⁰
Acetic acid ³⁷⁰	2-nitrotoluene ⁴⁰⁹	n-butylamine ³⁵¹
Propionic acid ³⁷⁰	4-nitrotoluene ⁴⁰⁹	Atrazine ⁴¹⁰
Hexanoic acid ³⁷⁰	2,4-dinitrotoluene ⁴⁰⁹	Ethene ⁴¹²
Dimethylformamide (DMF) ³⁷⁰	2,4,6-trichlorophenol ^{409, 411}	Propene ⁴¹²
Hexylamine ³⁷⁰	DMF ³⁵¹	1-decene ⁴¹²
Dimethylsulfoxide (DMSO) ³⁷⁰	Ethanol ³⁵¹	Peroxy nitrite ⁴¹³
Ethanol ³⁷⁰	Pyridine ^{351, 373}	trichloromethane ³⁶⁵
Ethyl acetate ³⁷⁰	Hexylamine ³⁵¹	bromomethane ³⁶⁵
Acetone ³⁷⁰	Acetonitrile ³⁵¹	chloropropane ³⁶⁵
Propyl ³⁶⁵	tert-butanol ³⁶⁵	sulfonate ³⁶⁵
hydroxyl ³⁶⁵	Acetone ³⁵¹	butanol ³⁶⁵
Hexanetriol ³⁷⁰	THF ³⁵¹	ethanol ³⁶⁵
Triethylphosphine ³⁷⁰	CH ₂ Cl ₂ ³⁵¹	methanol ³⁶⁵

TABLE 3.7 Selected studies on the interaction between porphyrins and volatile organic compounds or surfactants.

PORPHYRIN MACROCYCLE

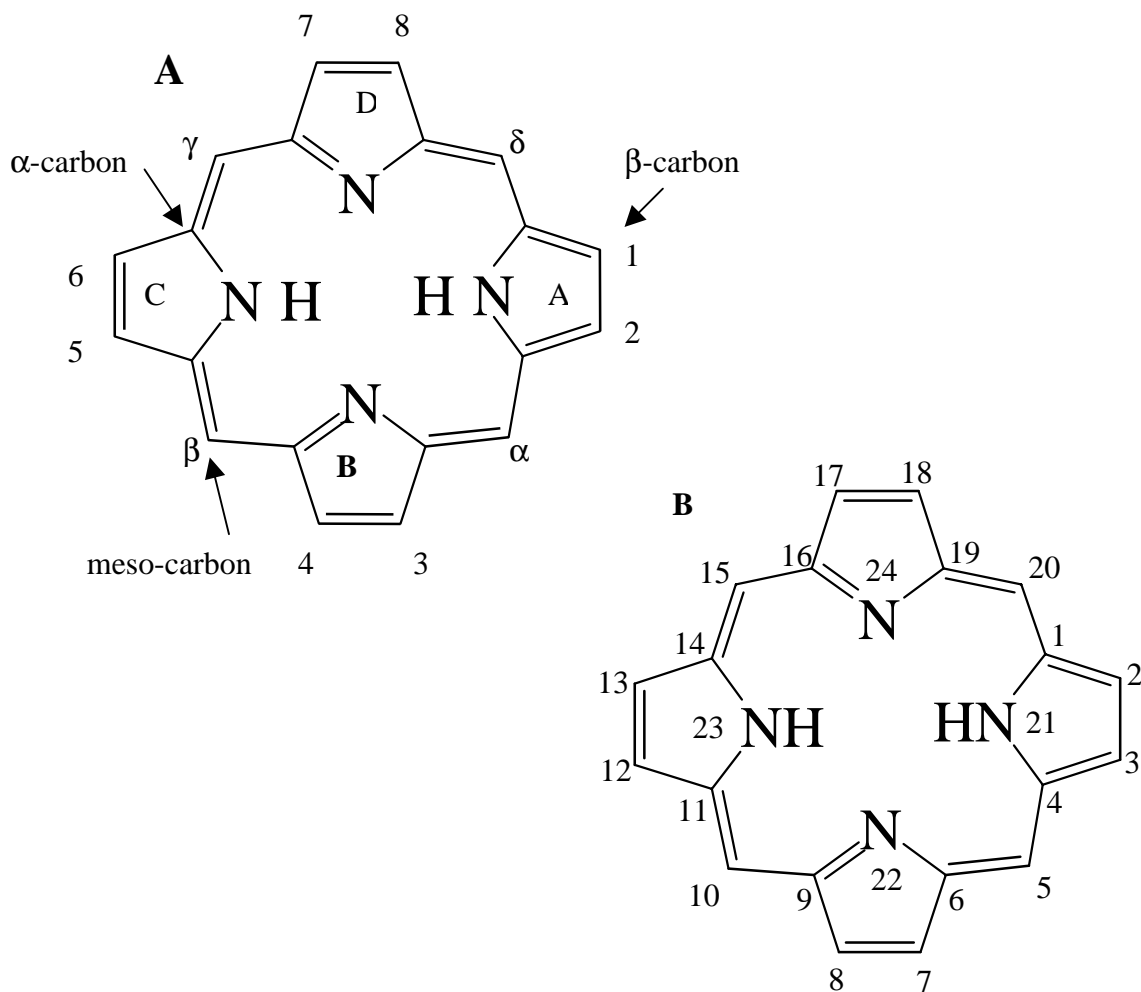


FIGURE 3.1 The porphyrin macrocycle consisting of twenty carbon atoms and four nitrogen atoms. (A) Fischer numbering system. (B) IUPAC numbering system.

NATURALLY OCCURRING PORPHYRINS

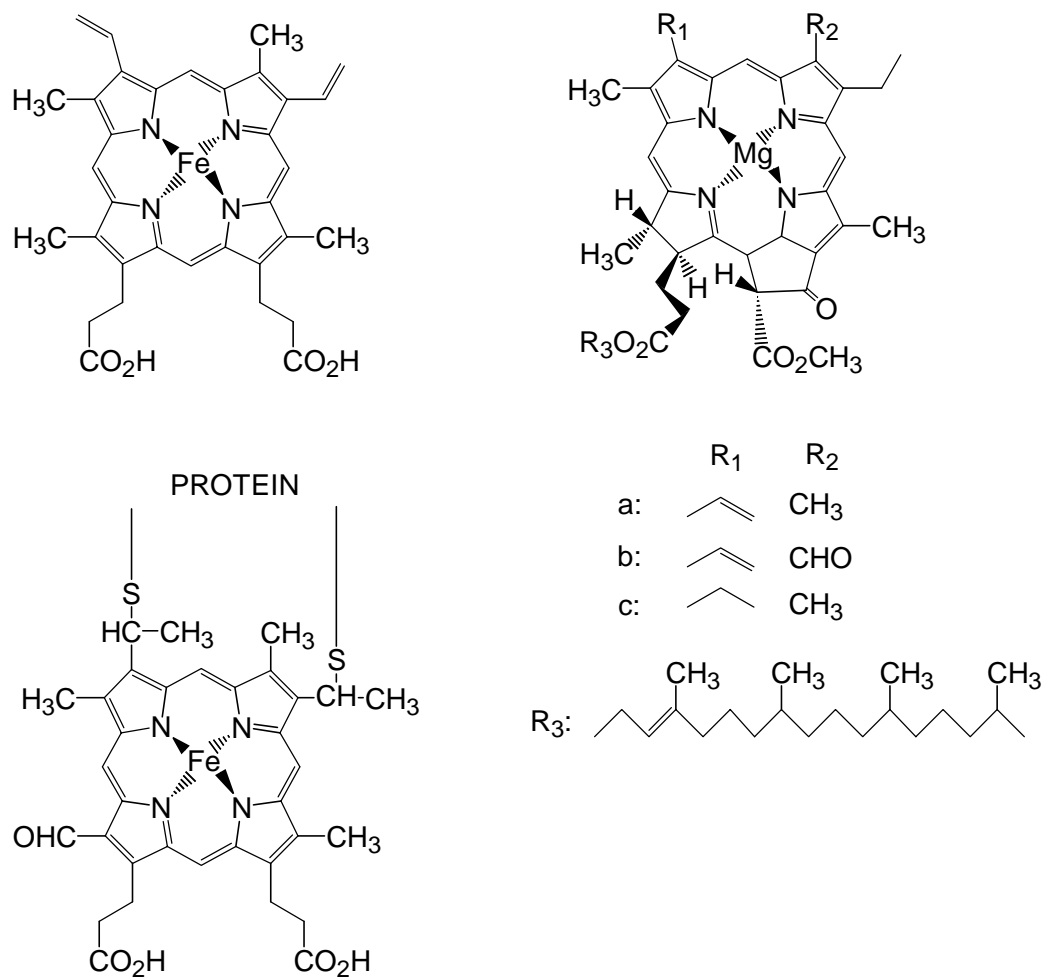


FIGURE 3.2 Porphyrins in nature: Heme *b* from hemoglobin and myoglobin, Heme *c* from cytochrome *c*, and chlorophyll.

FISCHER AND IUPAC NOMENCLATURE

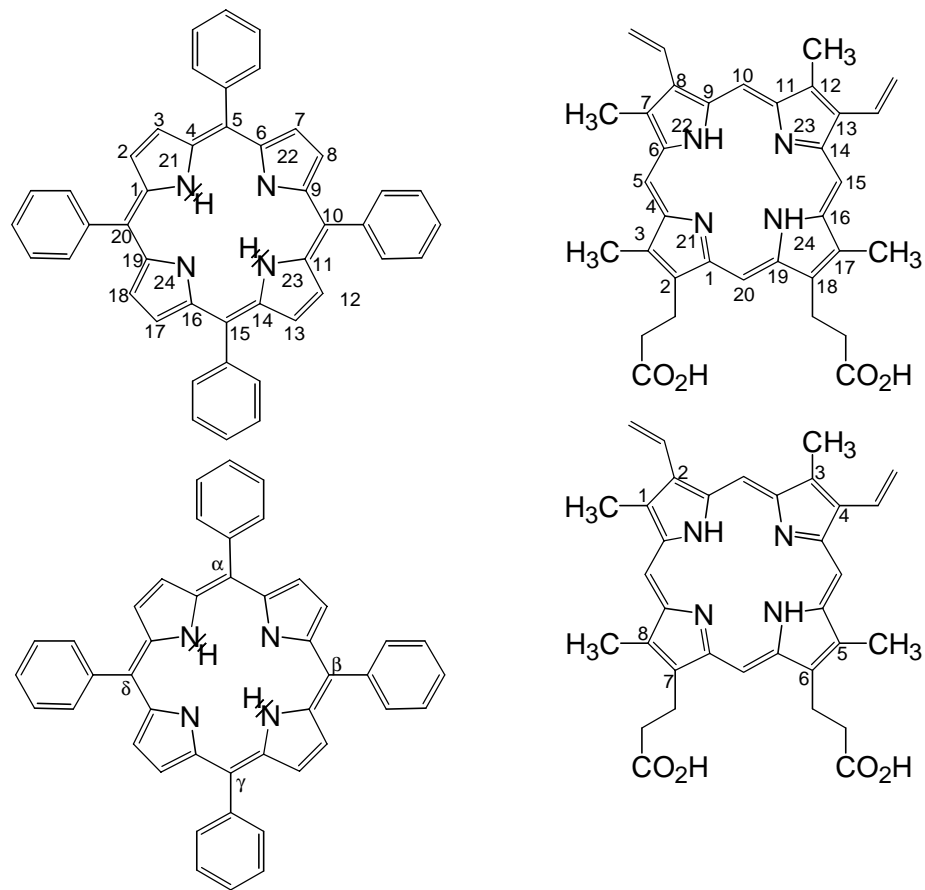


FIGURE 3.3 These structures show how the Fischer and IUPAC names for protoporphyrin IX and TPP [meso-tetraphenylporphyrin] are obtained.

ABSORBANCE SPECTRA AND SOLVENT EFFECTS

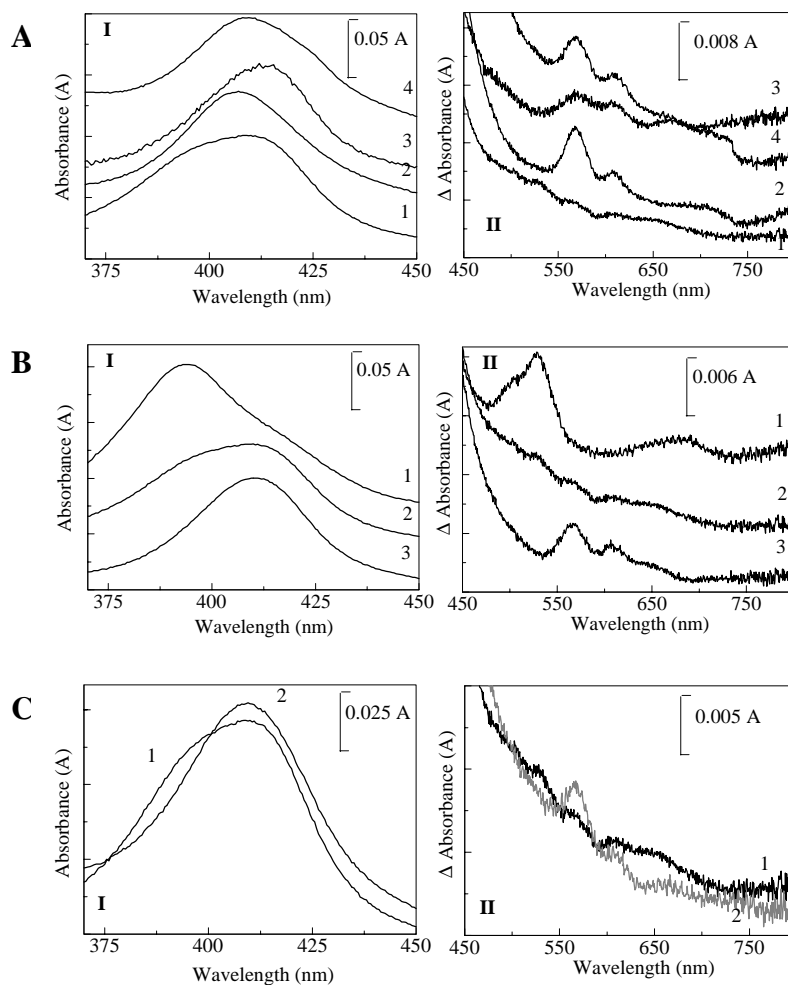


FIGURE 3.4 (A) The absorbance spectra of Fe-TPPS (0.8 μ M) in 50 mM NaPi pH 7 (Trace 1), 50 mM NaPi pH 7 with 50% ethanol (Trace 2), 50 mM NaPi pH 7 with 50% methanol (Trace 3), and 50 mM NaPi pH 7 with 50% DMSO (Trace 4). (B) The absorbance spectra of Fe-TPPS in 50 mM NaPi for pH 4.8 (Trace 1), pH 7.0 (Trace 2), and pH 9.2 (Trace 3). (C) The absorbance spectra of Fe-TPPS in pH 7 NaPi at 50 mM (Trace 1) and 500 mM (Trace 2). The Soret (I) and Q bands (II) are shown at different scales for emphasis.

ABSORBANCE SPECTRA AND STRUCTURAL EFFECTS

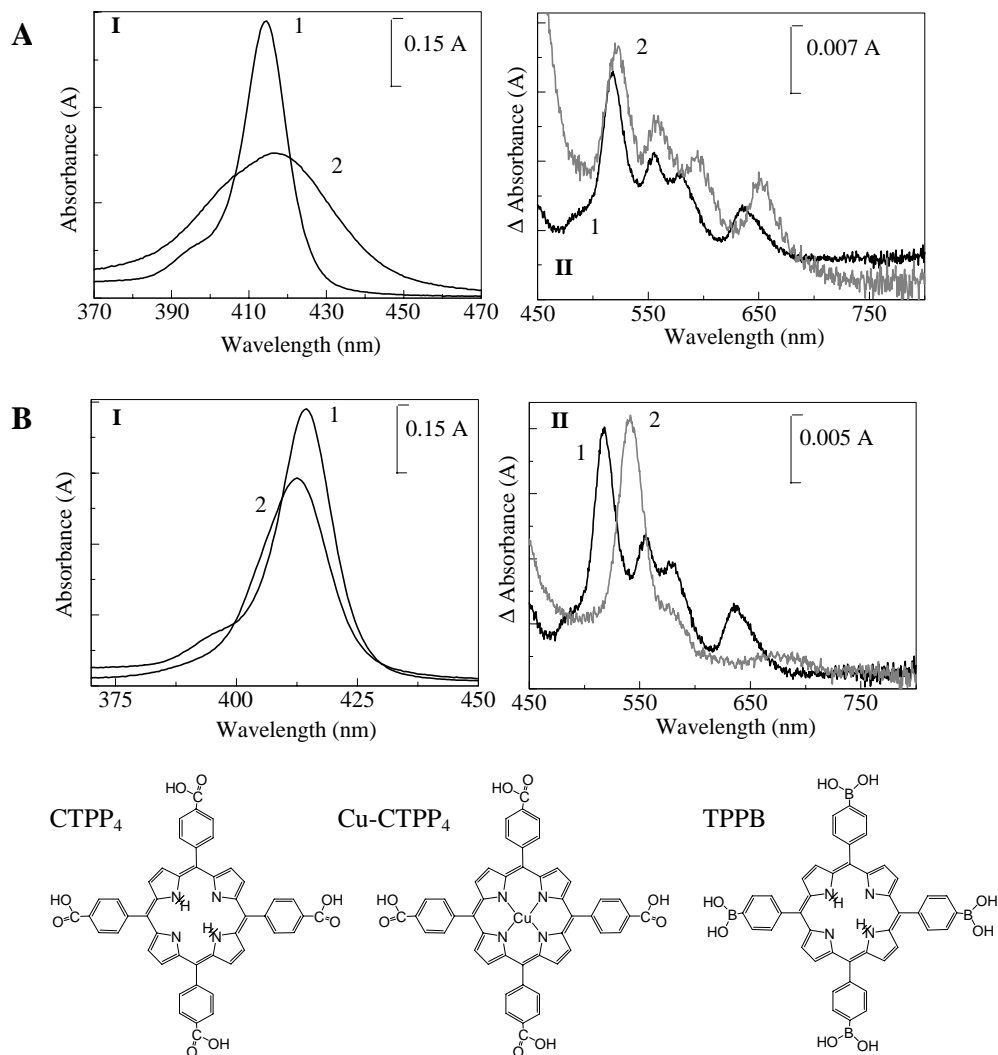


FIGURE 3.5 (A) The absorbance spectra of CTPP₄ (0.8 μM, Trace 1) and TPPB (0.8 μM, Trace 2) in 50 mM NaPi pH 7. (B) The absorbance spectra of CTPP₄ (0.8 μM, Trace 1) and Cu-CTPP₄ (0.8 μM, Trace 2) in 50 mM pH 7 NaPi. The Soret (I) and Q bands (II) are shown at different scales for emphasis.

Π - Π STACKING

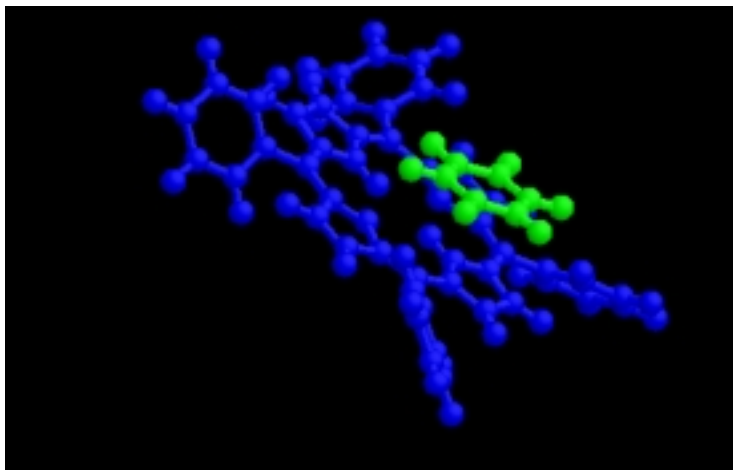


FIGURE 3.6 The cofacial interaction between TPP and benzene. Figure courtesy of Dr. H. J. Harmon.

CHAPTER 4

IMMOBILIZATION

4.1 BASIC CONSIDERATIONS: PROTEINS

There is no ideal method or support for immobilization of all proteins. The choices are made by weighing the required features for a given application against the limitations and properties of a combination of immobilization method and support. A soluble protein behaves in solution as any other analyte with freedom of movement. Immobilization restricts the motion of the protein, localizing a concentration. There are five basic methods for immobilization of proteins: adsorption, entrapment, encapsulation, cross-linking, and covalent binding. The book Immobilization of Enzymes and Cells gives a thorough review of these methods [424]. Points to be considered when choosing a support and method are described in Table 4.1 [424]. The following paragraphs briefly describe each method and mention some of the advantages/disadvantages for each one.

Adsorption is the simplest method involving reversible interactions between the support and the protein (Figure 4.1) [1]. The forces involved are typically electrostatic including van der Waals, ionic and hydrogen bonding, and hydrophobic/hydrophilic interactions. These forces are weak but sufficient to hold the proteins for some applications. The existing surface chemistry between the protein and the support is exploited, so no chemical modifications of the proteins are necessary. This means there will be little damage to the protein. Procedures generally involve mixing of the support and protein together under the proper pH, ionic strength, temperature, etc for some

incubation period. This is followed by harvesting of the immobilized material and thorough washing to remove any unbound protein. The primary disadvantage to this technique is dissociation of the protein from the support resulting from changes in pH, temperature, ionic strength or even substrate binding (Table 4.2) [424]. Interaction of contaminants, substrates, or products with the support may also result in dissociation of the protein. One other issue is overloading of the support. This can result in low catalytic activity as can the steric hindrance that occurs when the protein is too close to the support or to another protein.

Immobilization by entrapment involves restriction of the movement of the enzymes while still free in solution. This is generally accomplished using a gel with a controlled lattice structure. The structure must be tight enough to prevent the protein from passing yet loose enough to allow substrates and products to flow. This is a barrier to mass transfer and so may cause changes in the reaction kinetics for an enzyme. There are four major entrapment methods: ionic gelation involving cross-linking of a polymer, temperature-induced gelation taking advantage of phase transitions in compounds such as gelatin, chemical/photochemical organic polymerization of a mixture of monomers, and precipitation from immiscible solvent occurring by phase separation. The gelation methods often result in unstable, soft structures. Since the organic solvents used in the precipitation method are often not tolerated by proteins, this method is limited to highly stable enzymes.

Encapsulation, like entrapment, involves restricting the movement of proteins that are otherwise free in solution. Semi-permeable membranes are used to prevent large proteins from passing the barrier while substrates and products pass freely. The

difference here is that encapsulation involves surrounding a volume containing many enzyme while entrapment is a lattice structure with single (at most 2 or 3) proteins trapped in the gaps in the lattice. Nylon and cellulose nitrate are commonly used materials for membranes. Diffusion is still the main issue and may result in rupture of the membrane in cases of rapidly accumulating products and/or osmotic pressure. This method is very useful for immobilization of enzyme combinations, however.

Cross-linking is support free. Proteins are joined to each other to form large three-dimensional structures. Chemical cross-linking involves forming bonds between functional groups on the proteins using activators such as glutaraldehyde or toluene diisocyanate. Other molecules may be used as spacers to prevent difficulties with steric hindrance including albumin and gelatin. Many proteins are not tolerant of the activators limiting the applicability of this technique. Cross-linking lacks the mechanical properties and often results in unstable structures, so it is rarely used alone. Forming chemical bonds to the functional groups on a protein may modify the ability of an enzyme to function properly. This can alter substrate binding, catalytic mechanism, or changes in enzymatic reaction rates.

Covalent binding, similar to cross-linking, involves forming a covalent bond to a functional group on the surface of the protein. In this case the bond is between the support and an amino acid functional group. The most often used groups are the amino groups of lysine or arginine, the sulfhydryl group of cysteine, the hydroxyl group of serine or threonine, and the carboxyl group of aspartic acid and glutamic acid. Many supports are available for this type of immobilization. The primary factor for maintenance of enzymatic activity appears to be hydrophilicity of the surface making surfaces such as

dextran and cellulose, which bear sugar residues are popular. The sugar residues also provide hydroxyl groups that can be activated to form covalent bonds. Porous silicate glasses are also a popular choice. These glasses can be functionalized through silane linkages (described later).

Covalent binding is usually achieved through isourea linkage, diazo linkage, peptide bond, or alkylation reactions. The method must be chosen to accommodate the particular protein. If a carboxylic acid is involved in the active site, it would be more effective to choose a diazo linkage or an alkylation of an amino group rather than a peptide bond to a carboxylic acid group. There are generally two steps in the immobilization process: activation of the functional groups of the support generally forming strong electrophilic groups (electron deficient) and coupling of the enzyme to these groups via nucleophiles (electron donating) to form a covalent bond. A wide variety of possibilities can be realized using different supports and chemically modified supports.

4.2 DEVELOPMENT OF A METHOD

The sensor systems to be addressed in this document are to be used in a variety of environments, that is, samples in solution, vapor phase, or even solid state. To accommodate these situations, a covalent binding immobilization was chosen. This guarantees a constant protein density for the measurements with no dissociation of the enzyme into the sample even in large liquid volumes. The first enzyme addressed for immobilization was acetylcholinesterase (AChE, Type V-S from electric eel). A wide

variety of protocols used by different groups for immobilization of AChE exist [424-435].

4.2.1 FIRST STEPS

Catalysis in the AChE active site relies on a glutamic acid residue as well as serine and histidine residues, so an immobilization protocol taking advantage of amino-bearing residues was investigated [436]. Different supports were investigated in the early stages: ProbeOn™ Plus microscope slides and microwell plates, DNA-bind microwell plates, and Xenobind™ microwell plates. All of these have functionalized surfaces. Amino groups are bound to the microwell plates without requiring activation while the ProbeOn™ Plus slides do require activation. The investigation of microwell plates was abandoned early in the project, so the discussion to follow will focus on the work with ProbeOn™ Plus microscope slides although the principles are still effective for microwell plates. Silicate glass can be immersed in a solution of 3-aminopropyltriethoxysilane in acetone to prepare the amino-functionalized glass surfaces (Figure 4.2, protocol from Pierce Biotechnology Rockford, IL [437]). Following amino-functionalization ProbeOn™ Plus microscope slides are dipped into hydrochloric acid to protonate the amino groups. This improves surface hydrophilicity enhancing surface-solution interactions during the immobilization process.

Glutaraldehyde activation of amino groups is a common method used for covalent immobilization and cross-linking of proteins [9, 12, 438-441]. Figure 4.2 shows the alkylation of the surface amino group that takes place upon exposure to glutaraldehyde [442]. This reaction proceeds most favorably at pH 7.5 to pH 9.0. Following activation of the surface amino groups, an enzyme, porphyrin, or other amino group bearing

molecule (or cell) can be allowed to react with the remaining aldehyde group (similar pH conditions, Figure 4.2). This protocol was used for immobilization of AChE. In addition, several blocking agents were used including: Tris(hydroxymethyl)amino methane (TRIS, MW = 121), casein (6.4 kDa), gly-gly-gly (MW = 189), bovine serum albumin (BSA, 68 kDa), tricine (MW = 179), glycyl-glycine (MW = 132), lysine (MW = 146), and ethylenediamine tetra-acetic acid (EDTA, MW = 292). The blocking agents were used to bind any unreacted aldehyde groups remaining after binding of the enzyme to the surface. They play an additional role in that they fill the gaps between the enzymes, increasing the stability of the resulting protein matrix.

The success of the immobilization protocols is based on the enzymatic activity of the surface as determined by the Ellman method [443]. This protocol is described in detail in Chapter 5. The slides resulting from this protocol, regardless of blocking agent, showed very low enzymatic activity (Protocol 1, see section 4.4). The low enzyme activity was likely a consequence of the proximity of the enzyme to the surface, but could also indicate a very low enzyme density. As mentioned earlier, if an enzyme is too close to the support steric hindrance can result and therefore changes in reaction rates may be observed.

4.2.2 PAMAM DENDRIMERS

A macromolecule discovered in the 1980's by Dr. Tomalia at the Dow Chemical Company has been used in some immobilization protocols to both increase the number of available amino groups and provide a spacer between the enzyme and the support surface [444]. The macromolecules are referred to as dendrimers or "dense star" polymers because of their tree like branching structure (Figure 4.3). Unlike many polymers, the

PAMAM dendrimers show uniform molecular structure and have narrow molecular weight distribution as well as specific size and shape characteristics. The surface of the dendrimers also has a large number of terminal amino groups. The PAMAM dendrimers are classified into generations based on the number of growth steps used to achieve the molecule. Each subsequent growth step results in twice the number of surface amino groups and approximately double the molecular weight of the preceding step. Figure 4.3 shows the structure of PAMAM dendrimer generation 2. This polymer has molecular weight 3,260 with a diameter of 29 Å and 16 terminal amino groups. The dendrimer used for the following protocol was PAMAM dendrimer generation 4 (MW = 14,220; D = 45 Å, approx. 54 terminal amino groups). In the following text, PAMAM refers to the generation 4 dendrimer.

PAMAM can be immobilized to the glutaraldehyde activated amino-silicate glass in the same way as any other amino bearing molecule (Figure 4.4) except that the PAMAM will very likely bind several of the amino groups on the glass surface due to the high concentration of terminal amino groups on the dendrimer. The surface that results will also have many more exposed amino groups than the original glass surface. The unreacted aldehyde groups left on the surface of the slide can again be “blocked” with TRIS or one of the other blocking agents listed above. This surface can again be activated with glutaraldehyde. The activation of the dendrimer groups results in two possibilities for the terminal amino groups of the dendrimers: active aldehyde groups are formed allowing binding of another layer of amino group bearing molecules and the terminal amino groups of adjacent dendrimers become linked via the five carbon chain of glutaraldehyde (GA). Cross-linking of the dendrimer increases the stability of the first

layer and the enzyme (or porphyrin, etc) can be bound to the activated PAMAM. AChE immobilized surfaces produced using this protocol (Protocol 2) showed significantly higher enzymatic activity than slides produced using Protocol 1.

4.2.3 OPTIMIZATION OF THE PROTOCOL

Different blocking agents were tested with this protocol (TRIS, casein, gly-gly-gly, bovine serum albumin, tricine, glycyl-glycine, lysine, and ethylenediamine tetraacetic acid) both for optimize enzymatic activity and for surface stability under different storage conditions. Surfaces blocked using TRIS, casein, BSA, or a combination of casein and TRIS (steps 4 and 7, respectively) showed a higher degree of enzymatic activity than those blocked with the other molecules listed. As a result, the other potential blocking agents were not considered after this point. The surfaces were stored dry at room temperature, dry at 4°C, or in 50 mM pH 7 NaPi buffer at 4°C. Slides produced using TRIS and/or casein as the blocking agent retained some or all of the enzymatic activity when stored at 4°C for up to 7 days while those produced using BSA did not retain enzymatic activity after storage. The use of BSA as a blocking agent was abandoned at this point.

The effect of pH on the immobilization protocol was investigated. Protocol 2 was modified so that all steps took place at pH 5.5, 6, 7, 8, or 9. Slides produced at pH 5.5 and pH 6 showed little enzymatic activity; the Ellman reaction was allowed to proceed for 3 hours before a measurable color change occurred. Slides produced at pH 7 and pH 9 showed significantly higher enzymatic activity while slides produced at pH 8 showed double the activity of slides produced at pH 9. It is likely that some protein unfolding occurred during the immobilization of the enzyme in pH 9 buffer, reducing the number of

active enzymes that were immobilized. The reaction by which the aldehyde group of glutaraldehyde is replaced by the terminal nitrogen of the surface or the enzyme (etc) favors slightly alkaline conditions (above pH 7.5). It was later discovered that the enzymatically active lifetime of the slides could be extended by TRIS blocking at pH 9 while other steps were performed at pH 8.

Because the slides were to be used with a porphyrin indicator, the interaction of the porphyrin to be used, monosulfonate tetraphenyl porphyrin (TPPS₁), with the surfaces was investigated. A series of slides was produced using TRIS, casein, or combination TRIS/casein blocking after completion of only a portion of the protocol (Protocol 2): complete slide, slide completed through step 6, slide completed through 4, slide completed through step 3. TPPS₁ (370 nM) was applied to the surface in 50 mM pH 7 NaPi (50 % ethanol) and allowed to interact for 20 minutes. The absorbance spectra of the slides indicated a very strong interaction of TPPS₁ with casein. The absorbance intensity for this interaction was much larger than that for the TPPS₁-AChE interaction. For this reason, casein was eliminated as a possible blocking agent. TRIS was used for all subsequent slide production since the interaction with TPPS₁ is minimal.

4.2.4 FINAL MODIFICATIONS

As described in Chapter 2, the interaction of a substrate with ligand depends on the concentration of both. The implication for an enzyme based protocol is that a lower detection limit can be achieved with a greater enzyme density provided there are no factors such as overloading. It was believed that by providing a greater number of activated amino groups on the surface of the slide it may be possible to achieve binding of a larger enzyme density. To address this possibility, Protocol 2 was modified to

include the application of a second layer of PAMAM dendrimer to the slide surface (similar to Protocol 3 without steps 4 or 7, using concentrations from Protocol 2). It was also noted that a more homogeneous immobilization could be achieved by placing samples on an orbital shaker during incubation and by using a 200 μ l volume standing drop rather than 100 μ l.

Slides produced using this protocol showed six greater enzymatic activity than those produced using Protocol 2 (Figure 4.5). In addition, the TPPS₁-AChE peak for the slides showed more than three times the absorbance intensity of slides produced from the previous protocols. The addition of a third layer of PAMAM did not improve the intensity of the absorbance peak or the degree of enzymatic activity. Storage stability studies indicated the need for TRIS blocking between and following the PAMAM steps. The effect of the concentrations of AChE, PAMAM, and GA were investigated and optimized to achieve Protocol 3. This is the protocol used for immobilization of acetylcholinesterase, butyrylcholinesterase, glucose oxidase, organophosphorous hydrolase, and the lectins mentioned in later chapters. Myoglobin was immobilized by the steps listed in Protocol 1 using concentrations in Protocol 3 (myoglobin concentration 10 mg/ml).

4.3 OTHER METHODS

Though the PAMAM protocol proved successful for many enzymes, carbonic anhydrase showed very low enzymatic activity (method of determination of enzymatic activity described in Chapter 8) when immobilized through Protocol 3. Elimination of one of the PAMAM layers did not improve the activity of the surface. Section 4.1

mentions that the covalent bond in an immobilization scheme should not be made to a residue involved in catalytic activity. Catalysis in carbonic anhydrase (CA) relies on a threonine residue and a glutamic acid residue as well as histidine residues, so hydroxyl and carboxyl functional groups should not be used for immobilization, but binding to an amino group should not present any problem.

CA is much smaller than AChE having a molecular weight of about 26 kDa and an a surface area of 26,000 Å compared to 55 kDa and 51,000 Å. Carbonic anhydrase has seven arginine residues and twenty three lysine residues while AChE has twenty four arginine residues and twenty-six lysine residues, so the two proteins have about the same number of amino groups per surface area. Figures 4.6 and 4.7 show the distribution of the arginine and lysine residues for CA and AChE, respectively [445-446]. Though there is a slightly higher concentration of residues around the active site opening for CA, some enzymes should bind with their active sites accessible and others with the active site inaccessible. This is likely similar to what happens in the case of AChE.

It is likely that the limited activity of CA when immobilized by the PAMAM protocol is due to its small size rather than the distribution of amino groups. The large number of available binding sites on the surface could result in overloading of the surface and steric hindrance. A modified protocol was used for immobilization of CA. First CA was immobilized simply by activating the ProbeOn™ Plus slide surface as in step one of Protocol 3 and then applying carbonic anhydrase to the surface (0.3 mg/ml in 50 mM pH 8 NaPi). A slight increase in enzymatic activity was noted. Steric hindrance was thought to be a possible problem, so a spacer was added to the surface (Protocol 4). Arginine was added to the glutaraldehyde activate slide surface and the enzyme was bound to this

“tether” adding distance without increasing the number of functional groups. This did not improve the enzymatic activity of the slides.

The arginine tether added a spacer with about eight bonds. 1,12 diaminododecane is a twelve carbon chain with a terminal amino group on each end (Figure 4.8). Slides prepared using this tether showed activity slightly less than that of those prepared using the arginine tether. The arginine tethered enzymes showed activity for only two weeks based on an assay of esterase activity using p-nitrophenol acetate. LysLysLys was used to give a space of at least seven bonds and up to eighteen bonds from the surface (depending on the exact binding pattern). Using LysLysLys doubled the activity of the slides as compared to the surface using an arginine tether. The activity of the LysLysLys tethered enzymes dropped to 20% of the original activity within 2 months.

4.4 IMMOBILIZATION PROTOCOLS

Protocol 1

1. React ProbeOn™ Plus surface with glutaraldehyde at 0.29 M (40 µl stock solution in 100 µl 50 mM pH 8 NaPi) for 20 minutes.
2. Rinse surface with PBS (25 mM sodium phosphate 2.5 M NaCl solution at pH 9) to terminate.
3. React surface with AChE at 1 µM (100 µl 0.1 mg/ml in 100 µl 50 mM pH 8 NaPi) for 2 hours. Rinse with PBS to terminate.
4. React surface with 2% BSA solution in 50 mM pH 7 NaPi or 1 M TRIS pH 9 (or other blocking agent, see text) for 1 hour. Rinse excess away with deionized water.

Protocol 2

1. React ProbeOn™ Plus surface with glutaraldehyde at 0.29 M (40 µl stock solution in 100 µl 50 mM pH 8 NaPi) for 20 minutes.
2. Rinse surface with PBS (25 mM sodium phosphate 2.5 M NaCl solution at pH 9) to terminate.
3. React surface with PAMAM dendrimer generation 4 at 1.8 mM (2.5 µl stock solution in 100 µl 50 mM pH 8 NaPi) for 90 minutes. Rinse with PBS to terminate.
4. React surface with 2% BSA solution in 50 mM pH 7 NaPi or 1 M TRIS pH 9 (or other blocking agent, see text) for 1 hour. Rinse with PBS to terminate.
5. React surface with glutaraldehyde at 0.29 M for 20 minutes. Rinse with PBS to terminate.
6. React surface with AChE at 1 µM (100 µl 0.1 mg/ml in 100 µl 50 mM pH 8 NaPi) for 2 hours. Rinse with PBS to terminate.
7. React surface with 2% BSA solution in 50 mM pH 7 NaPi or 1 M TRIS pH 9 (or other blocking agent, see text) for 1 hour. Rinse excess away with deionized water.

Protocol 3

1. React ProbeOn™ Plus surface with glutaraldehyde at 0.17 M (40 µl stock solution in 200 µl 50 mM pH 8 NaPi) for 25 minutes.
2. Rinse surface with PBS (50 mM sodium phosphate 0.5 M NaCl solution at pH 7) to terminate.
3. React surface with PAMAM dendrimer generation 4 at 6.4 mM (20 µl stock solution in 200 µl 50 mM pH 8 NaPi) for 90 minutes. Rinse with PBS to terminate.

4. React surface with 1 M TRIS pH 9 for 20 minutes. Rinse with PBS to terminate.
5. React surface with glutaraldehyde at 0.17 M (40 μ l stock solution in 200 μ l 50 mM pH 8 NaPi) for 25 minutes. Rinse with PBS to terminate.
6. React surface with PAMAM dendrimer generation 4 at 6.4 mM (20 μ l stock solution in 200 μ l 50 mM pH 8 NaPi) for 90 minutes. Rinse with PBS to terminate.
7. React surface with 1 M TRIS pH 9 for 20 minutes. Rinse with PBS to terminate.
8. React surface with AChE at 200 nM (20 μ l 0.1 mg/ml in 200 ml 50 mM pH 8 NaPi) for 90 minutes. Rinse with PBS to terminate.
8. React surface with 1 M TRIS pH 9 for 40 minutes. Rinse excess away with 50 mM pH 7 NaPi.

Protocol 4

1. React ProbeOn™ Plus microscope slide surface with glutaraldehyde at 0.17 M (40 μ l stock solution in 200 μ l 50 mM pH 8 NaPi) for 25 minutes.
2. Rinse surface with PBS (50 mM sodium phosphate 0.5 M NaCl solution at pH 7) to terminate.
3. React surface with tether (in 200 μ l 50 mM pH 8 NaPi) for 90 minutes. Rinse with PBS to terminate. [Tethers: arginine at 900 μ M, LysLysLys at 900 μ M, and 1,12 diaminododecane at 350 μ M]
4. React surface with 1 M TRIS pH 9 for 20 minutes. Rinse with PBS to terminate.
5. React surface with glutaraldehyde at 0.17 M (40 μ l stock solution in 200 μ l 50 mM pH 8 NaPi) for 25 minutes.

6. React surface with CA at 12 μM (30 μl 2 mg/ml in 200 ml 50 mM pH 8 NaPi) for 90 minutes. Rinse with PBS to terminate.
7. React surface with 1 M TRIS pH 9 for 40 minutes. Rinse excess away with 50 mM pH 7 NaPi.

4.5 IMMOBILIZATION OF PORPHYRINS

Porphyryns can be immobilized in the same ways that proteins are: adsorption, entrapment, encapsulation, cross-linking, and covalent bonding. Entrapment and encapsulation have the disadvantage that the proximity of the support and/or the other porphyrin molecules will distort the π -bond conformation of the porphyrin altering the absorbance and response characteristics of the indicator. The other difficulty is the interference of the support with the measurement of absorbance or fluorescence characteristics of the porphyrins. Some work using cross-linking of the porphyrins is directed being at the study of the effect on the spectra though it hasn't yet been applied to detection technologies [379, 447-452]. The methods primarily used for immobilization of porphyrins are adsorption and covalent binding. Porphyrins have been immobilized to a variety of surfaces including quartz, glass, cellulose, Sephadex, and polystyrene [453-456].

Adsorption is again the simplest and cheapest though the porphyrin surface may be dissociate from the support. This method also distorts the absorbance/fluorescence characteristics and the characteristic response to analytes. This alteration, reported by several groups [455], is a result of the proximity of the porphyrin to the support and the sensitivity of the porphyrin to its environment. Several different porphyrins can be

immobilized to cellulose films and cellulose fibers by this method. The interaction of each porphyrin with the surface is strong enough to tolerate pH changes across the range from pH 5.5 to 10.5, media with ionic strengths ranging from that of deionized water to that of 2.5 M NaCl, and solvents such as DMF and ethanol (up to 75%). These immobilization protocols are given in section 4.6, Porphyrin Protocols 1 through 5. The porphyrin structures used in the studies presented here are shown in Figure 4.9.

The potential for modification of the substituent groups on the porphyrin makes the compounds ideal for formation covalently bound surfaces. Three types of covalent bound surfaces were used during the projects described in the following chapters. The Traut's Reagent substituent in the 4 position of one phenyl ring of TPPT [meso-tetra (4-carboxyphenyl) porphine monoethylene diamine coupled to Traut's reagent (2-iminothiolane)] makes it possible to form a covalent bond to gold (Figure 4.9). A gold evaporation technique was used to deposit gold onto the surface of standard microscope slides to varying degrees of reflectivity (provided by Dr. D. Peakheart, Physics Department, Oklahoma State University). Bond formation was accomplished by incubating the gold surface with 500 nM TPPT (see Porphyrin Protocol 6).

Covalent immobilization of TPPS-Si(OCH₃)₃ [meso tetra(4-sulfonatophenyl) porphyrin coupled to trimethoxysilane] to glass was accomplished similarly to the process for amino functionalization of glass (Figure 4.9). The protocol used was a modification of several common protocols for covalent bonding of triethoxy or trimethoxy compounds to glass [438, 457-458]. Adjustments were made to accommodate the solubility of the porphyrin and to optimize the porphyrin density on the surface. The protocol requires acidic conditions and uses a combination of methanol and

water to accommodate solubility and encourage dissociation of the methanol from the side chain (see Porphyrin Protocol 7).

Covalent immobilization of NH₂TPP [tetra(4-aminophenyl) porphyrin] to ProbeOn™ Plus microscope slides was accomplished in a manner similar to that of the myoglobin immobilization (Porphyrin Protocol 8). The reactivity of the immobilized porphyrin to analytes was unexpectedly reduced when PAMAM layers were used. Use of the PAMAM dendrimer would have made a higher porphyrin density possible but may have resulted in stacking effects or porphyrin-dendrimer interactions. The binding of this porphyrin to the surface was not guaranteed to be via a single bond (Figure 4.9). There could be up to four bonds between the porphyrin and the surface. In order to maximize porphyrin density on the surface, that is, limit the number of bonds to each porphyrin to one or two, a very high concentration of porphyrin was used for the immobilization (2 mM).

Some work was also done on the cross-linking of NH₂TPP both in solution and on the surface of the slide. In solution, there were no visible absorbance characteristics to indicate that glutaraldehyde cross-linking had been achieved. On the slide surface a repetition of steps 1 through 3 (Porphyrin Protocol 8) were used to create multiple layers of porphyrin. After application of four layers of porphyrin to the surface, the fluorescence of the slide (excitation 380-500 nm, emission 550-800 nm) was completely quenched. The absorbance intensity of the surface increased for each of the first three layers after which no further increase was noted for layers four through six.

4.6 PORPHYRIN PROTOCOLS

Porphyrin Protocol 1: TPPS on Cellulose Films

1. Cut cellulose film (SPECTRA/POR[®] molecular porous membrane tubing; Spectrum Houston, TX) down one side and fold open (flatten). Roll the film along the narrow direction to form a 2 inch cylinder (height). Place this film into a test tube and allow the roll to become loose. This allows space for the porphyrin solution between the cellulose layers.
2. Soak cellulose film in a solution of 1 mM TPPS in water for a minimum of 8 hours at 4° C.
3. Remove film from test tube, unroll, and lie flat to dry on clean surface (such as foil).
4. When the film is dry, soak in large excess of 1 M NaCl preferably on the orbital shaker (for 18 inches of film this is at least 0.5 l NaCl) for a minimum of 4 hours.
5. Remove film from salt solution and rinse with deionized water.
6. Soak film in large excess of 50/50 ethanol/water solution for minimum of 0.5 hours.
7. Rinse film with copious amounts of deionized water.
8. Allow film to dry and store at room temperature. Protect from dust and light.

Porphyrin Protocol 2: TPPT on Cellulose Films

1. Cut cellulose film (SPECTRA/POR[®] molecular porous membrane tubing; Spectrum Houston, TX) down one side and fold open (flatten). Roll the film along the narrow direction to form a 2 inch cylinder (height). Place this film into a test tube and allow the roll to become loose. This allows space for the porphyrin solution between the cellulose layers.

2. Soak cellulose film in a solution of 56 μM TPPT in 75% ethanol/ H_2O at room temperature for four hours.
3. Remove film from porphyrin solution and soak in excess 1M NaCl overnight in the dark.
4. Soak in 50% ethanol/water solution for 0.5 hours.
5. Rinse with deionized water.
6. Allow to dry. Store at room temperature. Protect from light and dust.

Porphyrin Protocol 3: TPPS₁ on Cellulose Fibers

1. Fold cellulose tissue (Kimwipes® EX-L, Fisher Scientific, Pittsburgh, PA) lengthwise and roll along the narrow direction to form a 2 inch cylinder (height). Place this tissue into a test tube and allow the roll to become loose. This allows space for the porphyrin solution between the cellulose layers.
2. Soak tissue in 1 mM TPPS₁ in N,N-dimethylformamide (DMF) for a minimum of 4 hours at 4° C.
3. Remove from tube and lie flat to dry.
4. When the tissue is dry, soak in large excess of 1 M NaCl preferably on the orbital shaker (at least 250 ml NaCl for one tissue) for a minimum of 4 hours.
5. Remove tissue from salt solution and rinse with deionized water.
6. Soak tissue in large excess of 50/50 ethanol/water solution for minimum of 0.5 hours.
7. Rinse tissue with copious amounts of deionized water.
8. Allow tissue to dry and store at room temperature. Protect from dust and light.

Porphyrin Protocol 4: NH₂TPP on Cellulose Fibers

As described for Porphyrin Protocol 3 with the exception that the porphyrin solution is 1 mM NH₂TPP in ethanol.

Porphyrin Protocol 5: TPPB on Cellulose Fibers

As described for Porphyrin Protocol 3 with the exception that the porphyrin solution is 1 mM TPPB in H₂O with NaOH at pH 10.

Porphyrin Protocol 6: TPPT on Gold Surface

1. Apply 200 µl 500 nM TPPT in 75% ethanol/H₂O to gold surface. Spread evenly.
2. Allow interaction for 2 hours before washing surface with copious amounts of deionized water.
3. Rinse surface with excess 1 M NaCl.
4. Rinse surface with excess 50/50% ethanol/water.
5. Allow surface to dry. Protect from dust and light. Store at room temperature.

Porphyrin Protocol 7: TPPS-Si(OCH₃)₃ on Glass

This protocol can be used for immobilization onto glass slides or other glass surfaces such as test tubes and fiber glass wool.

1. Prepare surface by soaking in nitric acid for 20 minutes. Rinse with deionized water repeatedly and allow to dry.
2. Using 1 N HCl, 0.87 mM (1 mg/ml) TPPS-Si(OCH₃)₃ in water, and acetone free methanol, mix directly onto surface in the following ratio: 4 parts porphyrin, 3 parts

- methanol, and 1 part HCl. (For example on a glass slide mix 200 μ l porphyrin, 150 μ l methanol, and 50 μ l HCl.) Distribute evenly over surface.
3. Place in oven or on hot plate at approximately 50 to 70° C for 6 hours or overnight.
 4. Soak in large excess of 1 M NaCl preferably on the orbital shaker for a minimum of 2 hours.
 5. Remove surface from salt solution and rinse with deionized water.
 6. Soak surface in excess of 50/50 ethanol/water solution for minimum of 0.5 hours.
 7. Rinse surface with copious amounts of deionized water.
 8. Allow tissue to dry and store at room temperature. Protect from dust and light.

Porphyrin Protocol 8: NH₂TPP on Amino-Silicate Glass

This protocol can also be used for the immobilization of TPPS₃-(CH₂)₁₀NH₂.

1. React ProbeOn™ Plus microscope slide surface with glutaraldehyde at 0.17 M (40 μ l stock solution in 200 μ l 50 mM pH 8 NaPi) for 25 minutes.
2. Rinse surface with PBS (50 mM sodium phosphate 0.5 M NaCl solution at pH 7) to terminate reaction.
3. React surface with 200 μ l porphyrin for 90 minutes. Rinse with PBS to terminate.
[Porphyrins: 2 mM NH₂TPP in DMF or 0.8 mM (1 mg/ml) TPPS₃-(CH₂)₁₀NH₂ in pH 8 50 mM NaPi]
4. Rinse surface with 50/50% ethanol/water several times followed by rinsing with water.
5. Allow surface to dry and store at room temperature. Protect from dust and light.

IMMOBILIZATION CONSIDERATIONS

PROPERTY	POINTS FOR CONSIDERATION
Physical	Strength, surface area, form (sheets, fibers, etc), permeability, density
Chemical	Hydrophobicity, inertness, density of functional groups, regenerability
Stability	Storage, maintenance of enzyme activity, regeneration of enzyme activity, stability of support material
Resistance	Bacteria/fungal, chemical, pH, temperature, organic solvents, proteases
Safety	Biocompatibility, toxicity of reagents, health issues for process workers and end users, special considerations for use with food, pharmaceuticals, and medical applications
Economic	Availability and cost of support and reagents, degree of skill required, feasibility for scale up, environmental impact, effective working life, reusability
Reaction	Enzyme loading, catalytic productivity, reaction kinetics, side reactions, multiple protein systems, diffusion limits

TABLE 4.1 Desirable properties and points for consideration when choosing an immobilization support and method [424].

PROPERTIES TO BE CONSIDERED

METHOD	ADVANTAGES/DISAVANTAGES
Adsorption	Little damage to proteins; simple, cheap, and quick; no chemical changes to support or protein; reversible allowing regeneration
	Leakage of protein from support; nonspecific binding; overloading of support; steric hindrance by support; coimmobilization may be difficult or impossible
Encapsulation	Little damage to proteins; simple, cheap, and quick; no chemical changes to support or protein; no leakage of protein; easily controlled loading; no toxic reagents; simplified coimmobilization
	Membranes subject to rupture; requires stable proteins; not reversible; mass transfer issues
Entrapment	No chemical changes to proteins; no leakage of protein
	Requires stable proteins, often involves toxic cross-linking agents, not reversible, steric hindrance by support; mass transfer issues; coimmobilization is difficult
Cross-linking	No protein leakage; no mass transfer issues; coimmobilization easily achievable; increased stability
	Toxic cross-linking reagents; steric hindrance; chemical changes to proteins
Covalent Binding	No protein leakage; no mass transfer issues; coimmobilization possible; easily controlled loading; increased stability
	Chemical changes to proteins; may or may not be reversible;

TABLE 4.2 Comparison of different immobilization strategies. Advantages versus disadvantages [1, 424].

TYPES OF IMMOBILIZATION

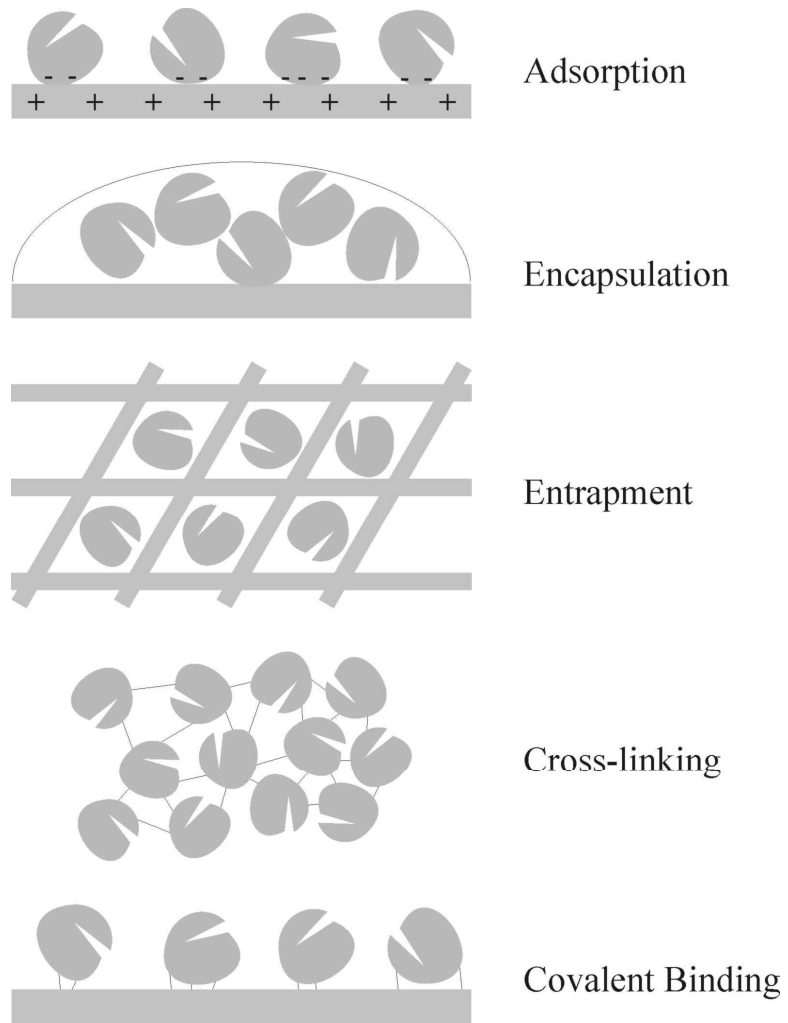


FIGURE 4.1 Schematic representations of the different types of immobilization [424].

IMMOBILIZATION ONTO AMINO-FUNCTIONALIZED GLASS

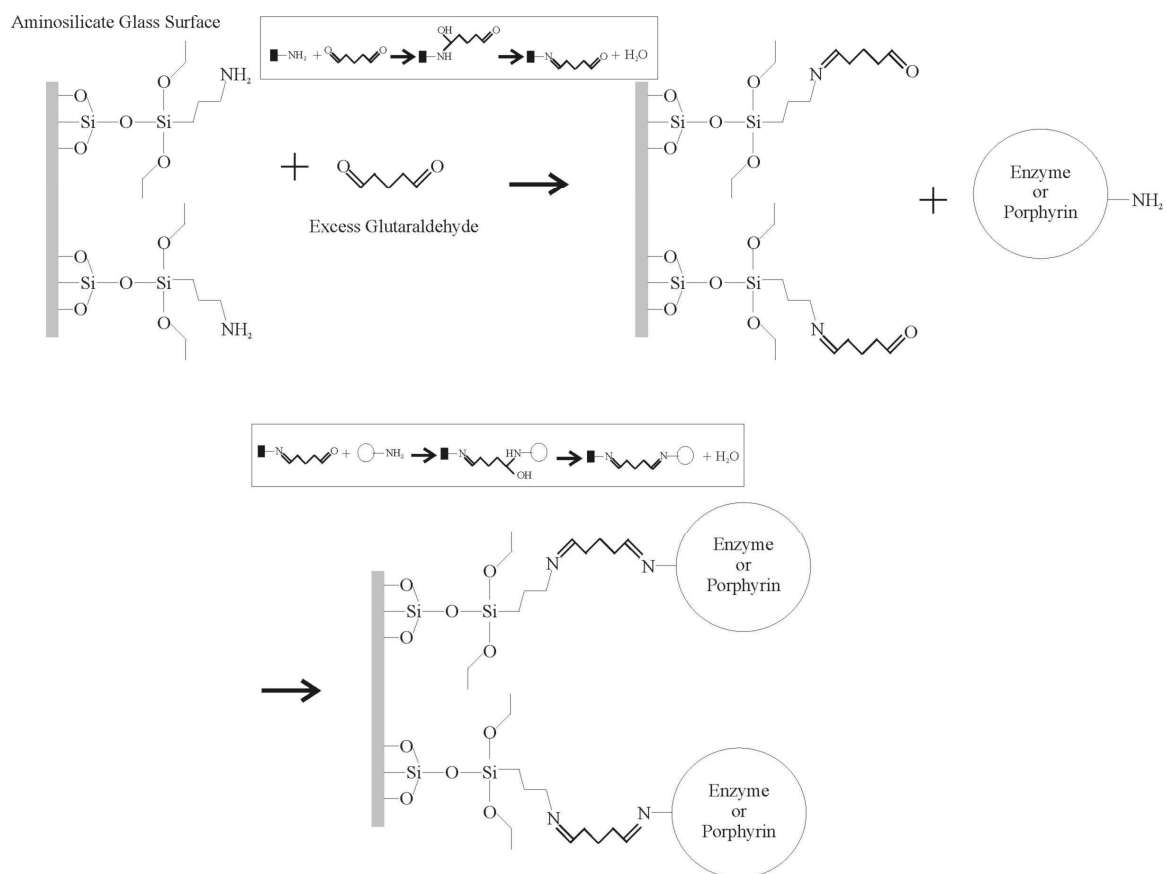


FIGURE 4.2 The steps involved in immobilization onto amino-silicate glass via glutaraldehyde linkage [437, 442].

PAMAM DENDRIMER

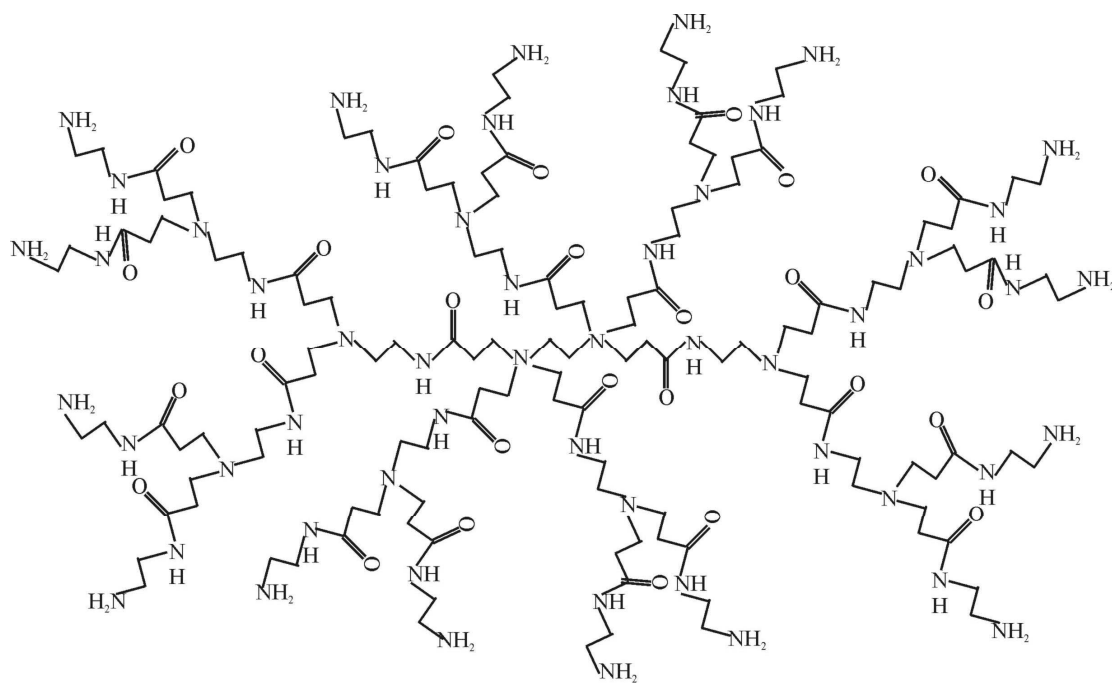
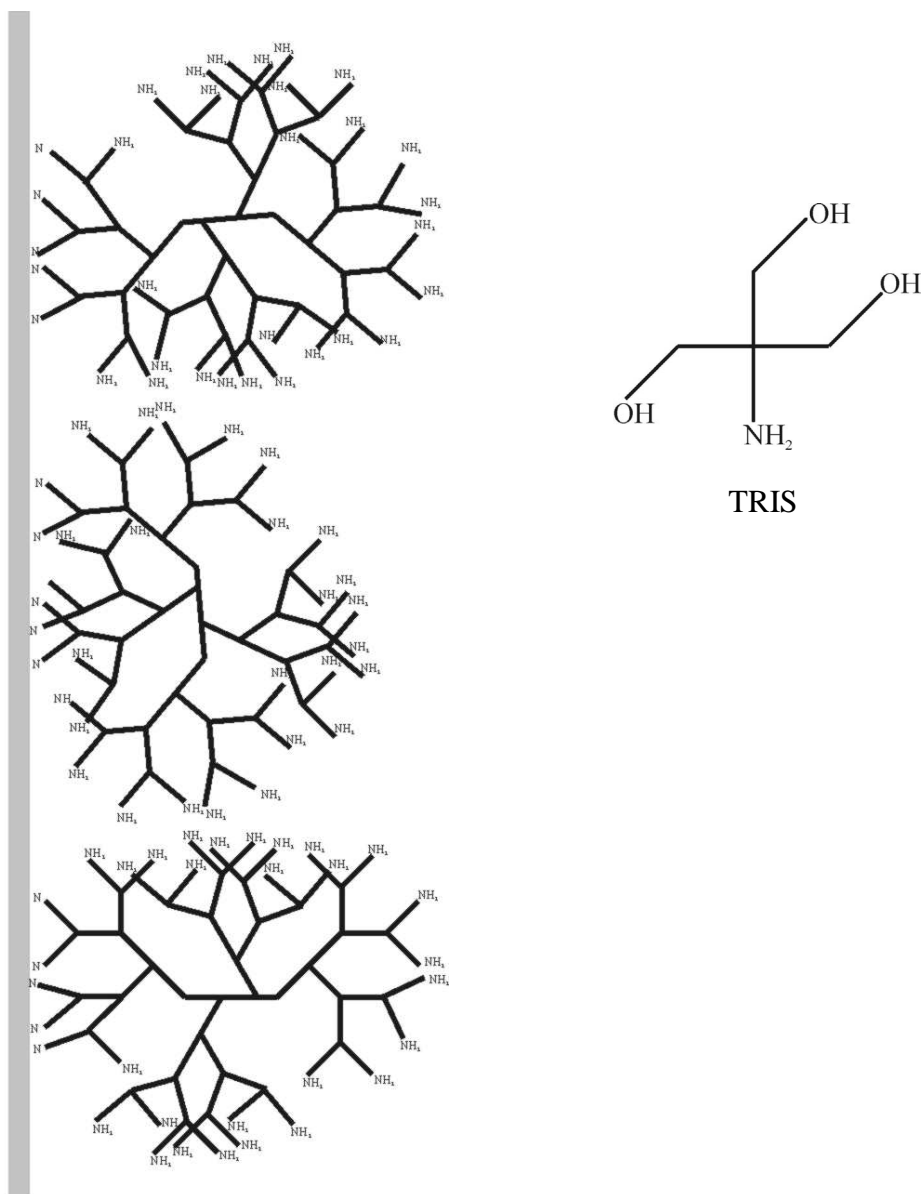


FIGURE 4.3 PAMAM dendrimer generation 2. Generation 4 has twice the number of functional groups and twice the molecular weight.

PAMAM DENDRIMER IMMOBILIZATION



Amino-glass PAMAM G4

FIGURE 4.4 Amino-silicate glass slide with PAMAM dendrimer Generation 4 bound through glutaraldehyde activation. Unreacted sites on glass are blocked with TRIS.

PAMAM DENDRIMER IMMOBILIZATION

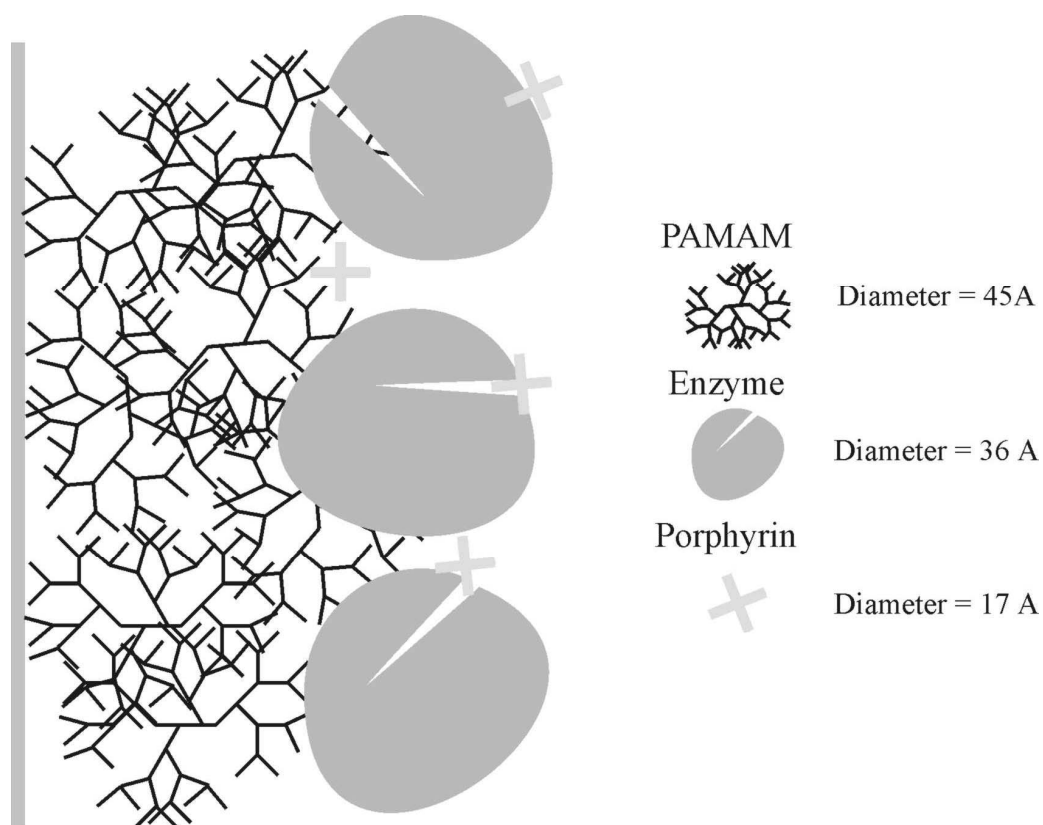


FIGURE 4.5 Amino-silicate glass slide with PAMAM dendrimer Generation 4 and AChE bound through glutaraldehyde activation. Unreacted sites are blocked with TRIS. Porphyrin is added as the final immobilization step. Approximate molecule diameters are given in angstroms (Å).

CARBONIC ANHYDRASE

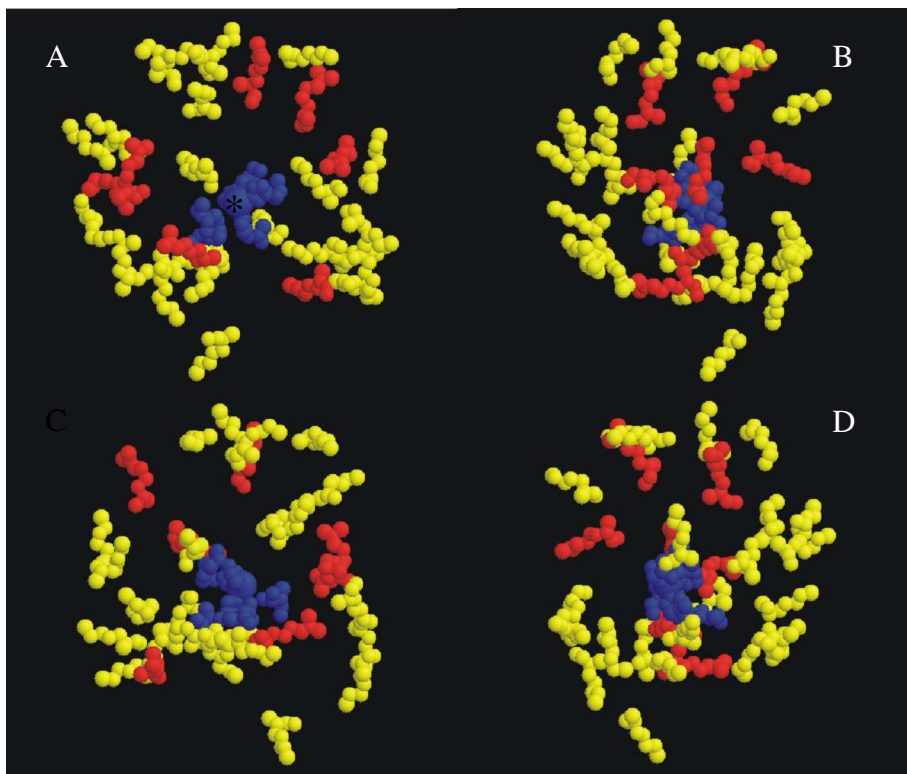


FIGURE 4.6 Arginine and lysine residues in carbonic anhydrase. View A looks into the active site showing the zinc atom (*). View B is a 90° rotation of View A around the z-axis. View C is a 90° rotation of View B around the z-axis. View D is a 90° rotation of C around the z-axis. Lysine = white, arginine = pink, active site residues shown in blue [445].

ACETYLCHOLINESTERASE

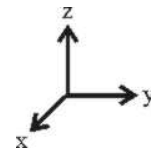
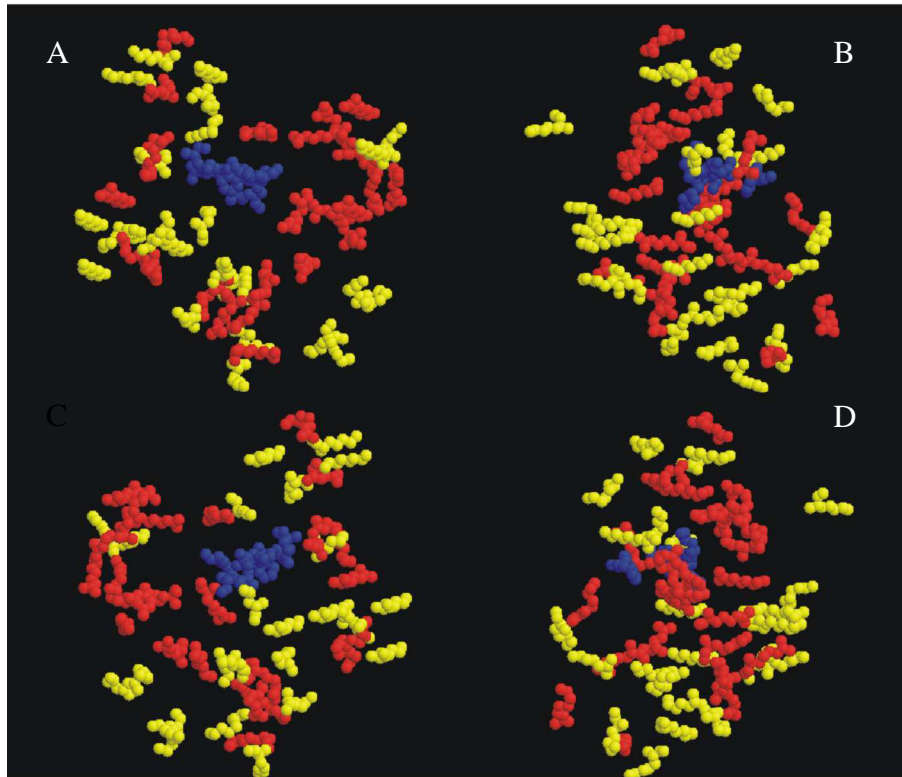
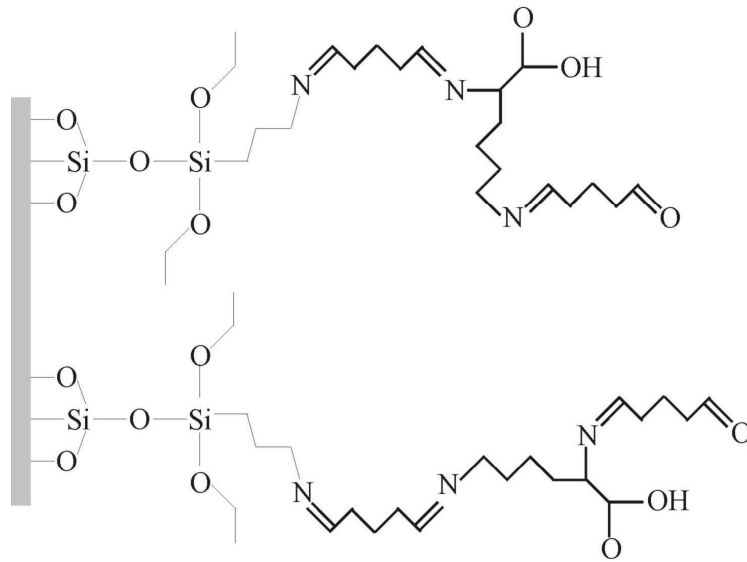


FIGURE 4.7 Arginine and lysine residues in acetylcholinesterase. View A looks into the active site. View B is a 90° rotation of View A around the z-axis. View C is a 90° rotation of View B around the z-axis. View D is a 90° rotation of C around the z-axis. Lysine = white, arginine = pink, active site residues shown in blue [446].

OTHER IMMOBILIZATIONS

Glutaraldehyde Activated Lysine



Glutaraldehyde Activated 1,12 diaminododecane

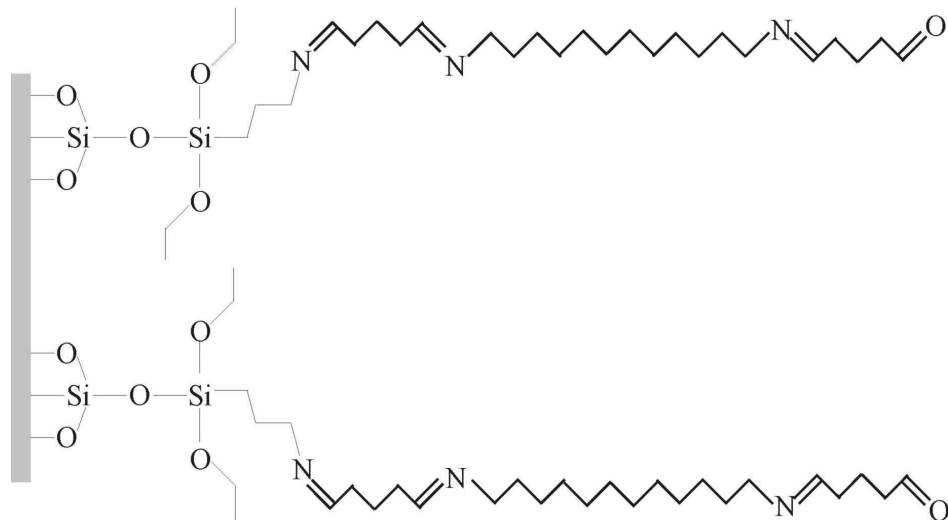


FIGURE 4.8 Amino-silicate glass slide with activated lysine or 1,12 diaminododecane bound through glutaraldehyde activation. Unreacted sites on the glass surface are blocked with TRIS.

PORPHYRIN STRUCTURES

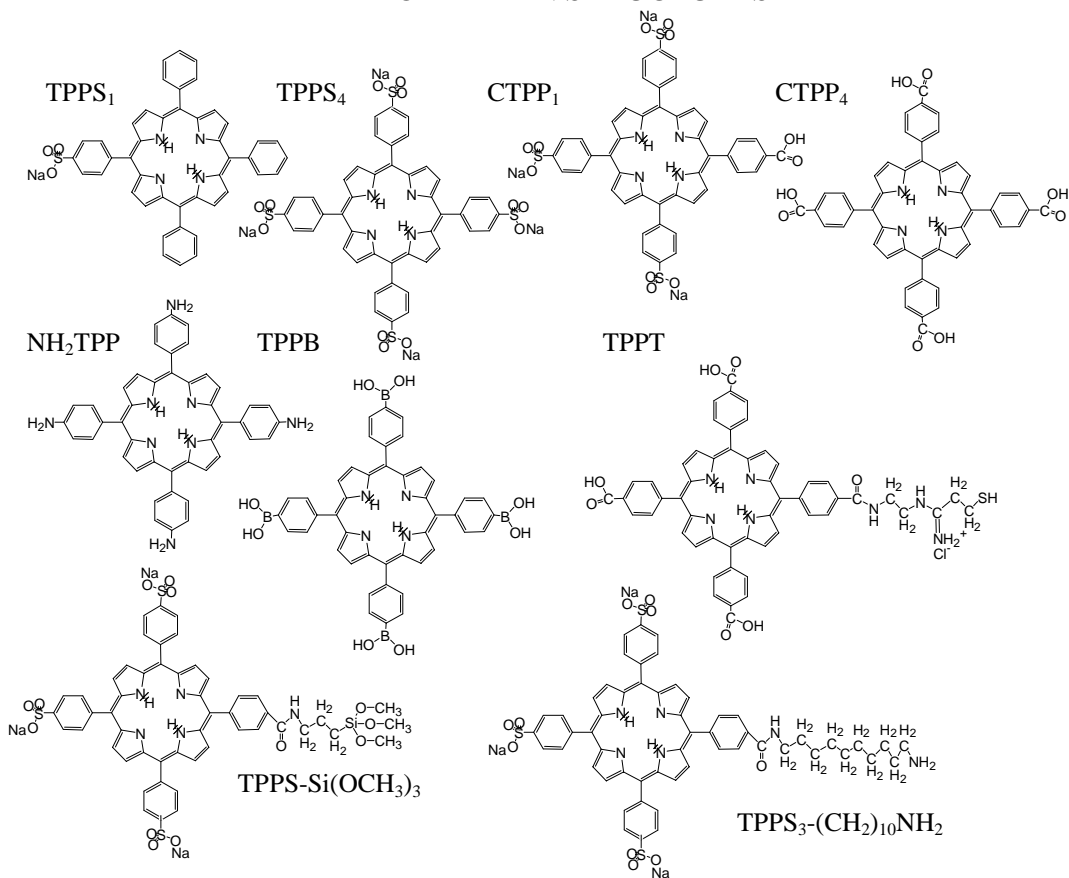


FIGURE 4.9 Molecular structures of several porphyrins mentioned in the text. TPPS₁ = mesonsulfonate tetraphenyl porphyrin, TPPS₄ = meso tetra(4-sulfonatophenyl)porphyrin, CTPP₁ = meso-tri(4-sulfonato phenyl) mono(4-carboxy phenyl) porphyrin, CTPP₄ = meso-tetra(4-carboxyphenyl)porphyrin, NH₂TPP = tetra(4-aminophenyl) porphyrin, TPPB = meso-tetra(4-boronic acid) porphyrin, TPPT = meso-tetra (4-carboxyphenyl) porphyrin monoethylene diamine coupled to Traut's reagent (2-iminothiolane), TPPS-Si(OCH₃)₃ = meso tetra(4-sulfonatophenyl)porphyrin coupled to trimethoxysilane, and TPPS₃-(CH₂)₁₀NH₂ = meso-tri(4-sulfonatophenyl) mono(4-carboxyphenyl) porphyrin coupled to 1,10 diamino decane.

CHAPTER 5

ACETYLCHOLINESTERASE

5.1 THE TARGET

The enzyme acetylcholinesterase (AChE, E.C. 3.1.1.7) terminates impulse transmission at cholinergic synapses by hydrolyzing the neurotransmitter acetylcholine to acetate and choline. Organophosphorous pesticides and nerve agents inhibit the activity of AChE resulting in constant impulse transmission and inducing symptoms ranging from increased salivation and headache to convulsion and suppressed breathing which can result in death [459]. First responders, military personnel, and other persons at risk for exposure to these compounds need an indicator that operates in real time and is reliable, cost effective, compact, portable, and sensitive.

Present sensors of nerve agents that inhibit acetylcholinesterase are based primarily upon comparison of catalytic rates of acetylcholinesterase, other cholinesterases, or OPH at a given time to a baseline, background, or pre-exposure level [9, 12, 425-427, 429, 440-441, 460-477]. The measurement of catalytic rates may involve multiple steps including the addition or changing of one or more reagent solutions, a somewhat undesirable operating characteristic.

Sensors can be broadly classified into two groups: detectors of specific agents (e.g., VX) [4, 12, 466, 478-480] and detectors of AChE inhibitors in general [12, 425-427, 429, 466-467, 465, 472, 481-482]. There is a need for both types of sensor. The central core technology of any sensor/detector is a system that transduces the presence of

the chemical into an optical, electronic, or other signal that can be processed either by eye or electronic circuitry.

The presence of individual organic molecules strongly affects the spectrophotometric characteristics of porphyrins [264, 283-284]. Amino acids and small peptides [376, 400] alter the absorbance spectra of porphyrins, each molecule resulting in unique spectral characteristics. Porphyrin-protein interactions also alter the spectra as shown by the interaction with serum albumin [385, 483-484] and other proteins [485]. In addition, porphyrins are enzyme inhibitors that have been shown to inhibit AChE activity [388-389]. They have been studied in this capacity as photoactivated insecticides [486] and for use in treating Alzheimer's disease and *myasthenia gravis* [487-488]. Porphyrins have been shown to inhibit telomerase and Hepatitis C virus serine protease [383] while metalloporphyrins have been shown to be potent inhibitors of human immunodeficiency virus (HIV) type 1 and 2 reverse transcriptases [387]. Porphyrins have also been shown to bind to DNA [401, 403] and are used in photodynamic therapy [489].

The following chapter outlines the development of a detection protocol for inhibitors of acetylcholinesterase based on reversible, competitive inhibition of the enzyme by a porphyrin which functions as a colorimetric indicator.

5.2 MATERIALS AND METHODS

Acetylcholinesterase (AChE, type V-S from electric eel), tetracaine HCl, procaine HCl, acetylcholine iodide (AChI), dithio-bis-nitrobenzoic acid (DTNB), glutaraldehyde, eserine salicylate salt (eserine), galanthamine hydrobromide, scopolamine hydrobromide, Triton X-100, and acetylthiocholine (ATC) were obtained from Sigma (St. Louis, MO).

Amino-terminated Starburst® (PAMAM) dendrimer (generation 4) was obtained from Aldrich (Milwaukee, WI). Monosulfonate tetraphenyl porphine (TPPS₁) was obtained from Frontier Scientific (Logan, UT) and used without further purification. ProbeOn™ Plus microscope slides were obtained from Fisher Biotech (Pittsburgh, PA.). Diazinon samples were obtained by stirring 2 g/L Ortho diazinon granules (Chevron Chemical Company, San Ramon, CA) in water for six hours followed by filtering of insoluble particles. This solution was then considered to be 40 ppm based on the concentrations specified on the granule label.

The activity of AChE was measured spectrophotometrically in 3 mL of 100 mM pH 8 phosphate buffer maintained at 25°C according to the method of Ellman [447] with slight modifications: (1) reaction rates were measured using a Gilford single beam spectrophotometer and (2) AChE was dissolved in 100 mM pH 7 phosphate buffer instead of gelatin and water. To minimize contributions from the absorption of TPPS₁ ($\lambda_{\text{max}} = 405 \text{ nm}$), reaction rates were measured at 435 nm instead of 412 nm. The absorbance of the yellow anion of 5-thio-2-nitro-benzoic acid, the reaction product, at 435 nm is 76% of that at 412 nm. Although the absorbance of TPPS₁ at 435 nm is 50% that at 412 nm, TPPS₁ absorbance is constant during the assays (being displaced by the substrate); the 435 nm absorbance due to 120 nM TPPS₁ is 0.043 A while the absorbance change of the assay mix is 0.043A. Linear fitting for Figure 5.6 was performed using PSI-Plot (V 6.0a) at a 99% confidence interval. Percent inhibition vs. concentration plots were generated for each inhibitor by addition of x mL of inhibitor in 100 mM pH 8 NaPi to $3-x$ mL buffer. Measurements were repeated in triplicate.

Absorbance spectra in solution of TPPS₁ in the presence/absence of AChE, tetracaine, procaine, and AChI were recorded in 5 mM pH 8 sodium phosphate (Sorenson) buffer with a Cary 4E spectrophotometer at 0.02 nm resolution. Difference spectra were obtained by subtraction of absolute spectra using Grams/32 (Galactic Industries, Salem, NH). PeakFit version 4 (SPSS Science, Chicago, IL) was used for analysis of peak positions. Final reagent concentrations are given in the text and figure captions.

Acetylcholinesterase was immobilized on ProbeOn™ Plus microscope slides by the PAMAM protocol described in Chapter 4. Briefly, microscope slides were activated with glutaraldehyde followed by reaction with PAMAM generation 4 and TRIS blocking. At this point in the procedure two options were tested. For the first option, the slide is activated with glutaraldehyde and to interact with AChE followed by TRIS blocking. For the second option, the slide is activated with glutaraldehyde followed by interaction with a second layer of PAMAM and TRIS blocking. The slide is again activated with glutaraldehyde and to interact with AChE followed by TRIS blocking. After the final blocking in both options, 740 μM TPPS₁ was allowed to react with the enzyme surface and the non-bound excess removed by washing with 50 mM pH 7 sodium phosphate buffer. The technique involving the use of two Starburst layers provides a greater number of immobilized enzymes. This allows for a higher ratio of TPPS₁ bound in the active site versus TPPS₁ bound to the other compounds or sites on the slide surface. The improved ratio results in an increased absorbance for interaction peak between TPPS₁ and AChE.

Reaction of the immobilized enzyme with other chemicals including TPPS₁ is accomplished by placing 200 µl of the reagent in solution on the surface of the slide for the 3 minutes. The solution is then blotted off the surface using a Kimwipe®. In the case of TPPS₁ the reaction time allowed was 30 minutes. The interaction time for other reagents was varied from 6 seconds to 15 minutes. While no further changes were observed after the six second exposure, 3 minute exposure time was used to assure completion of the reaction.

Absorbance spectra of the slides were collected using a dual wavelength spectrophotometer (SDB - 3 Johnson Research Foundation, University of Pennsylvania, Philadelphia, PA) at 0.125 nm intervals (Figures 5.9 and 5.10). The output light of the spectrophotometer was focused onto the round end of a 1/8" optical fiber bundle that terminates in a linear array (circular to linear bundle; Dolan-Jenner). The microscope slide (n = 1.5151) is butted against the linear array such that the light enters the plane of the glass. On the opposite side of the slide (1" distance), the slide butts against another linear to circular bundle to gather the light transmitted through and evanescently along the slide surface [490-492]. The circular end of the bundle is then placed for maximal illumination of the R928 photomultiplier of the SDB-3 unit (Figure 5.1). Alternatively, absorbance spectra of IES before and after exposure to inhibitors were collected using an Ocean Optics USB-2000 spectrometer [392] with the output of a LED of maximum wavelength at 434 nm and 83 nm HBW as a light source.

An enzyme that is not catalytically active may or may not bind inhibitors in the same way as a catalytically active enzyme, therefore the enzymatic activity of the immobilized AChE surfaces was monitored as an indication of viability. For

determination of enzymatic activity of enzyme immobilized on slide surfaces, 240 μL of 50 mM pH 7 sodium phosphate buffer (NaPi) containing 0.83 mM DTNB and 0.83 mM ATC were placed on the immobilized AChE surface. After ten minutes, the solution was removed to a 1 mL cuvette containing 800 μL of 50 mM pH 7 NaPi buffer. The absorbance spectrum was collected with a Cary 4E spectrophotometer at 0.02 nm resolution. The absorbance of the samples at 412 nm was corrected for spontaneous acetylcholine hydrolysis. Just after immobilization an AChE surface typically gives an absorbance intensity at 412 nm of about 2.0 A. As the slide ages, some enzymatic activity is lost and as a result the absorbance intensity will be less than that of a fresh slide. An absorbance intensity of 0.25 A or less indicates less active enzyme present on the surface than is necessary for application to the techniques used here for detection of inhibitors of AChE.

Five different storage methods were investigated to achieve maximum responsive lifetime for the immobilized AChE surface: 1) ambient room conditions; 2) dry at 4°C; 3) 1 M TRIS buffer pH 9 at 4°C; 4) 1 M TRIS buffer pH 6 at 4°C; and 5) under vacuum at room temperature. Three storage conditions were also investigated for slides following exposure to TPPS₁: 1) ambient room conditions; 2) dry at 4°C; and 3) under vacuum at room temperature. Slides stored prior to exposure to TPPS₁ were tested for AChE activity using the adapted Ellman method described above. The lifetime of slides stored following exposure to TPPS₁ was determined based on the change in the absorbance spectrum upon exposure to 0.50 ppm tetracaine.

5.3 RESULTS

5.3.1 SPECTROPHOTOMETRIC CHANGES

The absorbance spectrum of monosulfonate tetraphenyl porphyrin (TPPS₁) is shown in Figure 5.2 (Trace 1). Upon addition of AChE, the spectrum shows a shift to longer wavelengths (Figure 5.2, Trace 2) which is more clearly observed in the TPPS₁ + AChE minus TPPS₁ difference spectrum (Figure 5.2, Trace 3). The difference spectrum, which shows the changes in the TPPS₁ absorbance due to enzyme binding, displays a new absorption peak at 442 nm resulting from the TPPS₁-AChE complex and a trough at 402 nm resulting from a decrease in the amount of unbound TPPS₁. This spectral shift is independent of pH (7 to 11) and independent of salt concentration (2 mM to 100 mM).

The intensity of the peak at 442 nm resulting from the TPPS₁-AChE interaction is dependent on AChE concentration as shown in Figure 5.2. The absorbance of the 442 nm peak increases with increasing AChE concentration. The Benesi-Hilderbrand plot of this data is linear with a slope of 0.97 $\mu\text{M}/\text{A}$ and a y-intercept of 21.5 A^{-1} . The extinction coefficient of TPPS₁ is 50 A/mM and the total porphyrin concentration used was 730 nM. Fitting of the data using 1:1 and 2:1 (P:E) stoichiometric ratios was attempted, but neither fit matched the data (refer to Chapter 2). The interaction between porphyrin and enzyme is likely not limited to independent binding.

The fluorescence spectra resulting from excitation of TPPS₁ alone (50 mM pH 7 NaPi) from 375 nm to 450 nm with emission measured from 600 nm to 750 nm are shown in Figure 5.3. The peak fluorescence intensity occurs at 652 nm attaining a maximum when excited at 406 nm. In addition, a fluorescence band is observed in the region between 690 and 740 nm with maximum intensity achieved also at 406 nm

excitation. The peak emission intensity of this region is at 712 nm. These peaks may be more prominent when viewed as a contour plot (Figure 5.3).

Acetylcholinesterase does not itself exhibit fluorescence when excited from 375 nm to 450 nm (data not shown). The half-band width for the TPPS₁ fluorescence peak at 652 nm is 20 nm, while for the TPPS₁-AChE complex it is 18 nm (Figure 5.3). The TPPS₁-enzyme complex shows a shift in maximum emission (712 nm to 716 nm) and excitation wavelengths (406 nm to 413 nm) in the fluorescence bands in the region from 690 nm to 740 nm.

Figure 5.4 shows the fluorescence intensity for TPPS₁ alone (Figure 5.4) and in the presence of AChE (Figure 5.4) at 652 nm emission for all excitation wavelengths with the results of peak fitting. While addition of AChE does not affect the emission wavelength of TPPS₁, a shift is observed in the maximum intensity excitation wavelength from 407 nm to 412 nm (Figure 5.4) as seen by the new shifted position of the major band in the peak fitting results. The band in the region between 690 nm and 740 nm displays shifts in both peak emission and excitation wavelengths. The peak emission intensity of these bands is shifted from 712 nm to 716 nm (Figure 5.3). The excitation wavelength at which maximum intensity occurs shifts from 406 nm to 413 nm as evidenced by the fitted curves in Figure 5.3. The band constituting more than 85% of the total curve has a peak intensity which is shifted from 406 nm to 413 nm upon addition of AChE.

5.3.2 INHIBITION OF ACHE ACTIVITY

The Lineweaver-Burk plot of AChE activity at different substrate concentrations in the absence and presence of 470 nM TPPS₁ is shown in Figure 5.6. The linear plots intersect on the Y-axis. The intersection of the lines on the Y-axis indicates that TPPS₁ is a competitive inhibitor of AChE (Chapter 2). The K_m values for ATC are 87 and 141 μM in the absence and presence of 470 nM TPPS₁ respectively. These findings are consistent with the findings of Lee and co-workers [388-389], who suggest that porphyrins inhibit enzymes in either a mixed or a competitive manner. That the value of V_{max} is not changed and the K_m value for ATC increases in the presence of inhibitor are classical indicators that TPPS₁ is a competitive inhibitor. If TPPS₁ were a mixed inhibitor, both K_m and V_{max} values would be effected. The K_i for TPPS₁ is 760 nM as determined by K_m versus [TPPS₁] (data not shown), however, this is not necessarily the concentration which yields 50% inhibition [267]. At very high substrate concentration, the active site is occupied more frequently by substrate resulting in a change in K_m but the V_{max} at infinitely high substrate concentrations is not changed. As we shall see, substrate not only competes for the active site but dislodges TPPS₁ from the active site. The 50% inhibition of AChE by TPPS₁ occurs at 650 nM TPPS₁ (data not shown).

5.3.3 EFFECT OF SUBSTRATE/INHIBITOR

The difference spectrum TPPS₁ + AChE + AChI minus TPPS₁, resulting from addition of AChI and AChE to TPPS₁, shows the combined effect of substrate and enzyme on TPPS₁ (Figure 5.7, Trace 1). The difference spectrum displays a peak at 447 nm and trough at 402 nm. The TPPS₁ + AChE + AChI minus TPPS₁ + AChE difference spectrum (Figure 5.7, Trace 2), which shows the change in the TPPS₁ bound to AChE

due to the addition of the substrate, displays a narrowed peak at 447 nm and a trough at 402 nm. The peak at 442 nm is characteristic of TPPS₁ bound to AChE. A peak at 447 nm is characteristic of TPPS₁ bound to AChI (Table 5.1). The lack of an absorbance peak at 442 nm after addition of substrate to the TPPS₁-AChE complex indicates total dissociation of the complex with formation of an AChI-TPPS₁ complex.

Figure 5.7 (Trace 3) reiterates this point. When we subtract Trace 2 of Figure 5.7 from Trace 1 of Figure 5.7, the resulting spectrum (Figure 5.7, Trace 3) shows the same spectral characteristics as TPPS₁ + AChE minus TPPS₁ (Figure 5.2, Trace 3). Since Figure 5.7 (Trace 1) is the effect of substrate and enzyme on TPPS₁ and Figure 5.7 (Trace 3) is the change in the TPPS₁ by the enzyme, the difference in the TPPS₁ is likely attributable to the dissociation of the TPPS₁-enzyme complex. Thus, the presence of the 447 nm peak and 442 nm trough (seen as a shoulder on the 402 nm trough) in the TPPS₁ + AChE + AChI minus TPPS₁ + AChE difference spectrum are due to the changes in the TPPS₁ spectrum resulting from formation of TPPS₁-AChI complex as well as dissociation of the TPPS₁-enzyme complex. The narrowed 447 nm peak in the TPPS₁ + AChE + AChI minus TPPS₁ + AChE difference spectrum is due to the loss of the 442 nm band. As AChI displaces TPPS₁ from the active site, the 442 nm band due to TPPS₁ binding AChE decreases in intensity. Consistent with TPPS₁ being a competitive inhibitor, TPPS₁ is displaced at the active site by substrate.

Tetracaine has been shown to be a competitive inhibitor of AChE [493-494] while procaine has not, suggesting that tetracaine binds to the active site while procaine binds elsewhere, likely at the peripheral site located adjacent to the active site [493]. In the presence of tetracaine, the TPPS₁ + AChE + tetracaine minus TPPS₁ difference spectrum

(Figure 5.8, Trace 1) displays a trough at 402 nm and peak at 445 nm. The loss of the porphyrin-enzyme complex, represented by an absorbance band at 442 nm, is consistent with tetracaine displacing the TPPS₁ from the enzyme active site.

By comparison, the loss of the 442 nm peak is not observed when procaine (even at 2.0 mM, 550 ppm) is used in place of tetracaine (Figure 5.8, Trace 2). The TPPS₁ + AChE + procaine minus TPPS₁ difference spectrum shows peaks at 442 nm and 429 nm and a trough at 402 nm. The interaction between TPPS₁ and AChE is still present (442 nm band) and we observe an interaction between TPPS₁ and the procaine represented by the absorbance peak at 429 nm (Table 5.1). The binding of an inhibitor at a site other than the active site, therefore, does not effect the TPPS₁-enzyme interaction strongly enough to change the 442 nm absorbance characteristic.

The absorbance spectrum of a typical AChE immobilized slide treated with TPPS₁ is shown in Figure 5.9 (Trace 1); addition of acetylcholine iodide results in the spectrum shown in Figure 5.9 (Trace 2). Figure 5.9 (Trace 3), the difference in the spectra of TPPS₁ bound to immobilized AChE in the presence and absence of substrate, shows an absorbance peak centered at 446 nm. The peak at 446 nm represents the TPPS₁ interaction with the immobilized enzyme. The peak at 446 nm is not observed when TPPS₁ is added to a slide which has been through the immobilization procedure skipping the step involving exposure to AChE (data not shown), while the 429 nm peak is observed. Further, the spectral changes observed upon exposing the AChE-TPPS₁ slide to AChI are only at 446 nm (Figure 2, Trace 3). Thus we see a decrease only in the 446 nm band when TPPS₁ is removed from the active site of AChE by AChI. The TPPS₁ bound to other components of the slide surface is not affected; therefore, the 429 nm band

is not affected. The absence of a new absorbance band or an increase in the 429 nm band also indicates that TPPS₁ removed from the active site is washed off the slide surface.

As described previously [391], the addition of tetracaine to the TPPS₁-AChE complex in solution results in the remove of the TPPS₁ from the active site which is observed as a spectral change where the characteristic peak of AChE-TPPS₁ interaction (442 nm in solution compared to 446 nm with immobilized AChE) decreases in intensity. Similar experiments were performed with immobilized enzyme slides (IES). Addition of tetracaine, a competitive inhibitor of AChE, as observed in solution, displaces TPPS₁ from the active site, resulting in a decrease in absorbance at 446 nm (the wavelength of the immobilized TPPS₁-AChE complex). As seen in Figure 5.10, a decrease in absorbance at 446 nm is seen in the presence of 3ppb (10 nM) tetracaine, in both the absolute (Trace 2) and the difference spectrum (Trace 3).

5.3.4 INHIBITOR RESPONSE.

The detection of competitive inhibitors of AChE is accomplished by subtraction of the pre-exposure absorbance spectrum of the IES from the post-exposure absorbance spectrum IES following exposure to the inhibitor (IES + inhibitor minus IES). The absorbance intensity of the porphyrin-enzyme interaction peak at 446 nm is reduced upon exposure of the IES to a competitive inhibitor of AChE. The IES was tested for detection of the competitive inhibitors of AChE eserine [495], galanthamine [496], tetracaine [494], scopolamine, diazinon [497], and Triton X-100 [498]. For each of the inhibitors tested, the loss of 446 nm absorbance intensity is linearly dependent on the log of the

inhibitor concentration with a rate change occurring when the absorbance change reaches 0.002 A. (Figure 5.11).

The enzymatic activity in solution in the presence/absence of varying concentrations of inhibitors was measured by the Ellman method and the percent inhibition of AChE versus the inhibitor concentration was plotted (Figure 5.12). Linear fitting of this data was used to determine the concentration required to achieve 50% inhibition (IC_{50}) of the enzyme (Table 5.2).

The change in absorbance at 446 nm of the IES upon exposure to 50 ppb of each inhibitor is linearly dependent on the IC_{50} of the inhibitor in question as shown in Figure 5.13. The lower the concentration required to achieve 50% inhibition of AChE the greater the change in absorbance of the IES upon exposure to the inhibitor. This stands to reason as the percent inhibition will be less at fixed inhibitor concentration for higher IC_{50} , so the competitive inhibition test accurately reflects the binding affinity of the inhibitors and the displacement of $TPPS_1$.

5.3.5 LIFETIME EXPERIMENTS

Figure 5.12 shows the absorbance at 412 nm after reaction with ATC and DTNB for a group of slides stored under vacuum prior to $TPPS_1$ exposure. After 73 days the slides display 80% of the original enzymatic activity. Enzyme surfaces yielding greater than 0.25 A change at 412 nm for the Ellman assay respond as expected to tetracaine challenge (Table 5.3). Immobilized AChE surfaces yielding an absorbance change at 412 nm of less than 0.25 A for the Ellman assay responded to tetracaine challenge with a reduced absorbance change as compared to those shown in Table 5.3.

Slides stored at room temperature with no special consideration show no change in Ellman absorbance (Figure 5.12) or tetracaine response over a period of 49 days. After 81 days of storage in pH 9 TRIS at 4°C, slides show 65% of original Ellman activity and response to tetracaine challenge is unchanged. Slides stored at 4°C (atmospheric pressure, uncontrolled humidity) prior to TPPS₁ exposure maintained 75% of enzymatic activity after 25 days and bound 50% less TPPS₁ than slides stored under vacuum. These slides did not respond to tetracaine challenge after 12 days of storage. Slides stored at 4°C in pH 6 TRIS retained less than 40% of original Ellman activity after 16 days.

Slides bound with TPPS₁ stored at 4°C both with and without pH 9 TRIS as well as slides stored under ambient conditions showed rapid decline in response to tetracaine challenge beginning after six days, and no response was observed after 10 days. However, when stored under vacuum, the slides show consistent response to tetracaine challenge for more than 47 days (Figure 5.14).

5.4 DISCUSSION

TPPS₁ is found to be an effective reversible competitive inhibitor of AChE. Specific spectral changes at 402 nm and 442 nm occur in the TPPS₁ absorbance spectrum when the porphyrin binds to AChE in solution. The spectrum of the TPPS₁-AChE complex in the 442 nm region is altered by addition of compounds which bind at the active site of AChE, such as AChI and tetracaine, but not those which bind elsewhere (eg, procaine).

The immobilized sensor surface just described relies on the specificity of interaction of a competitive inhibitor of AChE, i.e. one that, like the nerve gasses and other inhibitors including pharmaceuticals, binds the active site. The covalently-immobilized AChE surface contains a porphyrin which we have shown [391] binds at the active site as a competitive inhibitor. The porphyrin exhibits a specific absorbance band at 446 nm when bound to the immobilized enzyme. As we have shown, a displacement of the porphyrin from the active site by another competitive inhibitor (e.g. tetracaine) results in a decrease in absorbance at 446 nm. This decrease in 446 nm absorbance is not observed when the non-competitive AChE inhibitor procaine is present. We expect that the 446 nm absorbance decrease will be observed in the presence of CW agents such as VX, Sarin, Soman, and Tabun or organophosphates that also bind specifically at the active site [459]. In this aspect, the surface will respond only to those inhibitors that bind the active site of AChE. As such, it is a broad spectrum sensor. Since the AChE surface contains a bound porphyrin (or other colorimetric compounds whose absorbance, fluorescence, or other spectrophotometric properties change upon association/dissociation with the inhibitor binding site) reagent-containing solutions need not be used, simplifying the size and complexity of actual operation. Only sample need be applied.

Detection of absorbance spectra through the use of an evanescent wave has been used for applications ranging from detection of pH changes using indicators to vitamin C concentration in orange juice samples [490-492, 499-503]. While the optical detection spectrophotometer utilized in this study was a bench-mounted unit, the absorbance changes have been recorded using a CCD/diode array-based-spectrometer (Ocean Optics). That the absorbance changes are observed at specific wavelengths also allows

for the use of small solid-state photodiodes fitted with bandpass filters at the appropriate wavelengths as the photodetector.

Exposure of the immobilized AChE-TPPS₁ complex to competitive inhibitors of AChE causes dissociation of TPPS₁ from AChE and consequently a loss in absorbance intensity at 446 nm with linear dependence on the log of the inhibitor concentration. A change in the slope of the absorbance change versus inhibitor concentration occurs at 0.002 A for each inhibitor and, therefore, is likely the result of the immobilized IES and not the inhibitor in question. The limits of detection commonly sought for nerve agents are approximately 5-15 micrograms per liter (5-15 ppb) [504]. Detection limits at 3:1 S/N for the competitive inhibitors of AChE are 37 ppt for eserine, 50 ppt for galanthamine, 100 ppt for scopolamine, 45 ppt for diazinon, 250 ppt for tetracaine, 83 ppb for Triton X-100. The response of the IES to 50 ppb inhibitor exposure is linearly dependent on the effectiveness (IC₅₀) of the inhibitors. Based on this response the IES should give detection limits of 250 ppt or less for untested competitive inhibitors of AChE with an IC₅₀ less than 100 μM making most pesticides and nerve agents easily within the detection limits at ppb levels. Other inhibitors with IC₅₀ greater than 100 μM this would be detected as well but only at higher concentrations.

In order to extend the lifetime of the immobilized enzyme surface for up to 73 days, a vacuum system can be used requiring approximately 20 minutes for exposure to TPPS₁ before putting into service, after which it is viable for 6 days under ambient conditions. It is possible that the extension of the enzymatic lifetime results from the removal of excess water from the surfaces. This would further stabilize the

immobilization matrix preventing partial unfolding of the enzyme as well as inhibiting any reactions that may otherwise degrade the enzyme.

We have shown that storage in vacuum preserves the lifetime of the immobilized enzyme-porphyrin surfaces for up to 49 days allowing for application without any preparation before use. Porphyrins are well known catalysts. Putting the enzyme-porphyrin complex under vacuum may inhibit the processes catalyzed by the porphyrin, thereby protecting the enzyme. This immobilized enzyme-porphyrin surface is effective as a detector for a variety of competitive inhibitors of acetylcholinesterase. The IES are stable and require only the application of a sample to measure its presence in less than six seconds.

Porphyrins have been used in sensor applications due to their sensitivity to chemicals in their environments. Shifts in absorbance [284] and fluorescence spectra [264] tend to be unique for different chemicals including different proteins [485]. Spectral shifts could be used as a “marker” for the presence of different proteins. It may be possible to use porphyrins as a sensor for detection of proteinaceous bacterial exotoxins such as botulinum toxin and those found in *Clostridium botulinum*, *Clostridium tetani*, *Clostridium perfringens*, *Escherichia coli*, cholera, and plague (*Yersinia pestis*). Though this possibility has not been addressed in this document, the use of porphyrin-enzyme combinations for other detection protocols will be.

CHARACTERISTIC PEAK/TROUGH LOCATIONS

Difference Spectrum	Peak	Trough
TPPS ₁ + AChE <u>minus</u> TPPS ₁	442 nm	402 nm
TPPS ₁ + AChE + AChI <u>minus</u> TPPS ₁ + AChE	447 nm	402 nm
TPPS ₁ + AChE + AChI <u>minus</u> TPPS ₁	447nm	402 nm
TPPS ₁ + AChI <u>minus</u> TPPS ₁	447 nm	402 nm
TPPS ₁ + AChE + tetracaine <u>minus</u> TPPS ₁	445 nm	402 nm
TPPS ₁ + tetracaine <u>minus</u> TPPS ₁	445 nm	402nm
TPPS ₁ + AChE + procaine <u>minus</u> TPPS ₁	442 nm and 429	402 nm
TPPS ₁ + procaine <u>minus</u> TPPS ₁	429 nm	402 nm

TABLE 5.1 The peak and trough locations in the difference spectra of TPPS₁ upon interaction with AChE, its substrate, and its inhibitors.

IC₅₀ AND SURFACE INTERACTION

Inhibitor	IC ₅₀ (μ M)	IC ₅₀ (ppb)	Δ Absorbance (A) at 446 nm 50 ppb exposure	Limit of Detection (ppb)
TPPS ₁	5	4600	-----	-----
Eserine salicylate	2.3	1000	0.0029	0.037
Diazinon	4.7	1440	0.0028	0.045
Galanthamine	6	2208	0.0028	0.050
Scopolamine	63	27600	0.0021	0.100
Tetracaine	100	30000	0.0017	0.250
Triton X-100	172	111500	0.0006	83

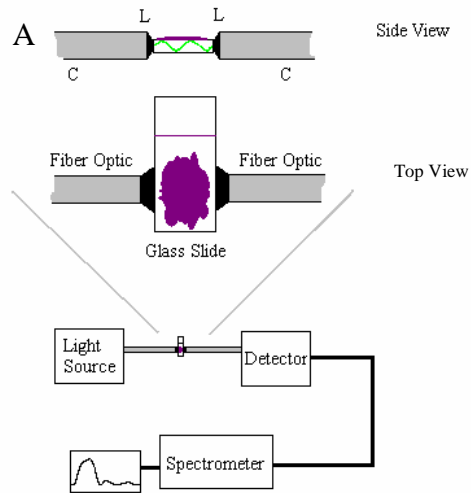
TABLE 5.2 Relationship between absorbance change at 446 nm of the IES to the association constant for each inhibitor.

LIFETIME EXPERIMENTS

Slide Age (days)	Change in absorbance upon tetracaine challenge (0.5 ppm)	Absorbance at 412 nm of DTNB (A)
3	0.0021	1.7706
16	0.0025	1.4610
27	0.0023	1.6520
51	0.0029	1.6096
62	0.0021	0.8873
71	0.0027	0.6200

TABLE 5.3 Comparison of Ellman activity and response to tetracaine challenge for slides stored under vacuum.

EVANESCENT WAVE MEASUREMENT TECHNIQUE



B



FIGURE 5.1 (A) The experimental setup for slide measurements. C = circular, L = linear optical fiber bundle [391]. (B) Photo of experimental setup using Ocean Optics USB2000 spectrophotometer.

INTERACTION OF TPPS₁ WITH AChE

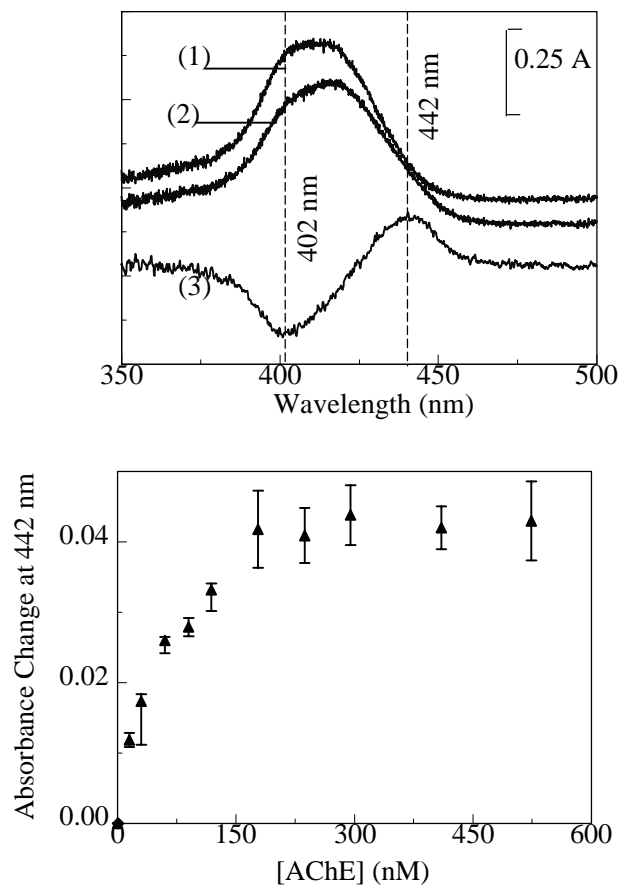


FIGURE 5.2 Absorbance spectra of TPPS₁ in the absence/presence of AChE at pH 8.

(A) The subtraction of the absolute spectrum of 730 nM TPPS₁ (Trace 1) from the absolute spectrum of 730 nM TPPS₁ + 30 nM AChE (Trace 2) yields the difference spectrum TPPS₁ + AChE minus TPPS₁ (Trace 3). (B) The dependence of the intensity of the peak at 442 nm on AChE concentration in the difference spectrum TPPS₁ (730 nM) + AChE minus TPPS₁ [391].

TPPS₁ FLUORESCENCE SPECTRA

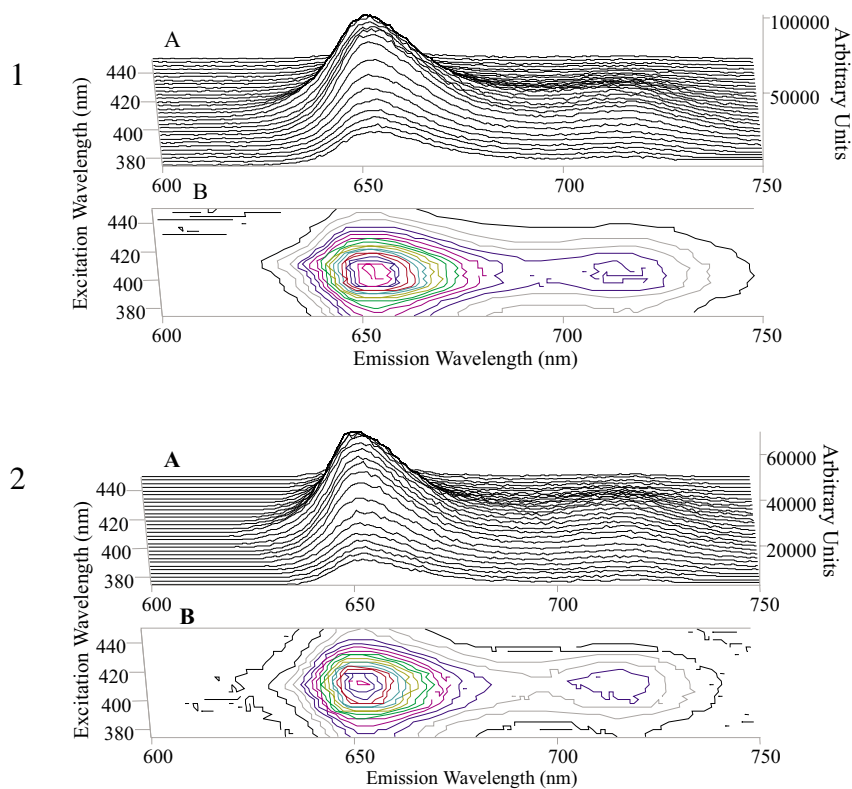


FIGURE 5.3 1. Fluorescence spectrum of TPPS₁ [391]. (A) The fluorescence spectrum of 125 nM TPPS₁ in 5 mM pH 7 sodium phosphate buffer. (B) The contour plot of the fluorescence spectrum shown in Figure 1A.

2. Fluorescence spectra of TPPS₁ + AChE [391]. (A) The fluorescence spectrum of 125 nM TPPS₁ + 30 nM AChE in 5 mM pH 7 sodium phosphate buffer. (B) The contour plot of the fluorescence spectrum shown in Figure 2A.

CHANGES IN THE TPPS₁ EXCITATION SPECTRUM

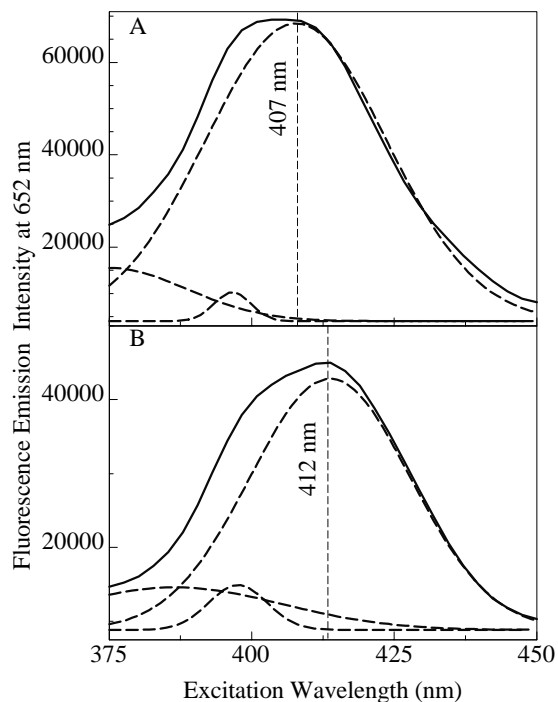


FIGURE 5.4 (A) Plot of the emission intensity at 652 nm for TPPS₁ in the absence of AChE as a function of excitation wavelength shown with results of PeakFit (dashed line) [391]. The peak centered at 407 nm constitutes 85% of the total area under the curve, while the peak 396 nm constitutes less than 1% of the total area. The peak at 376 nm constitutes approx. 14% of the total area. (B) Plot of the emission intensity at 652 nm for TPPS₁ in the presence of AChE as a function of excitation wavelength shown with results of PeakFit (dashed lines) [391]. The peak centered at 412 nm constitutes 82% of the total area under the curve, while the peak 396 nm constitutes less than 1% of the total area. The peak at 376 nm constitutes approx. 17% of the total area.

CHANGES IN THE TPPS₁ EMISSION SPECTRUM

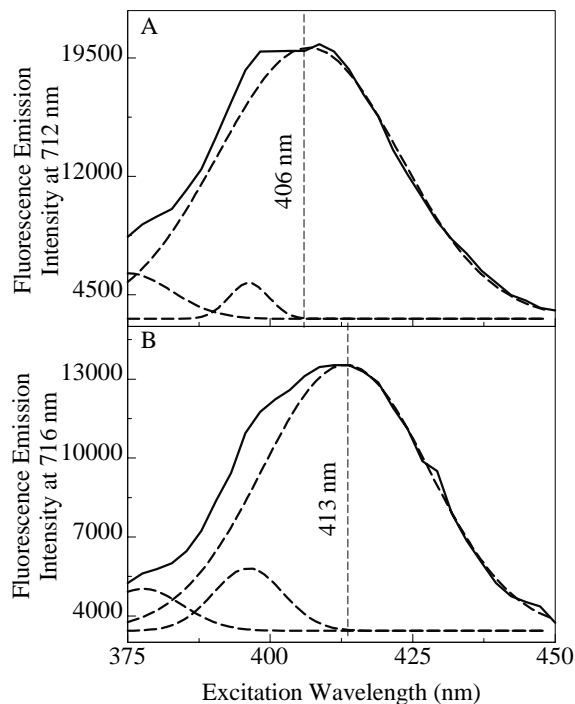


FIGURE 5.5 (A) Plot of the emission intensity at 712 nm for TPPS₁ in the absence of AChE as a function of excitation wavelength [391]. Dashed lines represent the results of peak fitting. The peak centered at 406 nm constitutes 90% of the total area under the curve, while the peak 396 nm constitutes less than 2% of the total area. The peak at 376 nm represents approx. 8% of the total area. (B) Plot of the emission intensity at 716 nm for TPPS₁ in the presence of AChE as a function of excitation wavelength [391]. Dashed lines represent the results of peak fitting. The peak centered at 413 nm constitutes 85% of the total area under the curve, while the peak 396 nm constitutes less than 6% of the total area. The peak at 376 nm represents 9% of the total area.

INHIBITION OF ACHE BY TPPS₁

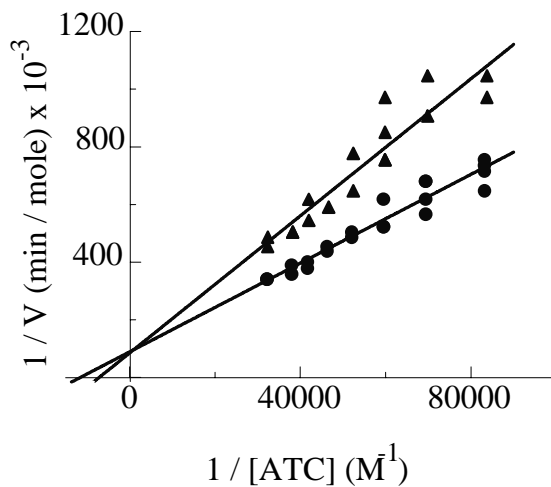


FIGURE 5.6 The Lineweaver-Burk plot of AChE activity at different ATC

concentrations [391]. In the absence of inhibitor (●) $K_m = 87 \mu\text{M}$. In the presence of 470 nM TPPS₁ (▲) $K_m = 141 \mu\text{M}$. Intersection of the curves occurs at the Y-axis ($V_{\max} = 12 \mu\text{mol/min}$). The lines show linear best fits performed with 99% confidence interval (PSI-Plot).

REVERSAL OF TPPS₁-ACHE COMPLEX FORMATION

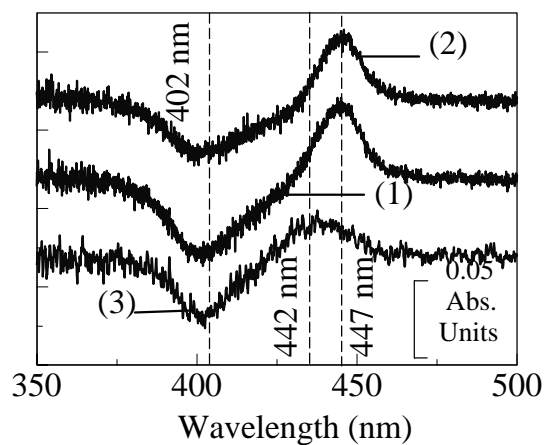


FIGURE 5.7 Spectral changes in the TPPS₁-AChE complex upon addition of AChI

[391]. Trace 1: the difference spectrum of TPPS₁ + AChE + AChI minus TPPS₁; Trace 2: the difference spectrum of TPPS₁ (730 nM) + AChE (30 nM) + AChI (18 μM) minus TPPS₁ + AChE, Trace 3: the double difference spectrum of (TPPS₁ + AChE + AChI minus TPPS₁) minus (TPPS₁ + AChE + AChI minus TPPS₁ + AChE) yields TPPS₁ + AChE minus TPPS₁

ADDITION OF INHIBITORS TO THE ACHE-TPPS₁ COMPLEX

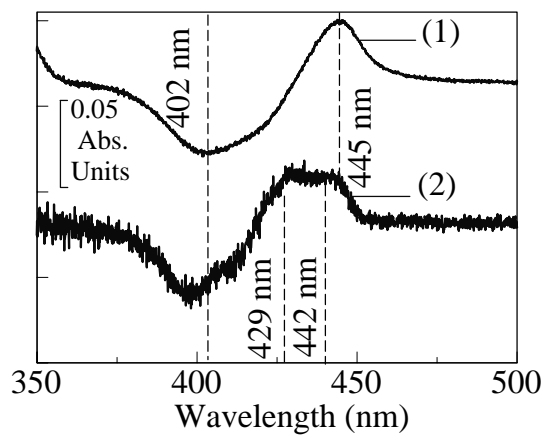


FIGURE 5.8 Trace 1: The interaction of the TPPS₁-AChE complex with tetracaine [391]. The difference spectrum of TPPS₁ (730 nM) + AChE (30 nM) + tetracaine (0.5 mM) minus TPPS₁. Trace 2: The difference spectrum of TPPS₁ (730 nM) + AChE (30 nM) + procaine (2.0 mM) minus TPPS₁ + procaine.

INTERACTION OF ACHI WITH IES

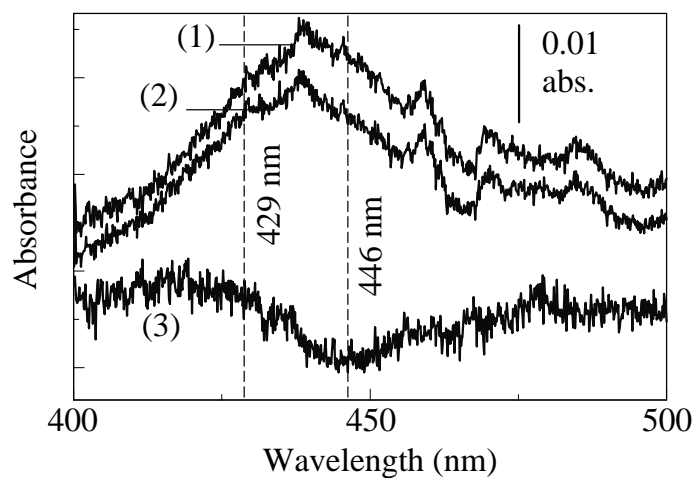


FIGURE 5.9 The absorbance spectra of the immobilized TPPS₁-AChE complex before (Trace 1) and after exposure to AChI (Trace 2). The difference spectrum TPPS₁ + AChE + AChI minus TPPS₁ + AChE is shown in Trace 3 [392].

INTERACTION OF TETRACAINE WITH IES

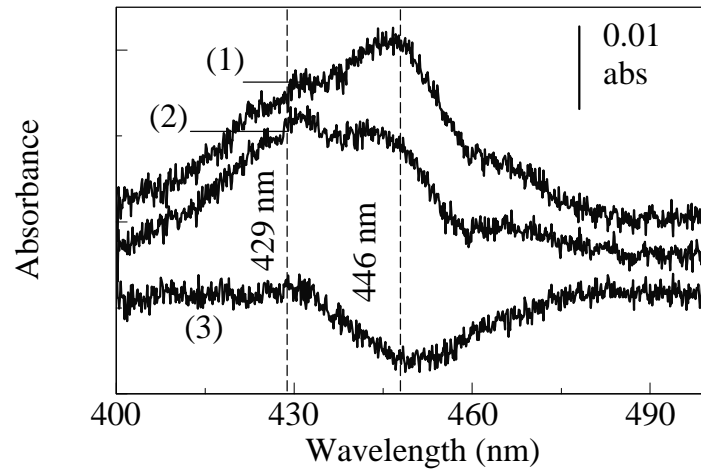


FIGURE 5.10 The absorbance spectra of the immobilized TPPS₁-AChE complex (Trace 1) and the effect of 3 ppb tetracaine exposure (Trace 2). The difference spectrum TPPS₁ + AChE + tetracaine minus TPPS₁ + AChE is shown in Trace 3 [392].

CONCENTRATION DEPENDENCE OF ABSORBANCE CHANGES

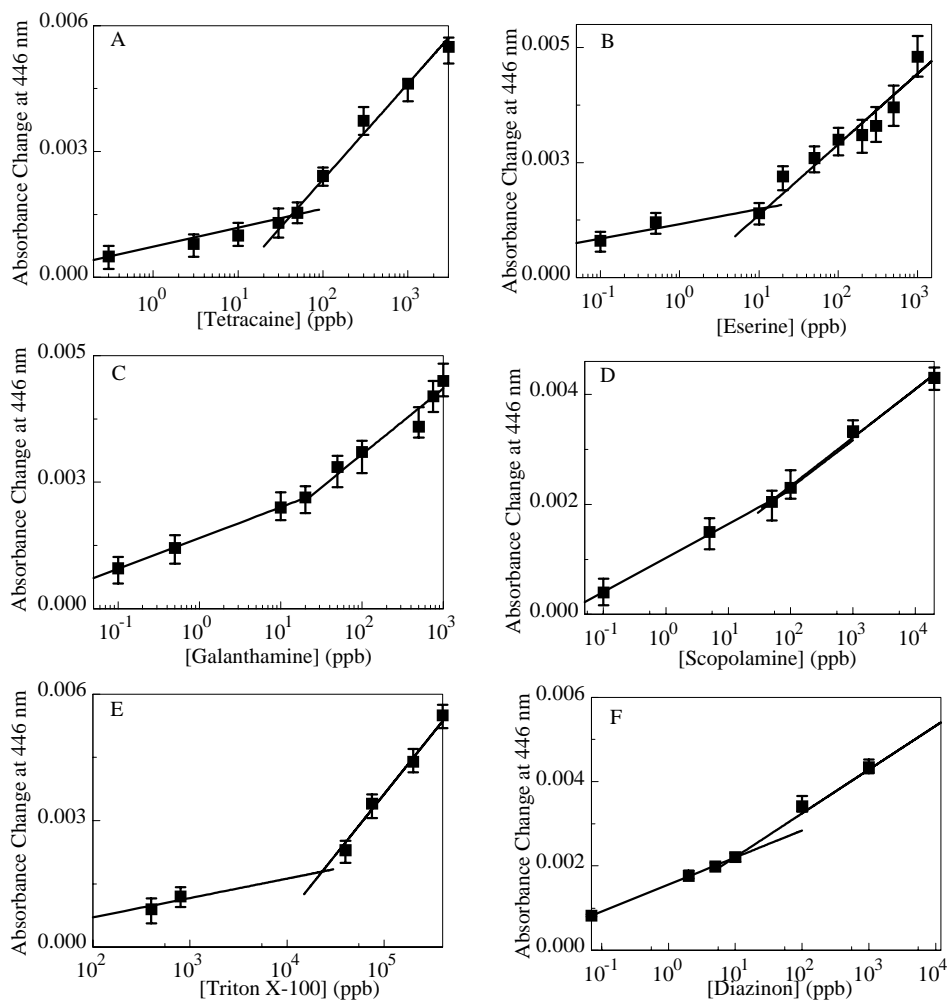


FIGURE 5.11 Loss in 446 nm absorbance intensity of immobilized TPPS₁-enzyme slide surface upon inhibitor exposure to: (A) tetracaine, (B) eserine, (C) galanthamine, (D) scopolamine, (E) Triton X-100, (F) diazinon [394].

PERCENT INHIBITION CURVES

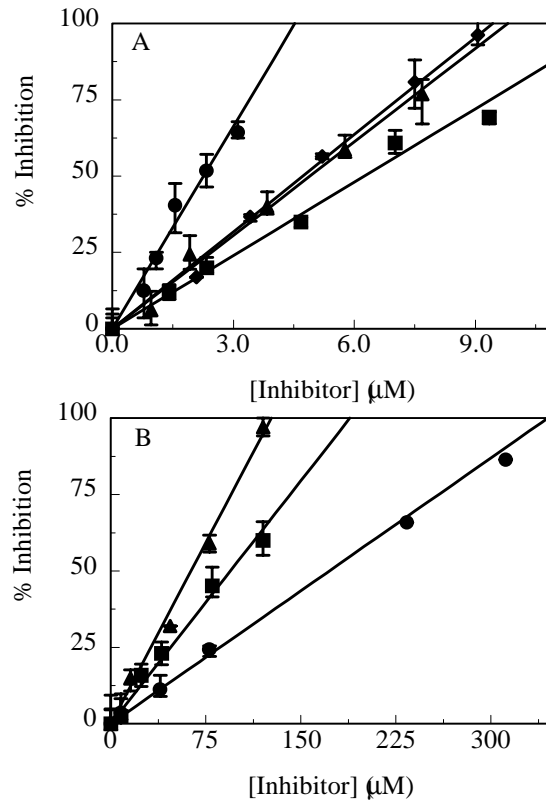


FIGURE 5.12 A. Percent inhibition of AChE activity versus inhibitor concentration for TPPS₁ (▲), eserine (●), diazinon (◆), and galanthamine (■).
B. Percent inhibition of AChE activity versus inhibitor concentration for Triton X-100 (●), scopolamine (▲), and tetracaine (■) [394].

RELATIONSHIP OF ABSORBANCE CHANGE TO IC_{50}

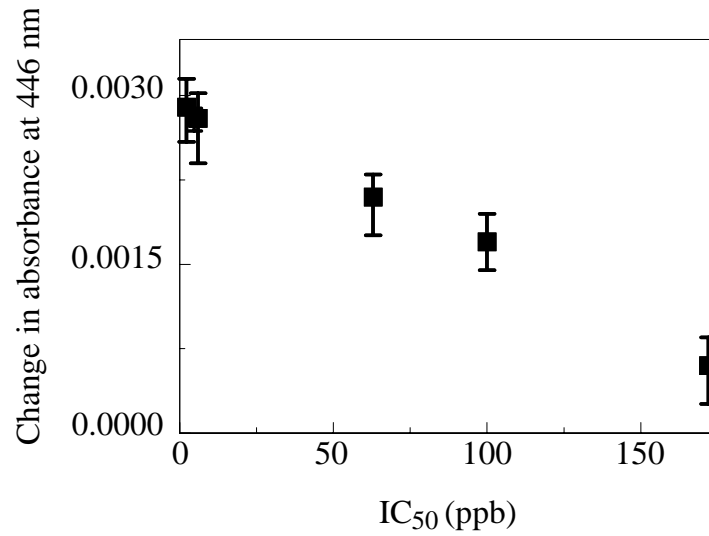


FIGURE 5.13 The response of the surface depends on the effectiveness of the inhibitor as shown by plotting the change in absorbance intensity upon exposure to 50 ppb inhibitor versus the IC_{50} (ppb) of the respective inhibitor [394].

SURFACE LIFETIMES

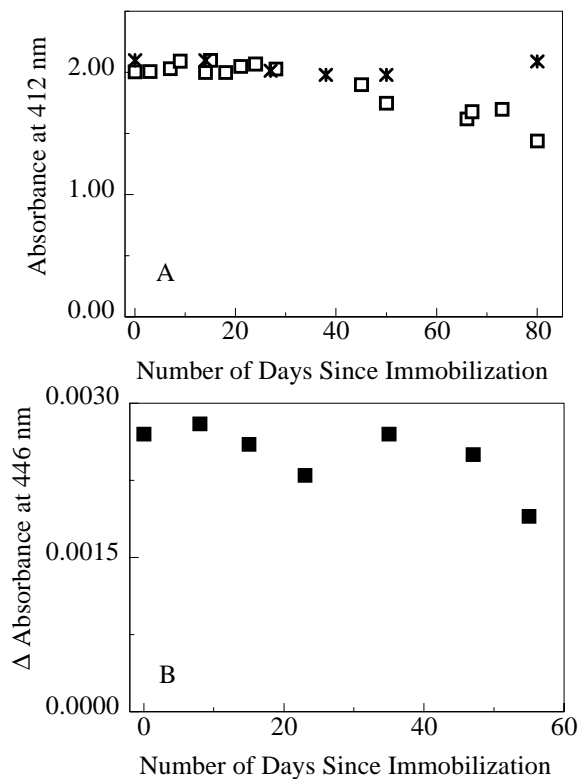


FIGURE 5.14 (A) Enzymatic activity of slide surfaces demonstrated as the OD of the Ellman reagent at 412 nm for slides stored under vacuum at room temperature (□) and under ambient conditions (*). (B) TPPS₁-AChE surface response to 0.5 ppm (1.7 μ M) tetracaine challenge after storage under vacuum shown as loss in absorbance intensity at 446 nm [394].

CHAPTER 6

EXTENTION OF THE CHOLINESTERASE SYSTEM

6.1 INTRODUCTION

Butyrylcholinesterase (BChE), also known as serum cholinesterase, hydrolyzes butyrylcholine (BCh) at rates similar to those for the hydrolysis of acetylcholine (ACh) by acetylcholinesterase (AChE). While AChE is known to terminate impulse transmission at cholinergic synapses, the biological role of BChE is poorly understood. There has been extensive comparison of the structure of horse serum BChE to that of *Torpedo* AChE (from electric eel). The enzymes show 73% similarity and 53% sequence identity. Both enzymes will hydrolyze ACh and BCh but at different rates and variations of the enzymes show differing affinities and degrees of inhibition by different OPs and other compounds [389, 459, 505-515].

Organophosphorous pesticides and nerve agents inhibit cholinesterases covalently bind to the active sites of cholinesterases resulting in irreversible inhibition of the enzymatic activity [459]. Other compounds including several drugs also inhibit the activity of cholinesterases by binding at the active sites, though this inhibition is typically reversible. The similarity of the interaction allows for use of these drugs as simulants for more the more dangerous pesticides and nerve agents.

Current methods of detection of these compounds use a comparison of the catalytic activity of immobilized enzymes before and after exposure to the inhibitor by monitoring the rate of production of one or more products of the enzyme-catalyzed reaction [466, 469-470, 516-519]. Changes in pH [517] or the oxidation current of

thiocholine [343, 516, 518], a hydrolysis product of acetylthiocholine and butyrylthiocholine, can be used to directly monitor the enzymatic activity of cholinesterases. Coupling of the cholinesterase reaction with the activity of choline oxidase allows the activity of AChE or BChE to be measured through the production of H_2O_2 [465, 482]. Additionally, the cholinesterase activity can be monitored spectrophotometrically through the use of dithio-bis-nitrobenzoic acid (DTNB) which reacts with thiocholine giving an absorbance increase at 412 nm [427, 443]. This process typically requires mixing of reagents and measurement of each reaction rate requires time precluding a fast real-time detection method.

In the previous chapter, we have shown that competitive inhibitors of acetylcholinesterase (AChE) can be detected spectrophotometrically by monitoring the changes in the absorbance spectrum of an immobilized enzyme-porphyrin complex [391-392]. Specifically, exposure to a competitive inhibitor results in dissociation of monosulfonate tetraphenyl porphyrin (TPPS₁), a reversible competitive inhibitor of AChE [392], from the enzyme causing a loss in absorbance of the characteristic peak for the AChE-TPPS₁ complex at 446 nm. Measurements of this type require only application of sample and can be completed in less than 6 seconds. Here we will show that, using the same techniques, reversible competitive inhibition of butyrylcholinesterase by TPPS₁ can be used to detect compounds that competitively inhibit BChE. We will additionally show that the use of two or more enzymes can be used not only to reduce false positives/negatives but also to help in identification of a particular inhibitor.

6.2 MATERIALS AND METHODS

Acetylcholinesterase (AChE, type V-S from electric eel, E.C. 3.1.1.7), butyrylcholinesterase (BChE, pseudocholinesterase from horse serum, E.C. 3.1.1.8), tetracaine HCl, eserine salicylate salt (eserine), galanthamine hydrobromide, scopolamine hydrobromide, amitriptyline, drofenine, Triton X-100, dithio-bis-nitrobenzoic acid (DTNB), acetylthiocholine (ATC) and butyrylthiocholine (BTC) were obtained from Sigma (St. Louis, MO). Monosulfonate tetraphenyl porphyrin (TPPS₁) was obtained from Frontier Scientific (Logan, UT) and used without further purification.

Butyrylcholinesterase and acetylcholinesterase were immobilized onto ProbeOn™ Plus microscope slides (Fisher Biotech, Pittsburgh, PA) by the PAMAM process described previously (Chapter 4). Combination BChE+AChE surfaces were generated by replacing the enzyme solution in the AChE immobilization procedure with a solution containing 39 units/mL of each enzyme. Absorbance spectra of the immobilized enzyme surfaces (IES) before and after exposure to inhibitors were collected using an Ocean Optics USB-2000 spectrometer [392] with the output of a LED of maximum wavelength at 434 nm and 83 nm HBW as a light source. The Ocean Optics spectra were collected as the average of 100 spectra collected with an integration time of 50 msec per spectrum. Data presented on concentration dependence represents the average of three sets of measurements. Spectral analysis was performed using Grams/32 (Galactic Industries, Salem, NH). Spectra of immobilized enzyme surfaces shown here (e.g., Figure 6.7) have been corrected for the absorbance of TPPS₁ bound non-specifically to slide surfaces that have completed the immobilization procedure in the absence of enzyme.

The activity of BChE using BTC as substrate was measured spectrophotometrically in 3 mL of 100 mM pH 8 phosphate buffer maintained at 25°C according to the method of Ellman [443] with BChE dissolved in 100 mM pH 7 phosphate buffer instead of gelatin and water. Linear fitting of the time-dependent absorbance increases was performed using PSI-Plot (V 7.0b) at a 99% confidence interval. IC₅₀ values for each inhibitor were taken from percent inhibition vs. concentration plots generated by addition of x mL of inhibitor in 100 mM pH 8 NaPi to $3-x$ mL buffer. Measurements were repeated in triplicate.

6.3 THE BCHE SYSTEM

The Lineweaver-Burk plots of BChE activity at different substrate concentrations in the absence and presence of 7.3 μ M TPPS₁ are shown in Figure 6.1. The intersection of the linear plots on the Y-axis indicates that TPPS₁ is a competitive inhibitor of BChE. The K_m values for BTC are 201 μ M and 1180 μ M in the absence and presence of TPPS₁ respectively. Competitive inhibition of enzymes by porphyrins has been demonstrated previously [388-389, 391].

The binding of TPPS₁ to BChE in solution results in decreased TPPS₁ absorbance at 398 nm and increased absorbance at 429 nm (Figure 6.2, Trace 1). Addition of a competitive inhibitor of BChE [520] to the BChE-TPPS₁ complex in solution results in a decrease in absorbance intensity at 429 nm and an increase at 398 nm. The difference spectrum TPPS₁ + BChE + drofenine minus TPPS₁ (Figure 6.2, Trace 2) shows the effect of drofenine, a competitive inhibitor of BChE, on the absorbance spectrum of the BChE-TPPS₁ complex. The peak/trough combination at 429 nm/398 nm observed in the TPPS₁

+ BChE minus TPPS₁ difference spectrum is no longer present. As with AChE [391], this demonstrates reversibility of the competitive inhibition of BChE by TPPS₁. The new peak-tough combination at 433 nm and 403 nm are the characteristic wavelengths for interaction of drofenine with TPPS₁ as indicated by the difference spectrum TPPS₁ + drofenine minus TPPS₁ (data not shown).

Figure 6.3 shows the absorbance spectrum for an immobilized BChE surface (IES) before and after exposure to 1 ppm (2.8 μM) drofenine (Traces 1 and 2, respectively). In order to determine the location of the immobilized TPPS₁-BChE interaction peak, a surface was made by the described immobilization procedure with the exception of the enzyme exposure step. The absorbance spectrum of the enzyme-lacking surface was then subtracted from the absorbance spectrum of the IES. The absorbance peak at 421 nm in the difference spectrum was then determined to be the result of the immobilized BChE-TPPS₁ interaction.

Upon exposure to competitive inhibitors of BChE, the IES absorbance spectrum shows a decrease in intensity at 421 nm, the characteristic peak for the TPPS₁-BChE surface, indicating dissociation of TPPS₁ from BChE (Figure 6.3, Traces 1 and 2). No change in the absorbance spectrum of the IES was observed upon exposure to non-competitive inhibitors. For the immobilized BChE-TPPS₁ no absorbance increase is observed upon exposure to inhibitor due to the removal of the newly dissociated TPPS₁ with the excess inhibitor solution by blotting (Figure 6.3, Trace 3).

The BChE surface has been tested against the competitive inhibitors of BChE eserine [495], amitriptyline [521], drofenine [520], and Triton X-100 [498]. For each competitive inhibitor of BChE tested, the IES showed a decrease in absorbance at 421 nm

with a linear dependence on the log of the inhibitor concentration (Figure 6.4).

Extrapolation of the data to 3:1 S/N indicates a theoretical detection limit of 40 ppb (62 nM) for Triton X-100, 91 ppt (260 pM) for drofenine, 72 ppt (230 pM) for amitriptyline, and 50 ppt (121 pM) for eserine.

The IC_{50} for each inhibitor of BChE was determined by the data shown in Figure 6.5. Table 6.1 shows the relationship between the IC_{50} for BChE of each inhibitor and the limits of detection. The data show that the greater the affinity of the inhibitor for the enzyme the lower the detection limit achieved. This is as expected. For the same inhibitor concentration, an inhibitor with a lower IC_{50} will displace a greater amount of TPPS₁ from the enzyme; thus a greater change in absorbance is observed leading to lower detection limits.

6.4 THE TWO ENZYME SYSTEM

The binding of TPPS₁ to BChE in solution results in decreased TPPS₁ absorbance at 398 nm and increased absorbance at 429 nm (Figure 6.6, Trace 1). The TPPS₁-AChE complex yields different interaction wavelength positions with the peak at 442 nm and trough at 402 nm in the TPPS₁ + enzyme minus TPPS₁ difference spectrum (Figure 6.6, Trace 2). The addition of a competitive inhibitor for either enzyme to the porphyrin-enzyme complex results in displacement of the porphyrin from the enzyme active site. This dissociation is observed as a loss in absorbance intensity at the wavelength of the characteristic peak of the porphyrin-enzyme complex as observed previously for AChE (Chapter 5).

Figure 6.7 (A, Trace 1) shows the absorbance spectrum of the immobilized BChE-TPPS₁ complex collected via the evanescent method. As in the case of solution, the immobilized BChE-TPPS₁ surfaces have peak positions different than those of the immobilized AChE-TPPS₁ surfaces (Figure 6.7 (A), Trace 2). Exposure of the BChE surface to competitive inhibitors of BChE results in decreased absorbance intensity at 421 nm while exposure of the AChE surface to competitive inhibitors of AChE results in decreased absorbance intensity at 446 nm [392]. The absorbance spectra of AChE-BChE immobilized combination cholinesterase surfaces show the characteristic peaks of both the AChE and BChE immobilized porphyrin complexes (Figure 6.7 (A), Trace 3).

The response of the mixed IES to competitive inhibitors of AChE alone, BChE alone, and both AChE and BChE was tested. The mixed IES responds to amitriptyline, a competitive inhibitor of BChE, with a loss in absorbance intensity at 421 nm only and responds to tetracaine, a competitive inhibitor of AChE, with a loss in absorbance intensity at 446 nm only (Figure 6.7 (B), Traces 1 and 2). Exposure of the mixed IES to eserine, a competitive inhibitor of AChE and BChE, showed a loss in absorbance intensity at both 421 nm and 446 nm (Figure 6.7 (B), Trace 3).

Eserine and Triton X-100 are competitive inhibitors of AChE and BChE [280, 291-292]. Figure 6.8 shows the linear dependence of the mixed IES response at each wavelength (421 nm and 446 nm) on the log of inhibitor concentration for eserine and Triton X-100. Table 6.2 shows the LOD of the mixed IES for tetracaine [494], scopolamine [522], and galanthamine [496], competitive inhibitors of AChE and for amitriptyline [521] and drofenine [520], competitive inhibitors of BChE as well as for eserine [495] and Triton X-100 [498], competitive inhibitors of both AChE and BChE.

Limits of detection were calculated base on linear fittings similar to those shown in Figure 6.8 with the LOD fixed at a 3:1 signal to noise ratio.

6.5 DISCUSSION

TPPS₁ is a reversible, competitive inhibitor of butyrylcholinesterase. Formation of the TPPS₁-BChE complex yields a characteristic peak at 429 nm in solution and 421 nm when immobilized. The absorbance intensity of the characteristic peak both for the immobilized porphyrin-enzyme complex and the complex in solution is reduced upon addition of a competitive inhibitor of BChE. The loss in absorbance intensity for the IES is linearly dependent on the log of the inhibitor concentration with detection limits dependent on the IC₅₀ for each inhibitor as shown in Table 6.1.

The spectrophotometric detection of competitive inhibitors through the use of an immobilized AChE-porphyrin complex via evanescent wave absorbance measurements has been demonstrated [392]. Here we have shown that the technique can be expanded for application to another enzyme. The technique could be applied to detection of inhibitors and/or substrates of any enzyme for which reversible competitive inhibition by a porphyrin or other compound with appropriate absorbance or fluorescence characteristics can be achieved. Detection via this method is specific for the inhibitors of the enzyme used rather than hydrolysis products [479].

Butyrylcholinesterase and acetylcholinesterase variants show different sensitivity and specificity for different inhibitors [466, 511, 523-524]. Eserine and Triton X-100 are competitive inhibitors of both AChE and BChE. The immobilized AChE and BChE complexes demonstrate limits of detection (LODs) of 37 ppt (89 pM) and 50 ppt (121

pM) respectively for eserine, while for Triton X-100 the LODs are 40 ppb (62 nM) and 83 ppb (128 nM) for BChE and AChE, respectively. The use of different enzymes will allow detection of differing ranges of inhibitors.

The TPPS₁ absorbance spectrum is sensitive to specific enzymes giving unique spectral changes even for very similar enzymes. The absorbance spectrum of the immobilized AChE-TPPS₁ complex has a characteristic peak at 446 nm while that of the immobilized BChE-TPPS₁ complex is 421 nm. The sensitivity of porphyrin absorbance spectra to different enzymes has been reported [485]. Variations in inhibitor affinities are reported to result from different charge distribution and hydrophobicity around the active site [525-529] and those differences likely affect the characteristic wavelength of the bound porphyrin. Porphyrin absorbance spectra are sensitive to the environment of the porphyrin responding to changes in charge distribution, ionic strength, and pH and are sensitive to slight variations in aromatic ring constituents [264, 283-284]. Different enzymes yielding different characteristic peaks upon inhibition by TPPS₁ (or similar compound) could be used to increase the specificity of this detection system. An immobilized enzyme surface consisting of both AChE and BChE can be used to specifically identify the presence of inhibitors interacting with the active site of either AChE, BChE, or both AChE and BChE with limits of detection very similar to those of the individual enzyme surfaces as long as the porphyrin enzyme-complexes exhibit different interaction wavelengths.

Because all inhibitors of AChE decrease the absorbance of the TPPS₁-AChE complex at 446 nm it is not possible to distinguish between them using the multi-enzyme technique presented here. Similarly, the technique does not allow for distinction between

different inhibitors of BChE, all of which decrease absorbance of the TPPS₁-BChE complex at 421 nm; however, it may be possible to differentiate between inhibitors which inhibit both AChE and BChE on the basis of the ratio of the change in absorbance at 421 nm and 446 nm. Using the change in absorbance per decade on the log scale shown in Figure 6.8 (A), AChE shows a 0.001 A/decade change for eserine while BChE shows a 0.0017 A/decade change. (Here, the rate of change for AChE is that of concentrations above the inflection point at 18 ppb.) The ratio of the AChE rate of change of absorbance to the BChE rate can be used to characterize the mixed IES giving 1:1.67 for eserine. Similarly, the ratio of the rates for Triton X-100 is 1:2.87, again using the AChE rate for concentrations above the inflection point. Characterization of the mixed IES using this type of ratio might allow for distinction between the various inhibitors affecting both AChE and BChE. A two enzyme system might not be able to distinguish components in mixture of inhibitors, although this might be possible with a larger group of enzymes.

While the measurement technique presented here is novel, the use of immobilized enzyme surfaces containing multiple enzymes for detection of competitive inhibitors of cholinesterases has been well documented [468-470]. Recent research has shown that mutation of AChE can yield variants with greater binding affinity for specific inhibitors (organophosphates) [515, 530]. The multi-enzyme techniques used for discrimination of cholinesterase inhibitors typically involve immobilization of enzymes on separate electrodes and combining the information from two or more electrodes for identification of the sample. Similarly, if we immobilize different AChE or BChE variants showing different binding affinities for various inhibitors on individual surfaces, the individual absorbance changes could possibly be used in concert for inhibitor discrimination without

the need for different porphyrin-enzyme interaction peaks. It is likely that the porphyrin-enzyme interaction peaks for the AChE variants will overlap as the enzymes vary by only a few amino acid residues.

A rapid reagent-less method for low level detection of competitive inhibitors of AChE and BChE has been presented which allows for discrimination between three groups of inhibitors: those which inhibit AChE, those which inhibit BChE, and those which inhibit both. While it is likely that one of the two methods described will allow for discrimination between inhibitors within the different groups, further research in this area is necessary.

IC₅₀ AND LOD VALUES FOR BCHE

Inhibitor	IC ₅₀ (mM)	IC ₅₀ (ppb)	LOD (ppb)
TPPS ₁	5	4600	-----
Eserine	2.7	1173	0.05
Amitriptyline	11	3454	0.072
Drofenine	42	14868	0.091
Triton X-100	70	45360	40

TABLE 6.1 Limits of detection (LOD) and 50 % inhibition constants (IC₅₀) for competitive inhibitors of butyrylcholinesterase [397].

LOD VALUES FOR MIXED IES

Inhibitors of:	Inhibitor	LOD (ppb)	Loss in Abs. Intensity at (nm)
BChE	Amitriptyline	0.072	421
	Drofenine	0.091	421
AChE	Galanthamine	0.05	446
	Scopolamine	0.1	446
	Tetracaine	0.26	446
Both	Eserine salicylate	0.05	421/ 446
	Triton X-100	81	421 / 446

TABLE 6.2 The ICCS limits of detection for competitive inhibitors of butyrylcholinesterase and acetylcholinesterase [395].

LINEWEAVER-BURK PLOT OF BCHE ACTIVITY

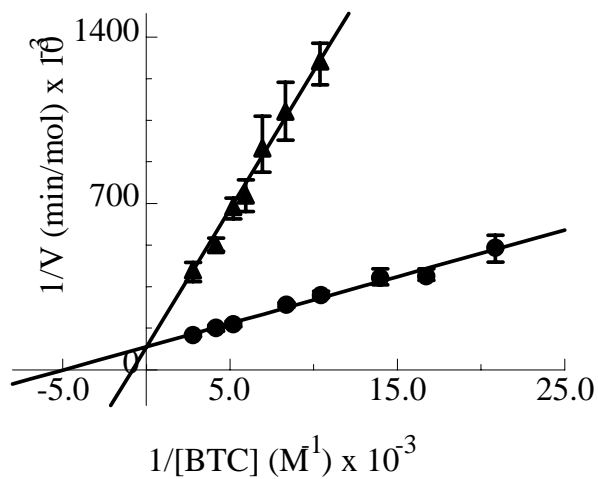


FIGURE 6.1 The Lineweaver-Burk plots of BChE activity at different BTC concentrations in the absence (●) and presence of 7.3 μM TPPS₁ (■). Intersection of the curves occurs at the Y-axis ($V_{\max} = 10.4 \mu\text{mol/min}$). The lines show linear best fits performed with 99% confidence interval [397].

BCHE/TPPS₁ INTERACTIONS IN SOLUTION

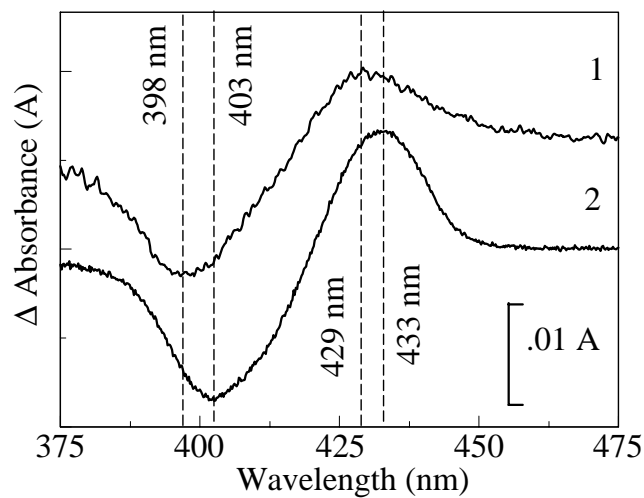


FIGURE 6.2 The response of the TPPS₁ absorbance spectrum to BChE (1) is demonstrated by the difference spectrum 1 μ M TPPS₁ + 30 nM BChE minus 1 μ M TPPS₁ (Trace 1). The difference spectrum 1 μ M TPPS₁ + 30 nM BChE + 1.7 μ M drofenine minus 1 μ M TPPS₁ shows the wavelengths for the TPPS₁-drofenine interaction [397].

EXPOSURE OF THE IES TO AN INHIBITOR

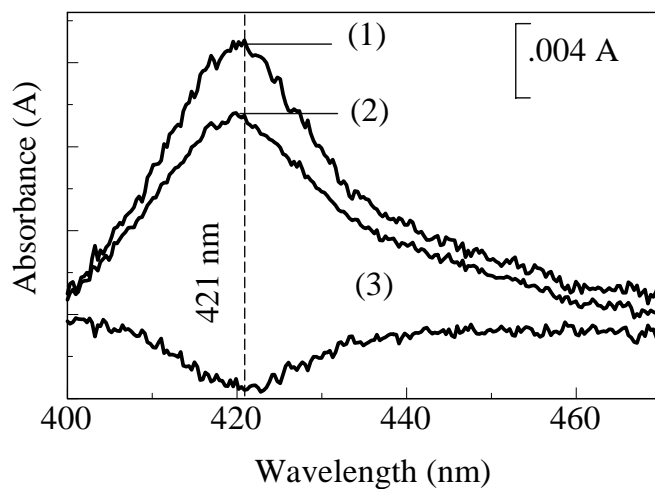


FIGURE 6.3 The absorbance spectrum of the immobilized TPPS₁-BChE (1) shows a loss at 421 nm upon exposure to 1 ppm (2.8 μM) drofenine (2). The change in absorbance is more easily observed in the difference spectrum TPPS₁-BChE + drofenine minus TPPS₁-BChE (3) [138].

CONCENTRATION DEPENDENCE OF ABSORBANCE CHANGE

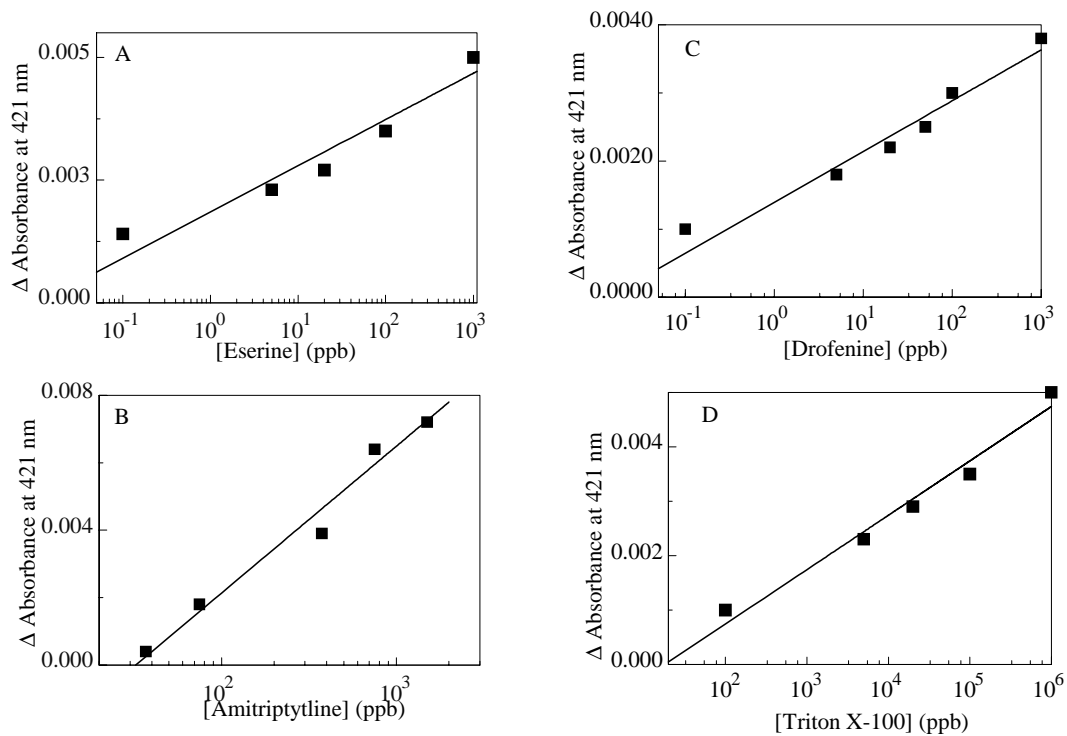


FIGURE 6.4 The concentration dependence of the loss in 421 nm absorbance intensity of immobilized TPPS₁-BChE slide surface upon inhibitor exposure to: (A) eserine, (B) amitriptyline, (C) drofenine, (D) Triton X-100 [397].

PERCENT INHIBITION CURVES FOR BChE

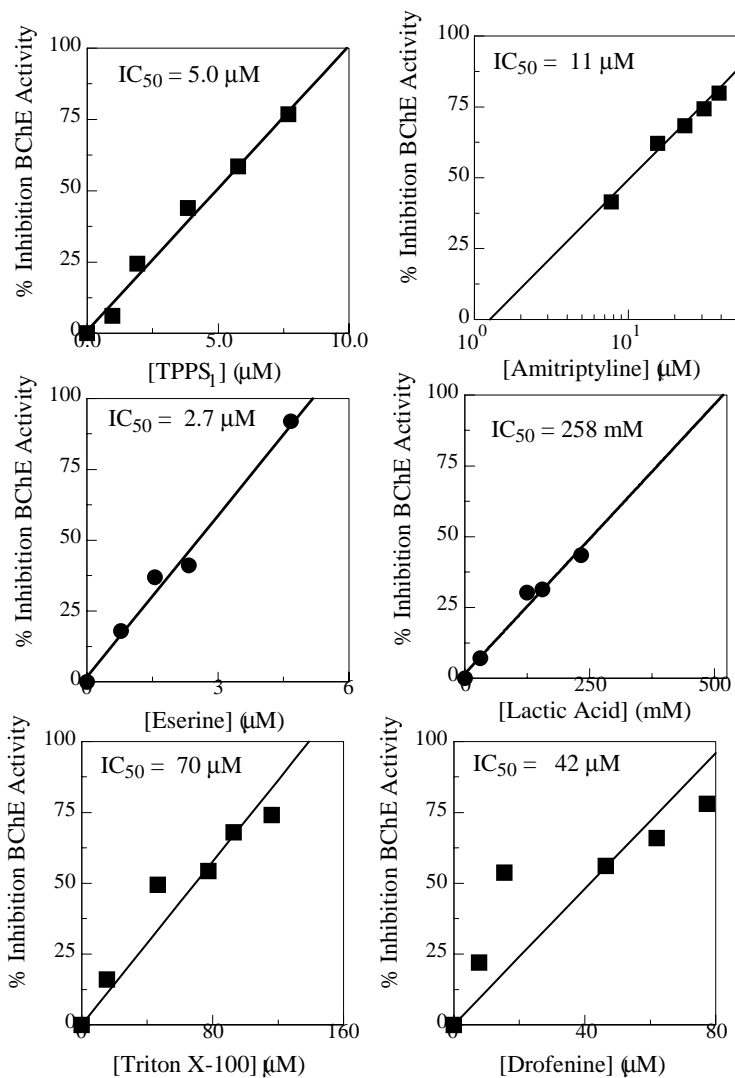


FIGURE 6.5 The dependence on inhibitor concentration of the percent inhibition of BChE activity.

INTERACTION OF TPPS₁ WITH CHOLINESTERASES

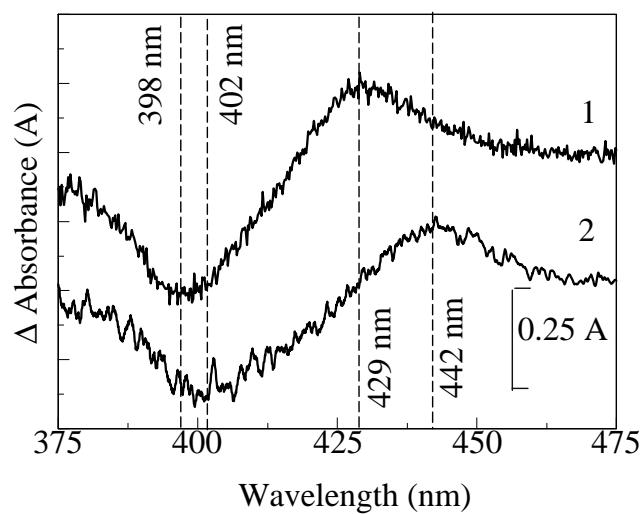


FIGURE 6.6 The difference spectra $1\mu\text{M TPPS}_1 + 30\text{ nM enzyme}$ minus TPPS_1 for BChE (1) and AChE (2) [395].

ABSORBANCE SPECTRA OF DIFFERENT IES

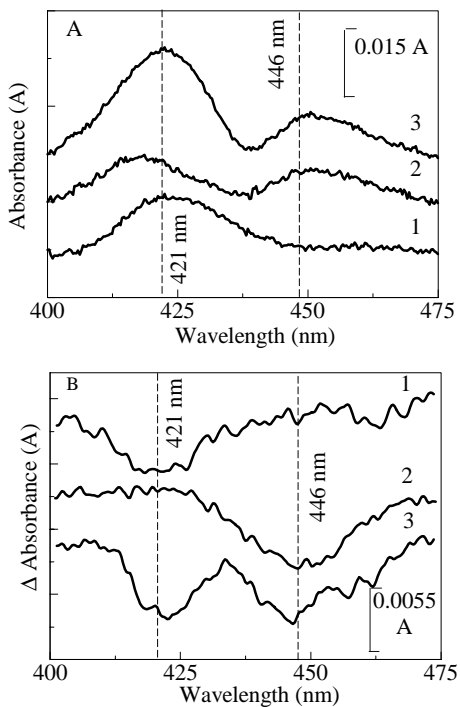


FIGURE 6.7 A. The absorbance spectra of the immobilized TPPS₁-BChE (1) and immobilized TPPS₁-AChE (2) complexes and the immobilized TPPS₁-BChE-AChE combination (3) were determined by subtraction of the absorbance spectrum of the enzyme-lacking slide from the individual absolute spectra of the three immobilized enzyme surfaces in order to isolate the porphyrin-enzyme interactions from the porphyrin interactions with the slide surface [395].

B. Difference spectra demonstrate the affect of different inhibitors on the ICCS. All traces smoothed by 4 point binomial method using Grams/32.

Trace 1. ICCS + 0.5 ppm amitriptyline minus ICCS

Trace 2. ICCS + 3 ppm tetracaine minus ICCS

Trace 3. ICCS + 4 ppm eserine minus ICCS [395]

CONCENTRATION DEPENDENCE FOR MIXED IES

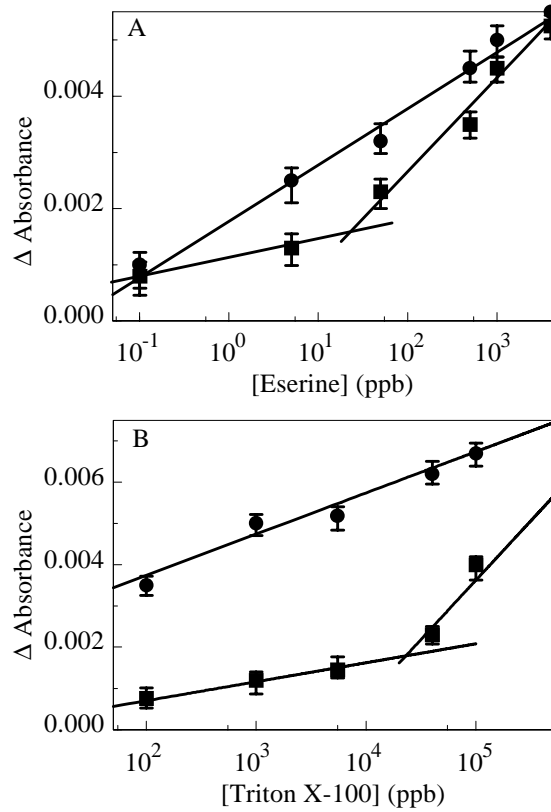


FIGURE 6.8 A. Loss in 421 nm (●) and 446 nm (■) absorbance intensity of immobilized TPPS₁-BChE-AChE combination slide surface upon inhibitor exposure to eserine [395].

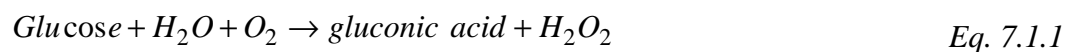
B. Loss in 421 nm (●) and 446 nm (■) absorbance intensity of immobilized TPPS₁-BChE-AChE combination slide surface upon inhibitor exposure to Triton X-100 [395].

CHAPTER 7

GLUCOSE OXIDASE

7.1 STRUCTURE AND FUNCTION

Glucose oxidase (GOD, E.C. 1.1.3.4) is an oxidoreductase which catalyses the oxidation of glucose to gluconic acid:



GOD is highly selective for β -D-glucose showing greatly reduced activity for even very similar sugars. The enzyme is highly stable showing activity over a broad pH range and it is easily immobilized. The result of these characteristics is the wide range of applications of GOD: determination of glucose in whole blood, food, and for agricultural applications; as a model system for development of new analytical approaches; and as a proposed cancer therapy [531].

Glucose oxidase is used for the detection and quantification of glucose through amperometric, potentiometric, chemiluminometric, spectrophotometric, or fluorometric methods. A thorough introduction to the application of these methods with glucose oxidase can be found in the review by Raba and Mottola [531]. Amperometric systems can be used for determination of H_2O_2 or O_2 production while potentiometric methods can be used for determination of gluconic acid production via pH change. Other methods use a coupled reaction and monitor the oxidation of an indicator compound. These methods are sensitive to the presence of the easily oxidized molecules ascorbate, urate, and L-cysteine as well as others. Sensitivity to these interferents has led to the development of methods to increase specificity including the use of coupled enzyme

systems and the use of selectively permeable polymer layers over the enzyme surface. Each of these solutions has problems. The polymer layers may crack or peel allowing penetration of the interferents to the enzyme surface. Using multiple enzymes (such as GOD with peroxidase) can also result in difficulty as each enzyme increases the complexity of the system and the immobilization procedure and each enzyme used eliminates only one interferent [439, 532].

In the following chapter, we will demonstrate the extension of the detection protocol discussed in Chapters 5 and 6 (the reversible, competitive inhibition of enzymes by porphyrins) to the enzyme glucose oxidase and we will show that this system can be applied for identification and quantification of glucose.

7.2 MATERIALS AND METHODS

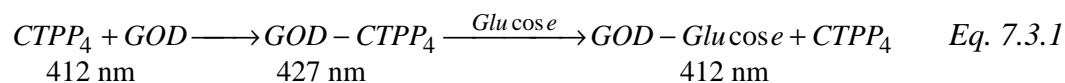
Glucose oxidase (from *Aspergillus niger*, E.C. 1.1.3.4) and (D)-(+)-glucose were obtained from Sigma (St. Louis, MO). Meso-tetra(4-carboxyphenyl)porphine (CTPP₄) was obtained from Frontier Scientific (Logan, UT) and used as delivered. Glucose oxidase was immobilized to PAMAM (generation 4, Aldrich - Milwaukee, WI) on ProbeOn™ Plus microscope slides (Fisher Biotech, Pittsburgh, PA) and porphyrin was incorporated into the surface as described previously (Chapter 4) [392]. Exposure of the immobilized CTPP₄-GOD surface was accomplished by applying 200 μL of the desired concentration of glucose in 50 mM pH 7 sodium phosphate buffer to the surface followed by blotting away the excess solution. Absorbance spectra of the immobilized enzyme-porphyrin surfaces (IES) before and after exposure to glucose was collected using an Ocean Optics USB-2000 spectrometer with the output of a LED of maximum wavelength

at 434 nm and 83 nm HBW as a light source (Chapter 5) [392]. Spectral analysis was performed using Grams/32 (Galactic Industries, Salem, NH).

7.3 RESULTS

Meso-tetra(4-carboxyphenyl)porphine binds immobilized glucose oxidase giving an absorbance peak at 427 nm and a shoulder at 412 nm as shown in Figure 1 (Trace 1). Addition of glucose to the immobilized CTPP₄-GOD complex results in a loss in absorbance at 427 nm as shown in the difference spectrum IES + glucose (Trace 2) minus IES (Trace 1) in Figure 1 (Trace 3). A surface that has completed the immobilization procedure with the exception of the enzyme exposure step gives a spectrum similar to that of the enzyme containing spectrum with the exception of the 427 nm peak; the peak at 412 nm due to CTPP₄ interaction with the surface persists.

That addition of glucose to the CTPP₄-GOD complex results in decreased intensity of the CTPP₄-GOD interaction peak at 427 nm indicates dissociation of CTPP₄ from GOD as illustrated below.



The amount of CTPP₄ bound to GOD decreases while the CTPP₄ non-specifically bound to the surface remains the same. An increase in 412 nm absorbance is not observed due to the removal of the newly dissociated CTPP₄ with excess glucose solution upon blotting of the surface.

The decrease in 427 nm absorbance is linearly dependent on the concentration of glucose to which the IES is exposed between 20 and 200 mg/dL (1.1 to 11.1mM) as seen in Figure 2. The LOD for the surface at 3:1 S/N is 20 mg/dL.

7.4 DISCUSSION

In order to be applicable for monitoring of glucose levels in whole blood samples by diabetic patients or in a clinical setting a system should operate in real time, be cost effective, and be interferent free. The glucose detector presented here is capable of operation in less than six seconds (the time required to collect a spectrum). The surface uses the specificity of the enzyme glucose oxidase so that only compounds interacting with glucose oxidase at the active site will affect the absorbance spectrum. The system used here uses an Ocean Optics USB2000; however, the cost could be greatly reduced through the use of wavelength specific diodes for detection of absorbance intensity changes.

This system does not require a polymer layer to prevent interference by reducing agents such as ascorbate or urate since the measurement is based on the dissociation of CTPP₄ from GOD as a direct result of the binding of glucose. The only interferents for a system of this type are compounds that bind GOD in a manner similar to glucose. Further investigation is needed to verify the response of the surface to whole blood samples and the affect of sugars such as 2-deoxy-D-glucose which are known to be oxidized by glucose [531].

The lifetime of this immobilized enzyme surfaces was not investigated beyond 35 days, however, GOD is known to be a very stable enzyme and the lifetime of similarly immobilized acetylcholinesterase surfaces is greater than 55 days (Chapter 5)[394].

IMMOBILIZED CTPP₄-GOD SURFACE

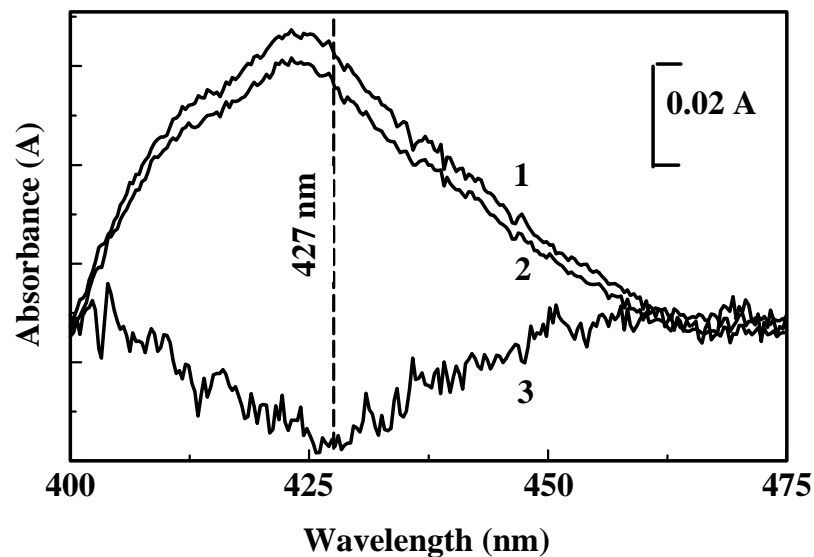


FIGURE 4.1 The absorbance spectra of the immobilized CTPP₄-GOD surface before (1) and after (2) exposure to 50 mg/dL (2.3 mM) glucose. The difference spectrum (3) IES + glucose minus IES shows the loss in absorbance at 427 nm. Trace 3 has been multiplied by 5 and smoothed by a 15% Fourier method in Grams/32 [398].

CONCENTRATION DEPENDENCE OF GLUCOSE RESPONSE

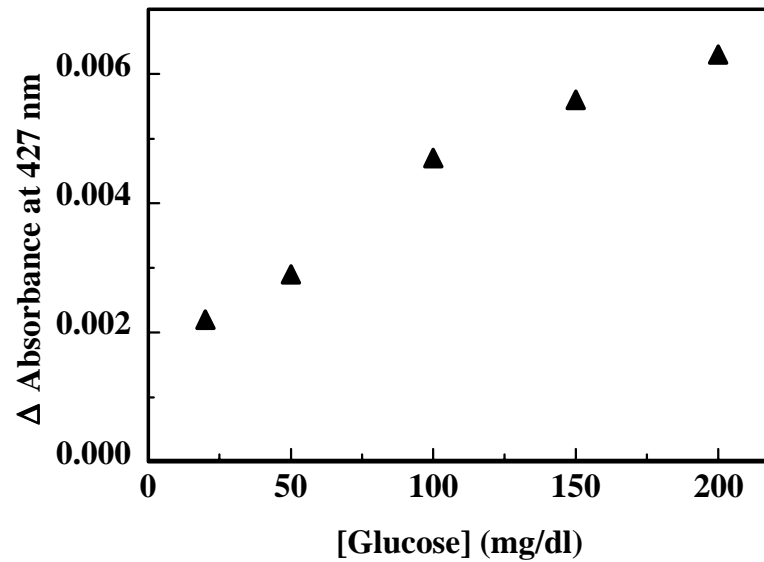


FIGURE 4.2 The change in absorbance at 427 nm in Figure 4.1 is linearly dependent on glucose concentration from 20 mg/dL (1.1 mM) to 200 mg/dL (11.1 mM) [398].

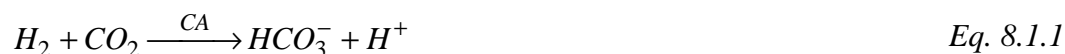
CHAPTER 8

CARBONIC ANHYDRASE

8.1 STRUCTURE AND FUNCTION

Zinc performs structural, regulatory, catalytic, and noncatalytic functions in metalloenzymes. Catalytic zinc atoms are found in all enzyme classes and include enzymes such as superoxide dismutase, RNA polymerase, carboxypeptidase, carbonic anhydrase (CA), pyruvate carboxylase, and organophosphate hydrolase (OPH) [533]. Catalytic zinc is often found in a four or five coordinated geometry in the active site with a water molecule or hydroxide ion in one ligand position. The work by Galdes and Vallee [534] suggests a two part mechanism for the role of zinc in catalysis. They indicate direct binding of the substrate to the metal without displacement of the metal-bound water molecule allowing the zinc atom to both polarize the substrate and activate the water molecule. The metal then facilitates the proper orientation of the substrate and the activated water to catalyze the reaction.

Carbonic anhydrase, a zinc metalloenzyme, catalyses the hydration of CO_2 to form



H_2CO_3 which dissociates to bicarbonate and a proton.

This reaction will proceed in the absence of CA, however, the turn over rate for this enzyme is extremely high. In humans there are seven isoenzymes of carbonic anhydrase (CA-I to CA-VII). Apart from hemoglobin, CA constitutes the principle protein of erythrocytes (red blood cells). It is found in saliva, mitochondria, and the cytosol of many cells. CA can also be found locations such as in secretory tissues where they are

involved in formation of ocular fluid, cerebrospinal fluid, and other secretions; the kidney where they mediate 85% of renal bicarbonate reabsorption; and in the capillaries of skeletal muscle, colon, reproductive tract, and cardiac muscle, as well as in lung tissue where it exists as a membrane associated glycoprotein. The physiological role of the enzyme is associated with the rapid hydration of carbon dioxide released into body tissues, dehydration of bicarbonate in the lungs, and transfer/accumulation of protons and bicarbonate ions in secretory organs such as the stomach.

The zinc ion in CA is at the base of the 15 Å active site. The zinc interacts with three His residues as well as one water molecule to form a tetrahedral metal coordination site. The interaction of the water molecule with the zinc reduces the pKa of the water significantly shifting the balance toward the hydroxide ion. The hydroxide ion is the catalytic nucleophile in the reaction. Competitive inhibition of metalloenzyme activity, that is, the binding at the active site of the enzyme by a compound other than the substrate, is observed in the presence of compounds such as imidazole [535], D-cysteine, penicillamine [536], 1,10-phenanthroline [537] and saccharin [538].

Porphyryns have been shown to competitively inhibit several enzymes including acetylcholinesterase [389, 391], butyrylcholinesterase [397], glucose oxidase [398], and heme oxygenase [539]. Here we will present data on the interactions of CA with several porphyryns and the resulting inhibition of enzymatic activity. We will also demonstrate how the reversible competitive inhibition of CA by a porphyrin can be used to monitor CO₂ and inhibitor levels.

8.2 MATERIALS AND METHODS

Carbonic anhydrase (CA, from bovine erythrocytes, E.C. 4.2.1.1), p-nitrophenol acetate (p-NPA), LysLysLys, arginine, glutaraldehyde, penicillamine, D-cysteine, 1,10-phenanthroline, saccharin, thiocyanate, p-nitrophenol acetate (p-NPA), 1,12-diaminododecane and dipicolinic acid (DPA) were obtained from Sigma (St. Louis, MO) and used without further purification. Sodium phosphate (NaPi) buffer salts were obtained from Fisher Scientific. Monosulfonate tetraphenyl porphyrin (TPPS₁), tetra(4-aminophenyl) porphyrin (NH₂TPP), meso-tri(4-sulfonato phenyl) mono(4-carboxy phenyl) porphyrin (CTPP₁), and meso-tetra(4-sulfonatophenyl)porphine (TPPS₄) were obtained from Frontier Scientific (Logan, UT) and used without further purification. Carbon dioxide (1%, 10,000 ppm) and nitrogen (99.998%) were obtained from Scott Specialty Gases (Plumsteadville, PA). Amino-terminated Starburst® (PAMAM) dendrimer (generation 4) and zinc acetate were obtained from Aldrich (Milwaukee, WI). Copper sulfate was obtained from Baker (Phillipsburg, NJ).

Absorbance spectra of the porphyrins in the presence and absence of CA and the various inhibitors of CA were recorded in 50 mM pH 7 sodium phosphate (Sorenson) buffer with a Cary 4E spectrophotometer at 0.2 nm resolution. Metal complex formation was monitored similarly. Difference spectra were obtained by subtraction of absolute spectra using Grams/32 (Galactic Industries, Salem, NH). Final reagent concentrations are given in the text and figure captions.

Porphyrin metal complexes were formed by mixing the respective porphyrin and copper sulfate (CuSO₄) or zinc acetate (C₄H₆O₄Zn) in solution in a one to one ratio at a concentration no greater than 30 μM and incubating overnight at 50°C. When higher concentrations of porphyrin are used, there is evidence of partial or no complex formation

(Figure 8.1) likely due to complications caused by aggregation of the porphyrins. The metallo-porphyrins used here should have only one or two Q-bands whereas the non-metallated versions have four Q-bands (as discussed earlier; Chapter 3). This can be used as an indicator of metal-complex formation. The shift in the Soret region can also be used to indicate complex formation, though overlap of the new and old peaks can make this difficult. In this case, peaks at 515, 553, 580, and 634 nm are observed in the TPPS₄ spectrum while peaks at 539 and 576 nm are observed in the CuTPPS₄ spectrum.

Thorslund and Lindskog [540] detail a method for spectrophotometric determination of the esterase activity of CA. CA will catalyze the hydrolysis of p-nitrophenol acetate to p-nitrophenol and acetate. At 348 nm, the ester p-nitrophenol acetate has insignificant absorbance while p-nitrophenol has a millimolar extinction coefficient of $5.54 \text{ mM}^{-1}\cdot\text{cm}^{-1}$. The enzymatic activity can be tracked by monitoring the change in absorbance at this wavelength as the concentration of p-NP increases (here using a Gilford single beam spectrophotometer). A slight modification of the proposed protocol was used. First, a background rate was measured for the each run using a 1 cm path length cuvette containing x ml 3mM p-NPA in 3% (v/v) acetone solution, (2.7 - x) ml 3% (v/v) acetone solution, and 0.3 ml 0.5 M NaPi pH 8. The reaction was initiated by adding 10 μl 2 mg/ml carbonic anhydrase (9700 Units/ml) to the above indicated cuvette. The initial velocity for the reaction was determined as described in Chapter 2 and it was corrected using the background rate. For determination of inhibition by the porphyrins, porphyrin was added as part of the (2.7 - x) ml 3% acetone solution. Linear fitting of the double-reciprocal data for the enzyme in the presence/absence of inhibitors was accomplished with PSI-Plot (V 7.0) at a 99.9% confidence interval.

In order to monitor the activity of the immobilized enzymes, 230 ml of 130 mM p-NPA in 100 mM pH 8 NaPi with 10% acetone is allowed to interact with the surface for 3 minutes. After this interaction period, 150 μ l is pipetted from the surface of the slide into 800 μ l of water. The absorbance of the solution is then measured with a Cary 4E spectrophotometer. The enzymatic activity of the slide surface is based on the absorbance at 412 nm compared to a background absorbance measurement.

Immobilization of carbonic anhydrase onto ProbeOn™ Plus (Fisher Biotech, Pittsburgh, PA.) microscope slides was attempted by the double dendrimer layer method described previously (Enzyme Protocol 3, Chapter 4)[392]. The result was a surface with very little enzymatic activity. It was found that a less tightly packed immobilization matrix resulted in higher enzymatic activity, so carbonic anhydrase was immobilized by the following procedure using one of three tethers (Protocol 4, Chapter 4). Each of the reaction steps was terminated by rinsing the slide surface with a 50 mM sodium phosphate 1 M NaCl solution at pH 9 (PBS). ProbeOn Plus™ Microscope slides were activated with 0.17 M glutaraldehyde for 25 minutes followed by reaction with 0.9 mM LysLysLys, 0.9 mM arginine, or 0.35 mM 1,12-diaminododecane in 50mM pH 7 phosphate buffer for 90 minutes. The slide was again activated by glutaraldehyde for 25 minutes followed by reaction with 12 μ M carbonic anhydrase for 90 minutes. This step was followed by interaction of the slide surface with 1M pH 9 TRIS to block all unreacted sites.

Slides were stored at room temperature after vacuum packing in three layer food saver bags using a FoodSaver (Vac360) from Tilia (San Francisco, CA). The lifetime of the immobilized enzyme surfaces based on the esterase activity as described above is less

than three months. If porphyrin is added to the surface of the slides, lifetimes based on the proper response to addition of inhibitor are less than seven days when stored under vacuum and less than 12 hours when stored under ambient conditions.

Absorbance spectra of immobilized enzyme-porphyrin complexes were collected using an Ocean Optics USB-2000 spectrometer (Chapter 5, Figure 5.1)[392] with the output of two LEDs (Mouser 430 nm - maximum wavelength at 434 nm and 83 nm HBW; Digikey 380 nm – maximum wavelength at 388 nm and 17 nm HBW) as a light source. A pair of LEDs was used to cover a spectral range not possible with a single LED. Inhibitors of CA were applied as 200 μ l drops of buffered solutions at the indicated concentrations and allowed to interact for 30 seconds. The excess solution was then blotted away before collection of the post-exposure difference spectrum. The difference spectra presented are the pre-exposure spectrum subtracted from the post-exposure spectrum. Slides were exposed to gaseous CO₂ as mixtures of 1% CO₂ (10,000 ppm) and 99% N₂. Constant pressure flow valves were used to dilute the 1% CO₂ to the desired concentrations. Absorbance spectra of the immobilized enzyme surfaces were collected before and after mixtures were allowed to flow across them for 20 seconds at 0.5 liters per minute.

Zinc was removed from the active site of carbonic anhydrase using a dialysis protocol outlined by Thompson and Jones [541]. The enzyme solution was dialyzed using Spectra/Por® membrane tubing (Molecular weight cut-off 6,000 to 8,000). The tubing containing 2 mg/ml CA in 0.1 M pH 7 NaPi was placed in pH 5.4 50 mM sodium acetate buffer containing 5 mM dipicolinic acid. This solution was stirred at 4°C for 20 hrs. The enzyme was reconcentrated and the DPA was removed from the sample using a

Microcon YM-10 micro-centrifuge filter (MWCO 10,000) to reduce the sample volume from 1.5 ml to approximately 0.2 ml. This process was repeated three times using 0.1 M pH 7 NaPi for the two subsequent dilutions. Zinc was replaced by addition of 2:1 zinc acetate to CA in 0.1 mM pH 7 sodium phosphate buffer followed by incubation overnight at 4°C. The work by Elbaum, et al. [542] and the work here demonstrate that CA readily binds zinc in solution, so no special considerations are necessary.

8.3 RESULTS

8.3.1 INTERACTIONS IN SOLUTION

In order to use a porphyrin as a colorimetric indicator for binding of substrate or inhibitor to an enzyme, the porphyrin must interact with the enzyme resulting in a detectable change in the porphyrin absorbance spectrum. With this in mind, the interaction of several porphyrins with carbonic anhydrase was investigated. The desired characteristic is a strong, specific absorbance change. The difference spectra porphyrin + CA (25 W-A units, 112 nM) minus porphyrin show the changes in the absorbance spectra of porphyrins upon interaction with carbonic anhydrase. The troughs in these spectra indicate the loss in absorbance intensity resulting from the decrease in concentration of the free porphyrin in solution while the peaks are the increase in absorbance intensity resulting from the formation of the porphyrin-CA complex.

Figure 8.2 shows the peak/trough pairs observed upon interaction of Cu^{2+} -TPPS₁ and TPPS₁ with carbonic anhydrase. There is a loss in absorbance intensity at 405 nm in the Cu^{2+} -TPPS₁ + CA minus Cu^{2+} -TPPS₁ difference spectrum (Trace 1) with an increase at 436 nm. The peak/trough locations in the difference spectrum for TPPS₁ (Trace 2) are

unique at 429 nm and 400 nm respectively. The wavelength shift upon interaction of a porphyrin with an analyte has been shown to be proportional to the association constant between the porphyrin and the molecule [284]. A shift of 31 nm for Cu^{2+} -TPPS₁ as opposed 29 nm for TPPS₁ indicates slightly greater affinity of the copper complexed TPPS₁ for CA.

Figure 8.3 shows the absorbance spectra for the pre- and post-CA addition for NH_2TPP and CuNH_2TPP . The Difference spectra $\text{NH}_2\text{TPP} + \text{CA}$ minus NH_2TPP for both the plain and copper complexed versions of NH_2TPP are also shown. Both CuNH_2TPP and NH_2TPP give the peak/trough locations at 465 nm / 418 nm upon interaction with CA, however the change in intensity is not the same for the interaction of CA with NH_2TPP as compared with CuNH_2TPP . Based a millimolar extinction coefficient of 48 (1 cm path length), the loss in absorbance intensity at 418 nm for Cu^{2+} - NH_2TPP is the result of the change in absorbance of 120 nM porphyrin while the change at 418 nm for NH_2TPP is the result of a change in absorbance of 39 nM porphyrin. The porphyrin concentration involved in an interaction gives an indication of the association constant between the porphyrin and the analyte. The involvement of 120 nM CuNH_2TPP in the interaction with CA indicates a 1:1 CA:porphyrin interaction. Similarly, the involvement of 39 nM NH_2TPP in the interaction with CA indicates only one in every two to three enzymes are interacting with a porphyrin indicating a greater association between the copper porphyrin and CA.

The copper-complexed CTPP_1 gives the same peak/trough (425 / 412 nm) locations in the $\text{CTPP}_1 + \text{CA}$ minus CTPP_1 difference spectrum as CTPP_1 with a larger change in absorbance intensity (Figure 8.4). Upon formation of the copper complex, the

CTPP₁ absorbance spectrum becomes slightly broadened in the Soret region and the millimolar extinction coefficient at 412 nm is reduced by 15% to 470 (1 cm path length). The change in the absorbance intensity at 412 nm results from the interaction of CA with 26 nM and 13 nM porphyrin for Cu²⁺-CTPP₁ and CTPP₁ respectively. The association constant between copper-complexed CTPP₁ and CA appears to be greater than that of CTPP₁ interacting at a rate of about one in four enzymes as compared to one in eight enzymes.

The changes in the TPPS₄ and CuTPPS₄ absorbance spectra upon interaction with CA are shown in Figure 8.5 along with the pre- and post CA addition absolute absorbance spectra. Both porphyrins show a loss in absorbance intensity at 412 nm. Additionally, TPPS₄ shows a peak in the difference spectrum at 422 nm. The interactions for both CuTPPS₄ and TPPS₄ with CA are weak. This is emphasized by the shift in the TPPS₄ spectrum which is only 10 nm and by the very low absorbance intensities in the difference spectra as compared to the overall porphyrin absorbance intensity (less than 1%).

Large changes in the Soret absorbance of TPPB occur upon copper complex formation. The FWHM is reduced from 28 nm to 7 nm while the extinction coefficient at 414 nm is increased by only 3%. The interaction between TPPB/CuTPPB and carbonic anhydrase was also investigated (Figure 8.6). The interactions between CA and both porphyrins are weak as evidenced by the low absorbance intensities in the difference spectra. In the TPPB difference spectrum there are two very broad features, a loss in absorbance intensity at 403 nm with an increase in absorbance intensity at 424 nm. In the

CuTPPB difference spectrum the features are more narrow with a decrease in absorbance intensity at 412 nm and an increase in absorbance intensity at 427 nm.

Lineweaver-Burk plots (Chapter 2) of carbonic anhydrase esterase activity in the absence/presence of porphyrins are shown in Figure 8.7. The y-intercept of each line is the inverse of the maximal enzymatic rate ($1/V_{\max}$) while the x-intercepts are the inverse of the concentration needed to achieve half of the maximal rate ($-1/K_m$). Competitive inhibition of an enzyme results in a change in K_m with no change in V_{\max} . In the absence of inhibitor, the value of K_m was determined to be 80 mM with a V_{\max} of 1 $\mu\text{M}/\text{min}$. In the presence of 3 μM CuTPPS₁ and 1.8 μM CuCTPP₁ the value of K_m is changed to 23 mM and 36 nM respectively with no change in the value of V_{\max} . No inhibition of CA activity was observed in the presence of non-metallated TPPS, CTPP₄, NH₂TPP, TPPS₁, or TPPB. CTPP₁ and CuTPPS₄ inhibited the activity of CA, but in a noncompetitive manner changing the value of V_{\max} with no change in the value of K_m . CuNH₂TPP and CuTPPB do not inhibit the activity of carbonic anhydrase.

Because CuTPPS₁ and CuCTPP₁ competitively inhibit the activity of CA, the rest of this chapter will focus on these two porphyrins. The reversibility of the CuTPPS₁ and CuCTPP₁ inhibition of CA was determined spectrophotometrically by monitoring the changes in the porphyrin absorbance spectrum upon addition of a another competitive inhibitor to the porphyrin-CA complex. Figure 8.8 (A) shows the difference spectrum CuTPPS₁ + CA + 1,10-phenanthroline minus CuTPPS₁ (Trace 1) indicating the effect of CA and the inhibitor on the absorbance spectrum of the porphyrin. Also shown is the difference spectrum CuTPPS₁ + 1,10-phenanthroline minus TPPS₁ (Trace 2) which shows the effect of the 1,10-phenanthroline alone on the absorbance spectrum of the

porphyrin. The two traces are similar in peak/trough position, shape, and intensity. The peak/trough pair indicative of the interaction between the porphyrin and CA is no longer present in the difference spectrum indicating dissociation of the porphyrin-CA complex. Had 1,10-phenanthroline not resulted in dissociation of the porphyrin-enzyme complex, the difference spectrum showing the interaction of the inhibitor and enzyme with the porphyrin (Figure 8.8 A, Trace 1) would have been the sum of the individual interactions of the enzyme and inhibitor with the porphyrin indicating no dissociation of the porphyrin-enzyme complexes and only formation of additional porphyrin-inhibitor complexes.

The identical effect is observed in the case of CuCTPP₁ as shown in Figure 8.8 (B). Similar experiments with D-cysteine and saccharin demonstrate the reversibility of the inhibition of CA by the two porphyrins as well (data not shown). The addition of thiocyanate, an uncompetitive of CA [543], does not result in the loss of the peak/trough pair observed upon interaction of CA with either CuTPPS₁ (Figure 8.9) or CuCTPP₁ (Figure 8.10). The results of these experiments are summarized in Table 8.1.

The difference spectra porphyrin + enzyme minus porphyrin shown in Figure 8.11 are the result of the interaction of CuCTPP₁ with carbonic anhydrase (Trace 1), zinc free carbonic anhydrase (Trace 2), and carbonic anhydrase after zinc replacement (Trace 3). In all three cases, there is a peak at 425 nm and a complex trough composed of a loss in absorbance intensity at two wavelengths 412 nm and 401 nm. The loss in absorbance intensity at 401 nm is greater for addition of CA where some or all of the zinc is missing while the loss in intensity at 412 nm is greater for addition of zinc containing CA. It appears that the trough at 412 nm is the result of the interaction of CuCTPP₁ with the

zinc-containing active site of CA and the trough at 401 nm results from interaction with other areas of the protein.

The interaction between CuTPPS₁ and zinc free carbonic anhydrase results in a very slight loss in absorbance intensity at 418 nm with no corresponding increase in absorbance intensity (Figure 8.12). When zinc is replaced in the CA, the peak trough pair expected for the interaction between CuTPPS₁ and CA is recovered (Figure 8.12, Trace 3). The change in the absorbance spectrum of CuNH₂TPP upon interaction with CA is the same regardless of the presence/absence of zinc in the active site (data not shown).

8.3.2 IMMOBILIZED ENZYME SURFACES

Figure 8.13 shows the absorbance spectrum of the immobilized CA surface after exposure to CuTPPS₁. The results of peak fitting indicate that there are two peaks involved in this spectrum at 427 and 454 nm. Exposure of the surface to cysteine results in changes at both of these peaks though not to the same degree. There is an 11% loss in absorbance intensity at 427 nm with a 45% loss in absorbance intensity at 454 nm. The use of the CA-CuTPPS₁ surface was not pursued due to the very broad loss in intensity, the shallow slope of the concentration dependence curve, and the lack of response to CO₂ exposure.

The absorbance spectrum of the immobilized carbonic anhydrase surface after exposure to CuCTPP₁ is shown in Figure 8.14. The absorbance spectrum between 375 and 500 nm can be fitted by three peaks at 404, 410, and 434 nm. Exposure of the immobilized porphyrin-enzyme surface to inhibitors of CA results in a loss in absorbance at 404 nm. This loss in absorbance shows a log-linear dependence on inhibitor

concentration for saccharin, 1,10-phenanthroline, and cysteine (Figure 8.15) with the slope of the concentration dependence varying depending on the inhibitor being used.

The ability of the immobilized carbonic anhydrase-CuCTPP₁ surface to detect gaseous CO₂ was also investigated. Exposure of the surface to CO₂-N₂ mixtures results in a loss in absorbance intensity at 404 nm with an increase in absorbance intensity at 434 nm (Figure 8.16). The dependence of this change in absorbance on concentration is shown in Figure 8.16. The expected half hyperbolic dependence on concentration is observed. The CO₂ limit of detection for this system based on a 3:1 S/N level is 1,000 ppm.

8.4 DISCUSSION

While competitive inhibition of the enzyme by the porphyrin does not guarantee binding of the zinc but may only block substrate access to the active site, the variation in the porphyrin-enzyme interaction peaks when zinc is removed from the active site of CA (Figures 8.11 and 8.12) strongly suggests and is consistent with the interaction of the porphyrin with the coordinated zinc. Data presented here indicate the copper complexed porphyrins bind at the active site while metal-free porphyrins do not. The ability of the metalloporphyrin to bind zinc in place of its original metal is greater than the ability of free porphyrin to bind zinc. Typical addition of zinc to porphyrins does not occur readily and is effected by refluxing the porphyrin with zinc. The improved ability to bind zinc may be the result of faster formation of metalloporphyrin species through metal substitution as compared to metallation of a free porphyrin ring [289-291]. In addition, it has been demonstrated that porphyrins with slightly deformed ring structures more readily exchange metal ions than those with less flexible rings [288]. The structure of

Cu^{2+} - NH_2TPP is highly symmetric while those of Cu^{2+} - TPPS_1 and Cu^{2+} - CTPP_1 have fewer symmetries and therefore less rigid rings. Thus both metal exchange factors and ring flexibility influence the binding of the porphyrins to the zinc containing active site of carbonic anhydrase.

The porphyrins TPPS_1 and CTPP_1 each have four phenyl rings as substituents with one phenyl bearing a sulfonate or carboxy group in the para position both of which are negatively charged at pH 7. The combination of the hydrophobicity of the phenyl rings together with the negative character of the substituents may also influence porphyrin-enzyme interaction as the interaction; the interaction of an inhibitor with the active site residues is an important factor in inhibitor binding. CuTPPS_1 and CuCTPP_1 have been shown to be reversible competitive inhibitors of the enzyme carbonic anhydrase while the positive charge bearing $\text{CuNH}_2\text{-TPP}$ does not inhibit the enzymatic activity and the more water soluble CuTPPS_4 does not bind at the active site of CA.

Preliminary results indicate that we will be able to use similar porphyrins to inhibit other zinc metalloenzymes. Organophosphorous hydrolase (OPH) is a zinc containing metalloenzyme that upon binding of a copper metalloporphyrin alters the absorbance spectrum of the porphyrin. The absorbance spectrum of the OPH-porphyrin complex is subsequently changed upon exposure to a competitive inhibitor of OPH indicating that the binding of the porphyrin likely takes place at the OPH active site. Based on the work presented here it seems likely that the porphyrin interacts with the zinc containing active site of OPH.

We have demonstrated the ability of copper metalloporphyrins to reversibly bind the active site of the zinc metalloenzyme carbonic anhydrase. Further, we have shown

the application of this interaction with immobilized CA for detection of compounds that bind at the active site of CA and for quantification of the CO₂ content of gas samples from 1,000 to 10,000 ppm (0.1 to 1%). Typical outdoor CO₂ levels are around 300 ppm (0.03%). Levels of CO₂ from 2,500 to 5,000 ppm (0.25 to 0.5%) can cause symptoms such as burning eyes, tiredness, and headaches. Levels of CO₂ in this range can result from improper building ventilation or from the used of unvented fuel-burning space heaters. The American Society of Heating Refrigeration and Air Conditioning Engineers (ASHRAE) standard 62-1989, Ventilation for Acceptable Indoor Air Quality indicates that indoor CO₂ levels should be below 1,000 ppm (0.1%). CO₂ levels of 100,000 ppm (10%) can cause loss of consciousness while levels of 200,000 ppm (20%) can cause respiratory paralysis. These levels of CO₂ can be encountered in caves by spelunkers. There is also interest in monitoring CO₂ levels in airplane cabins, on board shuttle missions, and on the International Space Station as these are nearly closed systems. CO₂ levels are also of interest for some environmental monitoring situations such as the CO₂ levels in a region following a violent lake turnover and the release of magmatic carbon dioxide.

INTERACTION OF PORPHYRINS WITH CARBONIC ANHYDRASE

Porphyrin	T (nm)	P (nm)	Inhibitors							
			PC-NH ₂		D-cys		1,10-P		Sacc	
			PB	RB	PB	RB	PB	RB	PB	RB
Cu-TPPS	No Interaction									
Cu-TPPS ₁	407	440	Yes	No	Yes	No	Yes	Yes	Red.	No
Cu-CTPP ₁	412	427	Yes	No	Yes	Yes	Yes	Yes	Yes	Red.
Cu-NH ₂ TPP	418	465	Yes	No	Yes	No	Yes	No	Yes	No
Cu-TPPT	412	428	Yes	No	Red.	No	Yes	Red.	Yes	No
Cu-TPPB	412	427	Yes	No	Yes	Yes	Yes	Yes	Yes	No
TPPS	412	425	Indet.	Indet.	Yes	No	Yes	Yes	No	No
TPPS ₁	400	429	Yes	No	No	No	Yes	Yes	No	No
CTPP ₁	413	424	Yes	Yes	Yes	Yes	Yes	Indet.	Yes	Yes
NH ₂ TPP	418	465	Yes	No	Yes	No	No	No	Yes	No
CTPP ₄	410	420	Indet.	Indet.	Yes	Yes	Yes	Yes	No	No
TPPT	412	428	No	No	Yes	No	No	No	Yes	No
TPPB	399	429	Yes	Yes	Yes	Yes	Yes	Yes	Yes	No

TABLE 8.1 Summary of the effects of inhibitors of carbonic anhydrase on the porphyrin-CA complexes. Inhibitors: PC-NH₂ = penicillamine, D-cys = D-cysteine, 1,10-P = 1,10-phenanthroline, and Sacc = Saccharin. Table Abbreviations: Indet. = indeterminate, Red. = reduces, P = peak, T = Trough, PB = prevents binding, and RB = reverses binding.

PORPHYRIN-METAL COMPLEX FORMATION

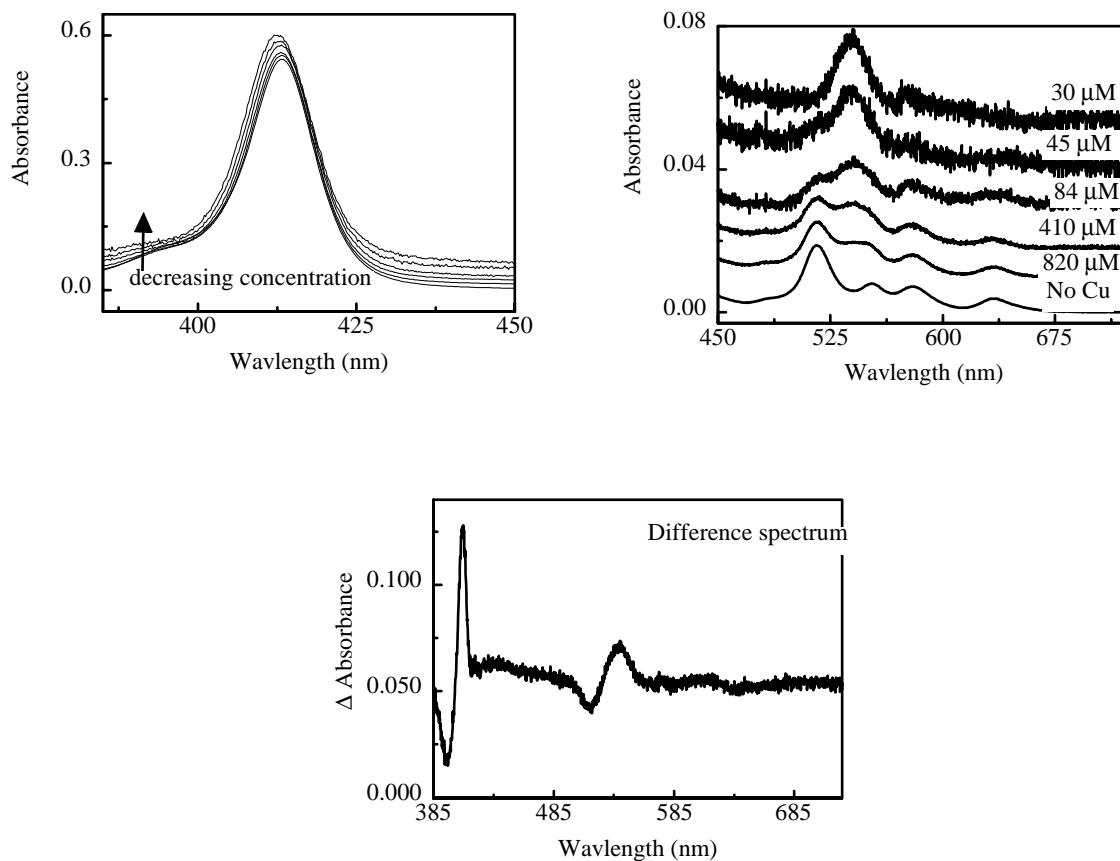


FIGURE 8.1 All curves have been scaled to match at the Soret peak and a factor has been added to achieve the separation between the curves. TPPS was incubated with CuSO_4 (both analytes at the indicated concentration) overnight (minimum 24 hrs) at room temperature. Spectra are measured in 50 mM NaPi at pH 7. The difference spectrum is CuTPPS from the 30 μM incubation minus TPPS.

CU-TPPS₁ AND TPPS₁ WITH CARBONIC ANHYDRASE

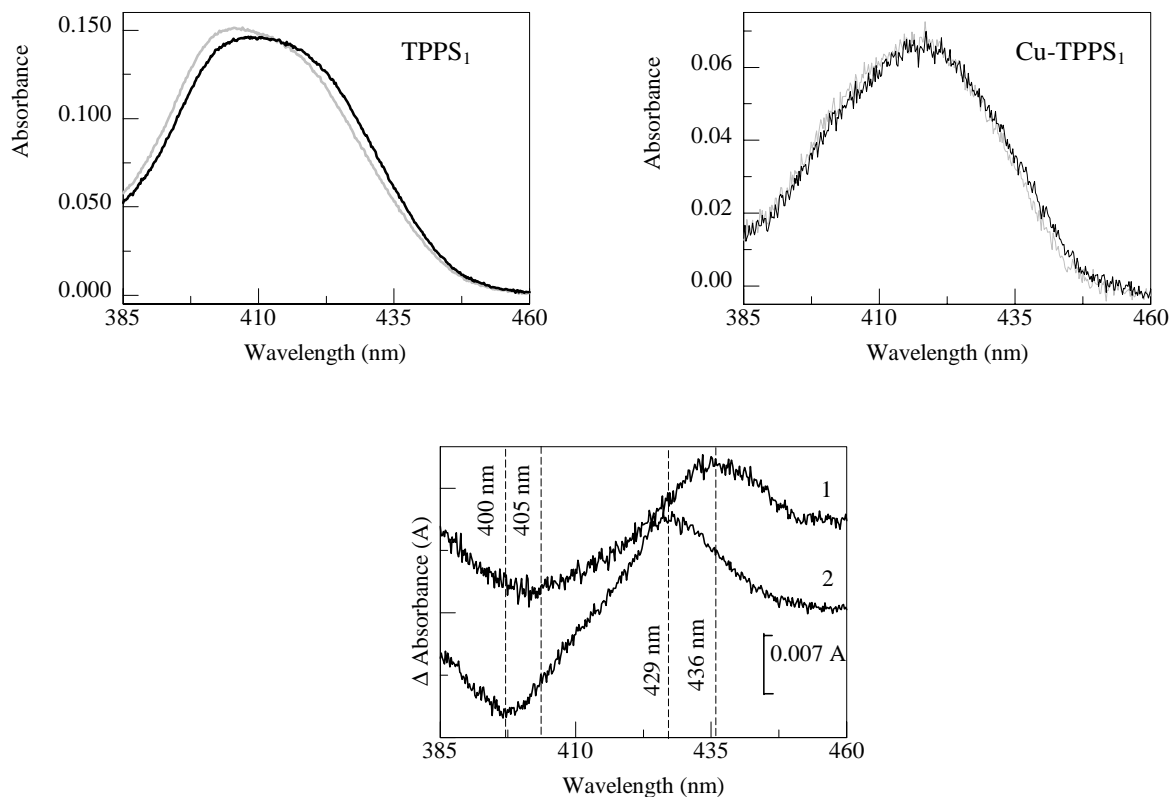


FIGURE 8.2 The spectra labeled TPPS₁ and Cu-TPPS₁ show the absorbance spectrum of the porphyrins before and after addition of CA. The (1) Cu-TPPS₁ (3 μM) + CA (112 nM) minus Cu-TPPS₁ [399] and (2) TPPS₁ (0.8 μM) + CA (112 nM) minus TPPS₁ difference spectra show that the porphyrin interaction wavelengths differ between the two porphyrins.

NH₂TPP AND CU-NH₂TPP WITH CARBONIC ANHYDRASE

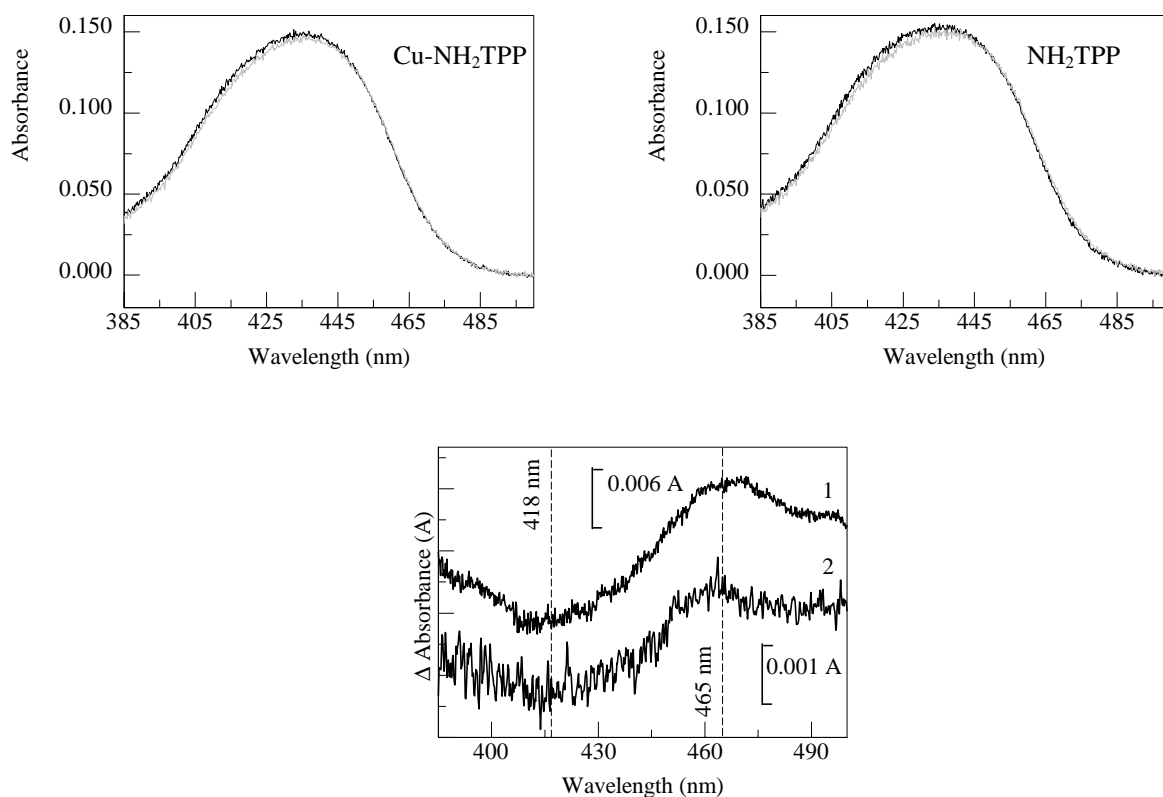


FIGURE 8.3 The spectra labeled NH₂TPP and Cu-NH₂TPP show the absorbance spectrum of the porphyrins before and after addition of CA. The (1) Cu-NH₂TPP (1.6 μM) + CA (112 nM) minus Cu-NH₂TPP [399] and (2) NH₂TPP (1.6 μM) + CA (112 nM) minus NH₂TPP difference spectra show that the porphyrin interaction wavelengths do not differ between the two porphyrins but the strength of the interaction does.

CTPP₁ AND CU-CTPP₁ WITH CARBONIC ANHYDRASE

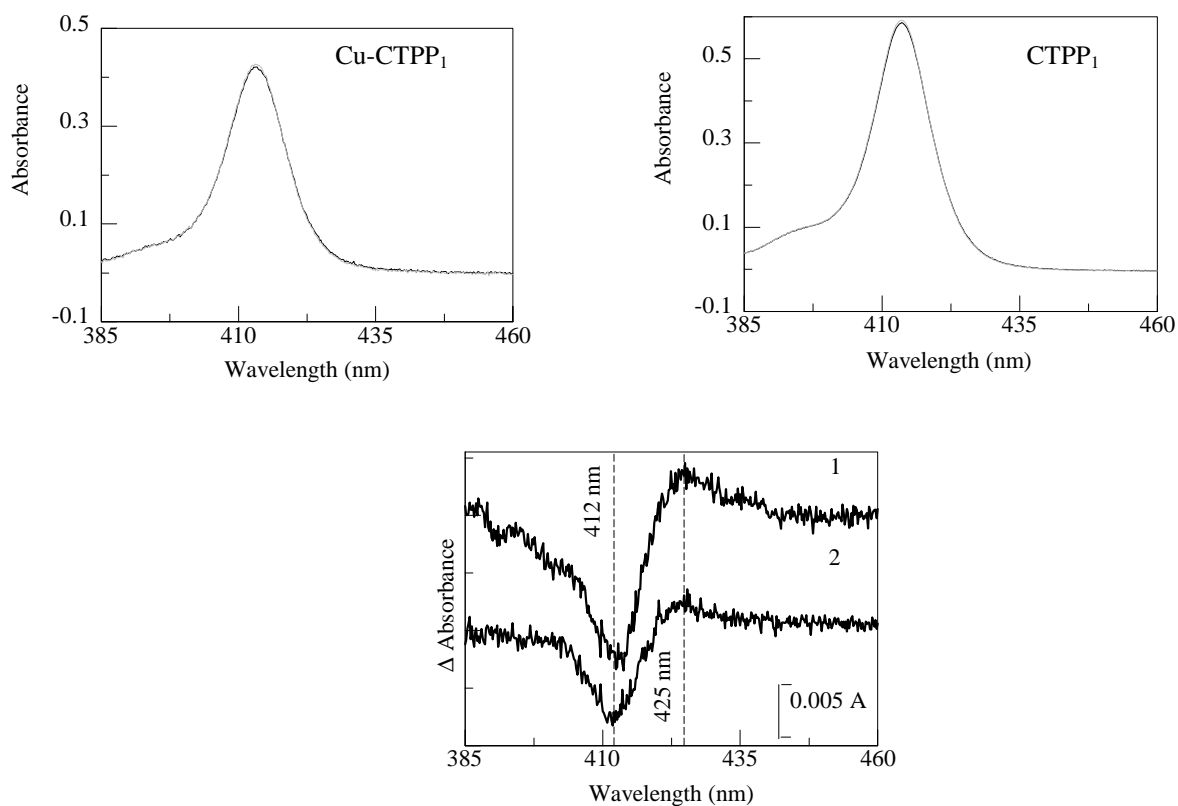


FIGURE 8.4 The spectra labeled CTPP₁ and Cu-CTPP₁ show the absorbance spectrum of the porphyrins before and after addition of CA. The (1) Cu-CTPP₁ (1.6 μ M) + CA (112 nM) minus Cu-CTPP₁ [399] and (2) CTPP₁ (1.6 μ M) + CA (112 nM) minus CTPP₁ difference spectra show that the porphyrin interaction wavelengths do not differ between the two porphyrins but the strength of the interaction does.

TPPS₄ AND CU-TPPS₄ WITH CARBONIC ANHYDRASE

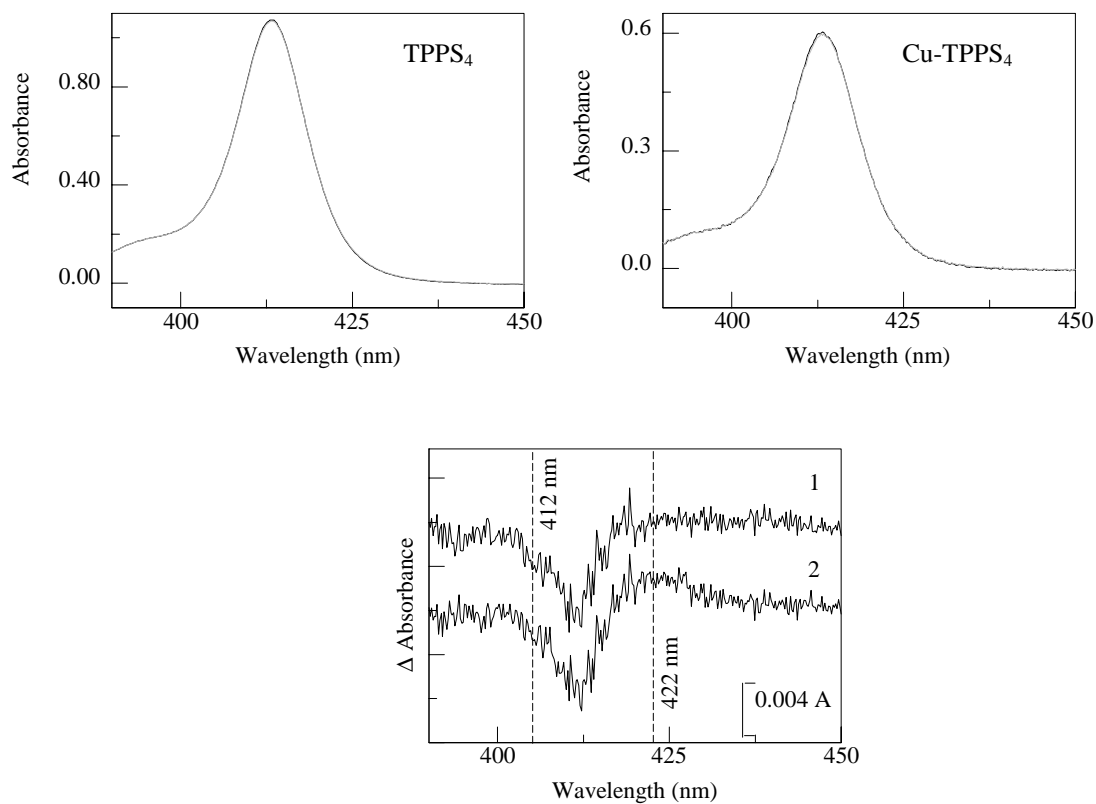


FIGURE 8.5 The spectra labeled TPPS₄ and Cu-TPPS₄ show the absorbance spectrum of the porphyrins before and after addition of CA. The (1) Cu-TPPS₄ (1.6 μ M) + CA (112 nM) minus Cu-TPPS₄ and (2) TPPS₄ (1.6 μ M) + CA (112 nM) minus TPPS₄ difference spectra show that while the troughs are at the same location in the difference spectra, the TPPS₄ spectrum has a peak at 422 nm that is not present in the Cu-TPPS₄ spectrum.

TPPB AND CU-TPPB WITH CARBONIC ANHYDRASE

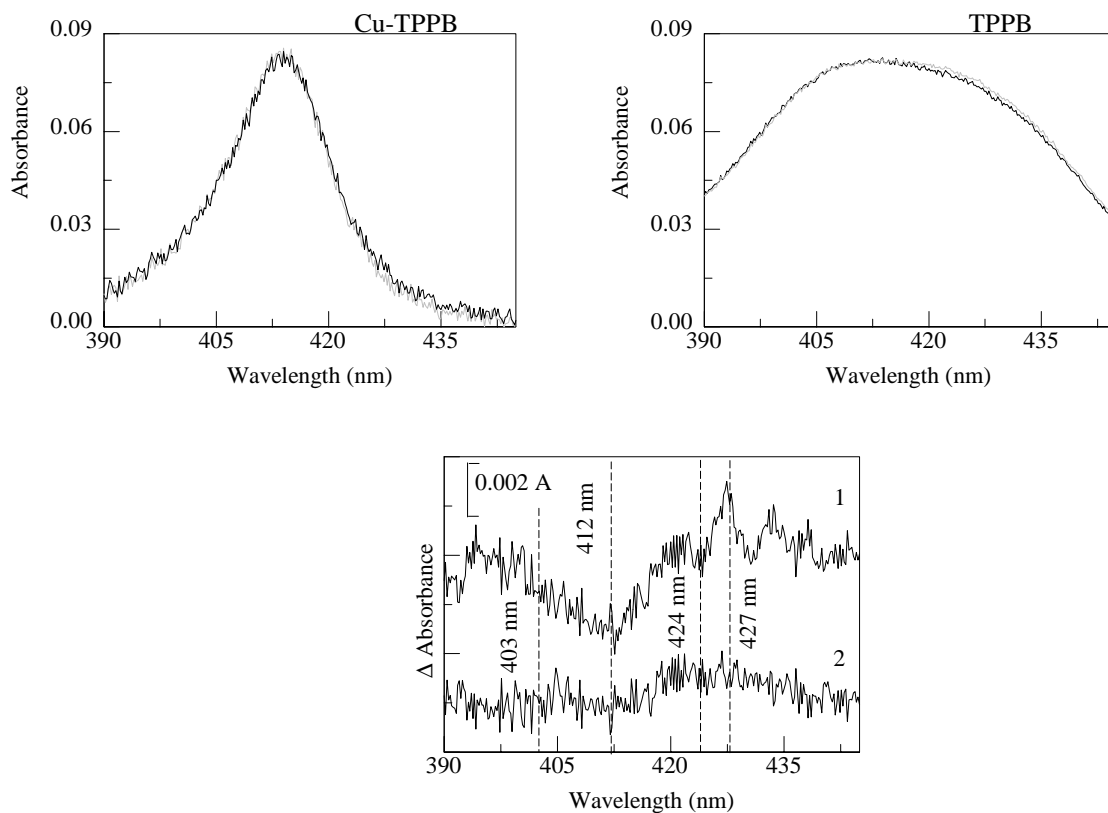


FIGURE 8.6 The spectra labeled TPPB and Cu-TPPB show the absorbance spectrum of the porphyrins before and after addition of CA. The (1) Cu-TPPB (1.6 μM) + CA (112 nM) minus Cu-TPPB and (2) TPPB (1.6 μM) + CA (112 nM) minus TPPB difference spectra show that the porphyrin interaction wavelengths differ between the two porphyrins as does the strength of the interaction.

LINEWEAVER-BURK PLOT OF CARBONIC ANHYDRASE ACTIVITY

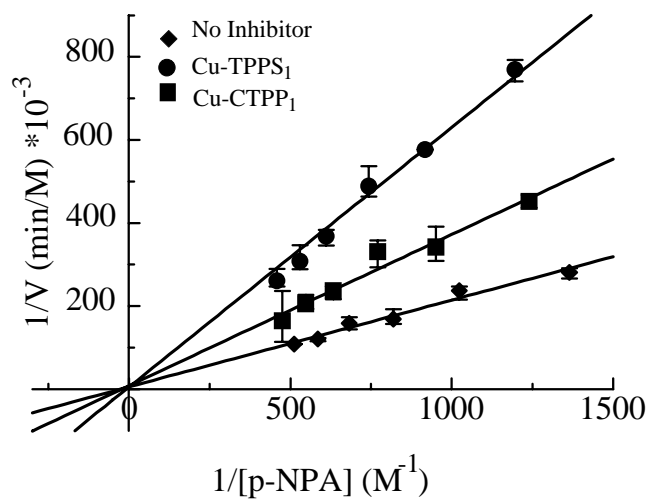


FIGURE 8.7 Enzymatic activity of carbonic anhydrase in the absence (◆)/presence of 3 μM Cu-TPPS₁ (●) and 1.8 μM Cu-CTPP₁ (■) shows a V_{max} of 170 $\mu\text{M}/\text{min}$ for p-NPA [399].

REVERSAL OF PORPHYRIN BINDING BY COMPETITIVE INHIBITORS

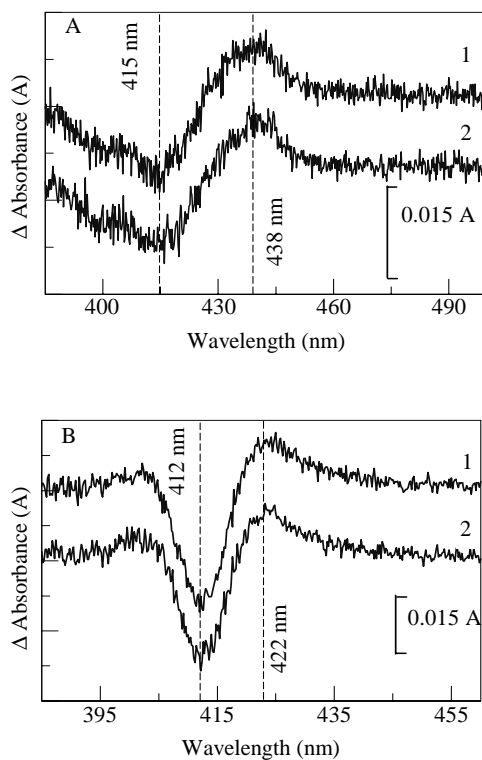


FIGURE 8.8 A. The reversal of Cu-TPPS₁ binding to CA demonstrated by the difference spectra Cu-TPPS₁ (1.8 μM)+ CA (112 nM)+ 1,10-phenanthroline (2 μM) minus Cu-TPPS₁ (1) and Cu-TPPS₁ (1.8 μM)+ 1,10-phenanthroline (2 μM) minus Cu-TPPS₁ (2) [399].

B. The reversal of Cu-CTPP₁ binding to CA demonstrated by the difference spectra Cu-CTPP₁ (1.8 μM)+ CA + 1,10-phenanthroline (2 μM) minus Cu-CTPP₁ (1) and Cu-CTPP₁ (1.8 μM)+ 1,10-phenanthroline (2 μM) minus Cu-CTPP₁ (2) [399].

EFFECT OF UNCOMPETITIVE INHIBITORS

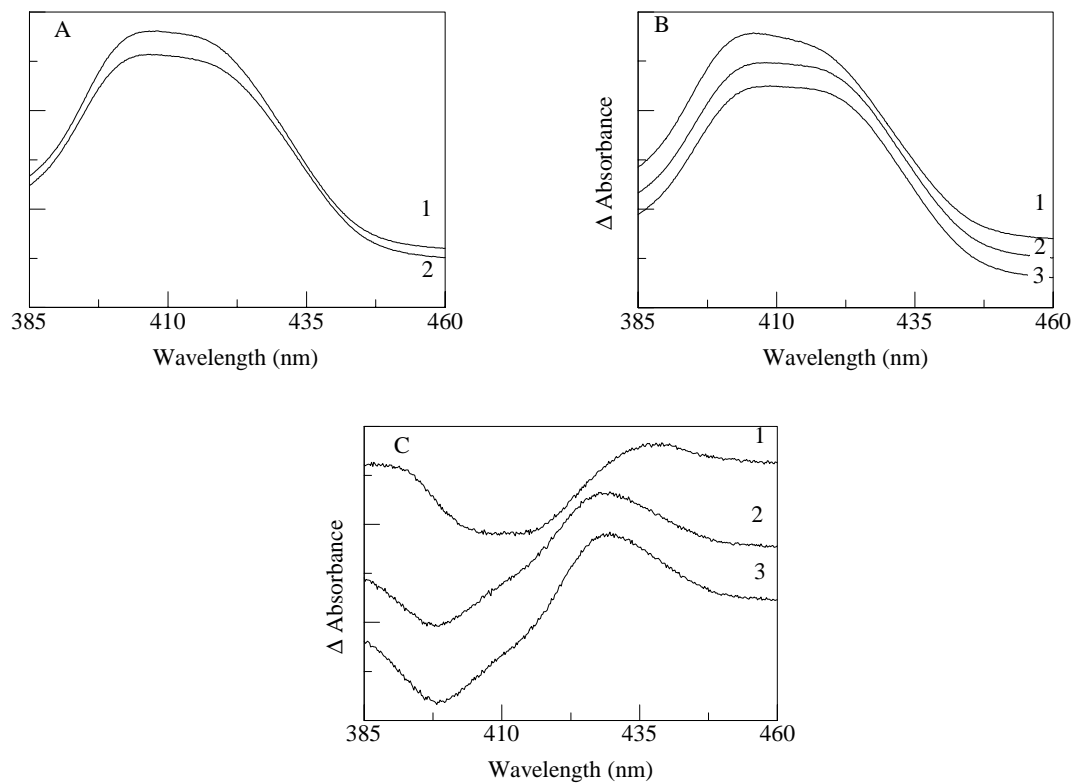


FIGURE 8.9 **A.** Cu-TPPS₁ (1) with 3.3 μ M sodium thiocyanate (2) a noncompetitive inhibitor of CA. **B.** Cu-TPPS₁ (1) with 112 nM carbonic anhydrase (2) and 3.3 μ M sodium thiocyanate (3). **C.** The difference spectra Cu-TPPS₁ (1.8 μ M) + sodium thiocyanate (3.3 μ M) minus Cu-TPPS₁ (1); Cu-TPPS₁ (1.8 μ M) + CA (112 nM) minus Cu-TPPS₁ (2); and Cu-TPPS₁ (1.8 μ M) + CA (112 nM) + sodium thiocyanate minus Cu-TPPS₁ (3). All samples are in 50 mM pH 7 NaPi.

EFFECT OF UNCOMPETITIVE INHIBITORS

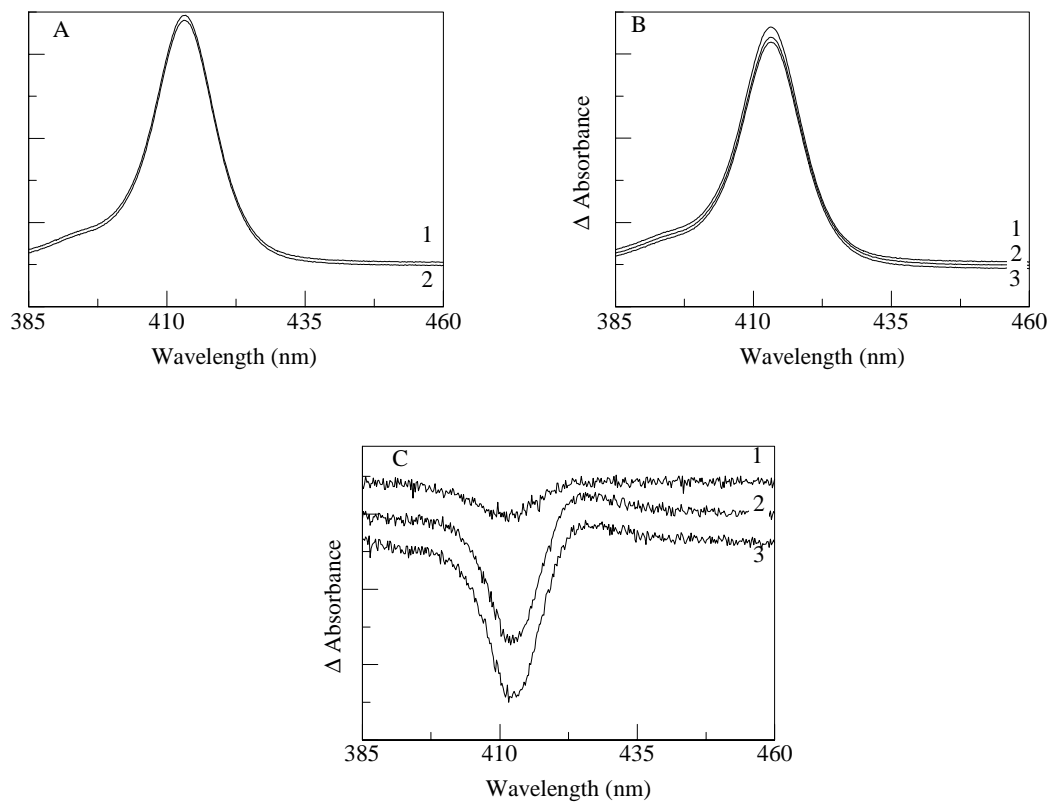


FIGURE 8.10 **A.** Cu-CTPP₁ (1) with 3.3 μ M sodium thiocyanate (2) a noncompetitive inhibitor of CA. **B.** Cu-CTPP₁ (1) with 112 nM carbonic anhydrase (2) and 3.3 μ M sodium thiocyanate (3). **C.** The difference spectra Cu-CTPP₁ (1.8 μ M) + sodium thiocyanate (3.3 μ M) minus Cu-CTPP₁ (1); Cu-CTPP₁ (1.8 μ M) + CA (112 nM) minus Cu-CTPP₁ (2); and Cu-CTPP₁ (1.8 μ M) + CA (112 nM) + sodium thiocyanate minus Cu-CTPP₁ (3). All samples are in 50 mM pH 7 NaPi.

CU-CTPP₁ INTERACTION WITH ZN-CONTAINING ACTIVE SITE

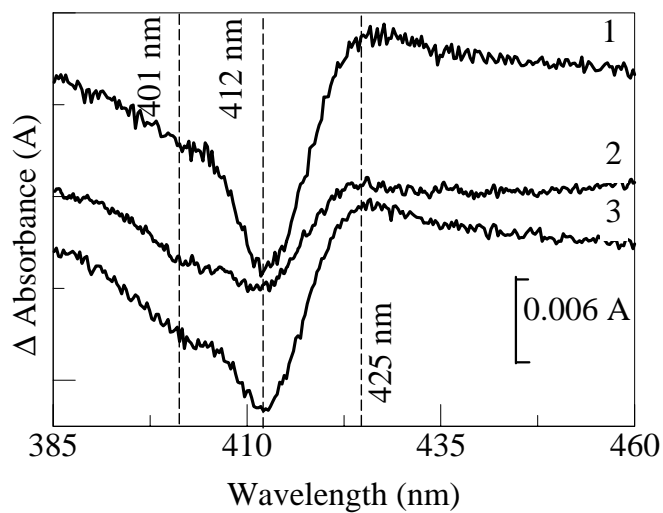


FIGURE 8.11 The difference spectra Cu-CTPP₁ + enzyme minus Cu-CTPP₁ for (1) carbonic anhydrase, (2) zinc free carbonic anhydrase, (3) zinc replaced carbonic anhydrase.

All samples are in 50 mM pH 7 NaPi [399].

Cu-TPPS₁ INTERACTION WITH ZN-CONTAINING ACTIVE SITE

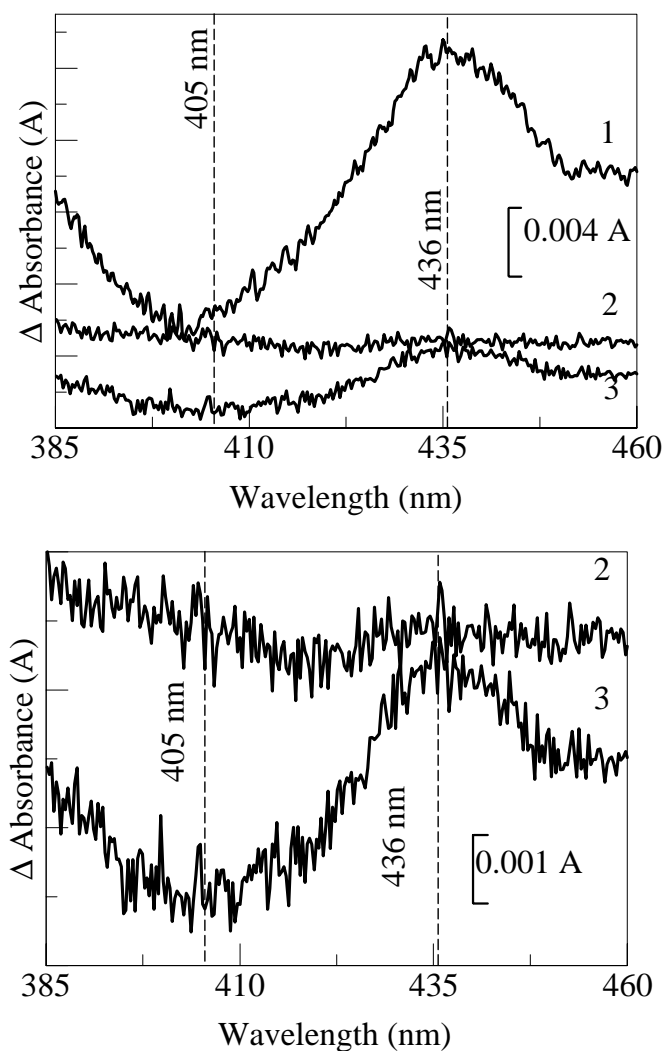


FIGURE 8.12 The difference spectra Cu-TPPS₁ + enzyme minus Cu-TPPS₁ for (1) carbonic anhydrase, (2) zinc free carbonic anhydrase, (3) zinc replaced carbonic anhydrase. All samples are in 50 mM pH 7 NaPi. The second figure shows Traces 2 and 3 on a more appropriate scale [399].

CU-TPPS₁ IES

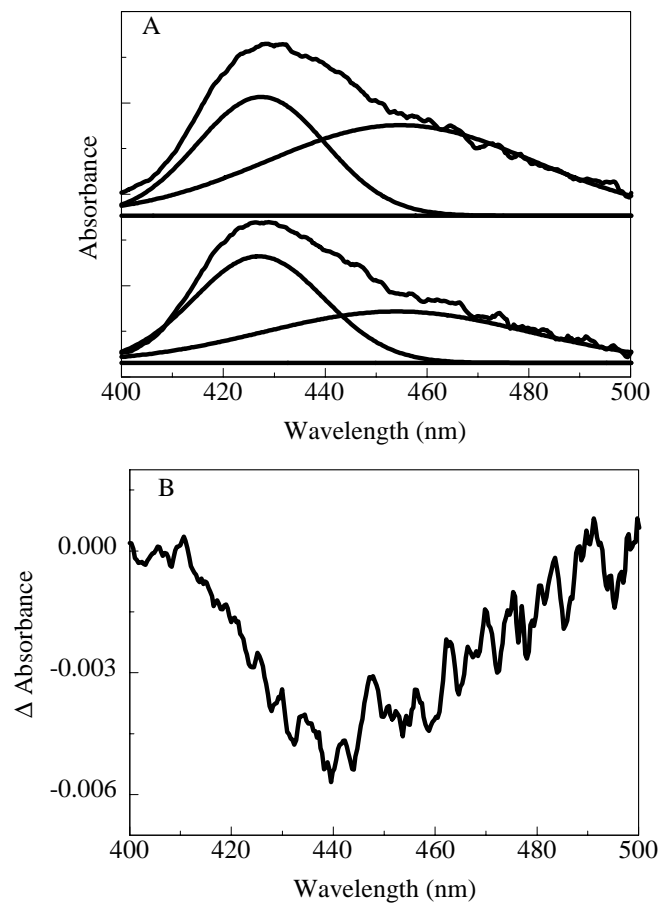


FIGURE 8.13 (A) The absorbance spectrum of the immobilized CuTPPS₁-CA complex before and after exposure to cysteine. (B) The difference spectrum CuTPPS₁ + CA + cysteine (10 ppm) minus CuTPPS₁ + CA for the immobilized CuTPPS₁-CA complex.

EXPOSURE OF IES TO INHIBITORS IN SOLUTION

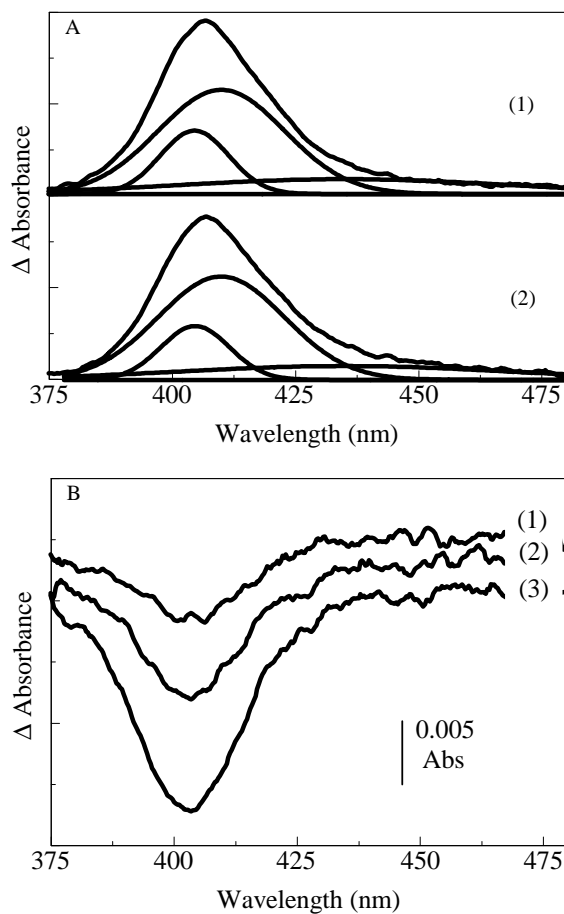


FIGURE 8.14 (A) The absorbance of the immobilized CA surface before (1) and after (2) exposure to cysteine shown with the results of peak fitting. (B) The difference spectra, IES + inhibitor minus IES, for 1 ppm 1,10-phenanthroline (1), 3 ppm cysteine (2), and 7 ppm saccharin (3) [399].

CONCENTRATION DEPENDENCE OF ABSORBANCE CHANGES

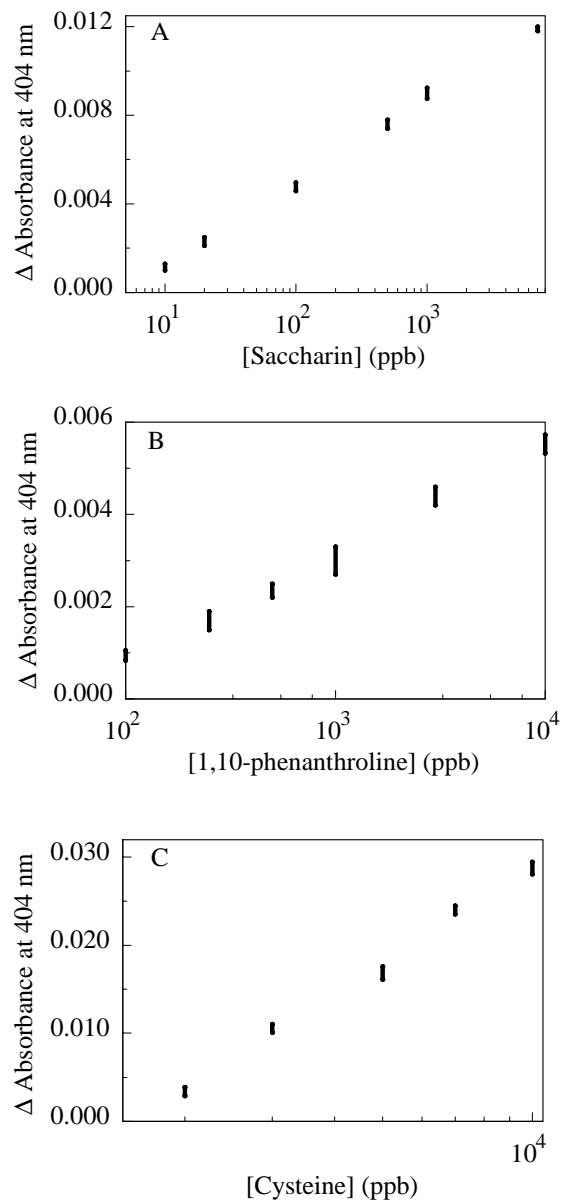


FIGURE 8.15 The dependence on concentration of the absorbance change at 404 nm upon exposure to: saccharin (A), 1,10-phenanthroline (B), cysteine (C) [399].

EXPOSURE OF IES TO CO₂ AS A VAPOR

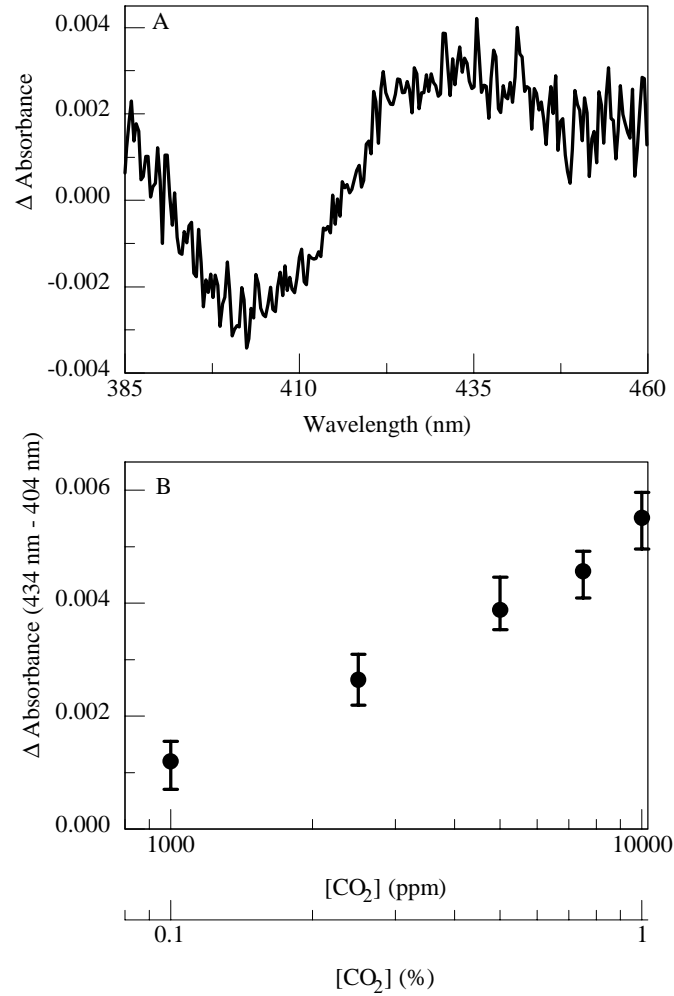


FIGURE 8.16 A. The difference spectrum CuCTPP₁ + CA + CO₂ (1%) minus CuCTPP₁ + CA for the immobilized CuCTPP₁-CA complex [399].

B. The concentration dependence of the absorbance change of the immobilized CuCTPP₁-CA complex upon CO₂ exposure [399].

CHAPTER 9

ORGANOPHOSPHORUS HYDROLASE

9.1 STRUCTURE AND FUNCTION

Organophosphorus compounds (OPs) are used as agricultural and domestic pesticides functioning as insecticides, fungicides, and herbicides. This class of compounds also includes chemical warfare agents such as sarin and soman. OPs inhibit the activity of cholinesterase in a nearly irreversible manner resulting in malfunction of nerve impulse transmission. The result in humans can be illness or even death. Exposure can result from occupational activities or can be a result of casual contact with contaminated air, food, or water. The potential health consequences of exposure make a simple, inexpensive detector of OPs desirable. Such a detector should be compact and light weight for portability and give a minimum of false positives/negatives with as little technical expertise as possible.

Organophosphorus hydrolase (OPH, often referred to as phosphotriesterase, systematic name aryltriphosphate dialkylphosphohydrolase) is capable of hydrolyzing a wide variety of OPs including those with P-O, P-F, P-CN, and P-S phosphoryl bonds to the phosphorus center (Figures 9.1 and 9.2). The protein active site contains two zinc atoms required for full catalytic activity [545]. The apo-enzyme can be activated by reconstitution with zinc (Zn^{2+}), cobalt (Co^{2+}), cadmium (Cd^{2+}), nickel (Ni^{2+}), or manganese (Mn^{2+}). Reconstitution with cobalt or cadmium results in a higher degree of enzymatic activity than that observed in the wild-type enzyme [546]. The enzymatic activity of OPH has been shown to be stable at temperatures up to 50° C [547].

The use of this enzyme for degradation of OPs as a decontamination protocol has been discussed extensively [547-557]. The hydrolysis rates of OPs by OPH exceed those of chemical hydrolysis using 0.1 N NaOH at 4° C by factors of 40 to 2450 times. OPH has also been used for detection of organophosphorus compounds both in microbial systems [472-473, 478] and as a purified enzyme [4, 10-12, 466, 480, 544, 558] using techniques such as optical, acoustic, potentiometric, and amperometric. Detection limits as low as 90 nM paraoxon and 70 nM methyl parathion have been demonstrated at a response time on the order of 10 seconds [4] and a theoretical limit of detection of 16 nM paraoxon has been reported for a slightly longer response time of 45 seconds [558].

9.2 MATERIALS AND METHODS

Monosulfonate tetraphenyl porphyrin (TPPS₁) and meso-tri(4-sulfonato phenyl) mono(4-carboxy phenyl) porphyrin (C₁TPP) were obtained from Frontier Scientific (Logan, UT). Copper metalloporphyrins were obtained by placing the porphyrin in solution at a concentration less than 45 μM with cupric sulfate overnight at 4° C. Diazinon, paraoxon, coumaphos, and malathion were obtained from Sigma (St. Louis, MO).

Organophosphorus hydrolase (OPH, EC 3.1.8.1) was obtained from the research group of Dr. A. Mulchandani using a protocol detailed by Omburo [546] using *E. coli* carrying plasmid pJK33. Cells are grown for 35 to 38 hrs at 31°C in a medium consisting of tryptone, yeast extract, glycerol, and potassium phosphate buffer. The cells were harvested by centrifugation and washed with water followed by resuspension in 50 mM HEPES buffer pH 8.5 containing 50 μM CoCl₂ with a protease inhibitor. The cells were

then lysed and the suspension was again centrifuged retaining the supernatant.

Polyethyleneimine was added to 0.4% followed by ammonium sulfate fractionation. The suspension was again centrifuged retaining the pellet. The pellet was then passed through a Sephadex G-150 column followed by a DEAE-Sephadex column. The protein was then concentrated by lyophilization, dialysed against the HEPES buffer and concentrated using a speed vac. The final specific activity of the protein was determined to be 7250 IU/mg protein based on the rate of p-nitrophenol (pNP) production per minute per milligram protein based on hydrolysis of 1 mM paraoxon in pH 8.5 at 30°C. The production of pNP can be monitored by the increase in absorbance at 412 nm (extinction coefficient 16500 M⁻¹ cm⁻¹). Purified enzyme was stored at less than 0°C.

The enzymatic activity of OPH in solution was measured spectrophotometrically at 412 nm at 37°C by the protocol of Mulchandani, et al. [441]. First, a background reaction rate was measured using a cuvette containing 2.7 ml 50 mM HEPES buffer pH 8.5 with 50 µM CoCl₂, x µl 10 mM paraoxon in methanol, (100 - x) µl methanol, y µl porphyrin, and (100 - y) µl water. After the background rate was measured, 20µl dilute OPH was added to the cuvette. The absorbance changes resulting from increasing pNP concentration were measured over time (see Chapter 2) at 412 nm.

OPH was immobilized to glass surfaces by the process described earlier for the cholinesterase systems (Chapters 4 and 5). Briefly, the ProbeOn™ Plus slides were activated by glutaraldehyde followed by interaction with amino-terminated Starburst® PAMAM dendrimer (generation 4, Aldrich, Milwaukee, WI). The remaining activated amino groups were blocked using TRIS. The resulting surface was again activated by glutaraldehyde and the steps repeated, that is, interaction with PAMAM dendrimer and

blocking of residual groups with TRIS. The surface coated now with two layers of PAMAM dendrimer was again activated with glutaraldehyde followed by exposure to the enzyme OPH (0.3 mg/ml) and blocking of remaining sites by TRIS. Slides were stored at room temperature after vacuum packing in three layer food saver bags using a FoodSaver (Vac360) from Tilia (San Francisco, CA). Binding of the porphyrin to the enzyme active site is accomplished by applying 0.5 mg/ml copper complexed meso-tri(4-sulfonato phenyl) mono(4-carboxy phenyl) porphyrin (Cu-CTPP₁) or copper complexed monosulfonate tetraphenyl porphyrin (Cu-TPPS₁) in 50 mM pH 7 sodium phosphate (Sorenson) buffer (NaPi) to the surface and allowing to interact for 15 minutes.

The enzymatic activity of the surfaces was measured as follows: 5 μ l 10 mM paraoxon in methanol and 195 μ l 100 mM pH 7 NaPi buffer were applied to the surface and allowed to interact for 3 minutes. A 1 ml cuvette was prepared containing 800 μ l H₂O and 150 μ l of the reacted solution was added. The spectrum of the resulting sample was measured using a Cary 4 at 2 nm resolution from 350 to 650 nm. The activity was monitored by the intensity of the absorbance at 412 nm.

The viability of the slides was also verified by challenging the immobilized porphyrin-enzyme complex with diazinon. Porphyrin was applied to the surfaces less than three hours prior to surface response testing. Response was determined by exposing the surface to 200 μ l 30 ppb diazinon in 50mM pH 7 NaPi for 3 minutes and measuring the resulting change in absorbance at 417 nm. The absorbance spectra of the slides was measured by the evanescent wave technique described previously (Chapter 5) using an Ocean Optics USB2000 spectrophotometer with an LED light source (maximum wavelength 434 nm, 83 nm FWHM).

9.3 RESULTS

We investigated the interaction of several porphyrins with OPH in order to determine those that elicited a peak-trough pair in the difference spectrum porphyrin + enzyme minus porphyrin upon interaction with OPH. Figure 9.3 shows the difference spectra porphyrin + OPH minus porphyrin for TPPS₁, NH₂TPP, CTPP₁, and TPPS₄. Though the absorbance spectra of TPPS₁ and NH₂TPP were strongly effected by the presence of OPH, no clear effect on the porphyrin-enzyme complex could be observed upon addition of diazinon. Diazinon was chosen rather than paraoxon because the hydrolysis product does not absorb in the region of interest.

Experiments with carbonic anhydrase (Chapter 8) [399] indicated that copper metalloporphyrins would be more likely to interact with the active site of OPH. Figure 9.4 shows the interaction of Cu-NH₂TPP with OPH as well as the effect of diazinon on the complex and the binding of Cu-NH₂TPP to the OPH-diazinon complex. Interaction of Cu-NH₂TPP with diazinon does not result in a change in the absorbance spectrum. Results of peak fitting of the data are also presented for emphasis. The data shows very little change in the absorbance spectrum of the porphyrin-enzyme complex upon addition of diazinon, however, binding of Cu-NH₂TPP to the OPH-diazinon complex shows strongly different results from those of binding to OPH alone. The indication is that the porphyrin binds to a site on the enzyme other than at the active site. The large difference in the binding of the porphyrin to OPH alone and the binding to the OPH-diazinon complex is likely due to the change in conformation of the enzyme allowing the

porphyrin to bind to a different combination of residues. In the case of Cu-NH₂TPP, this binding is much stronger than that to OPH alone.

The difference spectrum CuTPPS₁ + OPH minus CuTPPS₁ shows the changes in the CuTPPS₁ absorbance spectrum upon interaction with OPH with a peak at 422 nm and a trough at 400 nm (Figure 9.5, Trace 1). The interaction of CuTPPS₁ with diazinon results in a difference spectrum with a pair of troughs at 408 nm and 426 nm and no new peak (Figure 9.5, Trace 2). The characteristics of the difference spectrum for the interaction of CuTPPS₁ with OPH and diazinon (Figure 9.5, Trace 3) are different than the sum of the interactions with OPH (Trace 1) and diazinon (Trace 2) alone. The 419 nm peak observed in the OPH spectrum is no longer apparent, however, a peak at 417 nm observed for neither OPH nor diazinon is observed in this difference spectrum. This indicates that diazinon does effect the binding of CuTPPS₁ to OPH, but what effect it has it is not clear. CuTPPS₁ and CuC₁TPP absorbance spectra showed stronger, more specific changes than other copper-porphyrin absorbance spectra.

Cu-CTPP₄ and Cu-TPPS₄ did not give a peak trough pairs upon interaction with OPH. The interaction of Cu-CTPP₁ with OPH is shown in Figure 9.6. The interaction of Cu-CTPP₁ with OPH (shown in Figure 9.6, Trace A) results in a shift in the absorbance spectrum of Cu-CTPP₁ from 412 nm to 419 nm. The interaction of diazinon with Cu-CTPP₁ results in a shift in absorbance from 406 to 413 nm (Figure 9.6, Trace D). When the Cu-CTPP₁-OPH complex is exposed to diazinon, there is a loss in absorbance intensity for the Cu-CTPP₁-OPH complex at 403 nm with no corresponding increase in absorbance (Figure 9.6, Trace C). The difference spectrum Cu-CTPP₁ + OPH + diazinon minus Cu-CTPP₁ shows the effect of OPH and diazinon on the spectrum (Figure 9.6,

Trace B). The results of peak fitting this trace indicate that some of the Cu-CTPP₁-OPH interaction remains. This is apparent from the presence of trough at 419 and peak at 412 nm as in the Cu-CTPP₁ + OPH minus Cu-CTPP₁ spectrum. In the presence of diazinon these peaks have 80% of the intensity observed in the presence of OPH alone. This generally indicates partial reversal of binding, however, the peak/trough pair appearing in this spectrum at 423 and 401 nm are not the characteristic peaks for the Cu-CTPP₁-diazinon interaction as would be expected. If the porphyrin binds at an allosteric site on the enzyme rather than at the active site, the binding of a competitive inhibitor could cause a conformational change in the protein which would influence the spectral characteristics of the porphyrin. The result would be peaks in the difference spectrum characteristic for neither the porphyrin-inhibitor interaction nor the porphyrin-OPH interaction, as observed here.

Lineweaver-Burk plots of OPH activity in the absence/presence of porphyrin inhibitors are shown in Figure 9.7. The linear plots of rate⁻¹ versus substrate concentration⁻¹ indicate that inhibition of OPH by Cu-CTPP₁ and Cu-TPPS₁ is mixed type inhibition. Intersection of the two lines (absence/presence of porphyrin) at the y-axis would indicate no change in maximal enzymatic rate (V_{\max}) and therefore competitive inhibition. The substrate concentration needed to achieve half of V_{\max} (K_m) for paraoxon under the above described conditions is 76 μM with a V_{\max} of 1 mM/min. In the presence of 250 nM Cu-CTPP₁ both K_m and V_{\max} are changed giving 359 μM and 814 $\mu\text{M}/\text{min}$, respectively while in the presence of 150 nM Cu-TPPS₁ $K_m = 124 \mu\text{M}$ and $V_{\max} = 493 \mu\text{M}/\text{min}$. Cu-NH₂TPP did not inhibit the activity of OPH.

OPH was immobilized to ProbeOn Plus microscope slides and allowed to interact with Cu-CTPP₁. The immobilized OPH-Cu-CTPP₁ absorbance spectrum as measured by the evanescent technique is shown in Figure 9.8. Peak fitting this spectrum indicates the involvement of two peaks at 412 nm and 430 nm. Upon addition of paraoxon to the slide surface, a loss in intensity of the 412 nm peak is observed with no loss in intensity at the 430 nm peak. The implication is that the 412 nm peak is due to interaction of the porphyrin with the active site of the enzyme while the 430 nm peak results from nonspecific interaction with other areas of the enzyme or with other parts of the slide surface.

The loss in intensity at 412 nm shows log-linear dependence on paraoxon concentration (Figure 9.9) with a 3:1 S/N detection limit of 7 ppt. The interaction of other OPH substrates with the surface was also investigated. All substrates showed the log-linear dependence on concentration with limits of detection at 800 ppt diazinon, 250 ppt coumaphos, and 1.0 ppb malathion (Figures 9.9 and 9.10).

The lifetime of the slide surfaces is an important issue to be considered when designing a system to be used outside of a laboratory environment. Slides were stored under vacuum (as described above) prior to porphyrin exposure. The enzymatic activity of the slides was monitored over a period of 232 days and the response of porphyrin-enzyme complex to inhibitor exposure was monitored over a period of 100 days (Figure 9.11). No significant changes in enzymatic activity were observed using a paraoxon assay. Substrate challenge of the CuC₁TPP surfaces by 30 ppb diazinon in 50 mM pH 7 NaPi yielded the expected loss in absorbance at 412 nm throughout the trials.

9.4 DISCUSSION

We have demonstrated the use of CuC₁TPP as a colorimetric indicator for the binding of organophosphates to organophosphorus hydrolase. A log-linear relationship exists between the absorbance change at 412 nm and concentration for diazinon, paraoxon, coumaphos, and malathion. Unlike previously described work with other enzymes [393, 397-398], the inhibition of OPH by Cu-CTPP₁ is not competitive rather it is mixed type inhibition. Mixed-type inhibition involves the binding of inhibitor to two or more sites on the enzyme one of them being the active site. Cu-TPPS₁ also inhibits the activity of OPH in a mixed manner, however, the changes in absorbance upon substrate exposure for the Cu-TPPS₁-OPH complex were much less intense than those of the Cu-CTPP₁-OPH complex resulting in higher limits of detection. Our detection system will work for porphyrins binding at the active site of the enzyme regardless of whether they are competitive or mixed type inhibitors. 7 ppt (25 x 10⁻¹² M) paraoxon can be detected with immobilized Cu-CTPP₁-OPH complex exceeding the detection limits reported previously [4] for OPH based systems with a response time of less than 10 seconds. The surface relies on the binding specificity of the enzyme responding only to the presence of those compounds that bind at the active site of OPH.

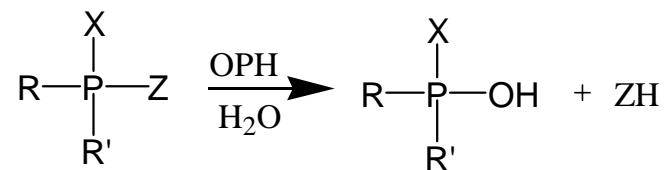
The prototype system for evanescent absorbance spectrum measurements includes a sample holder, Ocean Optics USB2000 with lithium battery pack, diode light source, and Compaq Pocket PC for a total weight of less than one kilogram (Figure 9.12). We have had limited success in developing a system employing small solid-state photodiodes fitted with bandpass filters for detection of absorbance changes. A system of this type

would be less expensive, lighter weight, and more compact, desirable characteristics for a system to be used by first responders or military personnel.

We have described a broad spectrum detection protocol for the presence of organophosphates. Identification of the specific compound involved is not possible using this system as described. In the cases of organophosphates with hydrolysis products that absorb in the region between 400 and 500 nm (paraoxon, coumaphos), identification may be possible based on the absorbance spectrum. For other organophosphate compounds, there are two possibilities for identification. For the first possibility, a range of concentrations can be assayed to obtain a slope that can be compared to the slope of the absorbance change versus concentration for known compounds. This requires much more time than a single measurement. Second, a combination of enzymes with varying sensitivity to OPs can be used to achieve a system capable of identifying the particular OP involved. Systems of this type have been described previously using OPH with acetylcholinesterase [466] or a combination of cholinesterases [395, 435, 470]. In a system of this type the different enzymes respond simultaneously, so that response time is not increased. There has been some work on mutation of OPH to change the binding specificity for different substrates [559-561] and there are other enzymes that bind OPs including organophosphorus acid anhydrase. Combinations of OPH as used here with other OP binding enzymes could be used in a system similar to the one described here allowing for identification of the detected analyte.

REACTION CATALYSED BY OPH

IN GENERAL:



PARAOXON:

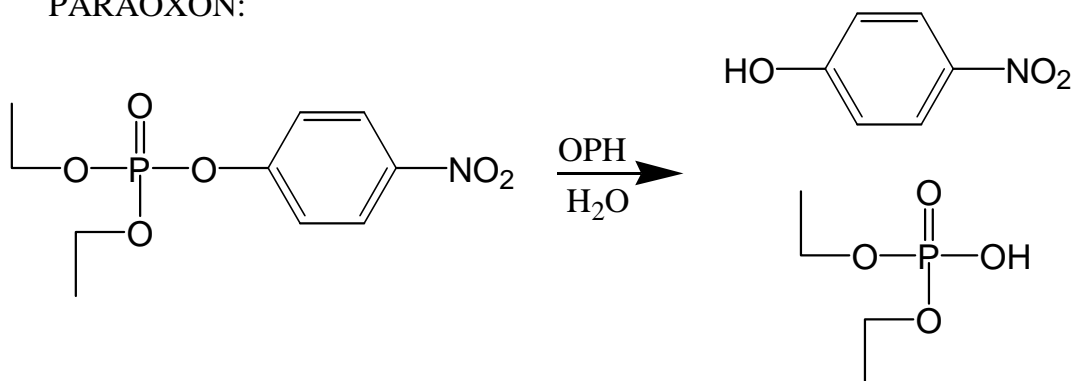


FIGURE 9.1 OPH catalyses the hydrolysis of the phosphoryl bond of OPs. Hydrolysis of paraoxon yields p-nitrophenol with an absorption peak at 412 nm ($\epsilon = 16500 \text{ M}^{-1} \text{ cm}^{-1}$) [544].

ORGANOPHOSPHATES

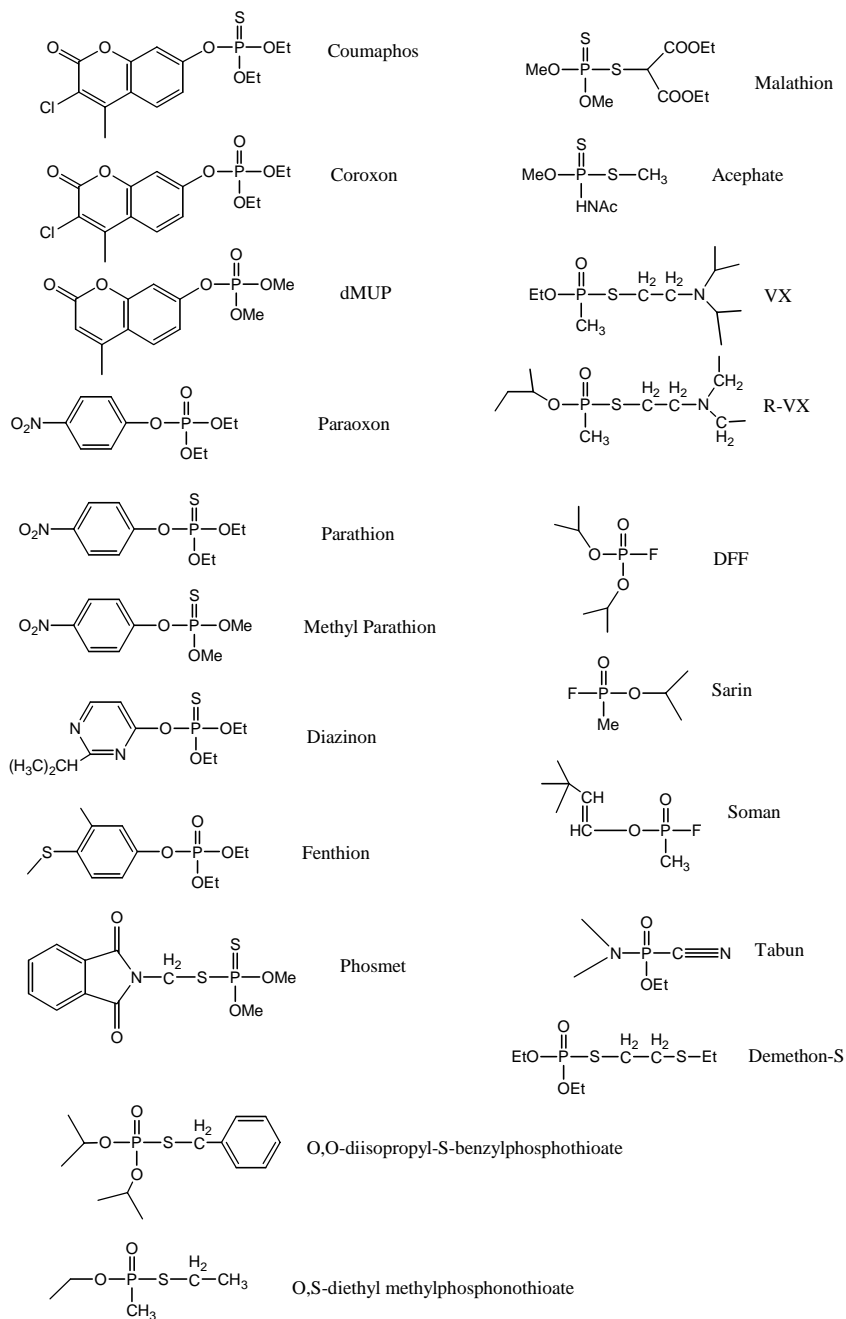


FIGURE 9.2 Structures of some organophosphate compounds.

INTERACTION OF OPH WITH PORPHYRINS IN SOLUTION

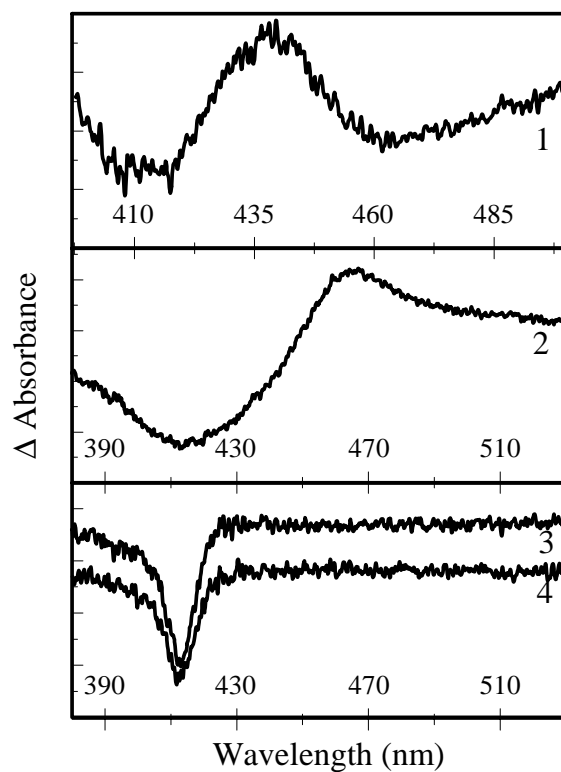


FIGURE 9.3 The interaction of TPPS₁ (Trace 1), NH₂TPP (Trace 2), CTPP₁ (Trace 3), and TPPS (Trace 4) with OPH shown as difference spectra, porphyrin + OPH minus porphyrin.

INTERACTION OF OPH WITH CU-NH₂TPP IN SOLUTION

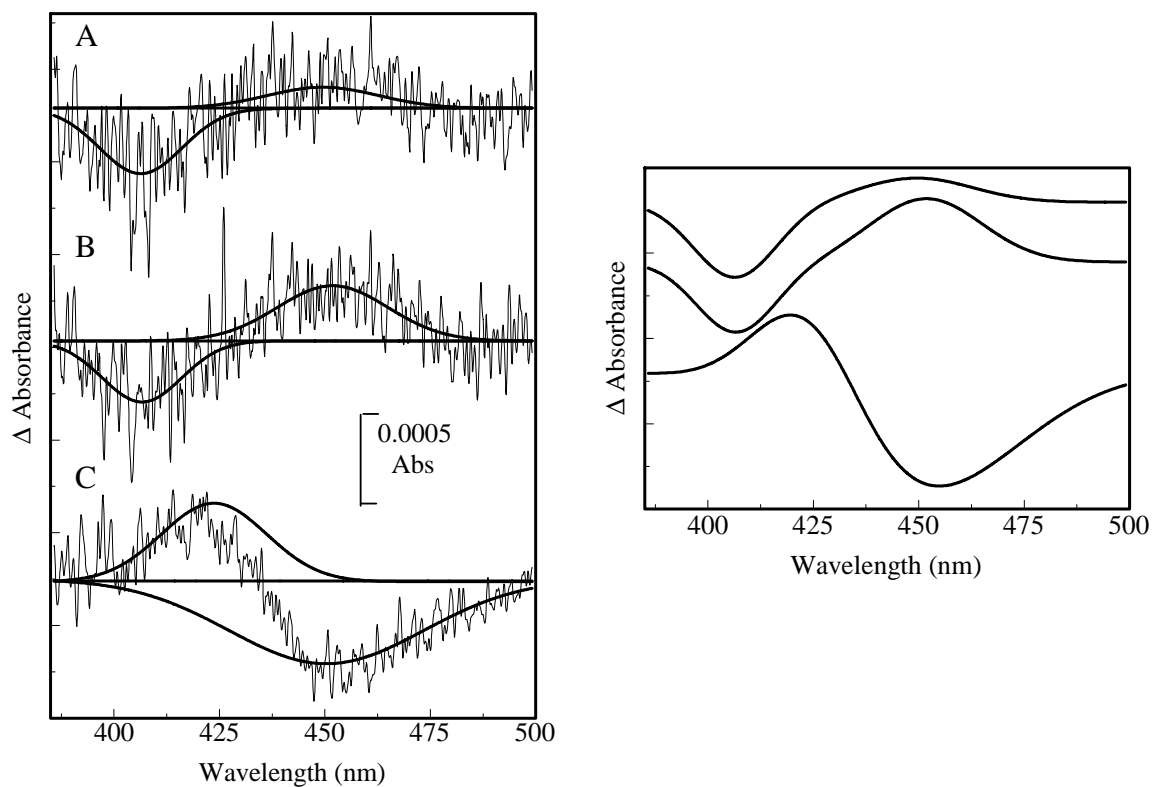


FIGURE 9.4 The difference spectra Cu-NH₂TPP + OPH minus Cu-NH₂TPP (A), Cu-NH₂TPP + OPH + Diazinon minus Cu-NH₂TPP (B), and Diazinon + OPH + Cu-NH₂TPP minus Cu-NH₂TPP (C) are shown along with the results of peak fitting the spectra in Grams/32.

INTERACTION OF OPH WITH CU-TPPS₁ IN SOLUTION

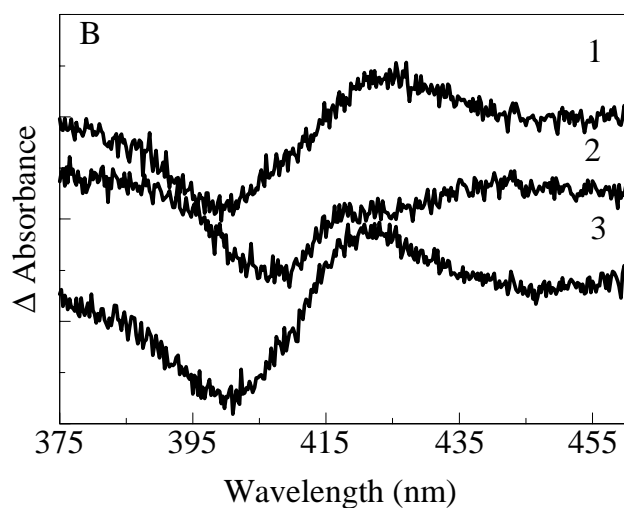


FIGURE 9.5 The interaction of CuTPPS₁ with OPH and diazinon:

CuTPPS₁ (1.0 μM) + OPH (3 μg, 7250 IU/mg) minus CuTPPS₁ (Trace 1);

CuTPPS₁ (1.0 μM) + diazinon (65 nM) minus CuTPPS₁ (Trace 2);

CuTPPS₁ (1.0 μM) + OPH (3 μg, 7250 IU/mg) + diazinon (65 nM) minus
CuTPPS₁ (Trace 3) [396].

INTERACTION OF OPH WITH CU-CTPP₁ IN SOLUTION

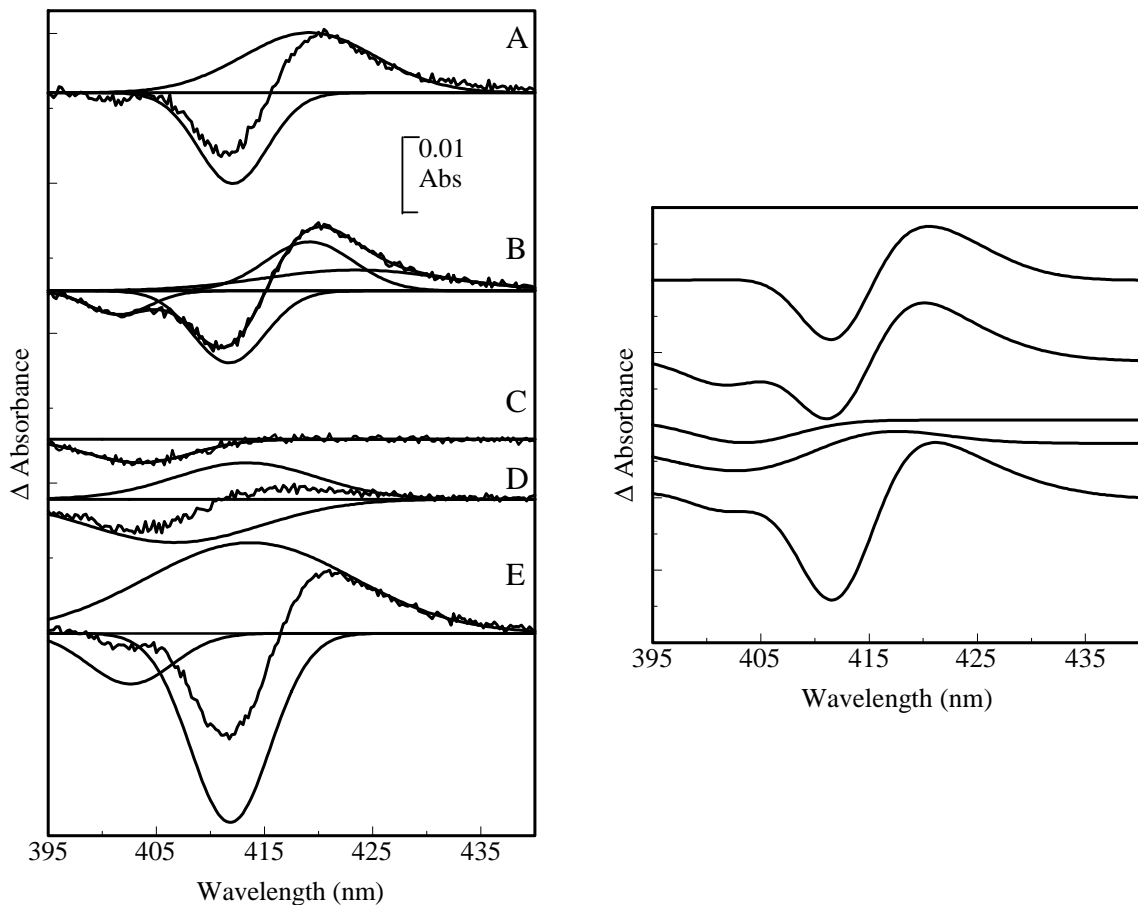


FIGURE 9.6 The difference spectra Cu-CTPP₁ (1.4 μM) + OPH (3 μg, 7250 IU/mg) minus Cu-CTPP₁ (A), Cu-CTPP₁ + OPH + Diazinon minus Cu-CTPP₁ (B), Cu-CTPP₁ (1.4 μM) + OPH (3 μg, 7250 IU/mg) + Diazinon (65 nM) minus Cu-CTPP₁ + OPH (C), Cu-CTPP₁ + Diazinon minus Cu-CTPP₁ (D), and Diazinon + OPH + Cu-CTPP₁ minus Cu-CTPP₁ (E) are shown along with the results of peak fitting the spectra in Grams/32 [396].

LINEWEAVER-BURK PLOT OF OPH ACTIVITY

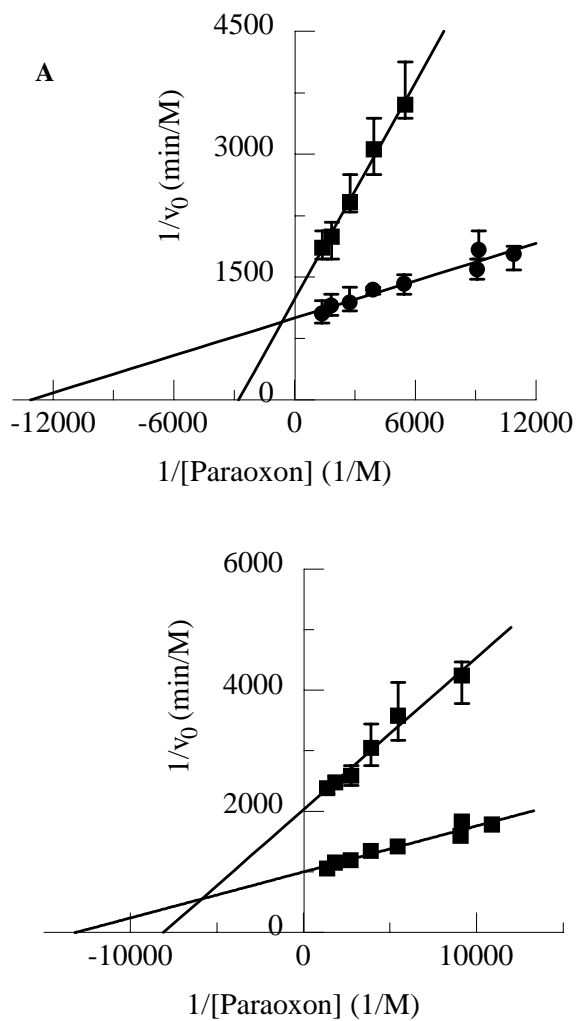


FIGURE 9.7 A. Lineweaver-Burk plot of organophosphorous hydrolase activity in the absence ($K_M = 76 \mu\text{M}$, $V_{\text{max}} = 1 \text{ mM/min}$) /presence of 250 nM Cu-CTPP₁ ($K_M = 359 \mu\text{M}$, $V_{\text{max}} = 814 \mu\text{M/min}$).

B. Lineweaver-Burk plot of organophosphorous hydrolase activity in the absence ($K_M = 76 \mu\text{M}$, $V_{\text{max}} = 1 \text{ mM/min}$) /presence of 150 nM Cu-TPPS₁ ($K_M = 124 \mu\text{M}$, $V_{\text{max}} = 493 \mu\text{M/min}$) [396].

OPH SLIDE RESPONSE TO ANALYTE EXPOSURE

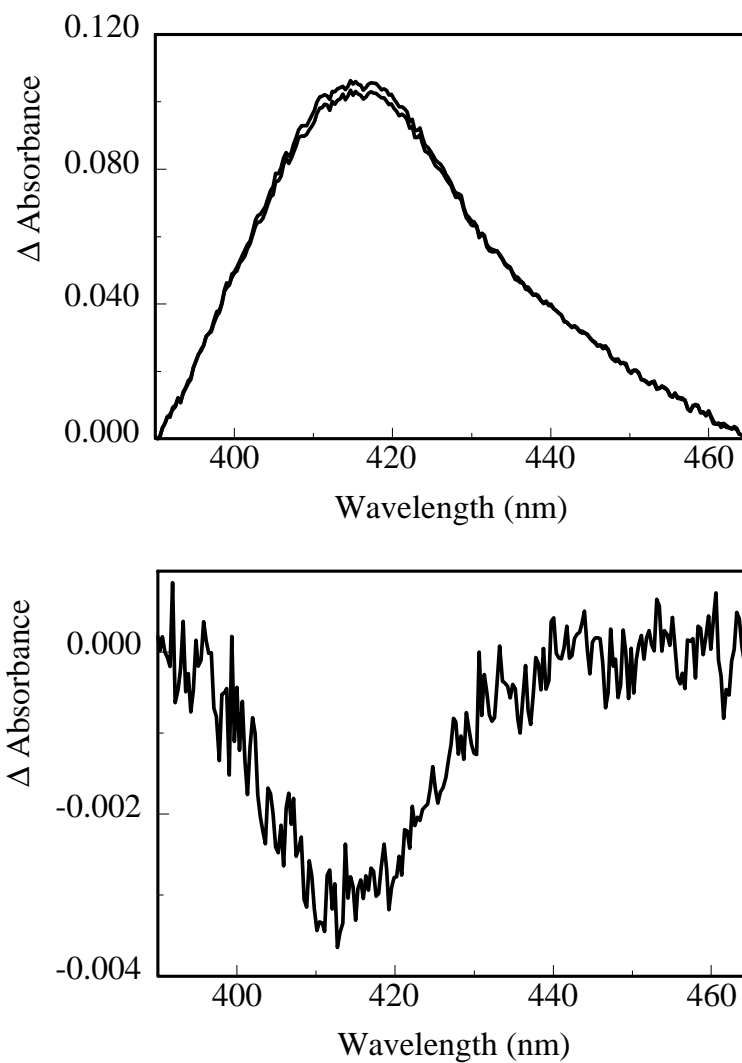


FIGURE 9.8 The change in absorbance of the immobilized CuCTPP₁-OPH complex upon exposure to 5 ppb paraoxon shown here as the difference spectrum CuCTPP₁-OPH + paraoxon minus CuCTPP₁-OPH [396].

CONCENTRATION DEPENDENCE OF OPH RESPONSE

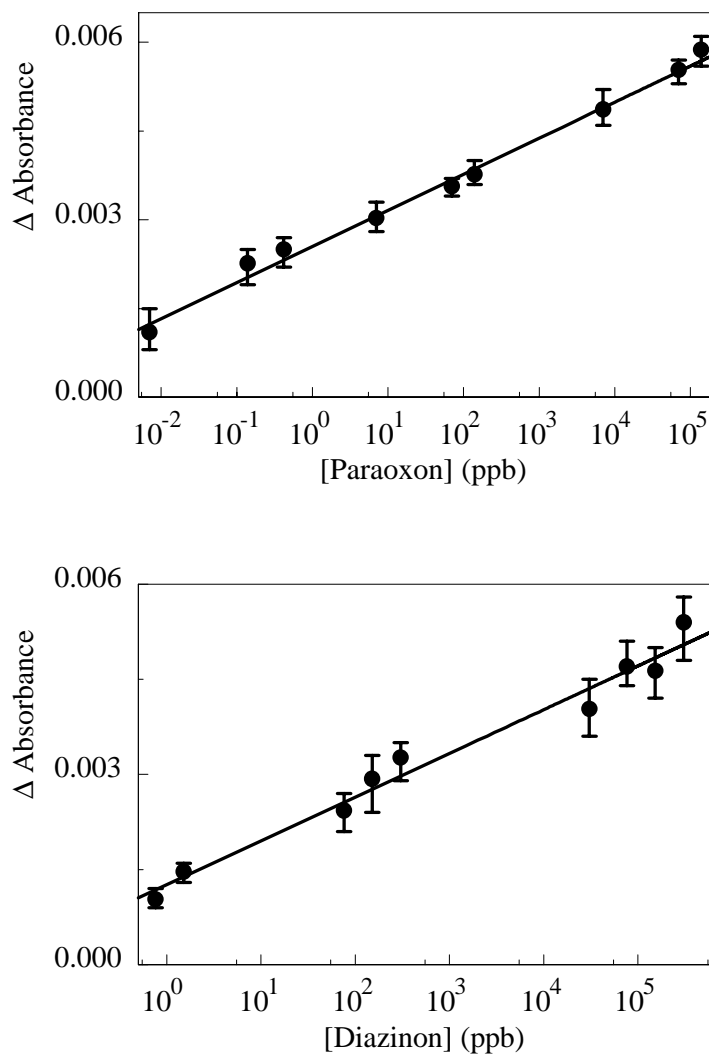


FIGURE 9.9 The concentration dependence of the change in absorbance at 414 nm of the immobilized Cu-CTPP₁-OPH complex upon exposure to paraoxon (A) and diazinon (B). All samples were buffered in 50 mM pH 7 NaPi [396].

OTHER OPH SUBSTRATES

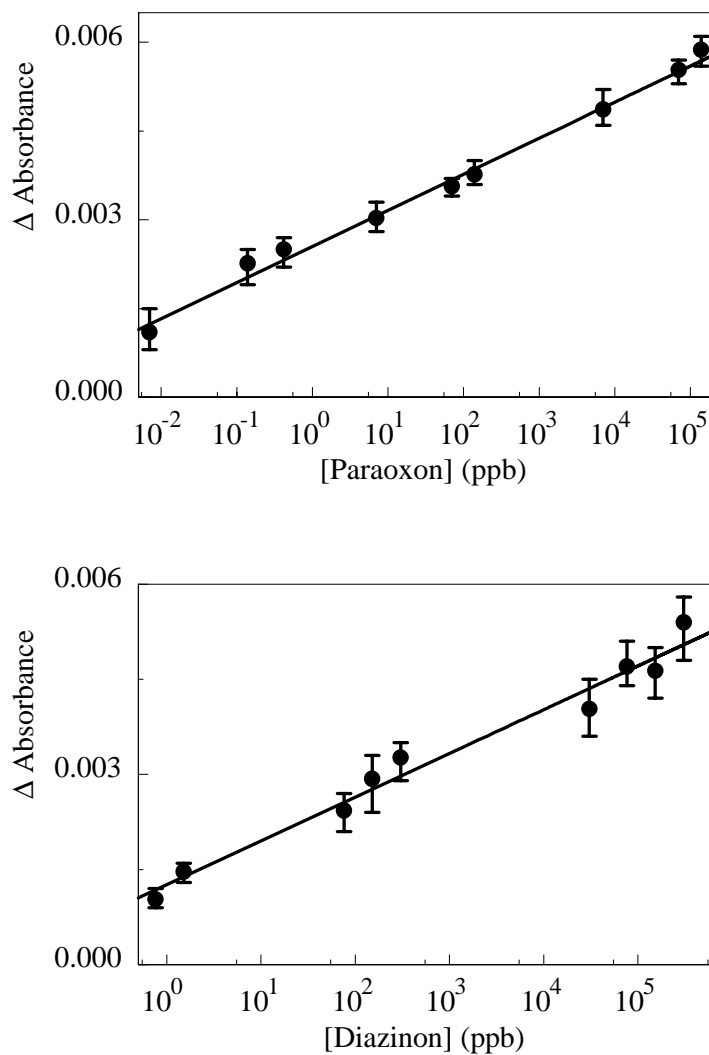


FIGURE 9.10 The concentration dependence of the change in absorbance at 412 nm of the immobilized Cu-CTPP₁-OPH complex upon exposure to coumaphos (A) and malathion (B). All samples were buffered in 50 mM pH 7 NaPi [396].

OPH SLIDE LIFETIMES

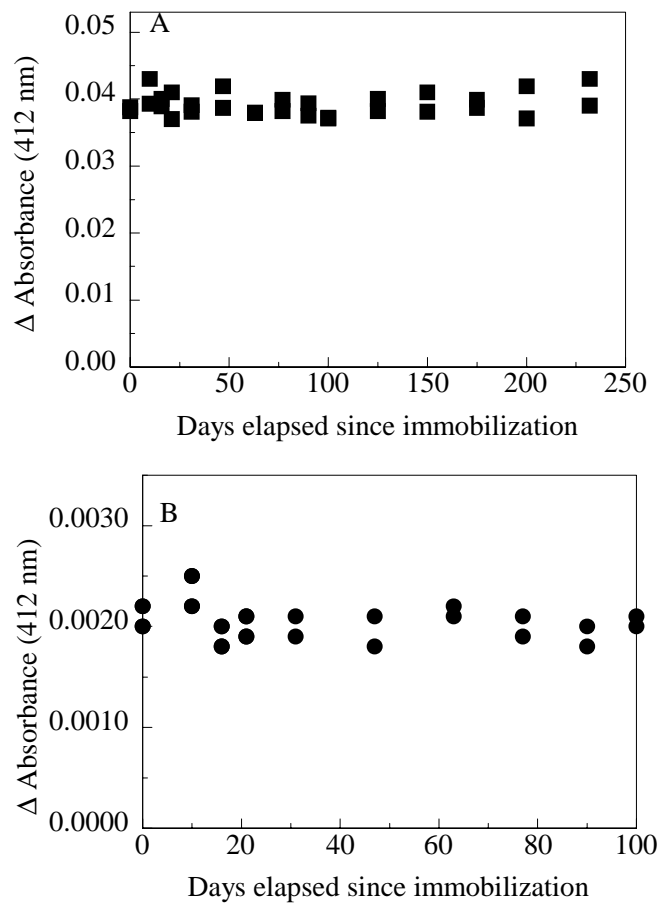


FIGURE 9.11 A. Activity of OPH slides over 232 days measured by paraoxon assay [396].
B. Activity of OPH slides over 100 days as measured by response to diazinon challenge [396].

PORTABLE UNIT



FIGURE 9.12 The portable experimental setup with USB2000 and PDA.

CHAPTER 10

DETECTION OF DIPICOLINIC ACID

10.1 BIOLOGICAL TARGETS

Dipicolinic acid (DPA) comprises from 5 – 15% of the total dry weight of bacterial spores [562]. DPA is a useful but non-specific indicator of the presence of bacterial spores such as *Bacillus anthracis* (anthrax) and *Clostridium botulinum* (botulism)[562] as well as members of the genus *Bacillus* that are non-virulent since it is a nearly universal component of *Bacillus* spores. Recent threats of contamination in the United States and the continuing danger to military personnel and civilians alike indicate the need for a detector of biological agents that operates in real time and that can function in a variety of environments. Several methods for detection of bacterial spores have been developed including PCR [563-564], immunofiltration assay [565-566], polymorphism analysis [567], direct detection of DNA sequences [568], liquid chromatography [569], FT-IR [570] and those which indicate bacterial spore presence by detection of DPA [571-581].

One method currently employed for detection of DPA is to measure the increase in terbium fluorescence when it binds DPA [566, 568, 569, 581]. In this method, solutions of DPA or bacterial spores are mixed with terbium solutions followed by separation of insoluble materials. Emission and excitation spectra are recorded from 450 nm to 640 nm and 270 nm to 280 nm respectively. The Tb fluorescence intensity increases without a wavelength shift in the emission spectrum [565-566, 568-569, 581]. However, phosphate containing compounds quench the fluorescence of the Tb-DPA

complex [569]; this problem can be solved by adding AlCl_3 to the solution prior to separation of insoluble particles [581] to remove phosphate from solution.

Porphyrins can be immobilized to a variety of surfaces including cellulose, polystyrene, glass, and quartz [454-456]. Immobilized meso-tetra (4-sulfonatophenyl) porphine (TPPS) has been shown to detect the presence of several analytes including naphthalene, ethanol, acetone, and formaldehyde [456]. Schneider and Wang [284] demonstrated that several aromatic compounds such as pyridine and benzoic acid interact with different porphyrins resulting in compound specific spectrophotometric shifts. Here we report the effect of dipicolinic acid on the visible spectrum of six water-soluble porphyrins and the corresponding zinc and copper metalloporphyrins at different pH values in solution. The data indicate that the absorbance spectra of three porphyrins are sensitive to the presence of low concentrations of DPA and could be useful in the detection of DPA.

10.2 MATERIALS AND METHODS

Monosulfonate tetraphenyl porphyrin (TPPS_1), tetra(4-aminophenyl) porphyrin (NH_2TPP), meso-tetra(4-boronic acid) porphyrin (TPPB), meso-tri(4-sulfonato phenyl) mono(4-carboxy phenyl) porphyrin (CTPP_1), meso-tetra(4-sulfonatophenyl)porphine (TPPS), meso-tetra(4-carboxyphenyl)porphine (CTPP_4), and meso-tri(4-sulfonatophenyl)mono(4-carboxyphenyl)porphine-cytosine amide (TPSC_1) were obtained from Frontier Scientific (Logan, UT) and used without further purification. Dipicolinic acid (DPA) was obtained from Sigma (St. Louis, MO). Picolinic acid and benzoic acid were obtained from Aldrich (Milwaukee, WI). Pyridine was obtained from Eastman Kodak (Rochester, NY). Porphyrin-copper and porphyrin-zinc complexes were formed

by mixing the respective porphyrin and cupric sulfate or zinc acetate in solution in a one to one ratio and allowing to incubate overnight at 4°C.

Visible light absorbance spectra of each porphyrin in the presence/absence of DPA, picolinic acid, benzoic acid, and pyridine were recorded at room temperature in 25 mM sodium phosphate (Sorenson) buffer (NaPi) at pH 5.5, 7, and 11 with a Cary 4E spectrophotometer at 0.02 nm resolution. Absorbance spectra of each porphyrin in the absence/presence of DPA were recorded at room temperature in buffer solution made in D₂O instead of H₂O and in 7 M urea at pH 7. Difference spectra were obtained by subtraction of absolute spectra using Grams/32 (Galactic Industries, Salem, NH). The peak positions indicated in the figures were determined using the 2nd derivative of the spectra taken with Grams/32. Linear fittings were preformed using PSI-Plot (V 6.0a) at a 99% confidence interval. The concentration dependence curves shown in Figures 10.1, 10.2, and 10.4 are the result of 5 separate titrations while those in Figures 10.3, 10.5, 10.6, and 10.7 are the result of 3 titrations. Extinction coefficients for the porphyrins were determined experimentally by measurement of the absorbance of solutions of different porphyrin concentrations. Fluorescence spectra were recorded as described for absorbance spectra with a SPEX Fluoromax 3 spectrofluorometer (JY-Horiba, Edison, NJ) using 2.5 nm resolution for excitation wavelength and 1.0 nm resolution for emission wavelength.

Covalent immobilization of NH₂TPP to glass was accomplished at room temperature on ProbeOn™ Plus microscope slides obtained from Fisher Biotech (Pittsburgh, PA.). Microscope slides were activated with glutaraldehyde rinsing with PBS (50 mM pH 9 sodium phosphate buffer with 50 mM NaCl). Slide surfaces were

then allowed to interact with 1 mM NH₂TPP in dimethyl formamide for 30 minutes followed by rinsing with water and ethanol to remove any unbound porphyrin (Chapter 4). The slide was exposed to DPA by placing 100µl of the appropriate concentration on the surface of the slide. After allowing 1 minute for interaction, the excess solution was blotted away. Measurements were collected as described previously (Chapter 5) using an Ocean Optics USB-2000 spectrometer with the output of a LED with maximum wavelength at 434 nm and 83 nm HBW.

Immobilization of porphyrins onto cellulose fibers (Kimwipes® EX-L, Fisher Scientific, Pittsburgh, PA) was accomplished as described (Chapter 4). Tissues were saturated with 1 mg/ml porphyrin in H₂O for TPPS, ethanol for NH₂TPP, and DMF for TPPS₁. Tubes were sealed and stored overnight followed by rinsing in 1M NaCl and 50% ethanol solutions and drying at room temperature. Spectra of Kimwipe®-immobilized porphyrins were recorded using a dual wavelength spectrophotometer (SDB - 3 Johnson Research Foundation, University of Pennsylvania, Philadelphia, PA) at 0.125 nm intervals in a 3 ml cuvette containing the indicated concentration of DPA.

10.3 RESULTS

10.3.1 NH₂TPP

Figure 10.1 shows the difference spectra of tetra(4-aminophenyl) porphyrin (NH₂TPP) + DPA minus NH₂TPP obtained by the subtraction of the absolute spectra of 1.8 µM NH₂TPP from the spectra of 1.8 µM NH₂TPP in the presence of 200 nM (33.5 ppb) DPA. The trough at 423 nm results from a loss in absorbance by unbound NH₂TPP, while the peak at 470 nm indicates a new weak absorbance band resulting from formation

of the DPA-NH₂TPP complex. The increase in absorbance at 470 nm in the difference spectrum shows hyperbolic dependence on DPA concentration with absorbance changes leveling off around 84 ppb (502 nM) as seen in Figure 10.1 at pH 11, 7, and 5.5.

Levels of DPA as low as 11 ppb (65 nM) in solution have been detected with NH₂TPP (Figure 10.1) with a signal to noise ratio of 5:1. Extrapolation of data to a 3:1 S/N limit indicates a theoretical limit of detection of 7 ppb (41 nM). The changes in the NH₂TPP spectrum described above upon addition of DPA are not seen in the presence of 7M urea or when D₂O is substituted for H₂O in the solution (data not shown), suggesting that the interaction likely involves hydrogen bonding [405].

10.3.2 TPPS₁

The difference spectra of 1.2 μM monosulfonate tetraphenyl porphyrin (TPPS₁) + 107 nM DPA (18 ppb) minus TPPS₁ at pH 11, 7, and 5.5 are shown in Figure 10.2. The peaks at 434 nm and 441 nm indicate new absorbance bands resulting from the formation of TPPS₁-DPA complex while the troughs at 403 and 416 nm indicate a decrease in the amount of unbound TPPS₁. Figure 10.2 shows the hyperbolic dependence of the increase in absorbance at 441 nm in the TPPS₁ absorbance spectrums resulting from DPA additions. Absorption spectra collected using D₂O or 7 M urea show only a 15% reduction in 434 nm and 441 nm absorbance as compared to those collected in 25 mM NaPi buffer, therefore, the interaction of DPA and TPPS₁ likely does not involve hydrogen bonding.

10.3.3 CTPP₄

The exposure of meso-tetra(4-carboxyphenyl)porphine (CTPP₄) to DPA resulted in a loss in absorbance intensity at 403 nm and a new absorbance peak at 415 nm as seen

in the difference spectra CTPP₄ + DPA minus CTPP₄ (Figure 10.3, Traces 1 and 2). No new peak was observed for the interaction between CTPP₄ and DPA at pH 5.5. The increase in absorbance at 415 nm is hyperbolically dependent on DPA concentration above the 50 ppb (270 nM) limit of detection for pH 7. The new absorbance peaks of CTPP₄ are not seen in the presence of D₂O or urea indicating the involvement of hydrogen bonding in the interaction.

10.3.4 TPPS

The interaction of meso-tetra(4-sulfonatophenyl)porphine (TPPS) with DPA produced a decrease in absorbance at 410 nm and a new peak at 419 nm at pH 7 (Figure 10.4, Trace 1); a new peak from the interaction between TPPS and DPA was not observed at pH 5.5 or at pH 11. The increase in absorbance at 419 nm at pH 7 is hyperbolically dependent on DPA concentration (Figure 10.4). The DPA-TPPS absorbance at 419 nm is only 15% as intense when absorption spectra are collected in D₂O or urea as compared to those collected in 25 mM NaPi, suggesting that DPA forms hydrogen bonds with TPPS.

10.3.5 OTHER PORPHYRINS

Meso-tetra(4-boronic acid) porphyrin (TPPB), meso-tri(4-sulfonato phenyl) mono(4-carboxy phenyl) porphyrin (CTPP₁), and meso-tri(4-sulfonatophenyl)mono(4-carboxyphenyl)porphine-cytosine amide (TPSC) were tested as possible candidate molecules for detection of DPA as well. The interaction of these porphyrins with DPA did not result in new characteristic absorbance peaks; however, specific losses in intensity much greater than those predicted by dilution of the sample by DPA addition were observed at 412 nm for TPPB and TPSC and 414 nm for CTPP₁.

TPSC and CTPP₁ interact with DPA, but only very poorly. TPSC interacts with DPA resulting in a loss at 412 nm (Figure 10.4, Trace 2) with no increase in absorbance at another wavelength. The loss in absorbance at 412 nm is linear to 223 ppb DPA. CTPP₁ interacts with DPA resulting in a loss in absorbance at 414 nm (Figure 10.4, Trace 3) that is linearly dependent on DPA concentration to 32 ppb. In the case of TPPB, interaction with DPA resulted in a loss of absorbance at 412 nm (Figure 10.4, Trace 4). The loss in absorbance at 412 nm upon interaction of TPPB with DPA was observed to be linear for the three pH values investigated (5.5, 7, and 11).

DPA did not induce changes in the absorbance spectra of the copper complexes of TPPS, TPPS₁, and NH₂TPP. Cu-CTPP₁ and Cu-TPPB responded to DPA in the same manner as the corresponding metal-free porphyrins. Zn-TPPS, Zn-CTPP₁, and Zn-TPPB did not respond to the presence of DPA while Zn-NH₂TPP responded in the same manner as the corresponding metal-free porphyrin. The difference spectrum Zn-TPPS₁ + DPA minus Zn-TPPS₁ resulted in a peak at 442 nm and a trough at 413 nm with the dependence on DPA concentration the same as with the metal-free TPPS₁.

The interaction of TPPS₁, TPPS, CTPP₄ and NH₂TPP with pyridine, benzoic acid, and picolinic acid was investigated because of the structural similarity of those compounds to dipicolinic acid. As shown in Table 10.1, the difference spectrum (porphyrin + reagent minus porphyrin) of each porphyrin exhibits absorbance increases at wavelengths different than those observed with DPA.

Fluorescence measurement of the DPA-porphyrin complexes are not presented due to the lack of changes in the fluorescence spectra of NH₂TPP and TPPS₁ upon exposure to DPA.

10.3.6 IMMOBILIZED PORPHYRINS

Immobilization of NH₂TPP onto glass results in a change in the absorbance spectrum of the surface similar to the change in the absorbance of CTPP₁ immobilized to glass reported by Kibbey and Meyerhoff [555] and as noted for immobilization of TPPS [456]. The difference spectrum NH₂TPP + DPA minus NH₂TPP for the immobilized complex shows a loss in absorbance at 445 nm and an increase in absorbance at 498 nm (Figure 10.5). The increase in absorbance at 498 nm is hyperbolically dependent on increasing DPA concentration; extrapolation of the data to 3:1 S/N limit indicates a detection limit of 16 ppb (95 nM) (Figure 10.5).

The difference spectrum NH₂TPP + DPA minus NH₂TPP resulting from addition of DPA to of NH₂TPP immobilized onto cellulose fibers shows a loss in absorbance at 434 nm and an increase in absorbance at 468 nm (Figure 10.6). The increase in 468 nm absorbance shows hyperbolic dependence on DPA concentration with a limit of detection of 14 ppb (84 nM) based on 3:1 S/N (Figure 10.6). The difference spectrum resulting from exposure of TPPS₁ immobilized onto cellulose fibers to DPA shows a loss in absorbance at 417 nm and an increase in absorbance at 434 nm (Figure 10.7). The increase in absorbance at 434 nm is hyperbolically dependent on DPA concentration; the data indicate a limit of detection of 1.5 ppb (9 nM) at 3:1 S/N (Figure 10.7). DPA induced no changes in the absorbance spectrum of immobilized TPPS (data not shown).

10.4 DISCUSSION

The small absorbance changes observed could possibly be due to dilution of the porphyrin-containing cuvette upon addition of DPA or the fact that very low levels of

DPA are being detected. That the former is not the case is shown by the fact that the absorbance changes in Figure 10.4 are >15 fold higher than those due to the addition of the volume of DPA solution. The effect of dilution on the absorbance spectrum is calculated by:

$$\Delta A = A_0 \left(\frac{V_a}{V_T} \right) \quad \text{Eq. 10.1}$$

where ΔA is the loss in absorbance at the peak, A_0 is the original peak intensity, V_a is the change in volume of the sample (the volume added) and V_T is the original sample volume. Further, a “dilution” effect would show only a “trough” in the DPA + porphyrin minus porphyrin difference spectrum; an increase in absorbance at a different wavelength would not be expected. Thus, the absorbance changes presented in the Figures 10.1 through 10.4 are due to the porphyrin-DPA interaction and not due to dilution upon adding DPA.

Each porphyrin exhibits a unique peak-trough combination in the porphyrin + analyte minus porphyrin difference spectra for DPA, pyridine, picolinic acid, and benzoic acid. Schneider and Wang [284] demonstrate that the Soret wavelength shift of a porphyrin upon exposure to an analyte is proportional to the free energy of association. This indicates a strong affinity of NH_2TPP for DPA or pyridine as compared to affinity to picolinic acid and benzoic acid.

The hyperbolic dependence of the absorbance intensity changes on DPA concentration is not unexpected (Chapter 2). This data can be replotted several in ways (semi-log, double reciprocal, x- or y- reciprocal) to yield a linear plot. A double reciprocal plot, which is the inverse of the change in absorbance versus the inverse of the substrate concentration, is referred to as a Benesi-Hilderbrand plot. The slope of the data

in this form together with the Y-intercept can be used to obtain the interaction constant between the porphyrin and DPA as well as the change in extinction coefficient upon complex formation for a 1:1 interaction (or an interaction at n independent sites under special conditions) as follows:

$$K_{11} = \frac{b}{m} \quad \text{Eq. 10.2}$$

$$\Delta\epsilon_{11} = \frac{1}{[S_t] \cdot b} \quad \text{Eq. 10.3}$$

$$\Delta\epsilon_{11} = \epsilon_{11} - \epsilon_s \quad \text{Eq. 10.4}$$

where b is the Y-intercept, m is the slope, S_t is the concentration of independent binding sites, ϵ_{11} is the extinction coefficient for the substrate-ligand complex at the considered wavelength, ϵ_s is the extinction coefficient for the free substrate at the considered wavelength, $\Delta\epsilon_{11}$ is the change in the extinction coefficient upon complex formation, and K_{11} is the association constant.

The double reciprocal plot of the data shown on the interaction of TPPS with DPA at pH 7 (Figure 10.4) gives a slope of 951 $\mu\text{M}/\text{A}$ and a Y-intercept of 146 A^{-1} . Using this information and assuming a 2:1 DPA:TPPS interaction similar to that of toluene stacking [582] we can determine $\Delta\epsilon_{11}$ to be 4.9 A/mM . This value indicates that 1.1 μM (200 ppb) DPA causes a change in the absorbance spectrum of 550 nM NH_2TPP under these conditions verifying the two to one interaction. Table 10.2 shows the slope and y-intercept for each set of data as well as the resulting K_{11} and $\Delta\epsilon_{11}$. In the case of the immobilized porphyrins for which an extinction coefficient has not been calculated and for which the total porphyrin concentration is unknown, $\Delta\epsilon_{11}$ remains undetermined. If the interaction of the porphyrins with DPA does not meet the conditions for this model,

that is a single binding site or n independent binding sites, the number of parameters to be determined increases based on the number of interactions involved. The absorbance data alone does not give enough information to determine parameters for this more complicated type of interaction.

Detection of DPA by photoluminescence involving the use of lanthanide metals, especially terbium (III), complexed with DPA [565-566, 568-569, 581] is successful with detection limits as low as 2 nM (0.3 ppb)[568]. However, the presence of phosphate-containing compounds results in false readings because of the high binding affinity of the terbium for phosphate [569].

In the measurements described here, the detection of DPA occurs in the presence of phosphate buffer and, therefore, does not require the use of AlCl_3 . Measurements can be completed quickly within the time to collect the spectrum (less than 45 sec). Separation of the porphyrins from the spore samples should not be necessary if dual wavelength spectroscopy or small amounts of spores are used to minimize light scattering effects. Some care is required with regard to measurement conditions as a result of the sensitivity to pH of the porphyrin response characteristics.

Detection of DPA by immobilized porphyrins has been demonstrated (Figure 10.5 to 10.7) with detection limits as low as 1.5 ppb (9 nM). Immobilization on cellulose fibers is inexpensive and requires no specialized equipment. However, the Kimwipes® are highly scattering, requiring reflectance measurements or collection of absorbance spectra by a dual wavelength instrument. The ability of porphyrins to detect DPA in intact and broken *Bacillus* spores is being investigated. Should it prove viable, a

porphyrin-tissue system used as a wipe test could provide a reagent-less and nearly instantaneous method of identifying the presence of *Bacillus* spores.

INTERACTION WAVELENGTHS

Porphyrin		Dipicolinic Acid	Pyridine	Picolinic Acid	Benzoic Acid
TPPS ₁	Peak	433 nm / 441 nm	428 nm / 438 nm	429 nm / 437 nm	427 nm / 437 nm
	Trough	403 nm / 416 nm	403 nm / 419 nm	403 nm / 418 nm	402 nm / 418 nm
NH ₂ -TPP	Peak	470 nm	467 nm	465 nm	461 nm
	Trough	423 nm	421 nm	427 nm	418 nm
TPPS	Peak	419 nm	none	none	none
	Trough	410 nm	410 nm	none	none
CTPP ₄	Peak	415 nm	421 nm	none	415 nm
	Trough	403 nm	410 nm	none	398 nm

TABLE 10.1 Characteristic porphyrin absorbance wavelengths for the interaction with DPA and three structurally similar compounds [583].

LINEAR FITTING PARAMETERS

Porphyrin	Slope (mM/A)	Y-intercept (A ⁻¹)	[Porphyrin] (μM)	<i>n</i>	K ₁₁ (μM) ⁻¹	Δε ₁₁ (A/mM)
NH ₂ TPP (pH 7)	767	77	1.8	1	100	7.2
NH ₂ TPP (pH 5.5)	650	51	1.8	1	78	11
NH ₂ TPP (pH 11)	680	187	1.8	1	275	3.0
TPPS ₁ (pH 7)	101	44	1.2	1	436	19
TPPS ₁ (pH 5.5)	57	54	1.2	1	947	15
TPPS ₁ (pH 11)	97	34	1.2	1	351	25
CTPP ₄ (pH 7)	13407	470	1.0	2	35	2.1
TPPS (pH 7)	951	146	0.7	2	154	9.8
NH ₂ TPP (on glass)	315	19	---	1	60	---
NH ₂ TPP (on cellulose)	2326	108	---	1	46	---
TPPS ₁ (on cellulose)	84	36	---	1	429	---

TABLE 10.2 The linear fitting parameters from the Benesi-Hilderbrand plots of concentration dependence and the resulting K₁₁ and Δε₁₁ values [583].

NH₂TPP IN SOLUTION

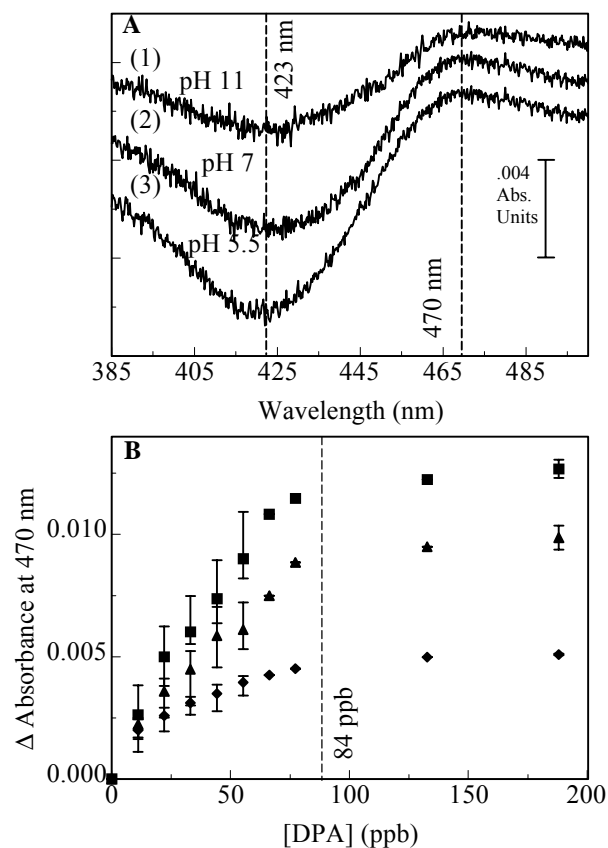


FIGURE 10.1 (A) The difference spectra NH₂-TPP (1.8 μM) + DPA (200 nM) minus NH₂-TPP shown for pH 11 (Trace 1), pH 7 (Trace 2), and pH 5.5 (Trace 3). (B) The concentration dependence of the peak at 470 nm in the difference spectra shown in Figure 1A at pH 11 (♦), pH 7(▲), and pH 5.5 (●) [583].

TPPS₁ IN SOLUTION

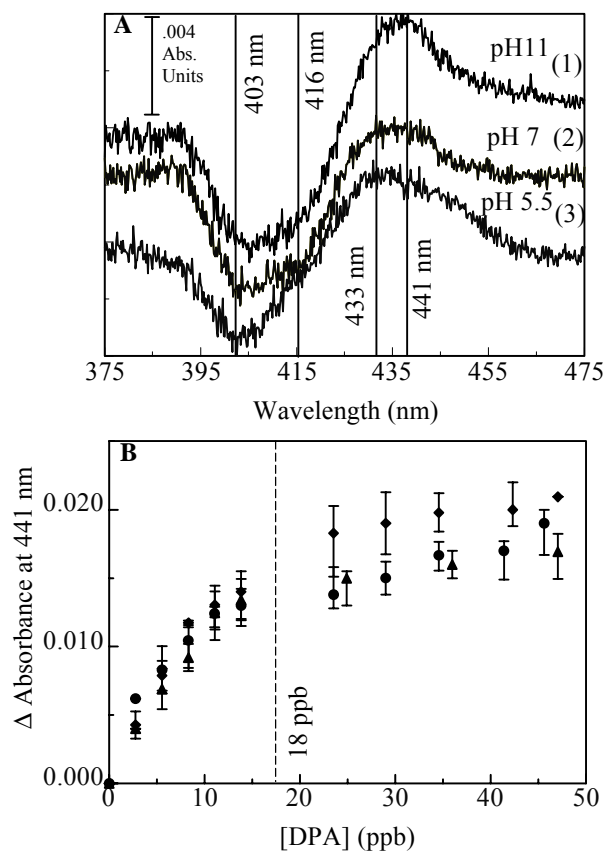


FIGURE 10.2 (A) The difference spectra TPPS₁ (1.2 μM) + DPA (107 nM) minus TPPS₁ shown at pH 11 (Trace 1), pH 7 (Trace 2), and pH 5.5 (Trace 3). (B) The concentration dependence of the peak at 441 nm in the difference spectra shown in Figure 2A at pH 11(♦), pH 7(▲), and pH 5.5 (●) [583].

CTPP₄ IN SOLUTION

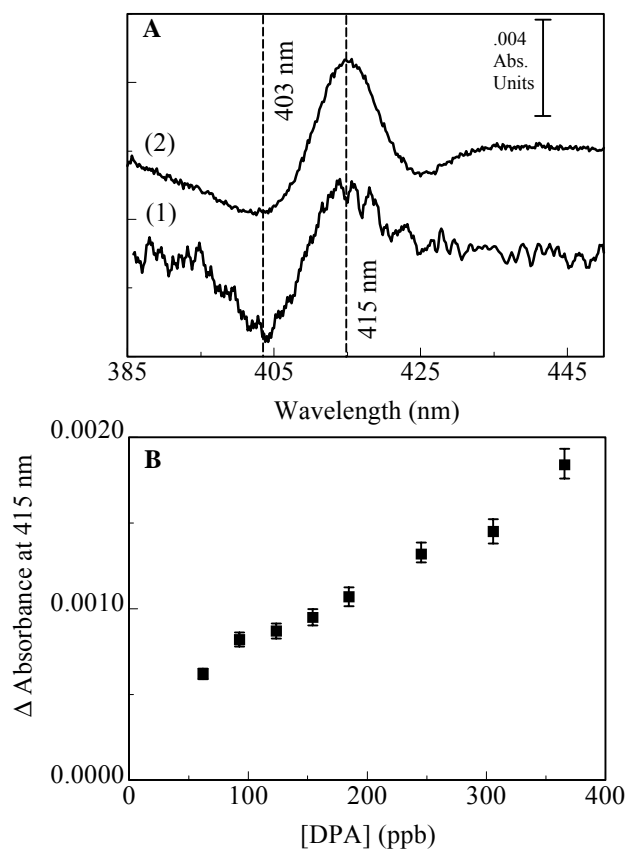


FIGURE 10.3 (A) The difference spectra CTPP₄ (220 nM) + DPA (1 μM) minus CTPP₄ for pH 11 (Trace 1, scaled up by a factor of 4), pH 7 (Trace 2). (B) The concentration dependence of the peak at 415 nm in the difference spectra shown in Figure 3A, Trace 2 [583].

OTHER PORPHYRINS IN SOLUTION

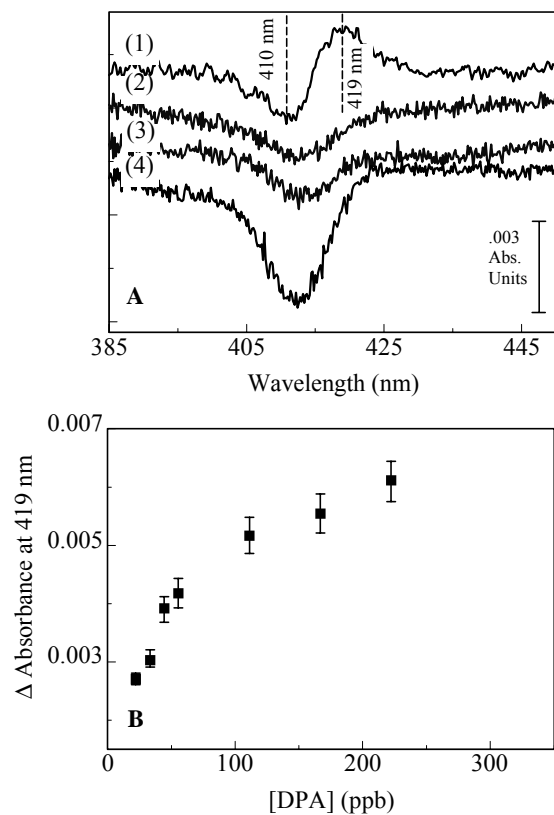


FIGURE 10.4 (A) The difference spectra resulting from the interaction of TPPS, TPSC, CTPP₁, and TPPB with DPA. Trace 1 shows the difference spectrum TPPS (700 nM) + DPA (50 nM) minus TPPS. Trace 2 shows the difference spectrum TPSC (355 nM) + DPA (400 nM) minus TPSC at pH 5.5. Trace 3 shows the difference spectrum CTPP₁ (650 nM) + DPA (500 nM) minus CTPP₁ at pH 7. Trace 4 shows the difference spectrum TPPB (1 μ M) + DPA (750 nM) minus TPPB at pH 11 [583]. (B) The concentration dependence of the peak in the pH 7 difference spectrum for TPPS shown in Figure 4A, Trace 1 [583].

NH₂TPP ON GLASS

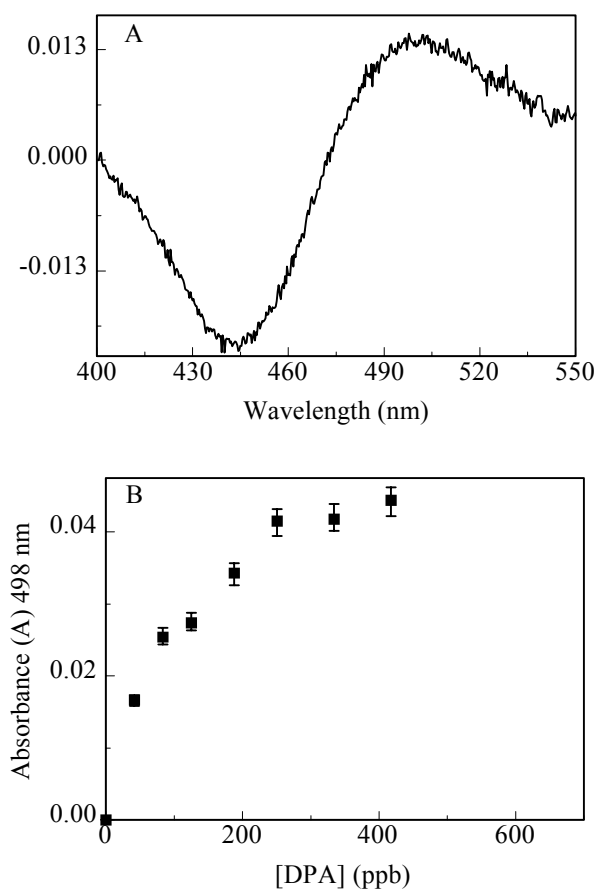


FIGURE 10.5 (A) The difference spectrum NH₂-TPP + DPA (500 nM) minus NH₂-TPP, resulting from the interaction of NH₂-TPP immobilized on glass with DPA [583]. (B) The concentration dependence of the peak in the difference spectrum [583].

NH₂TPP ON CELLULOSE FIBERS

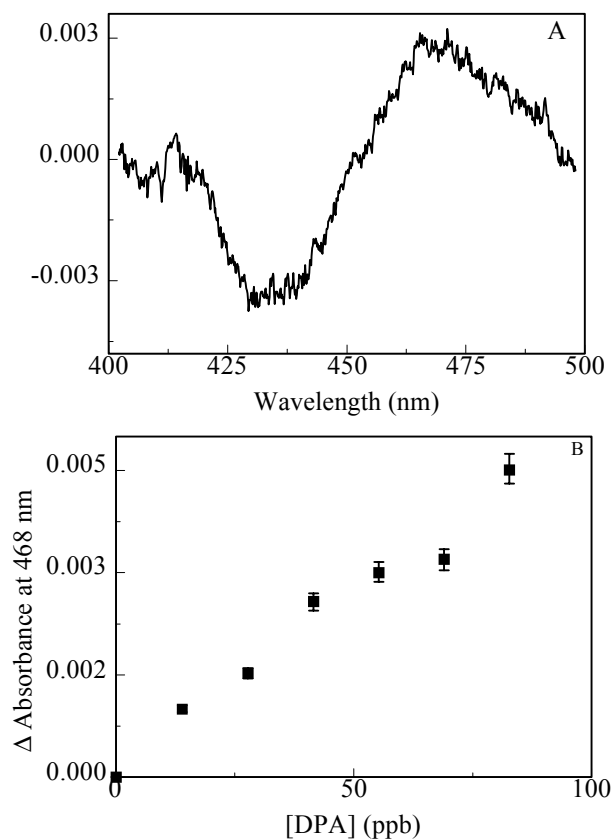


FIGURE 10.6 (A) The difference spectrum NH₂TPP + DPA (1 μM) minus NH₂TPP, resulting from the interaction of NH₂TPP immobilized on cellulose fibers with DPA [583]. (B) The concentration dependence of the peak in the difference spectrum [583].

TPPS₁ ON CELLULOSE FIBERS

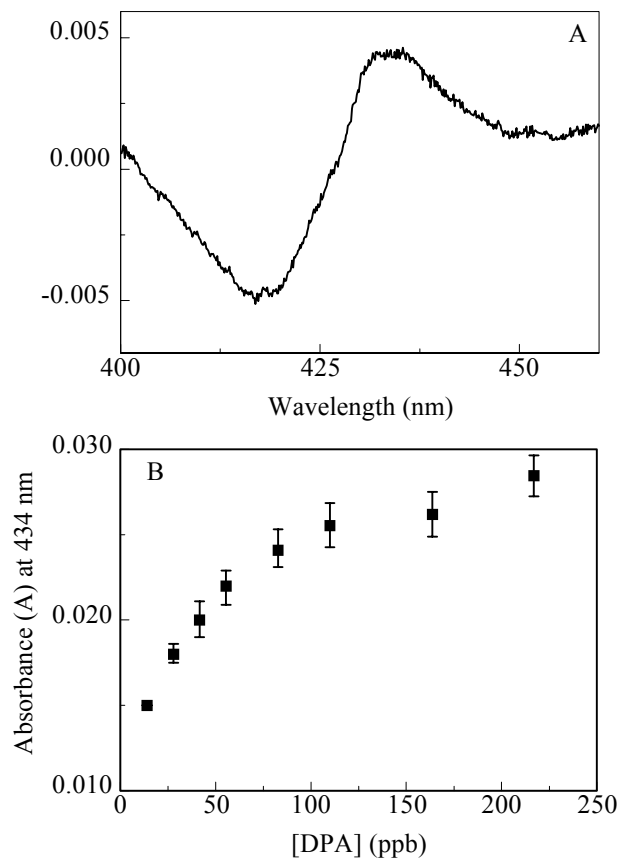


FIGURE 10.7 (A) The difference spectrum TPPS₁ + DPA (1 μM) minus TPPS₁, resulting from the interaction of TPPS₁ immobilized on cellulose fibers with DPA [583]. (B) The concentration dependence of the peak in the difference spectrum [583].

CHAPTER 11

PORPHYRIN DETERMINATION OF SUGARS

11.1 INTRODUCTION

Bacterial endospores are a very stable, dehydrated, heat-resistant, and non-growing state of certain types of gram positive bacteria. Bacterial endospores are a source of infection and disease and their resistance to extreme environmental conditions, disinfectants, and antibiotics makes them difficult to destroy. *Bacillus anthracis*, an endospore-forming bacterium, can be found in industrial waste from tanneries and water processing plants. *B. anthracis* can also be viewed as a biological threat agent due to the possibility of broadcasting the dry spores and the difficulty in detection and enumeration of the same. Some other spore producing bacteria of interest as biothreat agents are *Clostridium tetani* and *Clostridium botulinum*.

The surface of the bacterial endospores of some *Clostridium* and *Bacillus* species is composed of an exosporium structure on the outside of the spore coat. In *B. cereus* the major component of the exosporium is protein with 18% lipid and 20% carbohydrate. The exosporia of *B. anthracis*, *B. thuringiensis*, and *B. cereus* have been shown to contain glycoproteins, though glycosylation of proteins in bacteria is rare and the function is not yet clear [584-587].

Analysis of exosporium carbohydrate composition may be a likely method of distinguishing different endospores. A spore-specific carbohydrate, 3-*O*-methyl rhamnose, has been reported in the exosporia of *B. anthracis*, *B. cereus*, and *B. thuringiensis* [585-587]. This sugar is rare in nature, appearing almost exclusively in

members of the *Bacillus* genus. Other studies report rhamnose, galactose (and/or galactosamine), fucose, and 2-*O*-methyl rhamnose as exosporium components. The carbohydrate composition of *B. anthracis* differs from that of *B. cereus* and *B. thuringiensis* in that the former contains no fucose or 2-*O*-methyl rhamnose which are known components of the latter two bacterial endospores [585]. It has been proposed that the carbohydrate composition of the glycoproteins described in the three above mentioned members of the *Bacillus* genus consist of the sugars rhamnose, 3-*O*-methyl rhamnose, and galactosamine [584, 587-588].

Porphyrins have been used as colorimetric indicators for the detection of a wide range of compounds including sugars [292, 377-379] due to the specificity of the spectral response even for very similar compounds [283-284, 293]. In previous work, we have demonstrated the specificity of porphyrins for identification of the compound dipicolinic acid, which comprises 5 - 15% of the dry weight of the spore, as a non-specific indicator of bacterial endospore presence [585]. Here we will demonstrate the potential of porphyrins both in solution and immobilized onto cellulose fibers to identify and quantify rhamnose variants and other sugars using absorbance and fluorescence spectroscopy.

11.2 MATERIALS AND METHODS

Methyl α -L-rhamnopyranoside (MRP), L-rhamnose monohydrate (rhamnose), L(-)-fucose, and D(+)-galactosamine HCl were obtained from Sigma (St. Louis, MO) (Figure 11.1). Monosulfonate tetraphenyl porphyrin (TPPS₁), tetra(4-aminophenyl) porphyrin (NH₂TPP), and meso-tetra(4-boronic acid) porphyrin (TPPB) were obtained from Frontier Scientific (Logan, UT) and used without further purification (Figure 11.2).

Visible light absorbance and fluorescence spectra of each porphyrin in solution in the presence/absence of each of the sugars were measured to indicate which immobilized porphyrins would be likely to interact with the sugars. Absorbance spectra were recorded at room temperature in 50 mM sodium phosphate (Sorenson) buffer (NaPi) at pH 7 with a Cary 4E spectrophotometer at 0.02 nm resolution. The difference spectra porphyrin + sugar minus porphyrin were obtained by subtraction of absolute spectra using Grams/32 (Galactic Industries, Salem, NH). Characteristic wavelengths cited in Tables 11.1 and 11.2 are the peak and trough positions from the difference spectra as determined using the 2nd derivative of the spectrum as calculated using Grams/32. The difference spectra peak minus trough intensities were measured at varying concentrations. The double reciprocal plot of the concentration data was used for linear fittings at a 99% confidence interval using PSI-Plot (V 7.0) [583]. The fittings were subsequently used to determine the limits of detection as the concentration at which the absorbance change is three times the noise level in the measurement. Error bars are included to show the maximum and minimum absorbance changes observed for exposure to a given concentration of sugar.

Fluorescence spectra of each porphyrin in solution in the presence/absence of each sugar were recorded under the conditions described for absorbance spectra using a SPEX Fluoromax 3 spectrofluorometer (JY-Horiba, Edison, NJ). Wavelength resolution was set at 3.0 nm for both excitation and emission. Spectra were collected for excitation wavelengths from 380 to 600 nm and for emission wavelengths from 600 to 800 nm. Maximum fluorescence emission intensity is obtained for each porphyrin and porphyrin-sugar complex at the excitation and emission wavelengths listed in Tables 11.1 and 11.2.

Absorbance spectra of Kimwipe®-immobilized porphyrins were recorded using a dual wavelength spectrophotometer (SDB - 3 Johnson Research Foundation, University of Pennsylvania, Philadelphia, PA) at 0.125 nm intervals in a 3 ml cuvette containing the indicated sugar concentrations in 50 mM pH 7 NaPi. Spectral analysis is the same as cited for the porphyrins in solution with characteristic wavelengths listed in Tables 11.1 and 11.2. Fluorescence spectra were collected as described above with the excitation and emission wavelengths for maximum emission intensities listed in Tables 11.1 and 11.2. The fluorescence difference spectra shown are calculated by the point by point subtraction of the emission spectra, porphyrin + sugar minus porphyrin, for a particular excitation wavelength. The emission spectra are normalized to the same emission intensity at 693 nm before calculation of difference spectra. The 693 nm wavelength is used chosen because there is non-zero fluorescence emission for all of the porphyrins in this region of the spectrum. Scaling was used to compensate for the overall increase or decrease in fluorescence emission intensity observed upon interaction of some of the sugars with the porphyrins. The scaling allowed a comparison of the changes at the different wavelengths that would not have been seen due to the overall changes in intensity (Figure 11.3). The concept is to use ratios of the emission intensities at different wavelengths as indicators of emission profile changes.

Immobilization of porphyrins onto cellulose fibers (Kimwipes® EX-L, Fisher Scientific, Pittsburgh, PA) was performed at 4°C as described in Chapter 4 [583]. Briefly, tissues were placed in a test tube and saturated with 1 mg/ml porphyrin solution. Tubes were sealed and stored overnight at room temperature followed by soaking of the

tissues in NaCl and ethanol solutions to remove unbound porphyrin and drying at room temperature.

11.3 TETRA(4-AMINOPHENYL) PORPHYRIN

Tetra(4-aminophenyl) porphyrin (NH₂TPP) was chosen to identify sugars because of the sensitivity and selectivity for aromatic compounds observed previously [585]. Each of the four phenyl rings of this porphyrin has an amino substituent (Figure 11.2). We have demonstrated the interaction of this porphyrin both in solution and immobilized to cellulose and glass surfaces with compounds such as dipicolinic acid and benzene [585]. The characteristic wavelengths for each NH₂TPP-sugar combination in solution are unique indicating the potential of immobilized NH₂TPP to discriminate between the sugars (Figure 11.4). Immobilization on cellulose tissue was chosen for possible application as a “wipe test” for the presence of sugar. Though the exact peak / trough locations are unique for each sugar, the difference spectra resulting from exposure of the NH₂TPP tissues, excluding that for rhamnose, have broad overlapping features (Figure 11.5). The dependence of the absorbance changes on sugar concentration is shown in Figure 11.5. The expected half-hyperbolic dependence on concentration is observed in all cases with 3:1 signal to noise (S/N) detection limits at 13 ppb for MRP, 47 ppb for rhamnose, 45 ppb for galactosamine, and 60 ppb for fucose [263, 583].

In addition to the sugar-specific changes in the absorbance spectrum, changes in the NH₂TPP fluorescence spectrum are observed upon exposure to the sugars. Tables 11.1 and 11.2 shows the emission and excitation wavelengths for which maximum emission intensity are observed for NH₂TPP in the absence/presence of the sugars.

Though the maximum excitation and emission wavelengths for NH₂TPP and the sugar-porphyrin complexes are similar, fluorescence characteristics vary between the sugars. Figure 11.5 shows the changes in NH₂TPP tissue fluorescence emission for 416 nm excitation upon exposure to each of the sugars. The presence of either galactosamine or fucose causes an increase in NH₂TPP emission intensity at 649 nm while exposure to MRP or rhamnose results in a decrease in NH₂TPP emission intensity at 669 nm.

11.4 MONOSULFONATE TETRAPHENYL PORPHYRIN

We have demonstrated the interaction of monosulfonate tetraphenyl porphyrin (TPPS₁) with aromatic compounds [583] and enzymes [391-392, 397]. TPPS₁ has a single sulfonate group at the *para*-position of one phenyl ring (Figure 11.2). The three phenyl groups increase the hydrophobicity and the sensitivity of the porphyrin to aromatic compounds [583]. The interaction of TPPS₁ with each of the sugars in solution results in unique combinations of characteristic wavelengths and indicates detection limits significantly lower than when NH₂TPP is used (Tables 11.1 and 11.2, Figure 11.6). Unlike the NH₂TPP spectra, the characteristic wavelengths may include one or more troughs as well as one or more peaks (Figures 11.6 and 11.7). Upon exposure of the TPPS₁ tissue to MRP, there is a loss in absorbance intensity at 406, 417, and 432 nm and an increase in absorbance intensity at 444 nm (Figure 11.7). The features in the difference spectrum are, as in the case of NH₂TPP, broad and overlap in all cases. The concentration dependence for each sugar is half-hyperbolic (Figure 11.7). The detection limit at 3:1 S/N is 4 ppb for MRP, 80 ppb for rhamnose, 2 ppb for galactosamine, and 6 ppb for fucose.

The changes in the fluorescence spectrum of immobilized TPPS₁ at 416 nm excitation were similar for all sugars tested. Exposure to any of the sugars resulted in a relative increase in TPPS₁ emission intensity at 655 and 718 nm with a slight decrease around 741 nm (Figure 11.7). The only unique change in the TPPS₁ tissue emission was upon exposure to galactosamine where an overall increase in emission intensity as opposed to no change in maximum emission intensity is observed.

11.5 MESO-TETRA(4-BORONIC ACID) PORPHYRIN

Boronic acids form cyclic esters with saccharides through a reversible reaction at room temperature. Porphyrins and fluorophores with a boronic acid substituent have been used previously for spectrophotometric sugar detection [589-590]. Meso-tetra(4-boronic acid) porphyrin (TPPB) has four boronic acid substituents at the *para*-positions of the phenyl rings of the TPP molecule (Figure 11.2). This porphyrin showed unique characteristic interaction wavelengths for each sugar in solution with detection limits neither as good as those of TPPS₁ nor as poor as those of NH₂TPP (Figure 11.8). As in the case of TPPS₁, the TPPB difference spectra resulting from interaction with the sugars may include one or more peaks and troughs (Figures 11.8 and 11.9). The peak / trough positions for the interaction of the TPPB tissue with each sugar are unique (Tables 11.1 and 11.2). Additionally, the features in the difference spectra are easily distinguishable. Exposure to rhamnose results in a small peak /trough pair at 438 / 426 nm whereas MRP exposure results in a prominent peak / trough pair at 427 / 410 nm. Each of these changes is a bathochromic (red) shift where the absorbance intensities increase at longer wavelengths. Exposure of TPPB to galactosamine or to fucose results in a hypsochromic

(blue) shift with characteristic wavelengths at 418 / 434 nm for galactosamine and 427 / 449 nm for fucose. The features in the difference spectra are narrower than in the cases of TPPS₁ and NH₂TPP. The concentration dependence for each sugar gives the expected half-hyperbolic relation with detection limits of 14 ppb for MPR, 35 ppb for rhamnose, 16 ppb for galactosamine, and 85 ppb for fucose (Figure 11.9).

The TPPB fluorescence difference spectra for galactosamine and fucose exposure show similar, but distinguishable features (Figure 11.9). The emission intensity at 647 and 707 nm decreases and increases at 672 nm with galactosamine whereas fucose elicits a decrease at 654 and 707 nm and an increase at 680 nm. Exposure of TPPB to MRP results in an increase in 645 nm emission with a slight decrease in 683 nm emission whereas exposure to rhamnose results in an increase in 650 nm emission and a decrease 683 nm emission.

11.6 DISCUSSION

We have demonstrated the potential for identification of sugars using three immobilized porphyrin surfaces based on specific changes in absorbance and/or fluorescence spectra upon interaction of the sugars with the surfaces. Though both NH₂TPP and TPPS₁ showed promising results in solution and will likely be effective for use in detection of compounds such as those discussed in the previous Chapter [583], the TPPB tissues give the most easily distinguishable changes in absorbance and fluorescence spectra upon exposure to the sugars. Detection limits as low as 10 ppb are demonstrated here. The exosporium of the bacterial endospore makes up about 2% of the total dry weight of the spore [586]. Of this 2% approximately 20% consists of carbohydrate, so extremely low levels of sugar detection are desired.

If (i) the porphyrin-analyte complex is assumed to be 1:1; (ii) Beer's Law is followed by the porphyrin, analyte, and the porphyrin-analyte complex; and (iii) the extinction coefficients of the free reagents at the wavelength under consideration are significantly different from that of the porphyrin-analyte complex, we can derive the relationship between the absorbance change (ΔA) and the variables porphyrin concentration ($[P]$), analyte concentration ($[L]$), and complex stability constant (K_{11}) as follows [263] (see also Chapter 2). Beer's Law states:

$$A_0 = \varepsilon_p b P_t \quad \text{Eq. 11.1}$$

where A_0 is the initial absorbance of the porphyrin, P_t is the total porphyrin concentration, ε_p is the extinction coefficient at the wavelength under consideration, and b is the path length for the measurement. In the presence of analyte (total concentration L_t), the absorbance of a solution containing the same total porphyrin concentration is:

$$A_L = \varepsilon_p b [P] + \varepsilon_L b [L] + \varepsilon_{11} b [PL]. \quad \text{Eq. 11.2}$$

Here ε_L and ε_{11} are the extinction coefficients of the analyte and the complex, respectively and $[PL]$ is the concentration of the complex. Since $P_t = [P] + [PL]$ and $L_t = [L] + [PL]$, this can be rewritten as:

$$A_L = \varepsilon_p b P_t + \varepsilon_L b L_t + \Delta \varepsilon_{11} b [PL] \quad \text{Eq. 11.3}$$

(Note that $\Delta \varepsilon_{11} = \varepsilon_{11} - \varepsilon_p - \varepsilon_L$). If the reference spectrum is taken against a ligand spectrum at L_t or the ligand does not absorb in the considered region, this expression becomes:

$$A = \varepsilon_p b P_t + \Delta \varepsilon_{11} b [PL]. \quad \text{Eq. 11.4}$$

The stability constant for the 1:1 complex is:

$$K_{11} = \frac{[PL]}{[P][L]} \quad \text{Eq. 11.5}$$

and the total porphyrin concentration can be written as $P_t = [P] + [PL]$, so the change in absorbance can be written:

$$\Delta A = A - A_0 = \Delta \varepsilon_{11} b [PL] = K_{11} \Delta \varepsilon_{11} b [P][L] \quad \text{Eq. 11.6}$$

Note that the change in absorbance depends not only on the analyte concentration, but also on the porphyrin concentration. Though the exact relation will vary for more complex interactions such as those which are not 1:1 or those involving cooperative binding, the substrate and analyte concentrations can both affect the absorbance change. We have mentioned a similar result observed with immobilized enzyme surfaces [392] (Chapter 5). Improved detection limits, therefore, may be obtained by increasing the porphyrin density on the surface of the tissues. This may involve changing to a different type of cellulose surface and/or modifying the immobilization conditions. The density will need to be optimized to achieve the maximum number of porphyrins per area without involving porphyrin-porphyrin stacking effects, which will alter the absorbance intensity and typically the band positions as well [591-592].

Preliminary data has been collected using the tissues as wipes. A solution of rhamnose was dried onto a glass surface. The absorbance and fluorescence (at 416 nm excitation) spectra of a moistened TPPS₁ tissue were recorded and the tissue was subsequently used to wipe the glass surface. The changes in the spectral characteristics

were the same as reported for TPPS₁ tissues in solution (Tables 11.1 and 11.2) with troughs at 417 and 432 nm and a peak at 447 nm in the difference spectrum.

Preliminary work has also been done using intact and broken *Bacillus thuringensis* spores in solution (Figure 11.10). The changes in the porphyrin absorbance spectra are more complex than those observed upon exposure to the simple sugars. Figure 11.10 shows an absorbance difference spectrum with troughs at 397 and 403 nm and peaks at 422 and 434 nm. The changes in the fluorescence spectrum are very complex. This likely results from the interaction of the porphyrin not only with the sugars, but also with the lipid and protein components of the exosporium in the case of intact spores and with other spore components in the case of broken spores. Experiments with bacteria producing differing exosporia are necessary to determine the specificity of the detection protocol, however, we are hopeful that the protocol will be useful.

SUMMARY OF INTERACTIONS: MRP AND RHAMNOSE

Sugar	None		MRP					Rhamnose				
	Excitation (nm)	Emission (nm)	Trough (nm)	Peak (nm)	Excitation (nm)	Emission (nm)	LOD (ppb)	Trough (nm)	Peak (nm)	Excitation (nm)	Emission (nm)	LOD (ppb)
NH ₂ TPP	432	679	416	472	422	684	12	430	481	422	679	6
TPPS ₁	411	654	405	447	406	655	0.2	405/ 416	439	406	652	0.5
TPPB	411	650	404/ 426	459	417	653	10	415	435	417	650	0.5
Immobilized Porphyrins												
NH ₂ TPP	416	652	479	445	416	652	13	426	412	416	652	47
TPPS ₁	416	656	406/ 417/ 432	444	416	656	4	417/ 432	447	416	653	80
TPPB	423	663	410	427	423	660	14	426	438	423	663	35

TABLE 11.1 The characteristic wavelengths, limits of detection, and maximum fluorescence excitation and emission wavelengths for porphyrin-sugar interactions. Note: 405 / 416 indicates a complex trough involving two peaks centered at 405 and 416 nm [593].

SUMMARY OF INTERACTIONS: GALACTOSAMINE AND FUCOSE

Sugar	None		Galactosamine					Fucose				
	Excitation (nm)	Emission (nm)	Trough (nm)	Peak (nm)	Excitation (nm)	Emission (nm)	LOD (ppb)	Trough (nm)	Peak (nm)	Excitation (nm)	Emission (nm)	LOD (ppb)
NH ₂ TPP	432	679	425	460	430	673	2	425	460	430	676	2
TPPS ₁	411	654	405	432	417	654	5	405/ 416	432	417	654	2
TPPB	411	650	397	424	411	647	10	400	434	411	650	3
Immobilized Porphyrins												
NH ₂ TPP	416	652	416	445	416	649	45	472	439	423	652	60
TPPS ₁	416	656	417	439/ 447	416	656	2	417/ 432	444	416	653	6
TPPB	423	663	434	418	423	663	16	449	427	423	663	85

TABLE 11.2 The characteristic wavelengths, limits of detection, and maximum fluorescence excitation and emission wavelengths for porphyrin-sugar interactions. Note: 405 / 416 indicates a complex trough involving two peaks centered at 405 and 416 nm [593].

SUGAR STRUCTURES

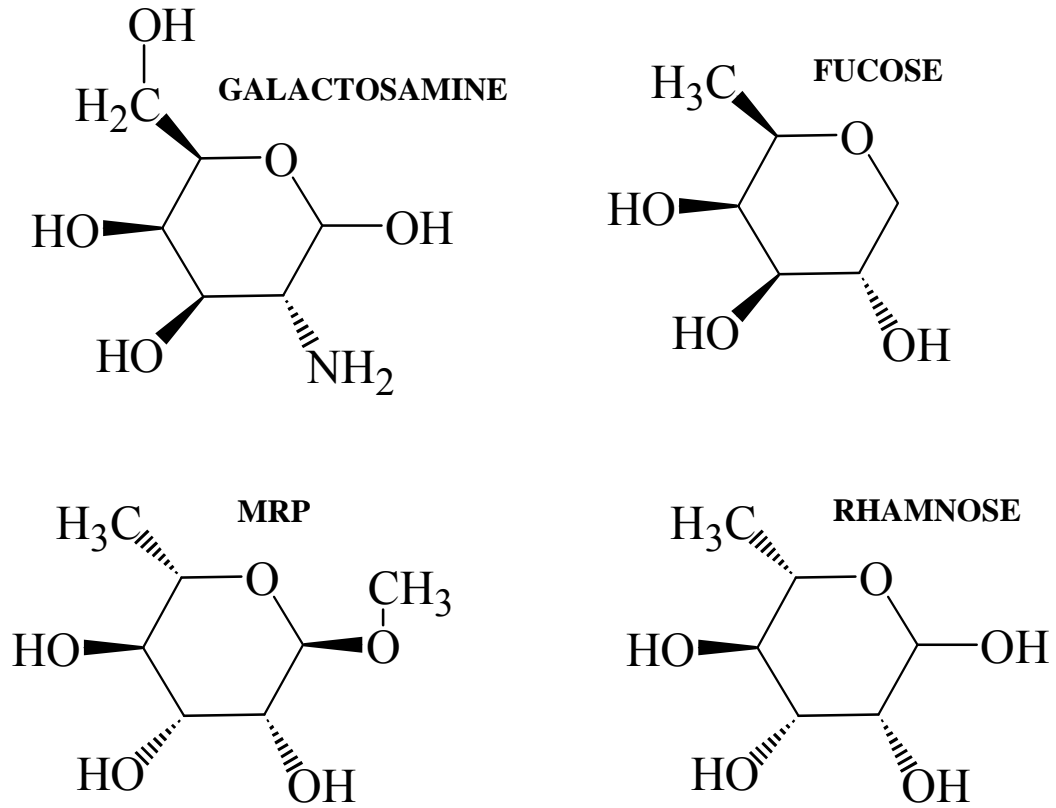


FIGURE 11.1 The structures of the sugars: methyl α -L-rhamnopyranoside (MRP), L-rhamnose, L(-)-fucose, and D(+)-galactosamine.

PORPHYRIN STRUCTURES

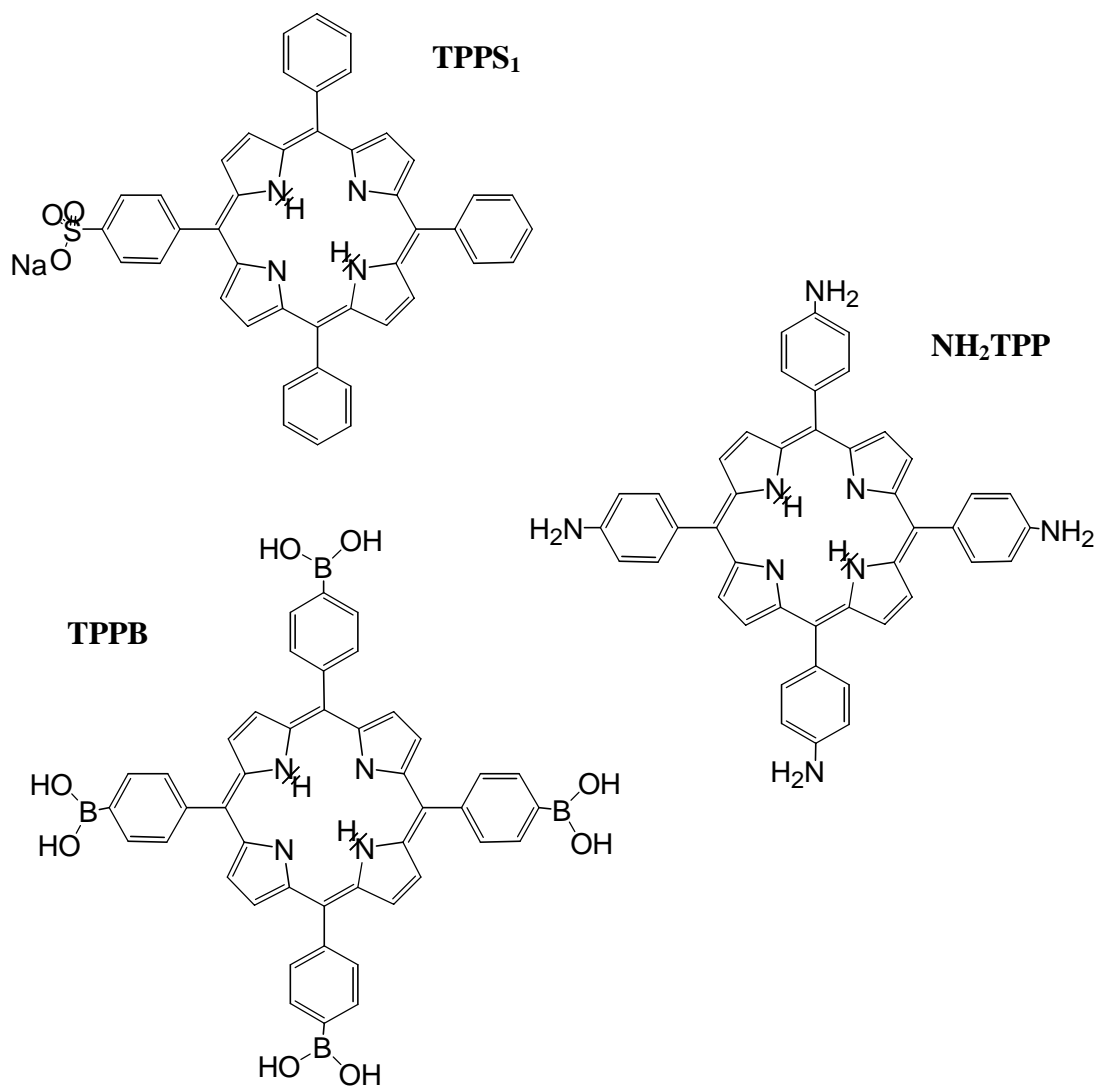


FIGURE 11.2 The structures of the porphyrins used for sugar determination: monosulfonate tetraphenyl porphyrin (TPPS₁), tetra(4-aminophenyl) porphyrin (NH₂TPP), and meso-tetra(4-boronic acid) porphyrin (TPPB).

SCALING OF FLUORESCENCE SPECTRA

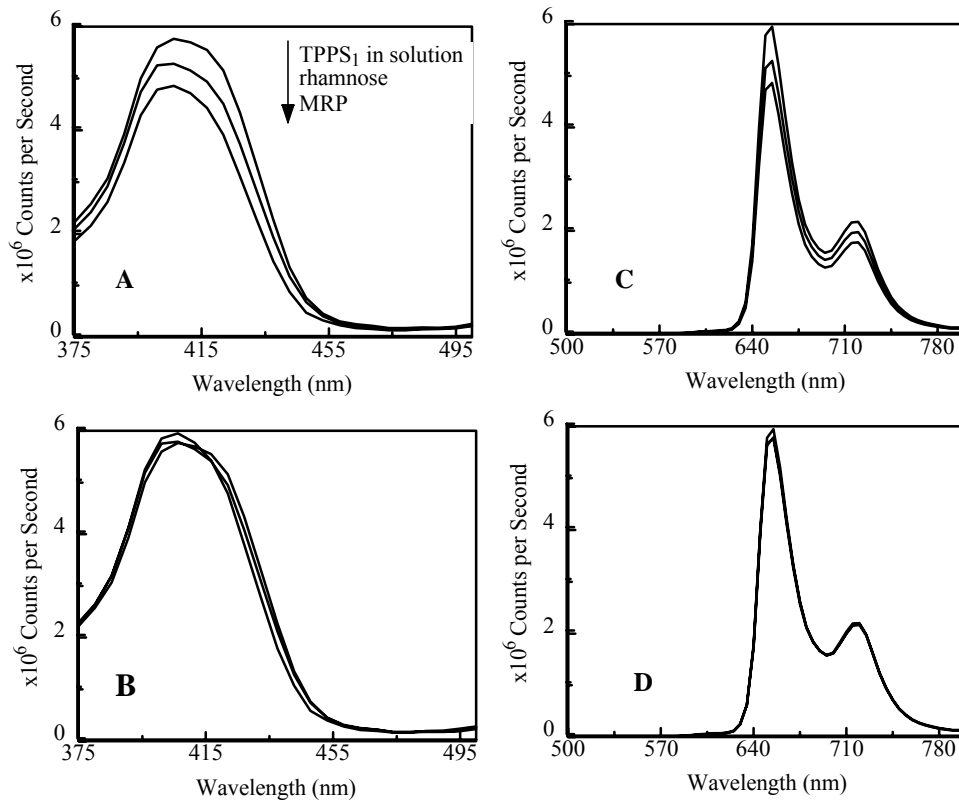


FIGURE 11.3 Fluorescence excitation and emission spectra for TPPS₁ in solution (50 mM pH 7 NaPi). (A) Excitation spectra of TPPS₁ in presence/absence of MRP and rhamnose. (B) Traces in (A) scaled to match at 693 nm emission. (C) Emission spectra of TPPS₁ in presence/absence of MRP and rhamnose. (D) Traces in (C) scaled to match at 693 nm emission.

NH₂TPP IN SOLUTION

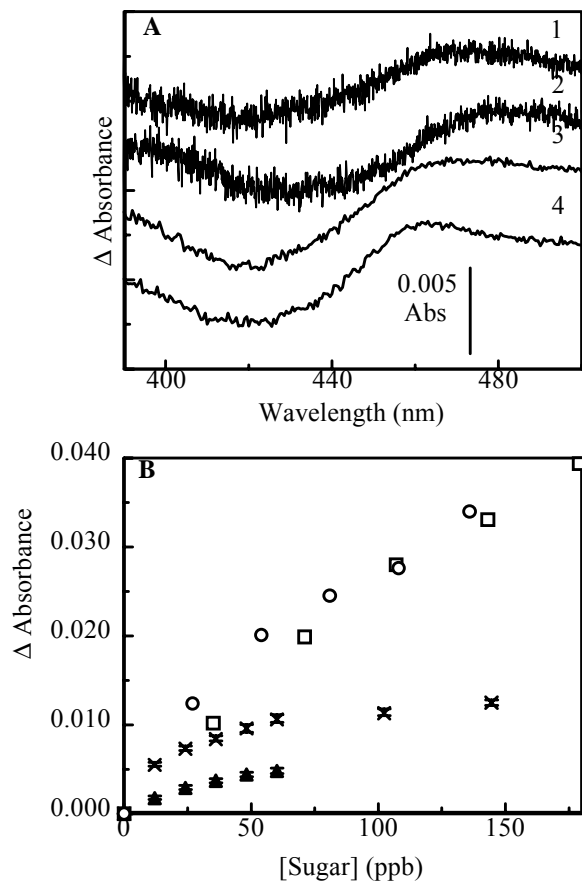


FIGURE 11.4 (A) The difference spectra NH₂TPP (1.8 μ M) + Sugar minus

NH₂TPP for MRP (50 ppb), rhamnose (50 ppb), fucose (27 ppb, scaled by 0.5), and galactosamine (35 ppb, scaled by 0.5). (B) The concentration dependence of the absorbance change upon exposure of NH₂TPP to MRP (x), rhamnose (\blacktriangle), fucose (\circ), and galactosamine (\square).

IMMOBILIZED NH₂TPP

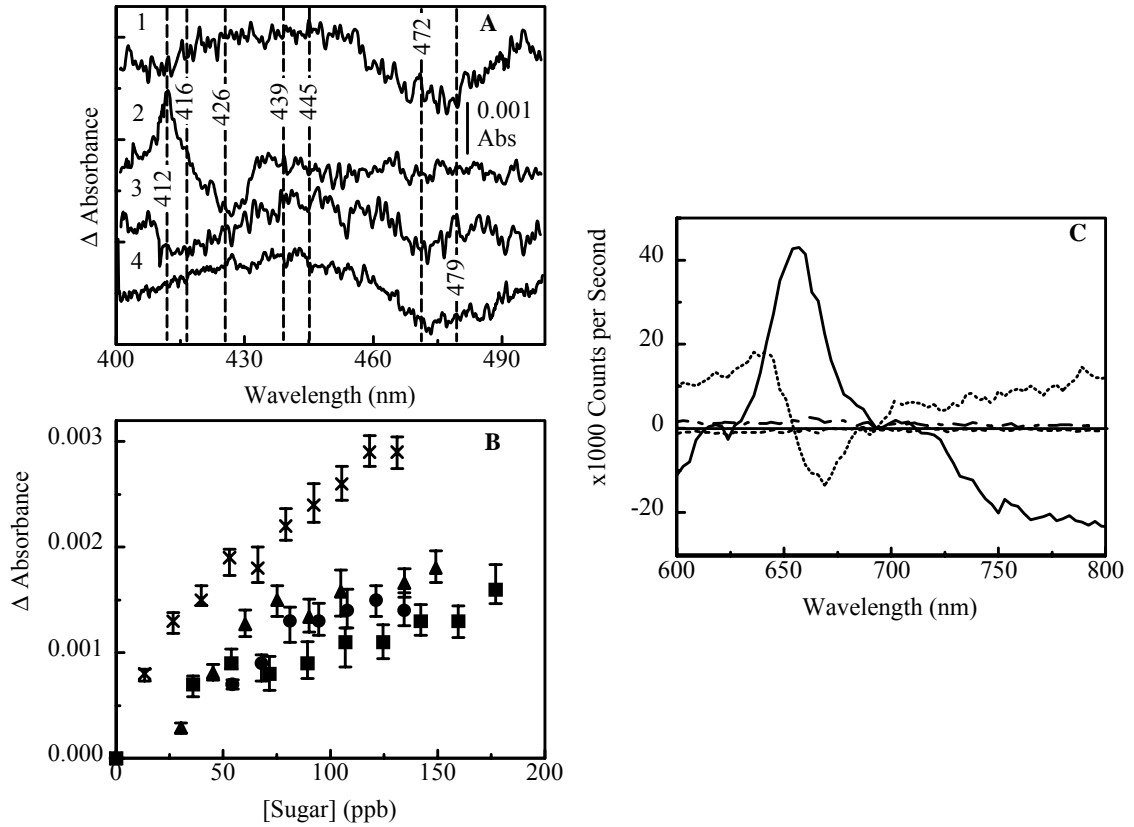


FIGURE 11.5 (A) The absorbance difference spectra NH₂TPP tissue + sugar minus NH₂TPP tissue in 50 mM pH 7 NaPi for MRP (Trace 1, 50 ppb), rhamnose (Trace 2, 50 ppb), galactosamine (Trace 3, 125 ppb), and fucose (Trace 4, 125 ppb) [343]. (B) The concentration dependence of the change in absorbance of NH₂TPP upon exposure to the sugars MRP (x), rhamnose (\blacktriangle), galactosamine (\blacksquare), and fucose (\bullet) [343]. (C) The fluorescence difference spectra NH₂TPP tissue + sugar (3 ppm, 16 μ M) minus NH₂TPP tissue in 50 mM pH 7 NaPi for MRP (...), rhamnose (—), galactosamine (— —), and fucose (- -) at 416 nm excitation [343].

TPPS₁ IN SOLUTION

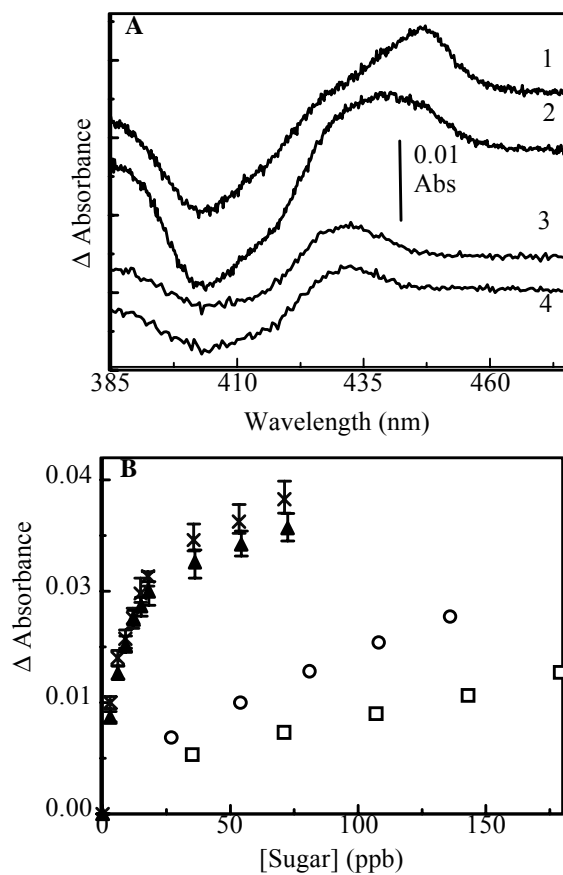


FIGURE 11.6 (A) The difference spectra TPPS₁ (1.8 μ M) + Sugar minus

TPPS₁ for MRP (50 ppb), rhamnose (50 ppb), fucose (27 ppb), and

galactosamine (71 ppb). (B) The concentration dependence of the

absorbance change upon exposure of TPPS₁ to MRP (x), rhamnose (▲),

fucose (○), and galactosamine (□).

IMMOBILIZED TPPS₁

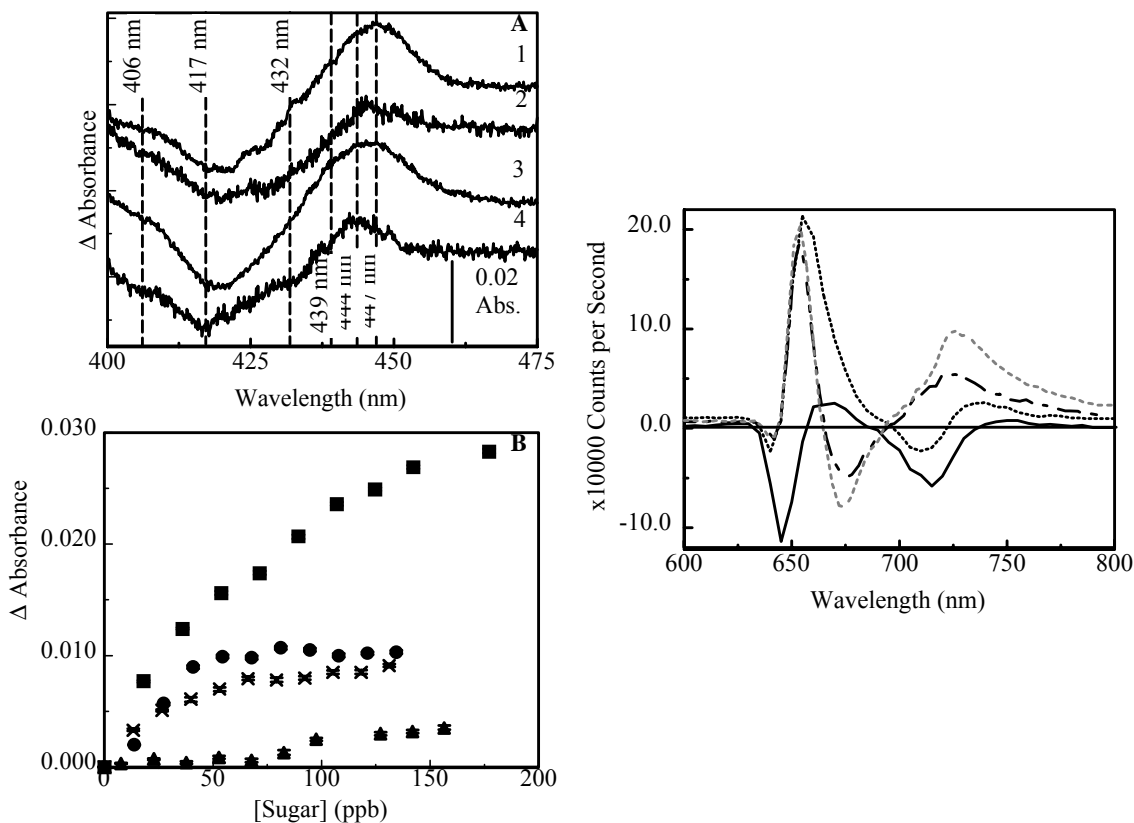


FIGURE 11.7 (A) The absorbance difference spectra TPPS₁ tissue + sugar (50 ppb) minus TPPS₁ tissue in 50 mM pH 7 NaPi for rhamnose (Trace 1), MRP (Trace 2, scaled up by a factor of 2), galactosamine (Trace 3), and fucose (Trace 4, scaled up by a factor of 2) [343]. (B) The concentration dependence of the change in absorbance of TPPS₁ upon exposure to the sugars MRP (x), rhamnose (\blacktriangle), galactosamine (\blacksquare), and fucose (\bullet) [343]. (C) The fluorescence difference spectra TPPS₁ tissue + sugar (3 ppm, 16 μ M) minus TPPS₁ tissue in 50 mM pH 7 NaPi for MRP (...), rhamnose (—), galactosamine (---), and fucose (- -) at 416 nm excitation [343].

TPPB IN SOLUTION

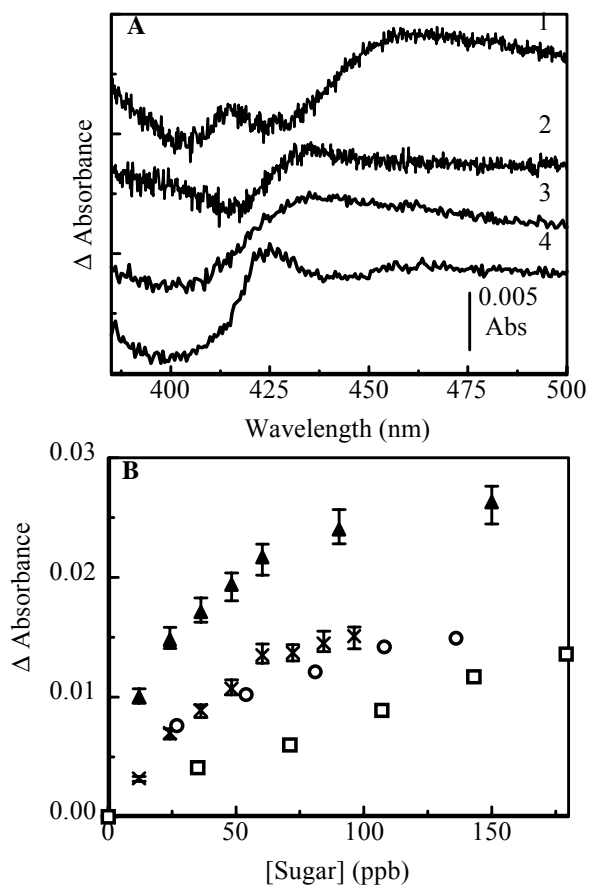


FIGURE 11.8 (A) The difference spectra TPPB (1.8 μ M) + Sugar minus TPPB for MRP (50 ppb), rhamnose (50 ppb), fucose (27 ppb), and galactosamine (107 ppb). (B) The concentration dependence of the absorbance change upon exposure of TPPB to MRP (x), rhamnose (\blacktriangle), fucose (\circ), and galactosamine (\square).

IMMOBILIZED TPPB

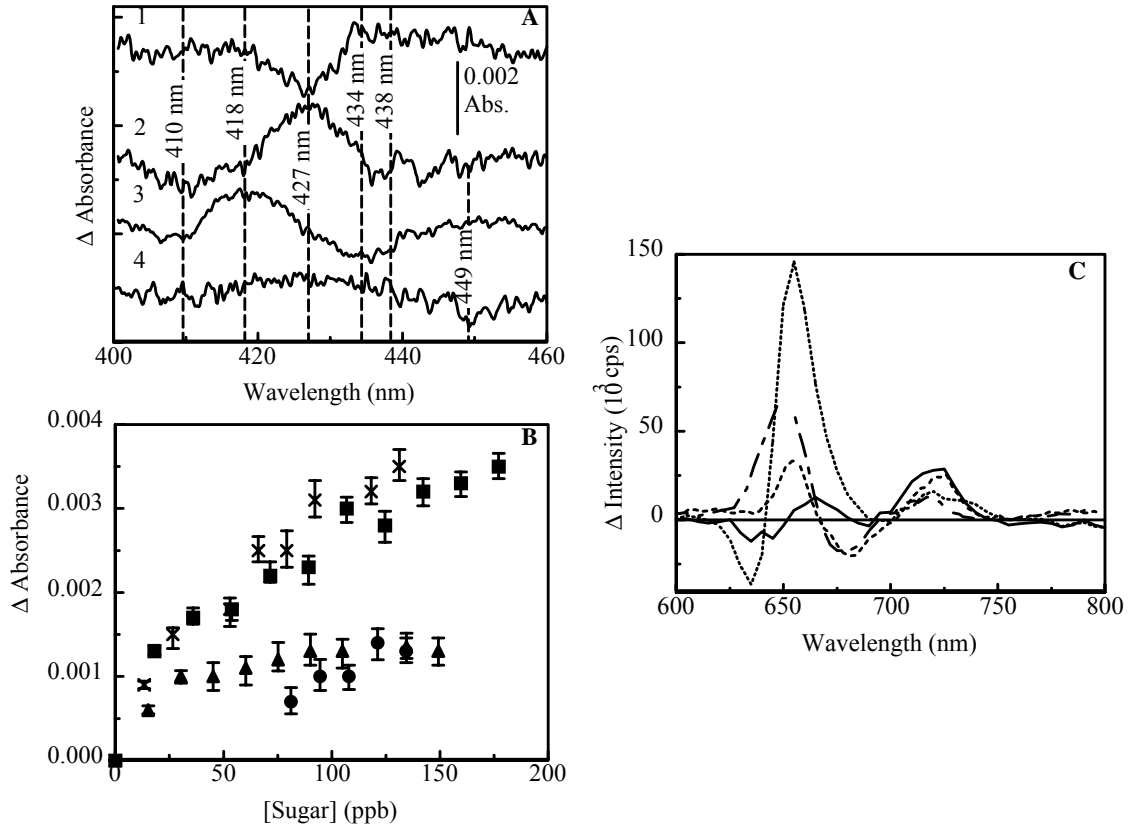


FIGURE 11.9 (A) The absorbance difference spectra TPPB tissue + sugar (125 ppb) minus TPPB tissue in 50 mM pH 7 NaPi for rhamnose (Trace 1), MRP (Trace 2), galactosamine (Trace 3), and fucose (Trace 4) [343]. (B) The concentration dependence of the change in absorbance of TPPB upon exposure to the sugars MRP (x), rhamnose (\blacktriangle), galactosamine (\blacksquare), and fucose (\bullet) [343]. (C) The fluorescence difference spectra TPPB tissue + sugar (3 ppm, 16 μ M) minus TPPB tissue in 50 mM pH 7 NaPi for MRP (...), rhamnose (—), galactosamine (— —), and fucose (- -) at 423 nm excitation [343].

BACILLUS THURINGENSIS SPORES

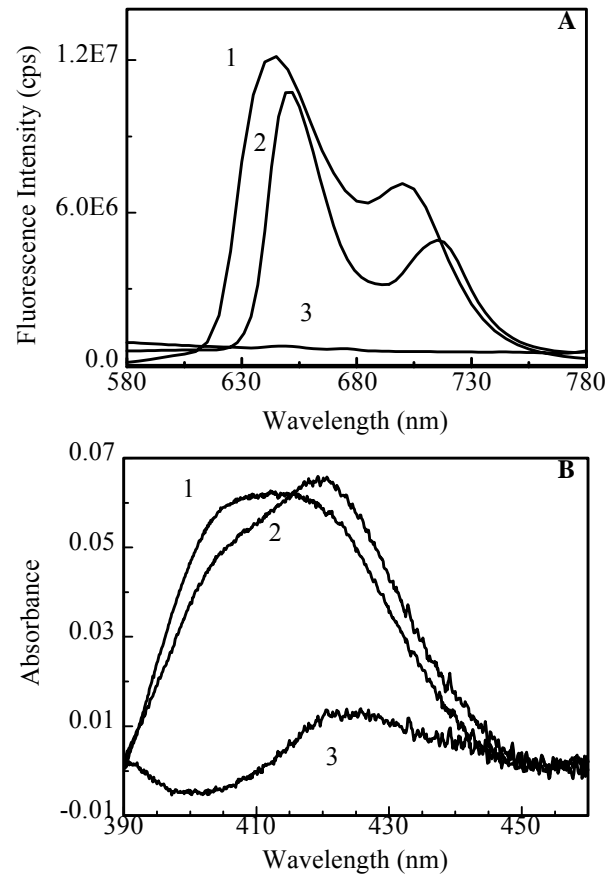


FIGURE 11.10 (A) Fluorescence emission spectrum of TPPS₁ (740 nM) at 411 nm excitation in the absence (Trace 1)/ presence (Trace 2) of *Bacillus thuringiensis* spores (0.2 mg/ml) and the fluorescence spectrum of *Bacillus thuringiensis* spores alone (0.2 mg/ml) (50 mM NaPi pH 7). (B) The absorbance spectra of TPPS₁ (740 nM) in the absence (Trace 1)/ presence (Trace 2) of *Bacillus thuringiensis* spores (0.2 mg/ml) and the difference spectrum TPPS₁ + *B. thuringiensis* minus TPPS₁. This data is for spores that have been cracked by repeated freezing and thawing in aqueous solution.

CHAPTER 12

DETECTION OF CYANIDE

12.1 CYANIDE

Cyanide is a commonly used chemical warfare (CW) agent and is used in a variety of industrial processes, such as electroplating, coke production, and cleaning of metallic parts. Its toxicity poses a threat to the safety of emergency personnel and the general public. There is great need for a detector of such CW agents as well as other toxic agents for use by first responders, emergency or military personnel, and chemical workers. A sensor that is agent-specific with a minimum of interferences and false positive readings and that is rapid, sensitive, solid-state and will report in real time would be ideal. The search for devices with as many of these characteristics as possible is ongoing.

Many cyanide sensors are in development or production and use various methods of detection. Current methods include electrochemical sensors as used by Dräger® and Enmet® and immobilized metal-complexed dyes [594]. Other companies such as RAE Systems® employ photoionization detectors. Chemiluminescence sensors have been used in cyanide detection [595]; chemiluminescence experiments involving enzymes such as rhodanese, sulfite oxidase, and peroxidase have been performed by Ikebukuro [596]. Metal anodes such as silver or gold have been used to amperometrically quantify cyanide in solution [597]. Oxygen electrodes have also been used extensively in the determination of cyanide; Lee and Karube [598] have been able to detect 200 ppb cyanide by inhibition of *Pseudomonas fluorescens* respiration using an oxygen electrode.

Enzymes such as cytochrome oxidase and horseradish peroxidase have been used in conjunction with electrodes extensively to detect and quantify cyanide [599-600]. Cyanide-specific electrodes have been explored as cyanide sensors as well [601] and are capable detecting less than 0.1 ppm (6.026 μM) cyanide. Spectroscopic [602] and spectrofluorometric methods [594, 603-606] have been used for detection and quantification of cyanide via light absorbing intermediates or reaction products.

Porphyrins are intensely colored biological molecules with absorbance spectra that are sensitive to the presence of different reagents and different conditions such as pH and ionic strength. Metalloporphyrins may be useful in detection of cyanide due to the affinity of cyanide for many metals such as rhodium, silver, gold, and copper. Cyanide has been shown to cause a shift in the Soret absorbance of a rhodium porphyrin from 417 nm in its absence to 427.5 nm in its presence with a detection limit of 7.84 ppm (160 μM)[604]. Porphyrins have been shown to be very sensitive to their environments and are highly selective for different reagents with a specific reagent giving peaks at specific wavelengths [264, 283-284]. Immobilization of porphyrins to a substrate such as a cellulose membrane, quartz, or other substance [453-456] permits usage and storage for extended periods.

Cyanide binds to hemoglobin, myoglobin, and cytochromes as well as other metallo-proteins and inhibits mitochondrial energy production by binding to cytochrome oxidase. Myoglobin has a strong absorbance spectrum that is sensitive to the interaction of ligands such as CN^- , CO , and O_2 with the heme. In this chapter two systems are reported for the detection of low levels of cyanide; first, copper porphyrin immobilized to cellulose film rapidly detects low levels of NaCN in aqueous solution; and second,

myoglobin immobilized to a glass surface can be used to detect the presence of 1.5 to 20ppb (31 nM and 408 nM respectively) NaCN in solution and the presence of HCN gas in less than ten seconds.

12.2 MATERIALS AND METHODS

Granular sodium cyanide, cupric sulfate 5-hydrate ($\text{CuSO}_4 \cdot 5\text{H}_2\text{O}$), and sodium chloride were obtained from J.T. Baker Chemical Co. (Phillipsburg, NJ).

SPECTRA/POR[®] molecular porous membrane tubing was obtained from Spectrum (Houston, TX). Meso-tetra (4-carboxyphenyl) porphine monoethylene diamine coupled to Traut's reagent (2-iminothiolane) here referred to as TPPT, was obtained from Frontier Scientific (Logan, UT). ProbeOn[™] Plus microscope slides were obtained from Fisher Biotech (Pittsburgh, PA). Myoglobin (Type III from horse heart, lyophilized powder) and glutaraldehyde were obtained from Sigma (St. Louis, MO). Cyanide gas (10 ppm HCN in N_2) was obtained from Drager (Pittsburgh, PA).

TPPT was bound to SPECTRA/POR[®] molecular-porous membrane tubing and complexed with copper through the procedure described in Chapter 4. Cellulose tubing was soaked in 56 μM TPPT solution at room temperature for four hours. The tubing was placed in 1M NaCl overnight in the dark followed by soaking in 50% ethanol for 0.5 hours to remove any unbound porphyrin. Deionized water was used to rinse the NaCl and ethanol from the tubing. At this point, copper was complexed to the membrane-bound TPPT by soaking the films in a 5 mM solution of CuSO_4 for four hours. Deionized water was used to rinse the uncomplexed copper from the films. These films were dried and stored at room temperature protected from dust in the dark.

Measurement of the films was accomplished by cutting strips to fit a standard 3 ml cuvette (0.9cm width). The films were held against the front wall of the cuvette with a custom made plastic clip. Measurements were made in 3 ml pH 7 sodium phosphate buffer (NaPi) 25 mM. Absorption spectra were collected using a Cary 4E UV-Visible spectrophotometer at 0.02 nm resolution in the presence/absence of NaCN. A scaling factor was determined for each data set by using the ratio of 0.065 A to the absorbance intensity of the porphyrin film at 416 nm in order to compensate variations in porphyrin density on the film surfaces. Each of the traces in the data series was then multiplied by this factor followed by calculation of difference spectra by subtraction of the scaled absolute spectra using Grams/32 (Galactic Industries, Salem, NH). The second derivative of the difference spectra were taken using Grams/32 to determine peak positions. Linear fitting was performed using PSI-Plot.

Immobilization of myoglobin onto glass was accomplished at room temperature on ProbeOn™ Plus microscope slides as described in Chapter 4. The slides were activated 0.17 M glutaraldehyde followed by rinsing with PBS. Slide surfaces were then allowed to interact with 10 mg/ml myoglobin in 50 mM pH 7 NaPi for 2 hours followed by rinsing with NaCl and ethanol solutions and H₂O to remove any unbound protein. The slide was exposed to NaCN in solution by placing 200µl of the appropriate concentration on the surface of the slide. The excess solution was immediately blotted away. The slide was exposed to HCN gas as a mixture of 10 ppm HCN and 99% N₂. Constant pressure flow valves were used to dilute the 10 ppm Drager HCN to the desired concentrations. Measurements were collected as described previously (Chapter 5) using an Ocean Optics

USB2000 spectrophotometer with the output of a LED with maximum wavelength at 434 nm and 83 nm HBW.

12.3 TPPT

The absorbance spectrum of immobilized CuTPPT in the absence/presence of 4 ppb (82 nM) NaCN is shown in Figure 12.1 (Traces 1 and 2, respectively). The CuTPPT immobilized onto the cellulose membrane gives apparent absolute absorbance peaks at 416 nm in the absence of cyanide and 417 nm in the presence of cyanide. The difference spectrum CuTPPT + NaCN minus CuTPPT is shown in Figure 12.1 (Trace 3). The shallow trough located at 411 nm indicates a decrease in the ligand-free CuTPPT while the 421 nm peak is a new absorption band that results from the formation of a CuTPPT-NaCN complex.

The apparent shallowness of the trough in the CuTPPT + NaCN minus CuTPPT difference spectrum is of some concern. The results (Figure 12.1) of peak fitting the absolute spectra shown in Figure 12.1 (Traces 1 and 2) indicate the involvement of three peaks in the absorbance spectrum of CuTPPT. All three of the peaks are changed upon exposure to NaCN (Table 12.1). The combination of the changes in the three peaks causes the shallowness of the trough in the difference spectrum.

As seen in Figure 12.2, the absorbance increase at 421nm in the difference spectrum shows a half hyperbolic dependence on NaCN concentration. Extrapolation of the data to a 3:1 signal:noise ratio indicates a detection limit of 0.7 ppb (14.3 nM). The changes in the absorbance spectrum level off around 75 ppb.

12.4 MYOGLOBIN

The absolute absorbance spectrum of immobilized myoglobin is shown in Figure 12.3 with peak fitting results at a 99.98% confidence interval. The Soret absorbance of myoglobin in solution is located at 406 nm. Upon immobilization, the absolute absorbance spectrum of myoglobin is altered. The peaks at 412, 448, and 476 nm shown in Figure 12.3 contribute to the absolute absorbance spectrum of myoglobin when immobilized onto glass, resulting in a broadened signal. The effect of immobilization on the absorbance spectrum of porphyrins has been previously documented [455]. Figure 12.3 shows the difference absorbance spectrum protein + NaCN minus protein for immobilized myoglobin. The heme-protein shows increased absorbance intensity at 400 nm and decreased absorbance intensity at 444 nm upon exposure to NaCN with an additional absorbance increase at 495 nm.

Figure 12.4 shows the concentration dependence of the change in the peak absorbance intensity (444 nm) for myoglobin upon exposure to NaCN in solution. The response of the protein surface is linear to 20 ppb after which the changes in the absorbance spectrum are greatly reduced suggesting saturation effects begin at 20 ppb.

As seen in Figure 12.5, reaction of the myoglobin surface to HCN gas is linearly dependent on HCN concentration over the range of values tested. Peak and trough positions for the protein + HCN gas minus protein difference spectra are identical to those for the myoglobin surface exposed to NaCN solution.

12.5 DISCUSSION

Methods such as electrochemical sensors, cyanide activated metal-complexed dyes, and optically sensitive molecules including porphyrins have been employed to detect cyanide [594, 597, 601, 607]. Calcein, a polyanionic fluorescein derivative, complexed to Cu^{2+} and bound to an Amberlite resin surface has been used to detect cyanide in wastewater. The copper-complexed calcein does not fluoresce while ligand-free calcein does. Addition of cyanide to the Cu^{2+} -Calcein complex results in fluorescence by removing the Cu^{2+} ligand [594]. However, any molecule that leads to the removal of the metal bound to the indicator will produce the same fluorescence intensity increase. In contrast, our porphyrin system relies on cyanide ions to bind to but not remove the copper bound to TPPT.

The method reported by Rao [597] employed silver electrodes in a silver dicyano complex; cyanide concentrations were obtained by calculating midpoint potentials, which is slow and requires many measurements. Immobilized *Saccharomyces cerevisiae* was used by Ikebukuro [608] to detect cyanide in river water. This method required time for the measurement of the respective rate before and after exposure to river water and the active element had a lifetime of only nine days.

Metalloporphyrins such as rhodium(III)-tetrakis(4-sulfonatophenyl)porphyrin (Rh-TPPS) have been used as cyanide scavengers [607]. Hambright [607] demonstrated the effectiveness of cyanide detection using Rh-TPPS in solution indicating that the reaction was first order with respect to cyanide concentration from 1.6 mM to 0.16 mM (104 ppm and 10.4 ppm respectively), within the levels of detection desired by the military (2 ppm; 41 μM) [504]. Detection of cyanide here using CuTPPT films exceeds

current detection level requirements by 1000-fold with a limit of detection less than 2 ppb (41 nM) and saturation of the surface at 75 ppb. Additional advantages of film immobilized CuTPPT are speed of detection (six seconds or less) as well as the ability of the films to be stored for years and retain their reactivity (data not shown). The CuTPPT films do not respond to the presence of HCN gas at concentrations up to 10 ppm. Early investigation of peak-trough positions for the interaction of CuTPPT with other metal binding compounds such as 1,10-phenanthroline and dipicolinic acid indicates highly specific response from the porphyrin with each of these compounds giving a unique signature from that of NaCN. This specificity is as expected based on previous reports [264, 283, 379].

Immobilized myoglobin surfaces demonstrate the ability to detect HCN gas from 1 ppm to 10 ppm. The myoglobin surface shows detection limits in solution of 1.5 ppb (31 nM) NaCN, with absorbance changes leveling off around 40 ppb (820 nM). The dynamic range of the surface is dependent on the amount of protein present. Using a variation of the described immobilization procedure, another set of surfaces gave absorbance intensities of 0.05 A as compared to 0.25 A for the surfaces described here and showed saturation points at 7 ppb. Increasing the surface density of myoglobin will increase the dynamic range of this sensor surface.

The minimization of false positives and negatives in a detection system is essential. The myoglobin system, showing absorbance increases at 400 nm and 495 nm and a decrease at 444 nm, gives an additional measurement wavelength that yields greater specificity for the detection system. If the decrease and increase in absorbance do not both appear or do not appear at the proper wavelengths, the signal is false and not due to

the desired analyte. Exposure of the immobilized myoglobin surface to CO gas results in a loss in absorbance intensity at 408 nm with an increase in absorbance intensity at 442 nm. The interaction of carbon monoxide with the slide surface can therefore be distinguished from that of cyanide gas. No change in absorbance was observed upon exposure of the myoglobin surface to a stream of N₂ gas.

Myoglobin slides have been used after storage for no more than 50 days thus far. Further information on the slide lifetime as well as the response of the surface to different conditions and the activity of possible interferents is needed before a system of this type could be put into operation.

PEAK FITTING RESULTS FOR FIGURE 12.1

	Peak Position (nm)	Height (A)	FWHM (nm)	% Total Area
CuTPPT	412	0.038	43	59
	416	0.036	15	20
	464	0.011	56	21
CuTPPT + NaCN	413	0.037	41	59
	417	0.038	15	24
	463	0.009	52	17

TABLE 12.1 The peak fitting results from Figure 12.1 help to explain the shallowness of the trough in the porphyrin + cyanide minus porphyrin difference spectrum [342].

EXPOSURE OF TPPT TO CYANIDE

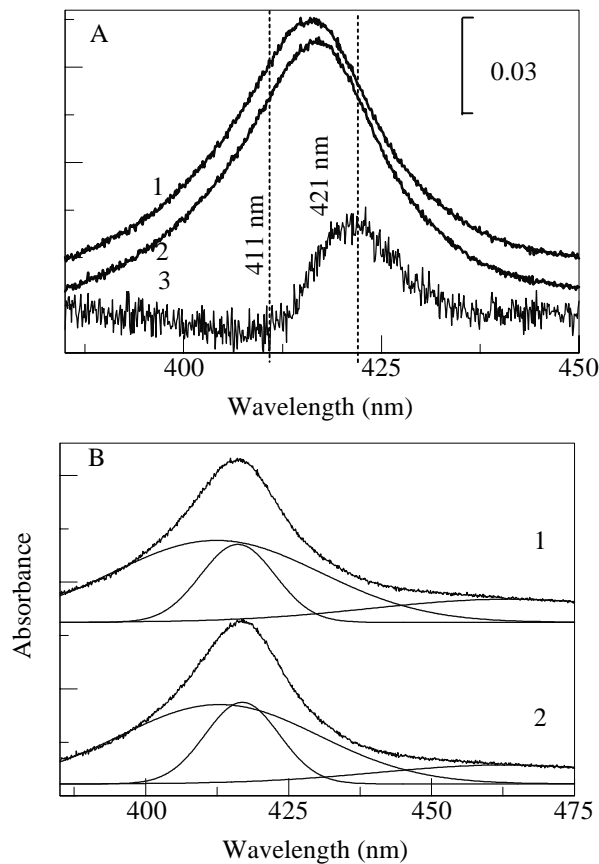


FIGURE 12.1 (A) Absorbance spectra of CuTPPT covalently immobilized onto dialysis tubing membrane in the absence (Trace 1) and presence (Trace 2) of NaCN (4 ppb) (82 nm) at pH 7. The difference spectrum CuTPPT + NaCN minus CuTPPT is shown in Trace 3 (scaled up by a factor of 3) [342]. (B) GRAMS/32 peak fitting at a 99.98% confidence interval for Traces 1 and 2 shown in Figure A demonstrates the involvement of three curves in the CuTPPT absorbance spectrum [342].

CONCENTRATION DEPENDENCE OF ABSORANCE CHANGE

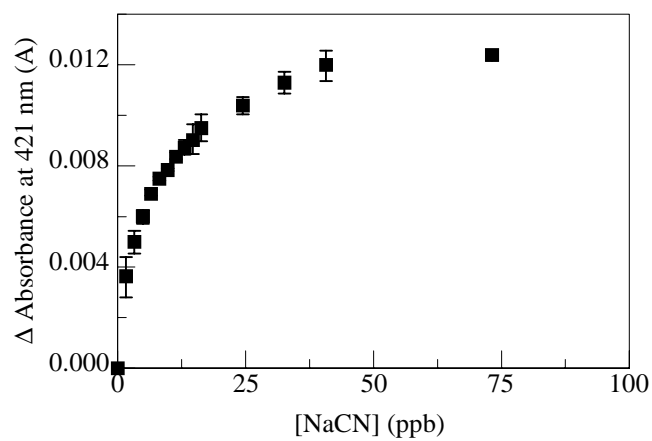


FIGURE 12.2 The change in absorbance intensity of immobilized CuTPPT at 421 nm as shown in Figure 12.1 (Trace 3) demonstrates a hyperbolic dependence on NaCN concentration [342].

CYANIDE EXPOSURE OF MYOGLOBIN SURFACE

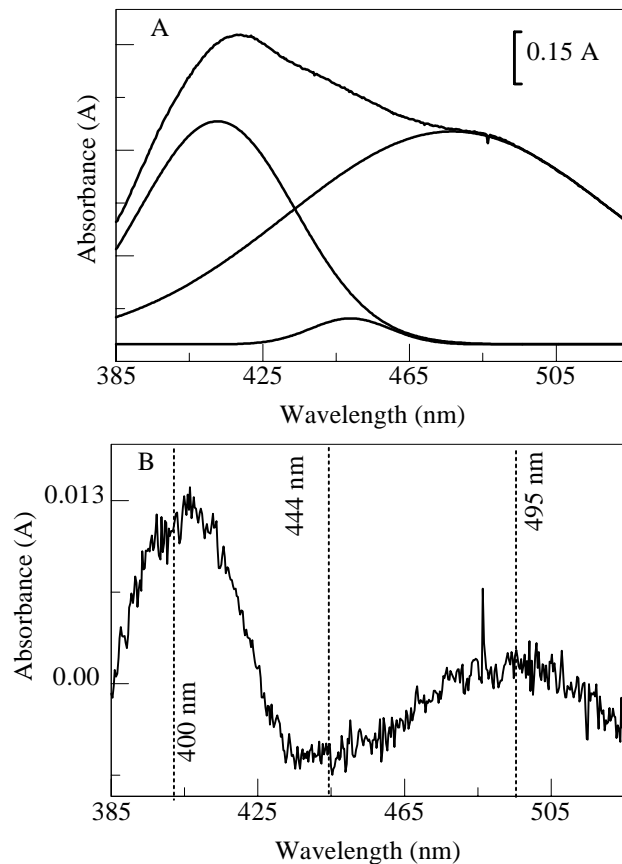


FIGURE 12.3 (A) The absolute spectrum of myoglobin immobilized onto a glass surface is shown with results of peak fit to demonstrate changes in absorbance spectrum upon immobilization [342]. (B) The difference spectrum myoglobin + NaCN minus myoglobin shows the result of immobilized myoglobin exposure to 20 ppb NaCN [342].

CYANIDE CONCENTRATION DEPENDENCE

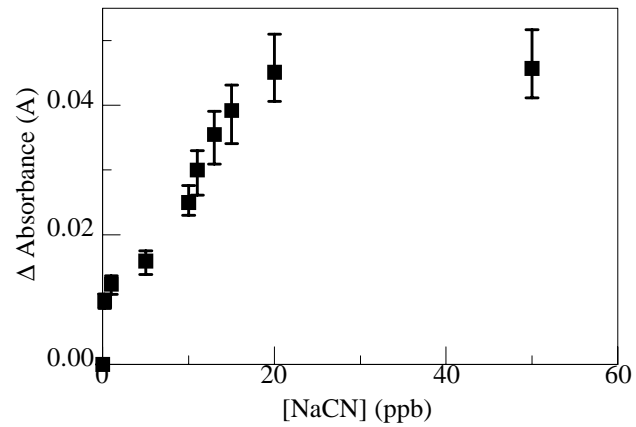


FIGURE 12.4 The intensity of the peak at 444 nm (Figure 12.3) in the difference spectrum myoglobin + NaCN minus myoglobin shows half hyperbolic dependence on NaCN concentration [342].

EXPOSURE OF MYOGLOBIN SURFACE TO HCN

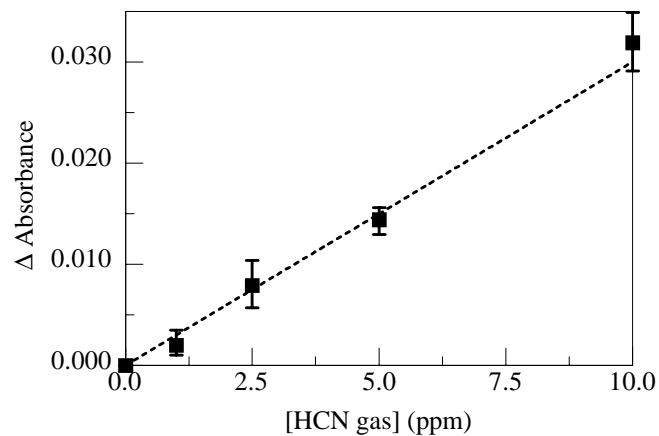


FIGURE 12.5 The peak minus trough difference 444 nm and 400 nm from the difference spectrum myoglobin + HCN gas minus myoglobin (data not shown) shows linear dependence on concentration of HCN in the gas mixture [342].

CHAPTER 13

FINAL STATEMENTS

The work presented here has been directed at the development of sensor surfaces for the optical detection and quantification of the presence of analytes of interest. All of the described surfaces have employed a porphyrin for signal transduction taking advantage of the strong absorbance characteristics of the porphyrin macrocycle and the high degree of sensitivity of these characteristics to changes in the environment of the porphyrin.

Chapters 10, 11, and 12 detail methods for detection of analytes based on immobilized porphyrin surfaces with the porphyrin acting as both transduction and recognition element. The data presented in these chapters demonstrates the high degree of sensitivity and specificity attainable through the use of the porphyrin surfaces for detection of compounds of interest ranging from sugars to volatile organic compounds. The porphyrins have been immobilized to cellulose films, cellulose tissues, and glass slides providing surfaces adaptable to a variety of different applications.

Chapters 5 through 9 deal with application of porphyrins for signal transduction in a novel system based on the reversible inhibition of enzymes. Six different enzyme based surfaces are discussed, all employing a glass microscope slide as the support surface though the immobilization techniques could be adapted to any amino-functionalized surface such as activated nylon or cellulose. The glass microscope slide is used as a planar waveguide allowing the absorbance spectrum of the immobilized porphyrin-enzyme surface to be collected by evanescent wave absorbance spectroscopy.

There are several advantages to this measurement technique. The sample is not applied between the light source and the detector, so correction for the absorbance of the sample is not necessary. The technique collects an absorbance spectrum with a 2.54 cm path length (1 inch) rather than a path length equal to the thickness of the coating allowing for a very thin layer (basically one enzyme thick) to be used while still obtaining a measurement with a good signal to noise ratio. This also prevents the diffusion issues faced by multilayer surfaces. The measurement that is obtained is effectively the average of the area covered by the longer path length as well as the broad linear fiber optic (1 cm). This averaging gives excellent reproducibility even when surfaces are produced in small groups. The discrepancies between the different slides and different areas on a single slide become obvious when measurements are collected perpendicularly to the surface with an instrument such as the Cary 4E.

Though the measurement protocol is not yet common, it is finding a great deal of popularity in new sensor applications. The novel aspect of the detection protocols described in Chapters 5 through 9 is the reversible inhibition of the enzyme by a colorimetric agent that gives a unique absorbance spectrum signature depending on if it is bound to the enzyme or not. To make the concept clear, the porphyrin interacts with the enzyme in the same place that the analyte (substrate or inhibitor) to be detected does. When the porphyrin-enzyme complex is exposed to the analyte, the porphyrin moves away from the enzyme and the analyte takes its place. When the porphyrin-enzyme complex is intact, the porphyrin absorbance spectrum has characteristics different from those of the porphyrin when it is not bound to the enzyme. The changes in the absorbance spectrum that occur upon dissociation of the porphyrin from the enzyme can

be used to indicate the presence of the analyte. In addition, the degree of change, that is how many porphyrins dissociate from enzymes, is related to the concentration of the analyte, so the intensity of the absorbance changes can be used to indicate analyte concentration.

The lack of diffusion considerations and the use of a direct event for indication of analyte presence and concentration allow this detection technique to be used in real time with time requirements imposed by the spectrophotometer and data handling. The technique has also proven to be exceptionally sensitive with limits of detection for organophosphorus compounds below the current safe drinking water standards. The detection of gaseous carbon dioxide and hydrogen cyanide has been demonstrated and presents a strong argument in favor of the ability of the other enzyme surfaces to detect analytes in vapor phase, though no guess at sensitivity can be made.

The surfaces described in Chapters 5, 6, and 9 are designed for the detection of organophosphorus compounds including pesticides and nerve agents. Though no data can be presented on detection of live agents such as sarin, the surfaces have not failed to respond to all inhibitor (substrate) challenges ranging from drugs for treatment of Alzheimer's disease to organophosphorus pesticides. Agent testing is planned for the surfaces, but time constraints prevent the inclusion of those results.

REFERENCES

- [1] A. Mulchandani and K. Rogers, "Enzyme and Microbial Biosensors: Techniques and Protocols," in *Methods in Biotechnology*, vol. 6. Totowa, NJ: Humana Press, 1998.
- [2] A. L. Simonian, J. K. Grimsley, A. W. Flounders, J. S. Schoeniger, T. C. Cheng, J. J. DeFrank, and J. R. Wild, "Enzyme-based biosensor for the direct detection of fluorine-containing organophosphates," *Analytica Chimica Acta*, vol. 442, pp. 15-23, 2001.
- [3] P. Mulchandani, W. Chen, and A. Mulchandani, "Flow injection amperometric enzyme biosensor for direct determination of organophosphate nerve agents," *Environmental Science & Technology*, vol. 35, pp. 2562-2565, 2001.
- [4] A. Mulchandani, P. Mulchandani, W. Chen, J. Wang, and L. Chen, "Amperometric thick film strip electrodes for monitoring organophosphate nerve agents based on immobilized organophosphorus hydrolase," *Analytical Chemistry*, vol. 71, pp. 2246-2249, 1999.
- [5] V. Sacks, I. Eshkenazi, T. Neufeld, C. Dosoretz, and J. Rishpon, "Immobilized parathion hydrolase: An amperometric sensor for parathion," *Analytical Chemistry*, vol. 72, pp. 2055-2058, 2000.
- [6] R. D. Richins, A. Mulchandani, and W. Chen, "Expression, immobilization, and enzymatic characterization of cellulose-binding domain-organophosphorus hydrolase fusion enzymes," *Biotechnology and Bioengineering*, vol. 69, pp. 591-596, 2000.

- [7] E. N. Efremenko, V. I. Lozinsky, V. S. Sergeeva, F. M. Plieva, T. A. Makhlis, G. M. Kazankov, A. K. Gladilin, and S. D. Varfolomeyev, "Addition of polybrene improves stability of organophosphate hydrolase immobilized in poly(vinyl alcohol) cryogel carrier," *Journal of Biochemical and Biophysical Methods*, vol. 51, pp. 195-201, 2002.
- [8] M. J. Schoning, R. Krause, K. Block, M. Musahmeh, A. Mulchandani, and J. Wang, "A dual amperometric/potentiometric FIA-based biosensor for the distinctive detection of organophosphorus pesticides," *Sensors and Actuators B-Chemical*, vol. 95, pp. 291-296, 2003.
- [9] J. Wang, R. Krause, K. Block, M. Musameh, A. Mulchandani, and M. J. Schoning, "Flow injection amperometric detection of OP nerve agents based on an organophosphorus-hydrolase biosensor detector," *Biosensors & Bioelectronics*, vol. 18, pp. 255-260, 2003.
- [10] A. L. Simonian, B. D. diSioudi, and J. R. Wild, "An enzyme based biosensor for the direct determination of diisopropyl fluorophosphate," *Analytica Chimica Acta*, vol. 389, pp. 189-196, 1999.
- [11] A. W. Flounders, A. K. Singh, J. V. Volponi, S. C. Carichner, K. Wally, A. S. Simonian, J. R. Wild, and J. S. Schoeniger, "Development of sensors for direct detection of organophosphates. Part II: sol-gel modified field effect transistor with immobilized organophosphate hydrolase," *Biosensors & Bioelectronics*, vol. 14, pp. 715-722, 1999.

- [12] P. Mulchandani, A. Mulchandani, I. Kaneva, and W. Chen, "Biosensor for direct determination of organophosphate nerve agents. 1. Potentiometric enzyme electrode," *Biosensors & Bioelectronics*, vol. 14, pp. 77-85, 1999.
- [13] K. R. Rogers, Y. Wang, A. Mulchandani, P. Mulchandani, and W. Chen, "Organophosphorus hydrolase-based assay for organophosphate pesticides," *Biotechnology Progress*, vol. 15, pp. 517-521, 1999.
- [14] I. Karube, K. Hara, H. Matsuoka, and S. Suzuki, "Amperometric Determination of Total Cholesterol in Serum With Use of Immobilized Cholesterol Esterase and Cholesterol Oxidase," *Analytica Chimica Acta*, vol. 139, pp. 127-132, 1982.
- [15] Suman and C. S. Pundir, "Co-immobilization of cholesterol esterase, cholesterol oxidase and peroxidase onto alkylamine glass beads for measurement of total cholesterol in serum," *Current Applied Physics*, vol. 3, pp. 129-133, 2003.
- [16] S. Singh, A. Chaubey, and B. D. Malhotra, "Amperometric cholesterol biosensor based on immobilized cholesterol esterase and cholesterol oxidase on conducting polypyrrole films," *Analytica Chimica Acta*, vol. 502, pp. 229-234, 2004.
- [17] A. Krug, R. Gobel, and R. Kellner, "Flow-Injection Analysis For Total Cholesterol With Photometric Detection," *Analytica Chimica Acta*, vol. 287, pp. 59-64, 1994.
- [18] H. Endo, M. Maita, M. Takikawa, H. F. Ren, T. Hayashi, N. Urano, and K. Mitsubayashi, "Enzyme sensor system for determination of total cholesterol in fish plasma," *Fisheries Science*, vol. 69, pp. 1194-1199, 2003.

- [19] C. K. Pires, B. F. Reis, C. X. Galhardo, and P. B. Martelli, "A multicommutated flow procedure for the determination of cholesterol in animal blood serum by chemiluminescence," *Analytical Letters*, vol. 36, pp. 3011-3024, 2003.
- [20] A. L. Crumbliss, J. Stonehuerner, R. W. Henkens, J. P. Odaly, and J. Zhao, "The Use of Inorganic Materials to Control or Maintain Immobilized Enzyme-Activity," *New Journal of Chemistry*, vol. 18, pp. 327-339, 1994.
- [21] V. Raghavan, K. Ramanathan, P. V. Sundaram, and B. Danielsson, "An enzyme thermistor-based assay for total and free cholesterol," *Clinica Chimica Acta*, vol. 289, pp. 145-158, 1999.
- [22] T. Nakaminami, S. Ito, S. Kuwabata, and H. Yoneyama, "Amperometric determination of total cholesterol at gold electrodes covalently modified with cholesterol oxidase and cholesterol esterase with use of thionin as an electron mediator," *Analytical Chemistry*, vol. 71, pp. 1068-1076, 1999.
- [23] L. Braco, J. A. Daros, and M. Delaguardia, "Enzymatic Flow-Injection Analysis in Nonaqueous Media," *Analytical Chemistry*, vol. 64, pp. 129-133, 1992.
- [24] X. J. Wu and M. M. F. Choi, "Hydrogel network entrapping cholesterol oxidase and octadecylsilica for optical biosensing in hydrophobic organic or aqueous micelle solvents," *Analytical Chemistry*, vol. 75, pp. 4019-4027, 2003.
- [25] A. Kumar, Rajesh, A. Chaubey, S. K. Grover, and B. D. Malhotra, "Immobilization of cholesterol oxidase and potassium ferricyanide on dodecylbenzene sulfonate ion-doped polypyrrole film," *Journal of Applied Polymer Science*, vol. 82, pp. 3486-3491, 2001.

- [26] K. V. Gobi and F. Mizutani, "Layer-by-layer construction of an active multilayer enzyme electrode applicable for direct amperometric determination of cholesterol," *Sensors and Actuators B-Chemical*, vol. 80, pp. 272-277, 2001.
- [27] A. Devadoss and J. D. Burgess, "Detection of cholesterol through electron transfer to cholesterol oxidase in electrode-supported lipid bilayer membranes," *Langmuir*, vol. 18, pp. 9617-9621, 2002.
- [28] O. Baticz and S. Tomoskozi, "Determination of total cholesterol content in food by flow injection analysis with immobilized cholesterol oxidase enzyme reactor," *Nahrung-Food*, vol. 46, pp. 46-50, 2002.
- [29] C. Bongiovanni, T. Ferri, A. Poscia, M. Varalli, R. Santucci, and A. Desideri, "An electrochemical multienzymatic biosensor for determination of cholesterol," *Bioelectrochemistry*, vol. 54, pp. 17-22, 2001.
- [30] S. Brahim, D. Narinesingh, and A. Giuseppi-Elie, "Interferent suppression using a novel polypyrrole-containing hydrogel in amperometric enzyme biosensors," *Electroanalysis*, vol. 14, pp. 627-633, 2002.
- [31] C. A. Marquette, B. D. Leca, and L. P. Blum, "Electrogenerated chemiluminescence of luminol for oxidase-based fibre-optic biosensors," *Luminescence*, vol. 16, pp. 159-165, 2001.
- [32] F. Cheillan, A. Albano, and M. Mascini, "Amperometric Biosensors For Measurement of Cholesterol and Application to Clinical-Samples," *Annali Di Chimica*, vol. 81, pp. 673-691, 1991.
- [33] A. M. N. Hendji, N. Jaffrezicrenault, M. Claude, A. A. Shulga, S. V. Dzydevich, A. P. Soldatkin, and A. V. Elskaya, "Enzyme Biosensor Based On a

- Micromachined Interdigitated Conductometric Transducer - Application to the Detection of Urea, Glucose, Acetylcholine and Butyrylcholine Chlorides,” *Sensors and Actuators B-Chemical*, vol. 21, pp. 123-129, 1994.
- [34] L. Doretto, D. Ferrara, S. Lora, F. Schiavon, and F. M. Veronese, “Acetylcholine Biosensor Involving Entrapment of Acetylcholinesterase and Poly(Ethylene Glycol)-Modified Choline Oxidase in a Poly(Vinyl Alcohol) Cryogel Membrane,” *Enzyme and Micro Tech*, vol. 27, pp. 279-285, 2000.
- [35] G. A. Evtugyn, E. E. Stoikova, R. R. Iskanderov, E. B. Nikolskaya, and G. K. Budnikov, “Electrochemical sample preparation for the enzymatic determination of cholinesterase inhibitors,” *Journal of Analytical Chemistry*, vol. 52, pp. 2-5, 1997.
- [36] H. Gulce, Y. S. Aktas, A. Gulce, and A. Yildiz, “Polyvinylferrocenium immobilized enzyme electrode for choline analysis,” *Enzyme and Microbial Technology*, vol. 32, pp. 895-899, 2003.
- [37] T. Inoue, J. R. Kirchhoff, and R. A. Hudson, “Enhanced measurement stability and selectivity for choline and acetylcholine by capillary electrophoresis with electrochemical detection at a covalently linked enzyme-modified electrode,” *Analytical Chemistry*, vol. 74, pp. 5321-5326, 2002.
- [38] A. N. Ivanov, G. A. Evtugyn, L. V. Lukachova, E. E. Karyakina, H. C. Budnikov, S. G. Kiseleva, A. V. Orlov, G. P. Karpacheva, and A. A. Karyakin, “New polyaniline-based potentiometric biosensor for pesticides detection,” *Ieee Sensors Journal*, vol. 3, pp. 333-340, 2003.

- [39] F. N. Kok, F. Bozoglu, and V. Hasirci, "Construction of an acetylcholinesterase-choline oxidase biosensor for aldicarb determination," *Biosensors & Bioelectronics*, vol. 17, pp. 531-539, 2002.
- [40] A. Guerrieri and F. Palmisano, "An acetylcholinesterase/choline oxidase-based amperometric biosensor as a liquid chromatography detector for acetylcholine and choline determination in brain tissue homogenates," *Analytical Chemistry*, vol. 73, pp. 2875-2882, 2001.
- [41] E. P. Medyantseva, S. S. Babkina, G. K. Budnikov, I. L. Fedorova, and N. N. Ibragimova, "Amperometric Immunoenzyme Electrode Based On an Immobilized Choline Esterase," *Journal of Analytical Chemistry*, vol. 47, pp. 806-810, 1992.
- [42] E. P. Medyantseva, M. G. Vertlib, G. K. Budnikov, S. S. Babkina, and S. A. Eremin, "Amperometric Biochemical Sensor-Based On Immobilized Cholinesterase in the Immunoassay of Pesticides," *Journal of Analytical Chemistry*, vol. 50, pp. 719-722, 1995.
- [43] L. Pogacnik and M. Franko, "Validation of different commercially available cholinesterases for pesticide toxicity test," *Annali Di Chimica*, vol. 92, pp. 93-101, 2002.
- [44] E. Wilkins, M. Carter, J. Voss, and D. Ivnitski, "A quantitative determination of organophosphate pesticides in organic solvents," *Electrochemistry Communications*, vol. 2, pp. 786-790, 2000.
- [45] S. S. Razola, S. Pochet, K. Grosfils, and J. M. Kauffmann, "Amperometric determination of choline released from rat submandibular gland acinar cells using

- a choline oxidase biosensor,” *Biosensors & Bioelectronics*, vol. 18, pp. 185-191, 2003.
- [46] T. Y. You, O. Niwa, M. Tomita, and S. Hirono, “Characterization of platinum nanoparticle-embedded carbon film electrode and its detection of hydrogen peroxide,” *Analytical Chemistry*, vol. 75, pp. 2080-2085, 2003.
- [47] T. Yao, T. Yano, Y. Nanjyo, and H. Nishino, “Simultaneous determination of glucose and (L)-lactate in rat brain by an electrochemical in vivo flow-injection system with an on-line microdialysis sampling,” *Analytical Sciences*, vol. 19, pp. 61-65, 2003.
- [48] A. D. Neklyudov, A. N. Ivankin, and M. I. Baburina, “Production and properties of pancreatin immobilized on carboxymethylcellulose,” *Applied Biochemistry and Microbiology*, vol. 34, pp. 57-60, 1998.
- [49] R. Rouillon, N. Mionetto, and J. L. Marty, “Acetylcholine Biosensor Involving Entrapment of 2 Enzymes - Optimization of Operational and Storage-Conditions,” *Analytica Chimica Acta*, vol. 268, pp. 347-350, 1992.
- [50] F. Mizutani and K. Tsuda, “Amperometric Determination of Cholinesterase With Use of an Immobilized Enzyme Electrode,” *Analytica Chimica Acta*, vol. 139, pp. 359-362, 1982.
- [51] T. H. Huang, L. Yang, J. Gitzen, P. T. Kissinger, M. Vreeke, and A. Heller, “Detection of Basal Acetylcholine in Rat-Brain Microdialysate,” *Journal of Chromatography B-Biomedical Applications*, vol. 670, pp. 323-327, 1995.

- [52] S. Fennouh, V. Casimiri, and C. Burstein, "Increased paraoxon detection with solvents using acetylcholinesterase inactivation measured with a choline oxidase biosensor," *Biosensors & Bioelectronics*, vol. 12, pp. 97-104, 1997.
- [53] A. A. Ciucu, C. Negulescu, and R. P. Baldwin, "Detection of pesticides using an amperometric biosensor based on ferrophthalocyanine chemically modified carbon paste electrode and immobilized bienzymatic system," *Biosensors & Bioelectronics*, vol. 18, pp. 303-310, 2003.
- [54] S. Q. Zhang, H. J. Zhao, and R. John, "A theoretical model for immobilized enzyme inhibition biosensors," *Electroanalysis*, vol. 13, pp. 1528-1534, 2001.
- [55] M. Snejdarkova, L. Svobodova, D. P. Nikolelis, J. Wang, and T. Hianik, "Acetylcholine biosensor based on dendrimer layers for pesticides detection," *Electroanalysis*, vol. 15, pp. 1185-1191, 2003.
- [56] P. C. Pandey, S. Upadhyay, H. C. Pathak, C. M. D. Pandey, and I. Tiwari, "Acetylthiocholine/acetylcholine and thiocholine/choline electrochemical biosensors/sensors based on an organically modified sol-gel glass enzyme reactor and graphite paste electrode," *Sensors and Actuators B-Chemical*, vol. 62, pp. 109-116, 2000.
- [57] S. Andreescu, L. Barthelmebs, and J. L. Marty, "Immobilization of acetylcholinesterase on screen-printed electrodes: comparative study between three immobilization methods and applications to the detection of organophosphorus insecticides," *Analytica Chimica Acta*, vol. 464, pp. 171-180, 2002.

- [58] S. Andreescu, D. Fournier, and J. L. Marty, "Development of highly sensitive sensor based on bioengineered acetylcholinesterase immobilized by affinity method," *Analytical Letters*, vol. 36, pp. 1865-1885, 2003.
- [59] C. Larosa, F. Pariente, L. Hernandez, and E. Lorenzo, "Determination of Organophosphorus and Carbamic Pesticides With an Acetylcholinesterase Amperometric Biosensor Using 4-Aminophenyl Acetate As Substrate," *Analytica Chimica Acta*, vol. 295, pp. 273-282, 1994.
- [60] L. Campanella, M. Achilli, M. P. Sammartino, and M. Tomassetti, "Butyrylcholine Enzyme Sensor For Determining Organophosphorus Inhibitors," *Bioelectrochemistry and Bioenergetics*, vol. 26, pp. 237-249, 1991.
- [61] N. Mionetto, J. L. Marty, and I. Karube, "Acetylcholinesterase in Organic-Solvents For the Detection of Pesticides - Biosensor Application," *Biosensors & Bioelectronics*, vol. 9, pp. 463-470, 1994.
- [62] L. Campanella, R. Cocco, and M. Tomassetti, "Determination of Compounds With Anticholinesterase Activity in Commercial Drugs By a New Enzyme Sensor," *Journal of Pharmaceutical and Biomedical Analysis*, vol. 10, pp. 741-749, 1992.
- [63] P. D. Beattle, P. P. Infelta, and H. H. Girault, "Determination of Butyrylcholinesterase Inhibition Using Ion Transfer Across the Interface Between 2 Immiscible Liquids," *Analytical Chemistry*, vol. 66, pp. 52-57, 1994.
- [64] E. V. Gogol, G. A. Evtugyn, J. L. Marty, H. C. Budnikov, and V. G. Winter, "Amperometric biosensors based on nafion coated screen-printed electrodes for

- the determination of cholinesterase inhibitors,” *Talanta*, vol. 53, pp. 379-389, 2000.
- [65] G. A. Evtugyn, A. N. Ivanov, E. V. Gogol, J. L. Marty, and H. C. Budnikov, “Amperometric flow-through biosensor for the determination of cholinesterase inhibitors,” *Analytica Chimica Acta*, vol. 385, pp. 13-21, 1999.
- [66] P. Skladal, “Detection of Organophosphate and Carbamate Pesticides Using Disposable Biosensors Based On Chemically Modified Electrodes and Immobilized Cholinesterase,” *Analytica Chimica Acta*, vol. 269, pp. 281-287, 1992.
- [67] S. S. Babkina, E. P. Medyantseva, H. C. Budnikov, and V. G. Vinter, “Enzyme Amperometric Sensor For the Determination of Cholinesterase-Inhibitors or Activators,” *Analytica Chimica Acta*, vol. 273, pp. 419-424, 1993.
- [68] G. Turdean, I. Popescu, and L. Oniciu, “Amperometric cholinesterase biosensors for the determination of organophosphorus pesticides,” *Canadian Journal of Chemistry-Revue Canadienne De Chimie*, vol. 80, pp. 315-331, 2002.
- [69] U. Wollenberger, K. Setz, F. W. Scheller, U. Loffler, W. Gopel, and R. Gruss, “Biosensors For Choline, Choline Esters and Inhibitors of Choline Esterase,” *Sensors and Actuators B-Chemical*, vol. 4, pp. 257-260, 1991.
- [70] E. V. Khaldeeva, E. P. Medyantseva, N. A. Imanaeva, and G. K. Budnikov, “Determination of gentamicin with an amperometric enzyme immunosensor,” *Journal of Analytical Chemistry*, vol. 57, pp. 1097-1102, 2002.

- [71] H. S. Lee, Y. A. Kim, Y. A. Cho, and Y. T. Lee, "Oxidation of organophosphorus pesticides for the sensitive detection by a cholinesterase-based biosensor," *Chemosphere*, vol. 46, pp. 571-576, 2002.
- [72] S. Reher, Y. Lepka, and G. Schwedt, "The potentiometric biosensor acetylcholine esterase as a model system," *Microchimica Acta*, vol. 140, pp. 15-20, 2002.
- [73] A. F. Danet, B. Bucur, M. C. Cheregi, M. Badea, and S. Serban, "Spectrophotometric determination of organophosphoric insecticides in a FIA system based on AChE inhibition," *Analytical Letters*, vol. 36, pp. 59-73, 2003.
- [74] J. Lui, M. Tan, C. Liang, and K. B. Ying, "Immobilized enzyme modulator microassay (IEMMA) for the detection of pesticide in fresh produce," *Analytica Chimica Acta*, vol. 329, pp. 297-304, 1996.
- [75] R. B. Shi and K. Stein, "Flow injection analysis of paraoxon with the use of an immobilized acetylcholinesterase reactor," *Analytica Chimica Acta*, vol. 324, pp. 21-27, 1996.
- [76] R. T. Andres and R. Narayanaswamy, "Fibre-optic pesticide biosensor based on covalently immobilized acetylcholinesterase and thymol blue," *Talanta*, vol. 44, pp. 1335-1352, 1997.
- [77] T. C. Rodrigues, M. Tubino, O. E. S. Godinho, and G. D. Neto, "Flow-injection spectrophotometric determination of paraoxon by its inhibitory effect on the enzyme acetylcholinesterase," *Analytical Sciences*, vol. 17, pp. 629-633, 2001.
- [78] Q. Xin and R. M. Wightman, "Enzyme modified amperometric sensors for choline and acetylcholine with tetrathiafulvalene tetracyanoquinodimethane as the electron-transfer mediator," *Analytica Chimica Acta*, vol. 341, pp. 43-51, 1997.

- [79] T. Neufeld, I. Eshkenazi, E. Cohen, and J. Rishpon, "A micro flow injection electrochemical biosensor for organophosphorus pesticides," *Biosensors & Bioelectronics*, vol. 15, pp. 323-329, 2000.
- [80] H. S. Lee, Y. A. Kim, D. H. Chung, and Y. T. Lee, "Determination of carbamate pesticides by a cholinesterase-based flow injection biosensor," *International Journal of Food Science and Technology*, vol. 36, pp. 263-269, 2001.
- [81] O. Niwa, T. Horiuchi, R. Kurita, and K. Torimitsu, "On-line electrochemical sensor for selective continuous measurement of acetylcholine in cultured brain tissue," *Analytical Chemistry*, vol. 70, pp. 1126-1132, 1998.
- [82] J. M. Abad, F. Pariente, L. Hernandez, H. D. Abruna, and E. Lorenzo, "Determination of organophosphorus and carbamate pesticides using a piezoelectric biosensor," *Analytical Chemistry*, vol. 70, pp. 2848-2855, 1998.
- [83] L. Pogacnik and M. Franko, "Detection of organophosphate and carbamate pesticides in vegetable samples by a photothermal biosensor," *Biosensors & Bioelectronics*, vol. 18, pp. 1-9, 2003.
- [84] V. G. Andreou and Y. D. Clonis, "A portable fiber-optic pesticide biosensor based on immobilized cholinesterase and sol-gel entrapped bromocresol purple for in-field use," *Biosensors & Bioelectronics*, vol. 17, pp. 61-69, 2002.
- [85] A. Makower, J. Halamek, P. Skladal, F. Kernchen, and F. W. Scheller, "New principle of direct real-time monitoring of the interaction of cholinesterase and its inhibitors by piezoelectric biosensor," *Biosensors & Bioelectronics*, vol. 18, pp. 1329-1337, 2003.

- [86] S. Kumaran and M. Morita, "Application of a Cholinesterase Biosensor to Screen For Organophosphorus Pesticides Extracted From Soil," *Talanta*, vol. 42, pp. 649-655, 1995.
- [87] N. Jaffrezic-Renault, A. Senillou, C. Martelet, K. Wan, and J. M. Chovelon, "ISFET microsensors for the detection of pollutants in liquid media," *Sensors and Actuators B-Chemical*, vol. 59, pp. 154-164, 1999.
- [88] G. A. Evtuyugin, L. V. Ryapisova, E. E. Stoikova, L. B. Kashevarova, S. V. Fridland, and V. Z. Latypova, "Enzymatic determination of hydrazonium salts of dialkyldithiophosphoric acids," *Journal of Analytical Chemistry*, vol. 53, pp. 869-875, 1998.
- [89] E. B. Nikol'skaya, L. P. Kuznetsova, and A. A. Prokopov, "New biosensors based on immobilized cholinesterase from squid optic ganglion for determining substances with anticholinesterase activity," *Journal of Analytical Chemistry*, vol. 53, pp. 658-662, 1998.
- [90] A. N. Reshetilov, O. V. Fedoseeva, T. P. Eliseeva, Y. V. Sergeev, E. P. Medyantseva, and G. K. Budnikov, "Characteristics of a Biochemical Sensor-Based On Cholinesterase Immobilized On a Field-Effect Transistor," *Journal of Analytical Chemistry*, vol. 50, pp. 414-417, 1995.
- [91] A. N. Diaz and M. C. R. Peinado, "Sol-gel cholinesterase biosensor for organophosphorus pesticide fluorimetric analysis," *Sensors and Actuators B-Chemical*, vol. 39, pp. 426-431, 1997.

- [92] J. Kondoh, Y. Matsui, S. Shiokawa, and W. B. Wlodarski, "Enzyme-Immobilized Sh-Saw Biosensor," *Sensors and Actuators B-Chemical*, vol. 20, pp. 199-203, 1994.
- [93] A. K. Singh, A. W. Flounders, J. V. Volponi, C. S. Ashley, K. Wally, and J. S. Schoeniger, "Development of sensors for direct detection of organophosphates. Part I: immobilization, characterization and stabilization of acetylcholinesterase and organophosphate hydrolase on silica supports," *Biosensors & Bioelectronics*, vol. 14, pp. 703-713, 1999.
- [94] M. Emteborg, K. Irgum, C. Gooijer, and U. A. T. Brinkman, "Peroxyoxalate chemiluminescence in aqueous solutions: Coupling of immobilized enzyme reactors and 1,1'-oxalyldiimidazole chemiluminescence reaction to flow-injection analysis and liquid chromatographic systems," *Analytica Chimica Acta*, vol. 357, pp. 111-118, 1997.
- [95] D. Martorell, F. Cespedes, E. MartinezFabregas, and S. Alegret, "Determination of organophosphorus and carbamate pesticides using a biosensor based on a polishable, 7,7,8,8-tetracyanoquinodimethane-modified, graphite-epoxy biocomposite," *Analytica Chimica Acta*, vol. 337, pp. 305-313, 1997.
- [96] A. Curulli, S. Dragulescu, C. Cremisini, and G. Palleschi, "Bienzyme amperometric probes for choline and choline esters assembled with nonconducting electrosynthesized polymers," *Electroanalysis*, vol. 13, pp. 236-242, 2001.
- [97] A. L. Hart, W. A. Collier, and D. Janssen, "The response of screen-printed enzyme electrodes containing cholinesterases to organo-phosphates in solution

- and from commercial formulations,” *Biosensors & Bioelectronics*, vol. 12, pp. 645-654, 1997.
- [98] J. L. Marty, N. Mionetto, T. Noguier, F. Ortega, and C. Roux, “Enzyme Sensors For the Detection of Pesticides,” *Biosensors & Bioelectronics*, vol. 8, pp. 273-280, 1993.
- [99] I. Karube, K. Yokoyama, and E. Tamiya, “Microbiosensors For Acetylcholine and Glucose,” *Biosensors & Bioelectronics*, vol. 8, pp. 219-228, 1993.
- [100] P. Skladal and M. Mascini, “Sensitive Detection of Pesticides Using Amperometric Sensors Based On Cobalt Phthalocyanine-Modified Composite Electrodes and Immobilized Cholinesterases,” *Biosensors & Bioelectronics*, vol. 7, pp. 335-343, 1992.
- [101] L. Pogacnik and M. Franko, “Optimisation of FIA system for detection of organophosphorus and carbamate pesticides based on cholinesterase inhibition,” *Talanta*, vol. 54, pp. 631-641, 2001.
- [102] A. Riklin and I. Willner, “Glucose and Acetylcholine Sensing Multilayer Enzyme Electrodes of Controlled Enzyme Layer Thickness,” *Analytical Chemistry*, vol. 67, pp. 4118-4126, 1995.
- [103] A. N. Ivanov, G. A. Evtyugin, K. Z. Brainina, G. K. Budnikov, and L. E. Stenina, “Cholinesterase sensors based on thick-film graphite electrodes for the flow-injection determination of organophosphorus pesticides,” *Journal of Analytical Chemistry*, vol. 57, pp. 1042-1048, 2002.

- [104] B. D. Leca, A. M. Verdier, and L. J. Blum, "Screen-printed electrodes as disposable or reusable optical devices for luminol electrochemiluminescence," *Sensors and Actuators B-Chemical*, vol. 74, pp. 190-193, 2001.
- [105] T. Kato, J. K. Liu, K. Yamamoto, P. G. Osborne, and O. Niwa, "Detection of basal acetylcholine release in the microdialysis of rat frontal cortex by high-performance liquid chromatography using a horseradish peroxidase-osmium redox polymer electrode with pre-enzyme reactor," *Journal of Chromatography B-Biomedical Applications*, vol. 682, pp. 162-166, 1996.
- [106] S. Kar and M. A. Arnold, "Fiberoptic Ammonia Sensor For Measuring Synaptic Glutamate and Extracellular Ammonia," *Analytical Chemistry*, vol. 64, pp. 2438-2443, 1992.
- [107] M. Smolander, G. Markovarga, and L. Gorton, "Aldose Dehydrogenase-Modified Carbon-Paste Electrodes As Amperometric Aldose Sensors," *Analytica Chimica Acta*, vol. 302, pp. 233-240, 1995.
- [108] X. B. Wang, M. P. Hughes, Y. Huang, F. F. Becker, and P. R. C. Gascoyne, "Nonuniform Spatial Distributions of Both the Magnitude and Phase of AC Electric-Fields Determine Dielectrophoretic Forces," *Biochimica Et Biophysica Acta-General Subjects*, vol. 1243, pp. 185-194, 1995.
- [109] T. J. Moore, G. G. Nam, L. C. Pipes, and L. A. Coury, "Chemically Amplified Voltammetric Enzyme Electrodes For Oxidizable Pharmaceuticals," *Analytical Chemistry*, vol. 66, pp. 3158-3163, 1994.
- [110] N. Adanyi, M. Toth-Markus, E. E. Szabo, M. Varadi, M. P. Sammartino, M. Tomassetti, and L. Campanella, "Investigation of organic phase biosensor for

- measuring glucose in flow injection analysis system,” *Analytica Chimica Acta*, vol. 501, pp. 219-225, 2004.
- [111] G. Aydin, S. S. Celebi, H. Ozyoruk, and A. Yildiz, “Amperometric enzyme electrode for L(+)-lactate determination using immobilized L(+)-lactate oxidase in poly(vinylferrocenium) film,” *Sensors and Actuators B-Chemical*, vol. 87, pp. 8-12, 2002.
- [112] M. Badea, A. Curulli, and G. Palleschi, “Oxidase enzyme immobilisation through electropolymerised films to assemble biosensors for batch and flow injection analysis,” *Biosensors & Bioelectronics*, vol. 18, pp. 689-698, 2003.
- [113] A. Bossi, L. Castelletti, S. A. Piletsky, A. P. F. Turner, and P. G. Righetti, “Towards the development of an integrated capillary electrophoresis optical biosensor,” *Electrophoresis*, vol. 24, pp. 3356-3363, 2003.
- [114] S. Brahim, D. Narinesingh, and A. Guiseppi-Elie, “Bio-smart materials: Kinetics of immobilized enzymes in p(HEMA)/p(pyrrole) hydrogels in amperometric biosensors,” *Macromolecular Symposia*, vol. 186, pp. 63-73, 2002.
- [115] L. Cen, K. G. Neoh, and E. T. Kang, “Surface functionalization of polypyrrole film with glucose oxidase and viologen,” *Biosensors & Bioelectronics*, vol. 18, pp. 363-374, 2003.
- [116] K. S. Chang, W. L. Hsu, H. Y. Chen, C. K. Chang, and C. Y. Chen, “Determination of glutamate pyruvate transaminase activity in clinical specimens using a biosensor composed of immobilized L-glutamate oxidase in a photo-crosslinkable polymer membrane on a palladium-deposited screen-printed carbon electrode,” *Analytica Chimica Acta*, vol. 481, pp. 199-208, 2003.

- [117] A. Chaubey, M. Gerard, R. Singhal, V. S. Singh, and B. D. Malhotra, "Immobilization of lactate dehydrogenase on electrochemically prepared polypyrrole-polyvinylsulphonate composite films for application to lactate biosensors," *Electrochimica Acta*, vol. 46, pp. 723-729, 2000.
- [118] A. Chaubey, M. Gerard, V. S. Singh, and B. D. Malhotra, "Immobilization of lactate dehydrogenase on tetraethylorthosilicate-derived sol-gel films for application to lactate biosensor," *Applied Biochemistry and Biotechnology*, vol. 96, pp. 293-301, 2001.
- [119] L. Chen and W. Gorski, "Bioinorganic composites for enzyme electrodes," *Analytical Chemistry*, vol. 73, pp. 2862-2868, 2001.
- [120] X. Chen, B. Q. Wang, and S. J. Dong, "Amperometric biosensor for hydrogen peroxide based on sol-gel/hydrogel composite thin film," *Electroanalysis*, vol. 13, pp. 1149-1152, 2001.
- [121] C. W. Chuang and J. S. Shih, "Preparation and application of immobilized C60-glucose oxidase enzyme in fullerene C60-coated piezoelectric quartz crystal glucose sensor," *Sensors and Actuators B-Chemical*, vol. 81, pp. 1-8, 2001.
- [122] A. Collins, E. Mikeladze, M. Bengtsson, M. Kokaia, T. Laurell, and E. Csoregi, "Interference elimination in glutamate monitoring with chip integrated enzyme microreactors," *Electroanalysis*, vol. 13, pp. 425-431, 2001.
- [123] G. Cui, J. H. Yoo, B. W. Woo, S. S. Kim, G. S. Cha, and H. Nam, "Disposable amperometric glucose sensor electrode with enzyme-immobilized nitrocellulose strip," *Talanta*, vol. 54, pp. 1105-1111, 2001.

- [124] G. Cui, J. H. Yoo, J. Yoo, S. W. Lee, H. Nam, and G. S. Cha, "Differential thick-film amperometric glucose sensor with an enzyme-immobilized nitrocellulose membrane," *Electroanalysis*, vol. 13, pp. 224-228, 2001.
- [125] F. Darain, S. U. Park, and Y. B. Shim, "Disposable amperometric immunosensor system for rabbit IgG using a conducting polymer modified screen-printed electrode," *Biosensors & Bioelectronics*, vol. 18, pp. 773-780, 2003.
- [126] V. T. Dimakis, V. G. Gavalas, and N. A. Chaniotakis, "Polyelectrolyte-stabilized biosensors based on macroporous carbon electrode," *Analytica Chimica Acta*, vol. 467, pp. 217-223, 2002.
- [127] I. Eshkenazi, E. Maltz, B. Zion, and J. Rishpon, "A three-cascaded-enzymes biosensor to determine lactose concentration in raw milk," *Journal of Dairy Science*, vol. 83, pp. 1939-1945, 2000.
- [128] E. Fujii, K. Nakamura, S. Sasaki, D. Citterio, K. Kurihara, and K. Suzuki, "Application of the absorption-based surface plasmon resonance principle to the determination of glucose using an enzyme reaction," *Instrumentation Science & Technology*, vol. 31, pp. 343-356, 2003.
- [129] A. Gambhir, M. Gerard, A. K. Mulchandani, and B. D. Malhotra, "Coimmobilization of urease and glutamate dehydrogenase in electrochemically prepared polypyrrole-polyvinyl sulfonate films," *Applied Biochemistry and Biotechnology*, vol. 96, pp. 249-257, 2001.
- [130] A. Guiseppi-Elie, N. F. Sheppard, S. Brahim, and D. Narinesingh, "Enzyme microgels in packed-bed bioreactors with downstream amperometric detection

- using microfabricated interdigitated microsensor electrode arrays,” *Biotechnology and Bioengineering*, vol. 75, pp. 475-484, 2001.
- [131] A. Guiseppi-Elie, C. H. Lei, and R. H. Baughman, “Direct electron transfer of glucose oxidase on carbon nanotubes,” *Nanotechnology*, vol. 13, pp. 559-564, 2002.
- [132] M. D. Gouda, M. S. Thakur, and N. G. Karanth, “Optimization of the multienzyme system for sucrose biosensor by response surface methodology,” *World Journal of Microbiology & Biotechnology*, vol. 17, pp. 595-600, 2001.
- [133] Y. Guemas, M. Boujtita, and N. El Murr, “Biosensor for determination of glucose and sucrose in fruit juices by flow injection analysis,” *Applied Biochemistry and Biotechnology*, vol. 89, pp. 171-181, 2000.
- [134] B. C. Hsieh, T. J. Cheng, T. Y. Wang, and R. L. C. Chen, “Use of chitosan membrane from the carapace of the soldier crab *Mictyris brevidactylus* for biosensor construction,” *Marine Biotechnology*, vol. 5, pp. 119-125, 2003.
- [135] D. Janasek and U. Spohn, “A chemiluminometric FIA procedure for the enzymatic determination of L-aspartate,” *Sensors and Actuators B-Chemical*, vol. 74, pp. 163-167, 2001.
- [136] S. Jawaheer, S. F. White, S. Rughooputh, and D. C. Cullen, “Development of a common biosensor format for an enzyme based biosensor array to monitor fruit quality,” *Biosensors & Bioelectronics*, vol. 18, pp. 1429-1437, 2003.
- [137] P. Jin, A. Yamaguchi, F. A. Oi, S. Matsuo, J. B. Tan, and H. Misawa, “Glucose sensing based on interdigitated array microelectrode,” *Analytical Sciences*, vol. 17, pp. 841-846, 2001.

- [138] S. I. Kang and Y. H. Bae, "A sulfonamide based glucose-responsive hydrogel with covalently immobilized glucose oxidase and catalase," *Journal of Controlled Release*, vol. 86, pp. 115-121, 2003.
- [139] S. Kasai, Y. Hirano, N. Motochi, H. Shiku, M. Nishizawa, and T. Matsue, "Simultaneous detection of uric acid and glucose on a dual-enzyme chip using scanning electrochemical microscopy/scanning chemiluminescence microscopy," *Analytica Chimica Acta*, vol. 458, pp. 263-270, 2002.
- [140] N. Kiba, S. Ito, M. Tachibana, K. Tani, and H. Koizumi, "Flow-through chemiluminescence sensor using immobilized oxidases for the selective determination of L-glutamate in a flow-injection system," *Analytical Sciences*, vol. 17, pp. 929-933, 2001.
- [141] N. Kiba, T. Miwa, M. Tachibana, K. Tani, and H. Koizumi, "Chemiluminometric sensor for simultaneous determination of L-glutamate and L-lysine with immobilized oxidases in a flow injection system," *Analytical Chemistry*, vol. 74, pp. 1269-1274, 2002.
- [142] E. Kosela, H. Elzanowska, and W. Kutner, "Charge mediation by ruthenium poly(pyridine) complexes in 'second-generation' glucose biosensors based on carboxymethylated beta-cyclodextrin polymer membranes," *Analytical and Bioanalytical Chemistry*, vol. 373, pp. 724-734, 2002.
- [143] M. A. Kumar, M. S. Thakur, A. Senthuran, V. Senthuran, N. G. Karanth, R. Hatti-Kaul, and B. Mattiasson, "An automated flow injection analysis system for on-line monitoring of glucose and L-lactate during lactic acid fermentation in a

- recycle bioreactor,” *World Journal of Microbiology & Biotechnology*, vol. 17, pp. 23-29, 2001.
- [144] A. S. Kumar and J. M. Zen, “Electrochemical investigation of glucose sensor fabricated at copper-plated screen-printed carbon electrodes,” *Electroanalysis*, vol. 14, pp. 671-678, 2002.
- [145] R. A. S. Lapa, J. Lima, and I. Pinto, “Development of a sequential injection analysis system for the simultaneous biosensing of glucose and ethanol in bioreactor fermentation,” *Food Chemistry*, vol. 81, pp. 141-146, 2003.
- [146] A. V. Lapierre, F. Battaglini, and J. Raba, “Rotating bioreactor based on an electron transfer mediated by osmium complexes incorporating a continuous-flow/stopped-flow system - Application to the determination of glucose in serum samples,” *Analytica Chimica Acta*, vol. 443, pp. 17-24, 2001.
- [147] M. D. Leonida, D. T. Starczynowski, R. Waldman, and B. Aurian-Blajeni, “Polymeric FAD used as enzyme-friendly mediator in lactate detection,” *Analytical and Bioanalytical Chemistry*, vol. 376, pp. 832-837, 2003.
- [148] Q. W. Li, G. A. Luo, J. Feng, Q. Zhou, L. Zhang, and Y. F. Zhu, “Amperometric detection of glucose with glucose oxidase absorbed on porous nanocrystalline TiO₂ film,” *Electroanalysis*, vol. 13, pp. 413-416, 2001.
- [149] S. Q. Liu and H. X. Ju, “Reagentless glucose biosensor based on direct electron transfer of glucose oxidase immobilized on colloidal gold modified carbon paste electrode,” *Biosensors & Bioelectronics*, vol. 19, pp. 177-183, 2003.

- [150] J. Losada and M. P. G. Armada, "An amperometric sensor based on covalent immobilization of glucose oxidase in electropolymerized chloranil-N-aminopyrrole films," *Electroanalysis*, vol. 13, pp. 1016-1021, 2001.
- [151] D. Losic, M. Zhao, J. G. Shapter, and J. J. Gooding, "Which parameters affect the response of the channel biosensor?," *Electroanalysis*, vol. 15, pp. 183-190, 2003.
- [152] Y. Lv, Z. J. Zhang, and F. A. Chen, "Chemiluminescence microfluidic system sensor on a chip for determination of glucose in human serum with immobilized reagents," *Talanta*, vol. 59, pp. 571-576, 2003.
- [153] H. B. Mao, T. L. Yang, and P. S. Cremer, "Design and characterization of immobilized enzymes in microfluidic systems," *Analytical Chemistry*, vol. 74, pp. 379-385, 2002.
- [154] C. A. Marquette, A. Degiuli, and L. J. Blum, "Fiberoptic biosensors based on chemiluminescent reactions," *Applied Biochemistry and Biotechnology*, vol. 89, pp. 107-115, 2000.
- [155] C. A. Marquette and L. J. Blum, "1,3-dichloro-5,5-dimethylhydantoin as triggering reagent for chemiluminescent biochip based on the luminol-H₂O₂ reaction," *Analytical Letters*, vol. 36, pp. 1697-1706, 2003.
- [156] P. B. Martelli, B. F. Reis, A. N. Araujo, M. Conceicao, and B. S. M. Montenegro, "A flow system with a conventional spectrophotometer for the chemiluminescent determination of lactic acid in yoghurt," *Talanta*, vol. 54, pp. 879-885, 2001.
- [157] S. A. M. Marzouk, H. E. M. Sayour, A. M. Ragab, W. E. Cascio, and S. S. M. Hassan, "A simple FIA-system for simultaneous measurements of glucose and

- lactate with amperometric detection,” *Electroanalysis*, vol. 12, pp. 1304-1311, 2000.
- [158] K. Matsumoto, K. Takayama, K. J. M. Abesundara, and T. Matsui, “Assay of alpha-glucosidase inhibitory activity using flow-biosensor system,” *Analytica Chimica Acta*, vol. 479, pp. 135-141, 2003.
- [159] J. J. Niu and J. Y. Lee, “Reagentless mediated biosensors based on polyelectrolyte and sol-gel derived silica matrix,” *Sensors and Actuators B-Chemical*, vol. 82, pp. 250-258, 2002.
- [160] H. Patel, X. Li, and H. I. Karan, “Amperometric glucose sensors based on ferrocene containing polymeric electron transfer systems - a preliminary report,” *Biosensors & Bioelectronics*, vol. 18, pp. 1073-1076, 2003.
- [161] M. Portaccio, M. El-Masry, N. R. Diano, A. De Maio, V. Grano, M. Lepore, P. Travascio, U. Bencivenga, N. Pagliuca, and D. G. Mita, “An amperometric sensor employing glucose oxidase immobilized on nylon membranes with different pore diameter and grafted with different monomers,” *Journal of Molecular Catalysis B-Enzymatic*, vol. 18, pp. 49-67, 2002.
- [162] J. M. Qian, X. X. Li, and H. Y. Huang, “Sol-gel-derived amperometric glucose biosensor based on covalent attachment of toluidine blue O to carrier,” *Polymers For Advanced Technologies*, vol. 14, pp. 207-211, 2003.
- [163] N. Rupcich and J. D. Brennan, “Coupled enzyme reaction microarrays based on pin-printing of sol-gel derived biomaterials,” *Analytica Chimica Acta*, vol. 500, pp. 3-12, 2003.

- [164] E. Salinas, P. Morcillo, M. I. Sanz, and J. Raba, "Continuous-flow/stopped-flow system incorporating a rotating bioreactor based on a double redox catalytic cycle and electron transfer mediated by osmium complexes. Application in the determination of extremely low levels of glucose," *Instrumentation Science & Technology*, vol. 30, pp. 281-293, 2002.
- [165] D. Shan, S. Cosnier, and C. Mousty, "HRP wiring by redox active layered double hydroxides: Application to the mediated H₂O₂ detection," *Analytical Letters*, vol. 36, pp. 909-922, 2003.
- [166] D. Stollner, W. Stocklein, F. Scheller, and A. Warsinke, "Membrane-immobilized haptoglobin as affinity matrix for a hemoglobin-A1c immunosensor," *Analytica Chimica Acta*, vol. 470, pp. 111-119, 2002.
- [167] A. Subramanian, P. I. Oden, S. J. Kennel, K. B. Jacobson, R. J. Warmack, T. Thundat, and M. J. Doktycz, "Glucose biosensing using an enzyme-coated microcantilever," *Applied Physics Letters*, vol. 81, pp. 385-387, 2002.
- [168] Y. Tian, L. Mao, T. Okajima, and T. Ohsaka, "Superoxide dismutase-based third-generation biosensor for superoxide anion," *Analytical Chemistry*, vol. 74, pp. 2428-2434, 2002.
- [169] J. Tkac, M. Navratil, E. Sturdik, and P. Gemeiner, "Monitoring of dihydroxyacetone production during oxidation of glycerol by immobilized *Gluconobacter oxydans* cells with an enzyme biosensor," *Enzyme and Microbial Technology*, vol. 28, pp. 383-388, 2001.
- [170] K. Tohda and M. Gratzl, "A microscopic, continuous, optical monitor for interstitial electrolytes and glucose," *Chemphyschem*, vol. 4, pp. 155-160, 2003.

- [171] A. A. J. Torriero, E. Salinas, F. Battaglini, and J. Raba, "Milk lactate determination with a rotating bioreactor based on an electron transfer mediated by osmium complexes incorporating a continuous-flow/stopped-flow system," *Analytica Chimica Acta*, vol. 498, pp. 155-163, 2003.
- [172] E. A. Ulasova, L. Micheli, L. Vasii, D. Moscone, G. Palleschi, S. V. Vdovichev, A. V. Zorin, S. A. Krutovertsev, E. E. Karyakina, and A. A. Karyakin, "Flow-injection analysis of residual glucose in wines using a semiautomatic analyzer equipped with a Prussian blue-based biosensor," *Electroanalysis*, vol. 15, pp. 447-451, 2003.
- [173] S. G. Wang, Q. Zhang, R. L. Wang, S. F. Yoon, J. Ahn, D. J. Yang, J. Z. Tian, J. Q. Li, and Q. Zhou, "Multi-walled carbon nanotubes for the immobilization of enzyme in glucose biosensors," *Electrochemistry Communications*, vol. 5, pp. 800-803, 2003.
- [174] C. Y. Wang and H. J. Huang, "Flow injection analysis of glucose based on its inhibition of electrochemiluminescence in a Ru(bpy)₃(²⁺)-tripropylamine system," *Analytica Chimica Acta*, vol. 498, pp. 61-68, 2003.
- [175] X. Wei, J. Cruz, and W. Gorski, "Integration of enzymes and electrodes: Spectroscopic and electrochemical studies of chitosan-enzyme films," *Analytical Chemistry*, vol. 74, pp. 5039-5046, 2002.
- [176] O. S. Wolfbeis, M. Schaferling, and A. Durkop, "Reversible optical sensor membrane for hydrogen peroxide using an immobilized fluorescent probe, and its application to a glucose biosensor," *Microchimica Acta*, vol. 143, pp. 221-227, 2003.

- [177] D. Xiao and M. M. F. Choi, "Aspartame optical biosensor with bienzyme-immobilized eggshell membrane and oxygen-sensitive optode membrane," *Analytical Chemistry*, vol. 74, pp. 863-870, 2002.
- [178] J. J. Xu and H. Y. Chen, "Amperometric glucose sensor based on glucose oxidase immobilized in electrochemically generated poly(ethacridine)," *Analytica Chimica Acta*, vol. 423, pp. 101-106, 2000.
- [179] F. Xu, L. Wang, M. N. Gao, L. T. Jin, and J. Y. Jin, "Amperometric sensor for glucose and hypoxanthine based on a Pd-IrO₂ modified electrode by a co-crosslinking bienzymic system," *Talanta*, vol. 57, pp. 365-373, 2002.
- [180] S. Yabuki, F. Mizutani, Y. Sato, and Y. Hirata, "Immobilization of polyglutamate-glucose oxidase onto a cysteamine-modified gold electrode," *Sensors and Actuators B-Chemical*, vol. 91, pp. 187-190, 2003.
- [181] T. Yao, Y. Nanjyo, T. Tanaka, and H. Nishino, "An electrochemical in vivo flow-injection system for highly selective and sensitive detection of L-glutamate using enzyme reactor involving amplification," *Electroanalysis*, vol. 13, pp. 1361-1366, 2001.
- [182] L. T. Yin, J. C. Chou, W. Y. Chung, T. P. Sun, K. P. Hsiung, and S. K. Hsiung, "Glucose ENFET doped with MnO₂ powder," *Sensors and Actuators B-Chemical*, vol. 76, pp. 187-192, 2001.
- [183] L. D. Zhu, Y. X. Li, F. M. Tian, B. Xu, and G. Y. Zhu, "Electrochemiluminescent determination of glucose with a sol-gel derived ceramic-carbon composite electrode as a renewable optical fiber biosensor," *Sensors and Actuators B-Chemical*, vol. 84, pp. 265-270, 2002.

- [184] J. Wang, Q. A. Chen, M. Pedrero, and J. M. Pingarron, "Screen-Printed Amperometric Biosensors For Glucose and Alcohols Based On Ruthenium-Dispersed Carbon Inks," *Analytica Chimica Acta*, vol. 300, pp. 111-116, 1995.
- [185] D. Odaci, S. Timur, and A. Telefoncu, "Carboxyl esterase-alcohol oxidase based biosensor for the aspartame determination," *Food Chemistry*, vol. 84, pp. 493-496, 2004.
- [186] C. B. Park and D. S. Clark, "Sol-gel encapsulated enzyme arrays for high-throughput screening of biocatalytic activity," *Biotechnology and Bioengineering*, vol. 78, pp. 229-235, 2002.
- [187] Y. Miao, L. S. Chia, N. K. Goh, and S. N. Tan, "Amperometric glucose biosensor based on immobilization of glucose oxidase in chitosan matrix cross-linked with glutaraldehyde," *Electroanalysis*, vol. 13, pp. 347-349, 2001.
- [188] M. Mifune, K. Sugimoto, A. Iwado, H. Akizawa, N. Motohashi, and Y. Saito, "Flow injection analysis of hydrogen peroxide using glass-beads modified with manganese(III)-tetra(4-carboxyphenyl)porphine derivative and its analytical application to the determination of serum glucose," *Analytical Sciences*, vol. 19, pp. 569-573, 2003.
- [189] J. Okuda, J. Wakai, N. Yuhashi, and K. Sode, "Glucose enzyme electrode using cytochrome b(562) as an electron mediator," *Biosensors & Bioelectronics*, vol. 18, pp. 699-704, 2003.
- [190] D. W. Pan, J. H. Chen, L. H. Nie, W. Y. Tao, and S. Z. Yao, "An amperometric glucose biosensor based on poly(o-aminophenol) and Prussian blue films at platinum electrode," *Analytical Biochemistry*, vol. 324, pp. 115-122, 2004.

- [191] R. B. Bhatia, C. J. Brinker, A. K. Gupta, and A. K. Singh, "Aqueous sol-gel process for protein encapsulation," *Chemistry of Materials*, vol. 12, pp. 2434-2441, 2000.
- [192] C. G. Tsiafoulis, M. I. Prodromidis, and M. I. Karayannis, "Development of amperometric biosensors for the determination of glycolic acid in real samples," *Analytical Chemistry*, vol. 74, pp. 132-139, 2002.
- [193] C. G. Tsiafoulis, M. I. Prodromidis, and M. I. Karayannis, "Development of a flow amperometric enzymatic method for the determination of total glucosinolates in real samples," *Analytical Chemistry*, vol. 75, pp. 927-934, 2003.
- [194] P. C. Pandey, S. Upadhyay, I. Tiwari, and V. S. Tripathi, "An organically modified silicate-based ethanol biosensor," *Analytical Biochemistry*, vol. 288, pp. 39-43, 2001.
- [195] F. Borzeix, F. Monot, and J. P. Vandecasteele, "Bi-Enzymatic Reaction For Alcohol Oxidation in Organic Media - From Purified Enzymes to Cellular-Systems," *Enzyme and Microbial Technology*, vol. 17, pp. 615-622, 1995.
- [196] H. Gulce, A. Gulce, M. Kavanoz, H. Coskun, and A. Yildiz, "A new amperometric enzyme electrode for alcohol determination," *Biosensors & Bioelectronics*, vol. 17, pp. 517-521, 2002.
- [197] N. G. Patel, S. Meier, K. Cammann, and G. C. Chemnitz, "Screen-printed biosensors using different alcohol oxidases," *Sensors and Actuators B-Chemical*, vol. 75, pp. 101-110, 2001.

- [198] Y. V. Rodionov, M. V. Sukhacheva, and O. I. Keppen, "Photometric assay for methanol in the presence of ethanol," *Applied Biochemistry and Microbiology*, vol. 38, pp. 607-609, 2002.
- [199] Y. V. Rodionov, O. I. Keppen, and M. V. Sukhacheva, "A photometric assay for ethanol," *Applied Biochemistry and Microbiology*, vol. 38, pp. 395-396, 2002.
- [200] S. Gaspar, H. Zimmermann, I. Gazaryan, E. Csoregi, and W. Schuhmann, "Hydrogen peroxide biosensors based on direct electron transfer from plant peroxidases immobilized on self-assembled thiol-monolayer modified gold electrodes," *Electroanalysis*, vol. 13, pp. 284-288, 2001.
- [201] M. Gundogan-Paul, S. S. Celebi, H. Ozyoruk, and A. Yildiz, "Amperometric enzyme electrode for organic peroxides determination prepared from horseradish peroxidase immobilized in poly(vinylferrocenium) film," *Biosensors & Bioelectronics*, vol. 17, pp. 875-881, 2002.
- [202] M. Gundogan-Paul, H. Ozyoruk, S. S. Celebi, and A. Yildiz, "Amperometric enzyme electrode for hydrogen peroxide determination prepared with horseradish peroxidase immobilized in polyvinylferrocenium (PVF+)," *Electroanalysis*, vol. 14, pp. 505-511, 2002.
- [203] B. X. Li, Z. J. Zhang, and Y. Jin, "Chemiluminescence flow biosensor for hydrogen peroxide with immobilized reagents," *Sensors and Actuators B-Chemical*, vol. 72, pp. 115-119, 2001.
- [204] O. Nozaki and H. Kawamoto, "Reactivation of inactivated horseradish peroxidase with ethyleneurea and allantoin for determination of hydrogen peroxide by micro-

- flow injection horseradish peroxidase-catalyzed chemiluminescence,” *Analytica Chimica Acta*, vol. 495, pp. 233-238, 2003.
- [205] S. S. Rosatto, G. D. Neto, and L. T. Kubota, “Effect of DNA on the peroxidase based biosensor for phenol determination in waste waters,” *Electroanalysis*, vol. 13, pp. 445-450, 2001.
- [206] J. Z. Xu, J. J. Zhu, Q. Wu, Z. Hu, and H. Y. Chen, “An amperometric biosensor based on the coimmobilization of horseradish peroxidase and methylene blue on a carbon nanotubes modified electrode,” *Electroanalysis*, vol. 15, pp. 219-224, 2003.
- [207] F. Pariente, E. Lorenzo, F. Tobalina, and H. D. Abruna, “Aldehyde Biosensor Based On the Determination of Nadh Enzymatically Generated By Aldehyde Dehydrogenase,” *Analytical Chemistry*, vol. 67, pp. 3936-3944, 1995.
- [208] A. Vertesi, L. M. Simon, I. Kiss, and B. Szajani, “Preparation, characterization and application of immobilized carboxypeptidase A,” *Enzyme and Microbial Technology*, vol. 25, pp. 73-79, 1999.
- [209] K. Endo, T. Miyasaka, S. Mochizuki, S. Aoyagi, N. Himi, H. Asahara, K. Tsujioka, and K. Sakai, “Development of a superoxide sensor by immobilization of superoxide dismutase,” *Sensors and Actuators B-Chemical*, vol. 83, pp. 30-34, 2002.
- [210] E. Akyilmaz, M. K. Sezginurk, and E. Dinckaya, “A biosensor based on urate oxidase-peroxidase coupled enzyme system for uric acid determination in urine,” *Talanta*, vol. 61, pp. 73-79, 2003.

- [211] T. K. V. Krawczyk, T. Moszczynska, and M. Trojanowicz, "Inhibitive determination of mercury and other metal ions by potentiometric urea biosensor," *Biosensors & Bioelectronics*, vol. 15, pp. 681-691, 2000.
- [212] R. Singhal, A. Gambhir, M. K. Pandey, S. Annapoorni, and B. D. Malhotra, "Immobilization of urease on poly(N-vinyl carbazole)/stearic acid Langmuir-Blodgett films for application to urea biosensor," *Biosensors & Bioelectronics*, vol. 17, pp. 697-703, 2002.
- [213] B. Tombach, J. Schneider, F. Matzkies, R. M. Schaefer, and G. C. Chemnitz, "Amperometric creatinine biosensor for hemodialysis patients," *Clinica Chimica Acta*, vol. 312, pp. 129-134, 2001.
- [214] J. H. Shin, Y. S. Choi, H. J. Lee, S. H. Choi, J. Ha, I. J. Yoon, H. Nam, and G. S. Cha, "A planar amperometric creatinine biosensor employing an insoluble oxidizing agent for removing redox-active interferences," *Analytical Chemistry*, vol. 73, pp. 5965-5971, 2001.
- [215] A. Erlenkotter, M. Fobker, and G. C. Chemnitz, "Biosensors and flow-through system for the determination of creatinine in hemodialysate," *Analytical and Bioanalytical Chemistry*, vol. 372, pp. 284-292, 2002.
- [216] K. V. Gobi, Y. Sato, and F. Mizutani, "Mediatorless superoxide dismutase sensors using cytochrome c-modified electrodes: Xanthine oxidase incorporated polyion complex membrane for enhanced activity and in vivo analysis," *Electroanalysis*, vol. 13, pp. 397-403, 2001.
- [217] E. Kilinc, M. Ozsoz, and O. A. Sadik, "Electrochemical detection of NO by inhibition on oxidase activity," *Electroanalysis*, vol. 12, pp. 1467-1471, 2000.

- [218] L. Q. Mao, F. Xu, Q. Xu, and L. T. Jin, "Miniaturized amperometric biosensor based on xanthine oxidase for monitoring hypoxanthine in cell culture media," *Analytical Biochemistry*, vol. 292, pp. 94-101, 2001.
- [219] Y. Nanjyo and T. Yao, "Rapid measurement of fish freshness indices by an amperometric flow-injection system with a 16-way switching valve and immobilized enzyme reactors," *Analytica Chimica Acta*, vol. 470, pp. 175-183, 2002.
- [220] J. I. Rhee, M. Yamashita, and T. Scheper, "Development of xylitol oxidase-based flow injection analysis for monitoring of xylitol concentrations," *Analytica Chimica Acta*, vol. 456, pp. 293-301, 2002.
- [221] A. Maines, M. I. Prodromidis, S. M. Tzouwara-Karayanni, M. I. Karayannis, D. Ashworth, and P. Vadgama, "An enzyme electrode for extended linearity citrate measurements based on modified polymeric membranes," *Electroanalysis*, vol. 12, pp. 1118-1123, 2000.
- [222] W. C. Mak, C. Y. Chan, J. Barford, and R. Renneberg, "Biosensor for rapid phosphate monitoring in a sequencing batch reactor (SBR) system," *Biosensors & Bioelectronics*, vol. 19, pp. 233-237, 2003.
- [223] F. Mizutani, Y. Sato, Y. Hirata, and S. Iijima, "Interference-free, amperometric measurement of urea in biological samples using an electrode coated with tri-enzyme/polydimethylsiloxane-bilayer membrane," *Analytica Chimica Acta*, vol. 441, pp. 175-181, 2001.

- [224] M. Situmorang, J. J. Gooding, D. B. Hibbert, and D. Barnett, "The development of a pyruvate biosensor using electrodeposited polytyramine," *Electroanalysis*, vol. 14, pp. 17-21, 2002.
- [225] G. S. Xuan, S. W. Oh, and E. Y. Choi, "Development of an electrochemical immunosensor for alanine aminotransferase," *Biosensors & Bioelectronics*, vol. 19, pp. 365-371, 2003.
- [226] S. Milardovic, Z. Grabaric, V. Rumenjak, and M. Jukic, "Rapid determination of oxalate by an amperometric oxalate oxidase-based electrode," *Electroanalysis*, vol. 12, pp. 1051-1058, 2000.
- [227] M. D. T. Sotomayor, I. M. Raimundo, G. O. Neto, and L. T. Kubota, "Bi-enzymatic optode detection system for oxalate determination based on a natural source of enzyme," *Analytica Chimica Acta*, vol. 447, pp. 33-40, 2001.
- [228] C. F. Wu, H. J. Cha, J. J. Valdes, and W. E. Bentley, "GFP-visualized immobilized enzymes: Degradation of paraoxon via organophosphorus hydrolase in a packed column," *Biotechnology and Bioengineering*, vol. 77, pp. 212-218, 2002.
- [229] Y. F. Tu and H. Y. Chen, "Studies of a disposable biosensor based on the beta-cyclodextrin inclusion complex as mediator," *Analytical Biochemistry*, vol. 299, pp. 71-77, 2001.
- [230] Y. F. Tu and H. Y. Chen, "A nano-molar sensitive disposable biosensor for determination of dopamine," *Biosensors & Bioelectronics*, vol. 17, pp. 19-24, 2002.

- [231] D. Shan, S. Cosnier, and C. Mousty, "Layered double hydroxides: An attractive material for electrochemical biosensor design," *Analytical Chemistry*, vol. 75, pp. 3872-3879, 2003.
- [232] V. S. Bezerra, J. L. De Lima, M. Montenegro, A. N. Araujo, and V. L. Da Silva, "Flow-injection amperometric determination of dopamine in pharmaceuticals using a polyphenol oxidase biosensor obtained from soursop pulp," *Journal of Pharmaceutical and Biomedical Analysis*, vol. 33, pp. 1025-1031, 2003.
- [233] S. Kiralp, L. Toppare, and Y. Yagci, "Immobilization of polyphenol oxidase in conducting copolymers and determination of phenolic compounds in wines with enzyme electrodes," *International Journal of Biological Macromolecules*, vol. 33, pp. 37-41, 2003.
- [234] P. Paranjpe, S. Dutta, M. Karve, S. Padhye, and R. Narayanaswamy, "A disposable optrode using immobilized tyrosinase films," *Analytical Biochemistry*, vol. 294, pp. 102-107, 2001.
- [235] J. S. Kim, J. D. Pike, D. Coucouvanis, and M. E. Meyerhoff, "Enzyme electrode with enhanced specificity using outer polymeric membrane doped with substrate selective ditopic carrier," *Electroanalysis*, vol. 12, pp. 1258-1262, 2000.
- [236] B. X. Li and Z. J. Zhang, "Chemiluminescence flow biosensor for determination of total D-amino acid in serum with immobilized reagents," *Sensors and Actuators B-Chemical*, vol. 69, pp. 70-74, 2000.
- [237] T. Yao, K. Takashima, and Y. Nanjyo, "Dual enzyme electrode with optical specificity for L- and D-amino acids," *Analytical Sciences*, vol. 18, pp. 1039-1041, 2002.

- [238] J. J. Gau, E. H. Lan, B. Dunn, C. M. Ho, and J. C. S. Woo, "A MEMS based amperometric detector for E-Coli bacteria using self-assembled monolayers," *Biosensors & Bioelectronics*, vol. 16, pp. 745-755, 2001.
- [239] K. V. Gobi and F. Mizutani, "Amperometric detection of superoxide dismutase at cytochrome c-immobilized electrodes: Xanthine oxidase and ascorbate oxidase incorporated biopolymer membrane for in-vivo analysis," *Analytical Sciences*, vol. 17, pp. 11-15, 2001.
- [240] M. H. Vela, D. S. de Jesus, C. Couto, A. N. Araujo, and M. Montenegro, "Electroimmobilization of MAO into a polypyrrole film and its utilization for amperometric flow detection of antidepressant drugs," *Electroanalysis*, vol. 15, pp. 133-138, 2003.
- [241] P. C. deJesus, J. J. Joao, P. L. F. daSilva, G. Burlin, and M. D. Nascimento, "Organogels: A new system for lipases immobilization and its application in organic synthesis," *Quimica Nova*, vol. 20, pp. 664-672, 1997.
- [242] E. Akyilmaz and E. Dinckaya, "Development of a catalase based biosensor for alcohol determination in beer samples," *Talanta*, vol. 61, pp. 113-118, 2003.
- [243] A. F. Danet, M. Badea, and H. Y. Aboul-Enein, "Flow injection system with chemiluminometric detection for enzymatic determination of ascorbic acid," *Luminescence*, vol. 15, pp. 305-309, 2000.
- [244] N. Kiba, Y. Inoue, M. Tachibana, K. Tani, and H. Koizumi, "Simultaneous determination of D-glucose and 3-hydroxybutyrate by chemiluminescence detection with immobilized enzymes in a flow injection system," *Analytical Sciences*, vol. 19, pp. 1203-1206, 2003.

- [245] I. Kubo, "Potentiometric phosphate-sensing system utilizing phosphate-binding protein," *Analytical and Bioanalytical Chemistry*, vol. 372, pp. 273-275, 2002.
- [246] Z. Naal, J. H. Park, S. Bernhard, J. P. Shapleigh, C. A. Batt, and H. D. Abruna, "Amperometric TNT biosensor based on the oriented immobilization of a nitroreductase maltose binding protein fusion," *Analytical Chemistry*, vol. 74, pp. 140-148, 2002.
- [247] L. Nagy, G. Nagy, R. E. Gyurcsanyi, M. R. Neuman, and E. Lindner, "Development and study of an amperometric biosensor for the in vitro measurement of low concentration of putrescine in blood," *Journal of Biochemical and Biophysical Methods*, vol. 53, pp. 165-175, 2002.
- [248] L. T. Ng, J. T. Guthrie, Y. J. Yuan, and H. J. Zha, "UV-cured natural polymer-based membrane for biosensor application," *Journal of Applied Polymer Science*, vol. 79, pp. 466-472, 2001.
- [249] H. Okuma and E. Watanabe, "Flow system for fish freshness determination based on double multi-enzyme reactor electrodes," *Biosensors & Bioelectronics*, vol. 17, pp. 367-372, 2002.
- [250] M. Ono, T. Nakajima, Y. Itoh, K. Shimada, and S. Yamato, "Specific determination of myo-inositol in multivitamin pharmaceutical preparations by a flow injection system using a myo-inositol dehydrogenase reactor coupled with a glucose eliminating enzyme reactor," *Journal of Pharmaceutical and Biomedical Analysis*, vol. 33, pp. 1175-1180, 2003.
- [251] P. Sarkar, "One-step separation-free amperometric biosensor for the detection of protein," *Microchemical Journal*, vol. 64, pp. 283-290, 2000.

- [252] N. Sato, K. Usui, and H. Okuma, "Development of a bienzyme reactor sensor system for the determination of ornithine," *Analytica Chimica Acta*, vol. 456, pp. 219-226, 2002.
- [253] Y. Sekiguchi, A. Nishikawa, H. Makita, A. Yamamura, K. Matsumoto, and N. Kiba, "Flow-through chemiluminescence sensor using immobilized histamine oxidase from *Arthrobacter crystallopoietes* KAIT-B007 and peroxidase for selective determination of histamine," *Analytical Sciences*, vol. 17, pp. 1161-1164, 2001.
- [254] N. Garcia-Villar, J. Saurina, and S. Hernandez-Cassou, "Flow injection differential potentiometric determination of lysine by using a lysine biosensor," *Analytica Chimica Acta*, vol. 477, pp. 315-324, 2003.
- [255] T. Yao, K. Takashima, and Y. Nanjyo, "Simultaneous determination of orthophosphate and total phosphates (inorganic phosphates plus purine nucleotides) using a bioamperometric flow-injection system made up by a 16-way switching valve," *Talanta*, vol. 60, pp. 845-851, 2003.
- [256] M. Yaqoob and A. Nabi, "Flow injection chemiluminescent assays for glycerol and triglycerides using a co-immobilized enzyme reactor," *Luminescence*, vol. 18, pp. 67-71, 2003.
- [257] J. Marcos and A. Townshend, "Fluoride Determination By Its Inhibitory Effect On Immobilized Liver Esterase," *Analytica Chimica Acta*, vol. 310, pp. 173-180, 1995.

- [258] M. Schoemaker, R. Feldbrugge, B. Grundig, and F. Spener, "The lipoxygenase sensor, a new approach in essential fatty acid determination in foods," *Biosensors & Bioelectronics*, vol. 12, pp. 1089-1099, 1997.
- [259] L. V. Sigolaeva, A. V. Eremenko, A. Makower, G. F. Makhaeva, V. V. Malygin, and I. N. Kurochkin, "A new approach for determination of neuropathy target esterase activity," *Chemico-Biological Interactions*, vol. 120, pp. 559-565, 1999.
- [260] P. J. Holt, N. C. Bruce, and C. R. Lowe, "Bioluminescent assay for heroin and its metabolites," *Analytical Chemistry*, vol. 68, pp. 1877-1882, 1996.
- [261] J. R. Lakowicz, *Principles of Fluorescence Spectroscopy*, 2nd ed. New York: Kluwer Academic, 1999.
- [262] L. Stryer, *Biochemistry*, 4th ed. New York: W.H. Freeman and Company, 1995.
- [263] K. A. Connors, *Binding Constants: The Measurement of Molecular Complex Stability*. New York: John Wiley & Sons, 1987.
- [264] D. Mauzerall, "Spectra of Molecular Complexes of Porphyrins in Aqueous Solution," *Biochemistry*, vol. 4, pp. 1801-1810, 1965.
- [265] P. Schuck, D. B. Millar, and A. A. Kortt, "Determination of binding constants by equilibrium titration with circulating sample in a surface plasmon resonance biosensor," *Analytical Biochemistry*, vol. 265, pp. 79-91, 1998.
- [266] C. Buron, C. Filiatre, F. Membrey, A. Foissy, and J. F. Argillier, "Interactions between gelatin and sodium dodecyl sulphate: binding isotherm and solution properties," *Colloid and Polymer Science*, vol. 282, pp. 446-453, 2004.
- [267] I. H. Segel, *Enzyme Kinetics*. New York: John Wiley & Sons, 1975.
- [268] D. Voet and J. Voet, *Biochemistry*, 2nd ed. New York: Wiley, 1995.

- [269] W. B. Person, "Criterion for Reliability of Formation Constants of Weak Complexes," *JACS*, vol. 87, pp. 167-181, 1965.
- [270] G. Norheim, "Optimum Conditions for Determination of the Stability of Weak Complexes," *Acta. Chem. Scand.*, vol. 23, pp. 2808-2814, 1969.
- [271] G. Weber and S. R. Anderson, "Multiplicity of Binding Range. Range of Validity and Practicle Test of Adair's Equation," *Biochemistry*, vol. 4, pp. 1942-1948, 1965.
- [272] D. A. Deranleau, "Theory of the Measurement of Weak Molecular Complexes. I. Consequences of Multiple Equilibria," *JACS*, vol. 91, pp. 4050-4049, 1969.
- [273] D. A. Deranleau, "Theory of the Measurement of Weak Molecular Complexes. I. General Considerations," *JACS*, vol. 91, pp. 4044-4050, 1969.
- [274] L. Michaelis and M. L. Menten, "The kinetics of invertase activity," *Biochemische Zeitschrift*, vol. 49, pp. 333, 1913.
- [275] G. E. Briggs and J. B. S. Haldane, "A note on the kinetics of enzyme action," *Biochemistry Journal*, vol. 19, pp. 338-339, 1925.
- [276] L. R. Milgrom, *The Colours of Life*. New York: Oxford University Press, 1997.
- [277] V. K. Skachkova and B. A. Begun, "Immobilization of porphyrin metallocomplexes on thermally structured poly(acrylonitrile)," *Polymer Science Series a*, vol. 42, pp. 963-966, 2000.
- [278] P. Hambright and E. B. Fleischer, "The Acid-Base Equilibria, Kinetics of Copper Ion Incorporation and acid catalyzed zinc ion displacement from the water-soluble porphyrin $\alpha,\beta,\gamma,\delta$ -Tetra(4-N-methylpyridyl)porphine," *Inorganic Chemistry*, vol. 9, pp. 1970, 1970.

- [279] D. Dolphin, "Irreversible Reactions on the Porphyrin Periphery (Excluding Oxidations, Reductions, and Photochemical Reactions)," in *The Porphyrins*, vol. VII, D. Dolphin, Ed. New York: Academic Press, 1979.
- [280] R. Bonnett, "Nomenclature," in *The Porphyrins*, vol. I, D. Dolphin, Ed. New York: Academic Press, 1979.
- [281] J.-H. Fuhrhop, "Irreversible Reactions on the Porphyrin Periphery (Excluding Oxidations, Reductions, and Photochemical Reactions)," in *The Porphyrins*, vol. II, D. Dolphin, Ed. New York: Academic Press, 1979.
- [282] J. W. Buchler, "Synthesis and Properties of Metalloporphyrins," in *The Porphyrins*, vol. I, D. Dolphin, Ed. New York: Academic Press, 1979.
- [283] J. A. Shelnutz, "Molecular Complexes of Copper Uroporphyrin with Aromatic Acceptors," *J. Phys. Chem*, vol. 87, pp. 605-616, 1983.
- [284] H.-J. Schneider and M. Wang, "Ligand-Porphyrin Complexes: Quantitative Evaluation of Stacking and Ionic Contributions," *J. Org. Chem*, vol. 59, pp. 7464-7472, 1994.
- [285] C. V. Banks and R. E. Bisque, "Spectrophotometric determination of zinc and other metals with alpha-,beta-, gamma-, delta-, tetraphenylporphyrine," *Analytical Chemistry*, vol. 29, pp. 522-526, 1957.
- [286] T. Yotuyanagi, H. Hoshino, and S. Igarashi, *Bunseki*, vol. 496, 1985.
- [287] M. Tabata and M. Tanaka, "Porphyrins as reagents for trace-metal analysis," *Trends in Analytical Chemistry*, vol. 10, pp. 128-132, 1991.
- [288] D. K. Lavalley, A. B. Kopelove, and O. P. Anderson, "Structures and Properties of N-Methyltetraphenylporphyrin Complexes. The Crystal and Molecular

- Structure of Chloro-N-methyl-a,b,g,d-tetraphenylporphinatozinc(II) and the Chelate Effect of Zn(II), Co(II), and Cd(II) N-Methylporphyrin Complexes,” *J. Amer. Chem. Soc.*, vol. 100, pp. 3025-30339, 1978.
- [289] M. Tabata, M. Ide, and K. Kaneko, “Thermochromism of Metal Exchange Reaction between Zinc(II) and Mercury(II) Porphyrins,” *Zeitschrift für Naturforschung*, vol. 50b, pp. 545-550, 1995.
- [290] S. Igarashi, T. Aihara, and T. Yotsuyanagi, “Flow injection spectrophotometric determination of ng ml^{-1} levels of cobalt(II) using the photochemical decomposition of a cadmium(II)-water soluble porphyrin complex,” *Anal. Chim. Acta*, vol. 323, pp. 63-67, 1996.
- [291] S. Igarashi and T. Yotsuyanagi, “Spectrofluorimetric determination of traces of zinc with the cadmium- $\alpha,\beta,\gamma,\delta$ -tetrakis(4-sulphophenyl)-porphine complex,” *Anal. Chim. Acta*, vol. 281, pp. 347-351, 1993.
- [292] P. Hambright, “Chemistry of Water Soluble Porphyrins,” in *The Porphyrin Handbook*, vol. 3, K. M. Kadish, K. M. Smith, and R. Guilard, Eds.: Academic Press, 2000, pp. 129-210.
- [293] T. Malinski, “Applications: Past, Present, Future,” in *The Porphyrin Handbook*, vol. 6, K. M. Kadish, K. M. Smith, and R. Guilard, Eds., 1st ed. New York: Academic Press, 2000, pp. 231.
- [294] G. Y. Yang, X. C. Dong, Y. Dai, Q. F. Hu, and G. Y. Yin, “Simultaneous determination of silver, nickel, lead, cadmium, and mercury by on-line column enrichment, followed by reversed phase high performance liquid

- chromatography,” *Journal of Liquid Chromatography & Related Technologies*, vol. 27, pp. 451-463, 2004.
- [295] P. G. P. Ab, J. W. Kampf, E. Rozniecka, Y. Kondratenko, E. Malinowska, and M. E. Meyerhoff, “Gallium(III) and indium(III) octaethylporphyrin dimeric complexes with a single mu-hydroxo bridge: synthesis, structure and stability in anion-containing organic media,” *Inorganica Chimica Acta*, vol. 355, pp. 302-313, 2003.
- [296] P. Aguirre, R. Sarriego, and S. A. Moya, “Ruthenium (II) complexes in catalytic oxidation,” *Journal of Coordination Chemistry*, vol. 54, pp. 401-413, 2001.
- [297] Y. Amao, T. Miyashita, and I. Okura, “Platinum tetrakis(pentafluorophenyl)porphyrin immobilized in polytrifluoroethylmethacrylate film as a photostable optical oxygen detection material,” *Journal of Fluorine Chemistry*, vol. 107, pp. 101-106, 2001.
- [298] Y. Amao, “Probes and polymers for optical sensing of oxygen,” *Microchimica Acta*, vol. 143, pp. 1-12, 2003.
- [299] M. K. Amini, J. H. Khorasani, S. S. Khaloo, and S. Tangestaninejad, “Cobalt(II) salophen-modified carbon-paste electrode for potentiometric and voltammetric determination of cysteine,” *Analytical Biochemistry*, vol. 320, pp. 32-38, 2003.
- [300] L. Angnes, C. M. N. Azevedo, K. Araki, and H. E. Toma, “Electrochemical detection of NADH and dopamine in flow analysis based on tetra-ruthenated porphyrin modified electrodes,” *Analytica Chimica Acta*, vol. 329, pp. 91-95, 1996.

- [301] B. Aveline, O. Delgado, and D. Brault, "Reaction of Singlet Oxygen With Vinyl-Substituted Porphyrins - a Kinetic-Study By Laser Flash-Photolysis," *Journal of the Chemical Society-Faraday Transactions*, vol. 88, pp. 1971-1976, 1992.
- [302] E. Baldini, V. C. Dall'Orto, C. Danilowicz, I. Rezzano, and E. J. Calvo, "Amperometric detection of peroxides using peroxidase and porphyrin biomimetic modified electrodes," *Electroanalysis*, vol. 14, pp. 1157-1164, 2002.
- [303] B. Boitrel, M. Breede, P. J. Brothers, M. Hodgson, L. Michaudet, C. E. F. Rickard, and N. Al Salim, "Bismuth porphyrin complexes: syntheses and structural studies," *Dalton Transactions*, pp. 1803-1807, 2003.
- [304] B. Boitrel, Z. Halime, L. Michaudet, M. Lachkar, and L. Toupet, "Structural characterisation of the first mononuclear bismuth porphyrin," *Chemical Communications*, pp. 2670-2671, 2003.
- [305] R. Carballo, V. C. Dall'Orto, A. Lo Balbo, and I. Rezzano, "Determination of sulfite by flow injection analysis using a poly [Ni-(protoporphyrin IX)] chemically modified electrode," *Sensors and Actuators B-Chemical*, vol. 88, pp. 155-161, 2003.
- [306] M. Cervantes, A. Clark, V. Terpigov, and F. Medrano, "Spectroscopic properties of rare-earth complexes of tetraphenyl porphyrin introduced into a silicate sol-gel matrix," *Journal of Optical Technology*, vol. 69, pp. 61-63, 2002.
- [307] D. Chabach, M. Tahiri, A. Decian, J. Fischer, R. Weiss, and M. E. Bibout, "Tervalent-Metal Porphyrin-Phthalocyanine Heteroleptic Sandwich-Type Complexes - Synthesis, Structure, and Spectroscopic Characterization of Their

- Neutral, Singly-Oxidized, and Singly-Reduced States,” *Journal of the American Chemical Society*, vol. 117, pp. 8548-8556, 1995.
- [308] W. H. Chan, R. H. Yang, and K. M. Wang, “Development of a mercury ion-selective optical sensor based on fluorescence quenching of 5,10,15,20-tetraphenylporphyrin,” *Analytica Chimica Acta*, vol. 444, pp. 261-269, 2001.
- [309] T. M. Chou, K. W. Woodburn, W. F. Cheong, S. A. Lacy, K. Sudhir, D. C. Adelman, and D. Wahr, “Photodynamic therapy: Applications in atherosclerotic vascular disease with motexafin lutetium,” *Catheterization and Cardiovascular Interventions*, vol. 57, pp. 387-394, 2002.
- [310] G. K. Chudinova, I. A. Nagovitsyn, R. E. Karpov, and V. V. Savranskii, “Immunosensor systems with the Langmuir-film-based fluorescent detection,” *Quantum Electronics*, vol. 33, pp. 765-770, 2003.
- [311] R. Czolk, J. Reichert, and H. J. Ache, “An Optical Sensor For the Detection of Cd(Ii) Ions,” *Sensors and Actuators a-Physical*, vol. 26, pp. 439-441, 1991.
- [312] J. R. C. da Rocha, L. Angnes, M. Bertotti, K. Araki, and H. E. Toma, “Amperometric detection of nitrite and nitrate at tetraruthenated porphyrin-modified electrodes in a continuous-flow assembly,” *Analytica Chimica Acta*, vol. 452, pp. 23-28, 2002.
- [313] D. Delmarre, R. Meallet, C. Bied-Charreton, and R. B. Pansu, “Heavy metal ions detection in solution, in sol-gel and with grafted porphyrin monolayers,” *Journal of Photochemistry and Photobiology a-Chemistry*, vol. 124, pp. 23-28, 1999.

- [314] N. Diab, J. Oni, A. Schulte, I. Radtke, A. Blochl, and W. Schuhmann, "Pyrrole functionalised metalloporphyrins as electrocatalysts for the oxidation of nitric oxide," *Talanta*, vol. 61, pp. 43-51, 2003.
- [315] G. D. Du and L. K. Woo, "Reductive coupling reactions of carbonyl compounds with low-valent titanium(II) and zirconium(II) porphyrin complexes," *Abstracts of Papers of the American Chemical Society*, vol. 225, pp. U125-U125, 2003.
- [316] Y. Duan, H. Z. Chang, G. Li, and W. J. Jin, "Oxygen sensor based on palladium-porphyrin room-temperature phosphorescence quenching," *Chinese Journal of Analytical Chemistry*, vol. 31, pp. 1069-1072, 2003.
- [317] H. Duval, V. Bulach, J. Fischer, M. W. Renner, J. Fajer, and R. Weiss, "Correlation of macrocycle distortion with oxidation potentials of iron(III) porphyrins: molecular structure of the sterically crowded chloro-iron(III) 7,8,17,18-tetrabromo-5,10,15,20-tetraphenylporphyrin," *Journal of Biological Inorganic Chemistry*, vol. 2, pp. 662-666, 1997.
- [318] B. Fabre, G. Bidan, and M. Lapkowski, "Poly(N-Methylpyrrole) Films Doped With Iron-Substituted Heteropolytungstates - a New Sensitive Layer For the Amperometric Detection of Nitrite Ions," *Journal of the Chemical Society-Chemical Communications*, pp. 1509-1511, 1994.
- [319] Y. J. Fang, H. Chen, Z. X. Gao, and X. Y. Jin, "Studies on the determination of palladium(II) by fluorescence quenching method with meso-tetra[4-(carboxymethylenoxy)phenyl]porphyrin," *Indian Journal of Chemistry Section a-Inorganic Bio-Inorganic Physical Theoretical & Analytical Chemistry*, vol. 41, pp. 521-524, 2002.

- [320] K. Farhadi, H. Shaikhlouei, R. Maleki, H. Sharghi, and M. Shamsipur, "Highly selective triiodide polymeric membrane electrode based on tetra(p-chlorophenyl)porphyrinato manganese (III) acetate," *Bulletin of the Korean Chemical Society*, vol. 23, pp. 1635-1639, 2002.
- [321] T. J. Foley, B. S. Harrison, A. S. Knefely, K. A. Abboud, J. R. Reynolds, K. S. Schanze, and J. M. Boncella, "Facile preparation and photophysics of near-infrared luminescent lanthanide(III) monoporphyrinate complexes," *Inorganic Chemistry*, vol. 42, pp. 5023-5032, 2003.
- [322] T. Fujihara, K. Tsuge, Y. Sasaki, Y. Kaminaga, and T. Imamura, "Synthesis, properties, and crystal structure of a novel anthracene-bridged molybdenum-zinc porphyrin dimer," *Inorganic Chemistry*, vol. 41, pp. 1170-1176, 2002.
- [323] C. D. George, T. Richardson, M. E. Hofton, C. M. Vale, M. G. M. Neves, and J. A. S. Cavaleiro, "Chlorine gas sensing using thin films of meso-tetra(p-stearamidophenyl)porphyrin," *Materials Science & Engineering C-Biomimetic and Supramolecular Systems*, vol. 8-9, pp. 559-563, 1999.
- [324] R. Giovannetti and V. Bartocci, "Determination of stability constants of Cu(II), Co(II), Zn(II), Ni(II) and Mn(II) chelates with 3,8,13,18-tetramethyl-21H,23H-porphine-2,7,12,27-tetrapropionic acid by reversed-phase high performance liquid chromatography," *Journal of Liquid Chromatography & Related Technologies*, vol. 22, pp. 2151-2157, 1999.
- [325] M. Gotardo, R. C. Sacco, C. S. Juvenal, A. G. Ferreira, A. C. Tedesco, and M. D. Assis, "A novel crowned porphyrin derived from meso-

- tetrakis(pentafluorophenyl)porphyrin,” *Journal of Porphyrins and Phthalocyanines*, vol. 7, pp. 399-404, 2003.
- [326] V. K. Gupta, S. Chandra, D. K. Chauhan, and R. Mangla, “Membranes of 5,10,15,20-tetrakis(4-methoxyphenyl) porphyrinatocobalt (TMOPP-Co) (I) as MoO₄²⁻-selective sensors,” *Sensors*, vol. 2, pp. 164-173, 2002.
- [327] J. H. Ha, H. S. Cho, J. K. Song, D. Kim, N. Arataini, and A. Osuka, “Excitonic coupling strength and coherence length in the singlet and triplet excited states of meso-meso directly linked Zn(II)porphyrin arrays,” *Chemphyschem*, vol. 5, pp. 57-67, 2004.
- [328] A. S. Holmes-Smith, A. Hamill, M. Campbell, and M. Uttamlal, “Electropolymerised platinum porphyrin polymers for dissolved oxygen sensing,” *Analyst*, vol. 124, pp. 1463-1466, 1999.
- [329] F. S. Hong, Z. G. Wei, and G. W. Zhao, “Mechanism of lanthanum effect on chlorophyll of spinach,” *Science in China Series C-Life Sciences*, vol. 45, pp. 166-176, 2002.
- [330] H. Huckstadt, A. Tutass, M. Goldner, U. Cornelissen, and H. Homborg, “Conformational heterogeneity in diphthalocyaninato(2-)metallates(III) of Sc, Y, In, Sb, Bi, La, Ce, Pr, and Sm,” *Zeitschrift Fur Anorganische Und Allgemeine Chemie*, vol. 627, pp. 485-497, 2001.
- [331] H. Y. Jia, W. Q. Xu, M. H. Qi, G. F. Liu, X. L. Li, and B. Zhao, “Spectral study of 5,10,5,20-tetra(p-chlorophenyl) porphyrin lanthanide complexes,” *Chemical Journal of Chinese Universities-Chinese*, vol. 25, pp. 338-341, 2004.

- [332] J. Z. Jiang, Y. Z. Bian, F. Furuya, W. Liu, M. T. M. Choi, N. Kobayashi, H. W. Li, Q. C. Yang, T. C. W. Mak, and D. K. P. Ng, "Synthesis, structure, spectroscopic properties, and electrochemistry of rare earth sandwich compounds with mixed 2,3-naphthalocyaninato and octaethylporphyrinato ligands," *Chemistry-a European Journal*, vol. 7, pp. 5059-5069, 2001.
- [333] J. H. Khorasani, M. K. Amini, H. Motaghi, S. Tangestaninejad, and M. Moghadam, "Manganese porphyrin derivatives as ionophores for thiocyanate-selective electrodes: the influence of porphyrin substituents and additives on the response properties," *Sensors and Actuators B-Chemical*, vol. 87, pp. 448-456, 2002.
- [334] K. Kilian and K. Pyrzynska, "Spectrophotometric study of Cd(II), Pb(II), Hg(II) and Zn(II) complexes with 5,10,15,20-tetrakis(4-carboxylphenyl)porphyrin," *Talanta*, vol. 60, pp. 669-678, 2003.
- [335] R. Konirova, M. Ernestova, V. Jedinakova-Krizova, and V. Kral, "Radioactively labelled porphyrin derivatives," *Czechoslovak Journal of Physics*, vol. 53, pp. A755-A761, 2003.
- [336] M. M. Koskelin, A. E. Soini, N. J. Meltola, and G. V. Ponomarev, "Phosphorescent labeling reagents of platinum(II) and palladium(II) coproporphyrin-II. Preparation and performance characteristics," *Journal of Porphyrins and Phthalocyanines*, vol. 6, pp. 533-543, 2002.
- [337] L. Kosminsky, R. C. Matos, M. H. Tabacniks, and M. Bertotti, "Electrochemical codeposition of platinum and molybdenum oxides: Formation of composite films

- with distinct electrocatalytic activity for hydrogen peroxide detection,” *Electroanalysis*, vol. 15, pp. 733-738, 2003.
- [338] K. Koyanagi and M. Tabata, “Synthesis of F28 tetraphenylporphyrin and its application to the separation and detection of lithium(I),” *Bunseki Kagaku*, vol. 51, pp. 803-807, 2002.
- [339] M. Kreitner, R. Ebermann, and G. Alth, “Quantitative determination of singlet oxygen. Production by porphyrins,” *Journal of Photochemistry and Photobiology B-Biology*, vol. 36, pp. 109-111, 1996.
- [340] T. S. Kurtikyan, G. G. Martirosyan, and M. E. Akopyan, “Spectral investigation of the interaction of carbon monoxide and dioxygen with low-temperature sublimates of Co(II) meso-tetraphenylporphyrinate: Evidences for oxidative catalysis,” *Kinetics and Catalysis*, vol. 42, pp. 281-288, 2001.
- [341] Y. Lee, B. K. Oh, and M. E. Meyerhoff, “Improved planar amperometric nitric oxide sensor based on platinized platinum anode. 1. Experimental results and theory when applied for monitoring NO release from diazeniumdiolate-doped polymeric films,” *Analytical Chemistry*, vol. 76, pp. 536-544, 2004.
- [342] J. A. Legako, B. J. White, and H. J. Harmon, “Detection of cyanide using immobilized porphyrin and myoglobin surfaces,” *Sensors and Actuators B-Chemical*, vol. 91, pp. 128-132, 2003.
- [343] Z. J. Li, Z. Z. Zhu, T. Jan, and J. M. Pan, “Synthesis of meso-tetra-(3,5-dibromo-4-hydroxyphenyl)- porphyrin and its application to second-derivative spectrophotometric determination of lead in clinical samples,” *Analyst*, vol. 124, pp. 1227-1231, 1999.

- [344] F. Li and H. L. Zheng, "Analysis of Pb(II), Cd(II) and Cu(II) in Chinese medicine by the system of porphyrin complexes and sulfhydryl cotton fiber," *Spectroscopy and Spectral Analysis*, vol. 24, pp. 197-199, 2004.
- [345] K. McEwan, K. Lewis, G. Y. Yang, L. L. Chng, Y. W. Lee, W. P. Lau, and K. S. Lai, "Synthesis, characterization, and nonlinear optical study of metalloporphyrins," *Advanced Functional Materials*, vol. 13, pp. 863-867, 2003.
- [346] E. Nyarko, N. Hanada, A. Habib, and M. Tabata, "Fluorescence and phosphorescence spectra of Au(III), Pt(II) and Pd(II) porphyrins with DNA at room temperature," *Inorganica Chimica Acta*, vol. 357, pp. 739-745, 2004.
- [347] K. Padmaja, R. Ramamurthi, and A. R. K. Prasad, "Inhibitory effect of selenium on enzymes involved in heme biosynthetic pathway in chick embryos," *Journal of Enzyme Inhibition*, vol. 11, pp. 1-11, 1996.
- [348] F. Ricchelli, P. Barbato, M. Milani, S. Gobbo, C. Salet, and G. Moreno, "Photodynamic action of porphyrin on Ca²⁺ influx in endoplasmic reticulum: a comparison with mitochondria," *Biochemical Journal*, vol. 338, pp. 221-227, 1999.
- [349] A. Rouhollahi and M. Shamsipur, "Triiodide PVC membrane electrode based on a charge-transfer complex of iodine with 2,4,6,8-tetraphenyl-2,4,6,8-tetraazabicyclo[3.3.0]octane," *Analytical Chemistry*, vol. 71, pp. 1350-1353, 1999.
- [350] H. Sakurai, T. Inohara, Y. Adachi, K. Kawabe, H. Yasui, and J. Takada, "A new candidate for insulinomimetic vanadium complex: synergism of

- oxovanadium(IV)porphyrin and sodium ascorbate,” *Bioorganic & Medicinal Chemistry Letters*, vol. 14, pp. 1093-1096, 2004.
- [351] S. Shahrokhian, A. Hamzehloei, and M. Bagherzadeh, “Chromium(III) porphyrin as a selective ionophore in a salicylate-selective membrane electrode,” *Analytical Chemistry*, vol. 74, pp. 3312-3320, 2002.
- [352] M. Shamsipur, G. Khayatian, and S. Tangestaninejad, “Thiocyanate-selective membrane electrode based on (octabromotetraphenylporphyrinato)manganese(III) chloride,” *Electroanalysis*, vol. 11, pp. 1340-1344, 1999.
- [353] V. C. Smith, T. Richardson, and H. L. Anderson, “Optical detection of chlorine gas using LB films of a zinc porphyrin dimer,” *Supramolecular Science*, vol. 4, pp. 503-508, 1997.
- [354] L. M. Stamp, S. A. Mang, A. B. Holmes, K. A. Knights, Y. R. de Miguel, and I. F. McConvey, “Polymer supported chromium porphyrin as catalyst for polycarbonate formation in supercritical carbon dioxide,” *Chemical Communications*, pp. 2502-2503, 2001.
- [355] K. Staninski, M. Kaczmarek, S. Lis, and M. Elbanowski, “Emission spectroscopic properties of water soluble porphyrins in hydrogen peroxide chemiluminescence system with d- and f-electron metals,” *Journal of Solid State Chemistry*, vol. 171, pp. 208-211, 2003.
- [356] W. L. Sun, J. Xue, J. S. Chen, L. Q. Mao, L. T. Jin, K. Yamamoto, S. G. Tao, and J. Y. Jin, “Measurement of dioxygen by electrocatalytic reduction on microelectrodes modified with Nafion and methyl viologen,” *Talanta*, vol. 49, pp. 345-356, 1999.

- [357] P. Tagliatesta and A. Pastorini, "Electronic and steric effects on the stereoselectivity of cyclopropanation reactions catalysed by rhodium meso-tetraphenylporphyrins," *Journal of Molecular Catalysis a-Chemical*, vol. 185, pp. 127-133, 2002.
- [358] K. Takamura and C. Matsubara, "Versatility of the Titanium(IV) - Porphyrin reagent for determining hydrogen peroxide," *Bulletin of the Chemical Society of Japan*, vol. 76, pp. 1873-1888, 2003.
- [359] M. Thamae, P. Westbroek, and T. Nyokong, "pH study of the electrocatalytic SO₂ detection at a glassy carbon electrode modified with iron(II)tetrakisulfophthalocyanine," *Microchimica Acta*, vol. 140, pp. 233-239, 2002.
- [360] C. Stinson and P. Hambright, "The Copper-Cadmium N-Methyltetraphenylporphyrin Electrophilic Substitution Reaction: Evidence for a Cis Attack," *JACS*, vol. 99, pp. 2357, 1976.
- [361] Y. Inada, Y. Sugimoto, Y. Nakano, and S. Funahashi, "Spectral Evidence and Kinetics for Formation of the Sitting-Atop Complex of Copper(II) Ion with 5,10,15,20-Tetraphenylporphyrin in Acetonitrile," *Chemistry Letters*, pp. 881-882, 1996.
- [362] D. A. Pearce, N. Jotterand, I. S. Carrico, and B. Imeriali, "Derivatives of 8-hydroxy-2-methylquinoline are powerful prototypes for zinc sensors in biological systems," *JACS*, vol. 123, pp. 5160, 2001.

- [363] M.-C. Richoux, P. Neta, P. A. Christensen, and A. Harriman, "Formation and Decay of Zinc Tetrakis(N-methyl-3-pyridyl)porphine π -Radical Cation in Water," *J. Chem. Soc., Faraday Trans. 2*, vol. 82, pp. 235-249, 1986.
- [364] M. Biesaga, K. Pyrzynska, and M. Trojanowicz, "Porphyrins in analytical chemistry. A review," *Talanta*, vol. 51, pp. 209-24, 2000.
- [365] K. M. Kadish, G. Royal, E. V. Caemelbecke, and L. Gueletti, "Metalloporphyrins in nonaqueous media: data base of redox potentials," in *The Porphyrin Handbook*, vol. 9, K. M. Kadish, K. M. Smith, and R. Guilard, Eds., 1st ed. New York: Academic Press, 2000, pp. 231.
- [366] S. L. Jia, W. Jentzen, M. Shang, X.-Z. Song, J.-G. Ma, W. R. Scheidt, and J. A. Schelnutt, "Axial Coordination and Conformational Heterogeneity of Nickel(II) Tetraphenylporphyrin Complexes with Nitrogenous Bases," *Inorg. Chem.*, vol. 37, pp. 4402-4412, 1998.
- [367] G. Guillaud, J. Simon, and J. P. Germain, "Metallophthalocyanines: Gas Sensors, Resistors, and Field Effect Transistors," *Coordination Chemistry Reviews*, vol. 178-180, pp. 1433-1484, 1998.
- [368] B. S. Jursic, "Spectroscopic and Molecular Mechanics Calculations of Discrimination between Enantiomers Possessing an Electron Rich Aromatic Group Directly Attached to the Chiral Carbon Atom with Optically Pure Benzoyl Derivatives," *J. Chem. Soc Perkin Trans.*, vol. 2, pp. 961-969, 1994.
- [369] T. R. E. Simpson, M. J. Cook, M. C. Petty, S. C. Thorpe, and D. A. Russell, "Surface Plasmon Resonance of Self-assembled Phthalocyanine Monolayers: Possibilities for Optical Gas Sensing," *Analyst*, vol. 121, pp. 1501-1505, 1996.

- [370] M. C. Drain, T. H. Joseph, K. S. Suslick, M. R. Wasielewski, and X. Chen, "A Perspective on Four New Porphyrin-Based Functional Materials and Devices," *JPP*, vol. 6, pp. 243-273, 2002.
- [371] A. A. Vaughan, M. G. Baron, and R. Narayanaswamy, "Optical Ammonia Sensing Films Based on an Immobilized Metalloporphyrin," *Anal. Comm.*, vol. 33, pp. 393-396, 1996.
- [372] O. Q. Munro, S. C. Shabalala, and N. J. Brown, "Structural, computational, and Co-59 NMR studies of primary and secondary amine complexes of Co(III) porphyrins," *Inorganic Chemistry*, vol. 40, pp. 3303-3317, 2001.
- [373] H. Ogoshi, T. Mizutani, T. Hayashi, and Y. Kuroda, "Porphyrins and Metalloporphyrins as Receptor Models in Molecular Recognition," in *The Porphyrin Handbook*, vol. 6, K. M. Kadish, K. M. Smith, and R. Guilard, Eds.: Academic Press, 2000, pp. 279.
- [374] H. Tamiaki, N. Matsumoto, S. Unno, S. Shinoda, and H. Tsukube, "Induced circular dichroism active complexes of synthetic gadolinium (III) porphyrinates with chiral amino acids," *Inorganica Chimica Acta*, vol. 300-302, pp. 243-249, 2000.
- [375] P. Kubat, K. Lang, J. Mosinger, and D. M. Wagnerova, "Reactions Photosensitized by Tetrakis(4-sulfonatophenyl)porphyrin: Protonation of the Triplet States and Effect of Amino Acids," *Zeitschrift Fur Physikalische Chemie*, vol. 210, pp. 243-256, 1999.

- [376] M. Aoudia and M. J. Rodgers, "Photoprocesses in Self-Assembled Complexes of Oligopeptides with Metalloporphyrins," *J. Amer. Chem. Soc.*, vol. 119, pp. 12859-12868, 1997.
- [377] S. Hamai, "Molecular Recognition of Malto-oligosaccharides by Free and Metal Tetrakis(4-sulfonatophenyl)porphyrins in Basic Aqueous Solutions," *J. Nanosci. and Nanotech.*, vol. 1, pp. 177-184, 2001.
- [378] J. Charvatova, O. Rusin, V. Kral, K. Volka, and P. Matejka, "Novel porphyrin based receptors for saccharide recognition in water," *Sensors and Actuators B-Chemical*, vol. 76, pp. 366-372, 2001.
- [379] N. A. Rakow and K. S. Suslick, "A colorimetric sensor array for odour visualization," *Nature*, vol. 406, pp. 710-713, 2000.
- [380] J. A. A. W. Elemans, M. B. Claase, P. P. M. Aarts, A. E. Rowan, A. P. H. J. Schenning, and R. J. M. Nolte, "Porphyrin Clips Derived from Diphenylglycoluril. Synthesis, Conformational Analysis, and Binding Properties," *J. Org. Chem.*, vol. 64, pp. 7009-16, 1999.
- [381] X. B. Zhang, Z. Z. Li, C. C. Guo, S. H. Chen, G. L. Shen, and R. Q. Yu, "Porphyrin-metalloporphyrin composite based optical fiber sensor for the determination of berberine," *Analytica Chimica Acta*, vol. 439, pp. 65-71, 2001.
- [382] R. Song, A. Robert, J. Bernadou, and b. Meunier, "Sulfonated and Acetamidofunctionalized Tetraarylporphyrins as Biomimetic Oxidation Catalysts Under Aqueous Conditions," *Inorganica Chimica Acta*, vol. 272, pp. 228, 1998.
- [383] R. T. Wheelhouse, D. Sun, H. Han, F. X. Han, and L. H. Hurley, "Cationic Porphyrins as Telomerase Inhibitors: the Interaction of Tetra-(*N*-methyl-4-

- pyridyl)porphine with Quadruplex DNA,” *J. Am. Chem. Soc.*, vol. 120, pp. 3261-62, 1998.
- [384] M. Lin and N. Wu, “A Model System for Protein-Porphyrin Binding Constant Measurement Using Capillary Electrophoresis,” *J. Liq. Chrom. and Rel. Technol.*, vol. 22, pp. 2167-2175, 1999.
- [385] J. Nakamura and S. Igarashi, “Highly Sensitive Spectrophotometric and Spectrofluorometric Determinations of Albumin with 5,10,15,20-tetrakis(4-sulfophenyl)porphine,” *Anal. Lett.*, vol. 29, pp. 981-989, 1996.
- [386] M. W. Stark, C. J. Hawker, G. J. Hart, A. Philippides, P. M. Petersen, J. D. Lewis, F. J. Leeper, and A. R. Battersby, “Biosynthesis of Porphyrins and Related Macrocycles. Part 40. Synthesis of a Spiro-lactam Related to the Proposed Spiro-intermediate for Porphyrin Biosynthesis: Inhibition of Cosynthetase,” *J. Chem. Soc. Perkin Trans. 1*, vol. 23, pp. 2875-92, 1993.
- [387] D. L. DeCamp, L. M. Babe, R. Salto, J. L. Lucich, M. S. Koo, S. B. Kahl, and C. S. Craik, “Specific Inhibition of HIV-1 Protease by Boronated Porphyrins,” *J. Med. Chem.*, vol. 4, pp. 3426-8, 1992.
- [388] B. H. Lee, M. B. Park, and B. S. Yu, “Inhibition of Electric Eel Acetylcholinesterase by Porphyrin Compounds,” *Bioorganic and Medicinal Chemistry Letters*, vol. 8, pp. 1467-1470, 1998.
- [389] S. C. Moon, J. H. Shin, B. H. Jeong, H. S. Kim, B. S. Yu, J. S. Lee, B. S. Lee, and S. K. Namgoong, “Synthesis of tetrakis(multifluoro-4-pyridyl)porphin derivatives as acetylcholinesterase inhibitors,” *Bioorganic & Medicinal Chemistry Letters*, vol. 10, pp. 1435-1438, 2000.

- [390] S. K. Namgoong, J. S. Lee, J. H. Shin, S. C. Moon, B. H. Jung, H. S. Kim, and B. S. Yu, "Synthesis of new tetrakis(multifluoro-4-pyridyl)porphyrin derivatives as the electric eel acetylcholinesterase inhibitors," *Bulletin of the Korean Chemical Society*, vol. 21, pp. 264-266, 2000.
- [391] B. J. White and H. J. Harmon, "Interaction of monosulfonate tetraphenyl porphyrin, a competitive inhibitor, with acetylcholinesterase," *Biosensors & Bioelectronics*, vol. 17, pp. 463-469, 2002.
- [392] B. J. White, J. A. Legako, and H. J. Harmon, "Reagent-less detection of a competitive inhibitor of immobilized acetylcholinesterase," *Biosensors & Bioelectronics*, vol. 17, pp. 361-366, 2002.
- [393] B. J. White and H. J. Harmon, "Reagent-less Biosensor of Inhibitors of Acetylcholinesterase," presented at 2002 Joint Service Scientific Conference on Chemical & Biological Defense Research, Hunt Valley Maryland, 2002.
- [394] B. J. White, J. A. Legako, and H. J. Harmon, "Extended Lifetime of Reagent-less Detector for Multiple Inhibitors of Acetylcholinesterase," *Biosensors & Bioelectronics*, vol. 18, pp. 729-734, 2003.
- [395] B. J. White, J. A. Legako, and H. J. Harmon, "Spectrophotometric detection of cholinesterase inhibitors with an integrated acetyl-/butyrylcholinesterase surface," *Sensors and Actuators B-Chemical*, vol. 89, pp. 107-111, 2003.
- [396] B. J. White, H. J. Harmon, and A. Mulchandani, "Optical solid-state detection of organophosphates using organophosphorus hydrolase," *Biosensors Bioelectronics*, vol. Submitted, 2004.

- [397] B. J. White, J. A. Legako, and H. J. Harmon, "Rapid reagent-less detection of competitive inhibitors of butyrylcholinesterase," *Sensors and Actuators B-Chemical*, vol. 91, pp. 138-142, 2003.
- [398] B. J. White and H. J. Harmon, "Novel optical solid-state glucose sensor using immobilized glucose oxidase," *Biochemical and Biophysical Research Communications*, vol. 296, pp. 1069-1071, 2002.
- [399] B. J. White and H. J. Harmon, "Competitive Inhibition of Carbonic Anhydrase by Water Soluble Porphyrins: Use of Carbonic Anhydrase as a CO₂ sensor," *Biosensors Bioelectronics*, vol. Submitted, 2004.
- [400] M. Takahashi, A. Ueno, T. Uda, and H. Mihara, "Design of Novel Porphyrin-Binding Peptides Based on Antibody CDR," *Bioorg. Medicinal Chem.*, vol. 8, pp. 2023-2026, 1998.
- [401] B. Mestre, A. Jakobs, G. Pratviel, and B. Meunier, "Structure/Nuclease Activity Relationships of DNA Cleavers Based on Cationic Metalloporphyrin-Oligonucleotide Conjugates," *Biochemistry*, vol. 35, pp. 9140-9, 1996.
- [402] Y. Feng and J. R. Pilbrow, "Porphyrin Intercalation and Non-specific 'Edge on' Outside Binding to Natural DNA," *Biophysical Chemistry*, vol. 36, pp. 117-31, 1990.
- [403] S. Mohammadi, M. Perree-Fauvet, N. Gresh, K. Hillairet, and E. Taillandier, "Joint Molecular Modeling and Spectroscopic Studies of DNA Complexes of a Bis(arginyl) Conjugate of Tricationic Porphyrin Designed to Target the Major Groove," *Biochemistry*, vol. 37, pp. 6165-78, 1998.

- [404] K. Zaruba, Z. Tomankova, D. Sykora, J. Charvatova, I. Kavenova, P. Bour, P. Matejka, J. Fahrnich, K. Volka, and V. Kral, "Interaction of porphyrin and sapphyrin macrocycles with nucleobases and nucleosides Spectroscopic, quantum chemical, and chromatographic investigation," *Anal. Chim. Acta*, vol. 437, pp. 39-53, 2001.
- [405] H. J. Harmon, "Specific Visible Spectral Changes Induced by Guanine Binding to Cytosine-derivatized porphyrin," *J. Porphyrins Phthalocyanines*, vol. 6, pp. 73-77, 2002.
- [406] R.-H. Yang, K.-M. Wang, D. Xiao, X.-H. Yang, and H.-M. Li, "A selective optical chemical sensor for the determination of Tween-60 based on fluorescence enhancement of tetraphenylporphyrin," *Anal. Chim. Acta*, vol. 404, pp. 205-211, 2000.
- [407] S. C. M. Gandini, V. E. Yushmanov, and M. Tabak, "Interaction of Fe(III)- and Zn(II)-tetra(4-sulfonatophenyl) porphyrins with ionic and nonionic surfactants: aggregation and binding," *Journal of Inorganic Biochemistry*, vol. 85, pp. 263-277, 2001.
- [408] S. L. H. Rebelo, M. M. Q. Simoes, M. G. P. M. S. Neves, and J. A. S. Cavaleiro, "Oxidation of alkylaromatics with hydrogen peroxide catalysed by manganese(III) porphyrins in the presence of ammonium acetate," *J. Molec. Cat. A*, vol. 291, pp. 9-22, 2003.
- [409] S. Hasan, J.-G. Cho, K. L. Sublette, D. Pak, and A. Maule, "Porphyrin-catalyzed degradation of chlorinated phenols and nitro-substituted toluenes," *J. Biotech.*, vol. 24, pp. 195-201, 1992.

- [410] V. Hequet, P. Le Cloirec, C. Gonzalez, and B. Meunier, "Photocatalytic Dgradation of Atrazine by Porphyrin and Phthalocyanine Complexes," *Chemosphere*, vol. 41, pp. 379, 2000.
- [411] M. Sanchez, N. Chap, J. B. Cazaux, and B. Meunier, "Metallophthalocyanines linked to organic copolymers as efficient oxidative supported catalysts," *European Journal of Inorganic Chemistry*, pp. 1775-1783, 2001.
- [412] G. S. Long, B. Snedeker, K. Bartosh, M. L. Werner, and A. Sen, "Transition metal phthalocyanine and porphyrin complexes as catalysts for the polymerization of alkenes," *Canadian Journal of Chemistry-Revue Canadienne De Chimie*, vol. 79, pp. 1026-1029, 2001.
- [413] M. P. Jensen and D. P. Riley, "Peroxynitrite Decomposition Activity of Iron Porphyrin Complexes," *Inorg. Chem.*, vol. 41, pp. 4788-4797, 2002.
- [414] R. Paolesse, C. Di Natale, M. Burgio, E. Martinelli, E. Mazzone, G. Palleschi, and A. D'Amico, "Porphyrin-based array of cross-selective electrodes for analysis of liquid samples," *Sensors and Actuators B-Chemical*, vol. 95, pp. 400-405, 2003.
- [415] Akrajas, M. M. Salleh, and M. Yahaya, "Enriching the selectivity of metalloporphyrins chemical sensors by means of optical technique," *Sensors and Actuators B-Chemical*, vol. 85, pp. 191-196, 2002.
- [416] R. Paolesse, D. Monti, L. La Monica, M. Venanzi, A. Froiio, S. Nardis, C. Di Natale, E. Martinelli, and A. D'Amico, "Preparation and self-assembly of chiral porphyrin diads on the gold electrodes of quartz crystal microbalances: A novel potential approach to the development of enantioselective chemical sensors," *Chemistry-a European Journal*, vol. 8, pp. 2476-2483, 2002.

- [417] A. D'Amico, C. Di Natale, R. Paolesse, A. Macagnano, and A. Mantini, "Metalloporphyrins as basic material for volatile sensitive sensors," *Sensors and Actuators B-Chemical*, vol. 65, pp. 209-215, 2000.
- [418] R. Paolesse, C. Di Natale, V. C. Dall'Orto, A. Macagnano, A. Angelaccio, N. Motta, A. Sgarlata, J. Hurst, I. Rezzano, M. Mascini, and A. D'Amico, "Porphyrin thin films coated quartz crystal microbalances prepared by electropolymerization technique," *Thin Solid Films*, vol. 354, pp. 245-250, 1999.
- [419] C. Di Natale, R. Paolesse, A. Macagnano, V. I. Troitsky, T. S. Berzina, and A. D'Amico, "Pattern recognition approach to the study of the interactions between metalloporphyrin Langmuir-Blodgett films and volatile organic compounds," *Analytica Chimica Acta*, vol. 384, pp. 249-259, 1999.
- [420] A. D'Amico, C. Di Natale, A. Macagnano, F. Davide, A. Mantini, E. Tarizzo, R. Paolesse, and T. Boschi, "Technologies and tools for mimicking olfaction: status of the Rome "Tor Vergata" electronic nose," *Biosensors & Bioelectronics*, vol. 13, pp. 711-721, 1998.
- [421] P. S. Barker, J. R. Chen, N. E. Agbor, A. P. Monkman, P. Mars, and M. C. Petty, "Vapor Recognition Using Organic Films and Artificial Neural Networks," *Sensors and Actuators B-Chemical*, vol. 17, pp. 143-147, 1994.
- [422] N. Inagaki, s. Tasaka, and Y. Sei, "Plasma Polymer Thin Films of Zinc Phthalocyanies for NO₂ Gas Sensor Device," *Polymer Bulletin*, vol. 36, pp. 601-607, 1996.
- [423] E. Moons, A. Goossens, and T. Savenije, "Surface Voltage of Porphyrin Layers Using the Kelvin Probe Technique," *J. Phys. Chem. B*, vol. 101, pp. 8492, 1997.

- [424] G. F. Bickerstaff, *Immobilization of Enzymes and Cells*, vol. 1. Totowa, NJ: Humana Press, 1997.
- [425] C. Cremisini, S. D. Sario, J. Mela, R. Pilloton, and G. Palleschi, "Evaluation of the Use of Free and Immobilized Acetylcholinesterase for Paraoxon Detection with an Amperometric Choline Oxidase Based Biosensor," *Anal Chim Acta*, vol. 311, pp. 273-280, 1995.
- [426] M. E. Leon-Gonzales and A. Townshend, "Flow-Injection Determination of Paraoxon by Inhibition of Immobilized Acetylcholinesterase," *Anal Chim Acta*, vol. 236, pp. 267-272, 1990.
- [427] V. K. Nguyen, C.-M. Wolff, J.-M. Warter, and P. Poindron, "Stabilization of Dry Immobilized Acetylcholinesterase on Nitrocellulose Membrane for Rapid Colorimetric Screening of its Inhibitors in Water and Biological Fluids," *Analytical Letters*, vol. 31, pp. 2457-2473, 1998.
- [428] M. Stoytcheva, V. Sharkova, and J.-P. Magnin, "Electrochemical Approach in Studying the Inactivation of Immobilized Acetylcholinesterase by Arsenate (III)," *Electroanalysis*, vol. 10, pp. 994-8, 1998.
- [429] I. A. Takruni, A. M. Almuaibed, and A. Townshend, "Flow-Injection Study of Inhibition and Reactivity of Immobilized Acetylcholinesterase: Determination of the Pesticides Paraoxon and Carbamoylcholine," *Analytica Chimica Acta*, vol. 282, pp. 307, 1993.
- [430] S. Yabuki, F. Mizutani, and Y. Hirata, "Preparation of an acetylcholine sensor based on an enzyme-immobilized polyion complex membrane," *Bunseki Kagaku*, vol. 50, pp. 899-901, 2001.

- [431] L. Dziri, B. Desbat, and R. M. Leblanc, "Polarization-modulated FT-IR spectroscopy studies of acetylcholinesterase secondary structure at the air-water interface," *Journal of the American Chemical Society*, vol. 121, pp. 9618-9625, 1999.
- [432] L. Dziri, S. Boussaad, N. J. Tao, and R. M. Leblanc, "Acetylcholinesterase complexation with acetylthiocholine or organophosphate at the air/aqueous interface: AFM and UV-Vis studies," *Langmuir*, vol. 14, pp. 4853-4859, 1998.
- [433] T. K. V. Krawczyk, "Analytical applications of inhibition of enzymatic reactions," *Chemia Analityczna*, vol. 43, pp. 135-158, 1998.
- [434] P. Skladal, "Biosensors based on cholinesterase for detection of pesticides," *Food Technology and Biotechnology*, vol. 34, pp. 43-49, 1996.
- [435] P. Skladal, M. Pavlik, and M. Fiala, "Pesticide Biosensor Based On Coimmobilized Acetylcholinesterase and Butyrylcholinesterase," *Analytical Letters*, vol. 27, pp. 29-40, 1994.
- [436] J. L. Sussman, M. Harel, F. Frolow, C. Oefner, G. Adrian, L. Toker, and I. Silman, "Atomic Structure of Acetylcholinesterase from *Torpedo californica*: A Prototypic Acetylcholine-Binding Protein," *Science*, vol. 25, pp. 872-9, 1991.
- [437] C. Communications, "Pierce Biotechnology: Technical Resources," , vol. 2004: Pierce Biotechnology, 2002.
- [438] M. Abo, Y. Ogasawara, Y. Tanaka, A. Okubo, and S. Yamazaki, "Amperometric dimethyl sulfoxide sensor using dimethyl sulfoxide reductase from *Rhodobacter sphaeroides*," *Biosensors & Bioelectronics*, vol. 18, pp. 735-739, 2003.

- [439] J. J. Burmeister and G. A. Gerhardt, "Self referencing ceramic based multisite microelectrodes for the detection and elimination of interferences from the measurement of L-glutamate and other analytes," *Analytical Chemistry*, vol. 73, pp. 1037-1042, 2001.
- [440] Y.-G. Li, Y.-X. Zhou, J.-L. Feng, Z.-H. Jiang, and L.-R. Ma, "Immobilization of Enzyme on Screen-Printed Electrode by Exposure to Glutaraldehyde Vapour for the Construction of Amperometric Acetylcholinesterase Electrodes," *Analytica Chimica Acta*, vol. 382, pp. 277-282, 1999.
- [441] A. Mulchandani, P. Mulchandani, and W. Chen, "Enzyme biosensor for determination of organophosphates," *Field Analytical Chemistry and Technology*, vol. 2, pp. 363-369, 1998.
- [442] E. H. Cordes and W. P. Jencks, "On the Mechanism of Schiff Base Formation and Hydrolysis," *JACS*, vol. 84, pp. 832-836, 1961.
- [443] G. L. Ellman, K. D. Courtney, V. Andres, and R. M. Featherstone, "A New and Rapid Colorimetric Determination of Acetylcholinesterase Activity," *Biochemical Pharmacology*, vol. 7, pp. 88-95, 1961.
- [444] I. Dendritech, "PAMAM Dendrimers," , vol. 2004: Dendritech, Inc., 2002.
- [445] A. E. Eriksson, T. A. Jones, and A. Liljas, "Refined structure of human carbonic anhydrase II at 2.0 Å resolution," *Proteins*, vol. 4, pp. 274, 1988.
- [446] M. Harel, G. Kryger, T. L. Rosenberry, W. D. Mallender, T. Lewis, R. J. Fletcher, J. M. Guss, I. Silman, and J. L. Sussman, "Three-Dimensional Structures of *Drosophila Melanogaster* Acetylcholinesterase and of its Complexes with Two Potent Inhibitors," *Protein Sci.*, vol. 9, 2000.

- [447] G. D. Zhang, A. Harada, N. Nishiyama, D. L. Jiang, H. Koyama, T. Aida, and K. Kataoka, "Polyion complex micelles entrapping cationic dendrimer porphyrin: effective photosensitizer for photodynamic therapy of cancer," *Journal of Controlled Release*, vol. 93, pp. 141-150, 2003.
- [448] P. M. R. Paulo, R. Gronheid, F. C. De Schryver, and S. M. B. Costa, "Porphyrin-dendrimer assemblies studied by electronic absorption spectra and time-resolved fluorescence," *Macromolecules*, vol. 36, pp. 9135-9144, 2003.
- [449] K. Sugiura, "An adventure in macromolecular chemistry based on the achievements of dendrimer science: Molecular design, synthesis, and some basic properties of cyclic porphyrin oligomers to create a functional nano-sized space," in *Dendrimers V: Functional and Hyperbranched Building Blocks, Photophysical Properties, Applications in Materials and Life Sciences*, vol. 228, *Topics in Current Chemistry*, 2003, pp. 65-85.
- [450] O. Finikova, A. Galkin, V. Rozhkov, M. Cordero, C. Hagerhall, and S. Vinogradov, "Porphyrin and tetrabenzoporphyrin dendrimers: Tunable membrane-impermeable fluorescent pH nanosensors," *Journal of the American Chemical Society*, vol. 125, pp. 4882-4893, 2003.
- [451] G. D. Zhang, N. Nishiyama, A. Harada, D. L. Jiang, T. Aida, and K. Kataoka, "PH-sensitive assembly of light-harvesting dendrimer zinc porphyrin bearing peripheral groups of primary amine with poly(ethylene glycol)-b-poly(aspartic acid) in aqueous solution," *Macromolecules*, vol. 36, pp. 1304-1309, 2003.
- [452] M. J. Frampton, S. W. Magennis, J. N. G. Pillow, P. L. Burn, and I. D. W. Samuel, "The effect of intermolecular interactions on the electro-optical

- properties of porphyrin dendrimers with conjugated dendrons,” *Journal of Materials Chemistry*, vol. 13, pp. 235-242, 2003.
- [453] R. M. Crooks and A. J. Ricco, “New Organic Materials Suitable for Use in Chemical Sensor Arrays,” *Accounts of Chem. Res.*, vol. 31, pp. 219-227, 1998.
- [454] L.-H. Guo, G. McLendon, H. Razafitrimo, and Y. Gao, “Photo-active and Electro-active Protein Films Prepared by Reconstitution with Metalloporphyrins Self-Assembled on Gold,” *J. Mater. Chem.*, vol. 6, pp. 369--374, 1996.
- [455] C. E. Kibbey and M. E. Meyerhoff, “Preparation and Characterization of Covalently Bound Tetraphenylporphyrin Silica-Gel Stationary Phases For Reversed- Phase and Anion-Exchange Chromatography,” *Analytical Chemistry*, vol. 65, pp. 2189-2196, 1993.
- [456] H. J. Harmon, “Porphyrins as detectors of CB agents,” presented at Proceedings of the Joint Conference on Point Detection for Chemical and Biological Defense, Williamsburg, VA, 2000.
- [457] A. V. Krasnoslobodtsev and S. N. Smirnov, “Effect of water on silanization of silica by trimethoxysilanes,” *Langmuir*, vol. 18, pp. 3181-3184, 2002.
- [458] N. Nishimura, M. Ooi, K. Shimazu, H. Fujii, and K. Uosaki, “Post-assembly insertion of metal ions into thiol-derivatized porphyrin monolayers on gold,” *Journal of Electroanalytical Chemistry*, vol. 473, pp. 75-84, 1999.
- [459] S. Reutter, “Hazards of Chemical Weapons Release during War: New Perspectives,” *Environmental Health Perspectives*, vol. 107, pp. 985-990, 1999.

- [460] M. Bernabei, C. Cremisini, M. Mascini, and G. Palleschi, "Determination of Organophosphorus and Carbamic Pesticides with a Choline and Acetylcholine Electrochemical Biosensor," *Analytical Letters*, vol. 24, pp. 1317, 1991.
- [461] C. Dumschat and H. Muller, "Pesticide-sensitive ISFET based on enzyme inhibition," *Analytica Chimica Acta*, vol. 252, pp. 7-9, 1991.
- [462] K. R. Rogers, M. Foley, S. Alter, P. Koga, and M. Eldefrawl, "Light Addressable Potentiometric Biosensor for the Detection of Anticholinesterases," *Analytical Letters*, vol. 24, pp. 191, 1991.
- [463] M. Stoytcheva, "Acetylcholinesterase-Based Amperometric Sensor," *Electroanalysis*, vol. 7, pp. 560-2, 1995.
- [464] J.-W. Choi, J. Min, J.-W. Jung, H.-W. Rhee, and W. H. Lee, "Fiber-Optic Biosensor for the Detection of Organophosphorus Compounds Using AChE-Immobilized Viologen LB Films," *Thin Solid Films*, vol. 327-329, pp. 676-80, 1998.
- [465] I. Palchetti, A. Cagnini, M. Del Carlo, C. Coppi, M. Mascini, and A. P. F. Turner, "Determination of Anticholinesterase Pesticides in Real Samples Using a Disposable Biosensor," *Anal Chim Acta*, vol. 337, pp. 315-321, 1997.
- [466] A. L. Simonian, E. I. Rainina, and J. R. Wild, "A new approach for discriminative detection of organophosphate neurotoxins in the presence of other cholinesterase inhibitors," *Analytical Letters*, vol. 30, pp. 2453-2468, 1997.
- [467] A. L. Simonian, J. K. Grimsley, A. W. Flounders, J. S. Schoeniger, T. C. Cheng, J. J. DeFrank, and J. R. Wild, "Enzyme-based biosensor for the direct detection of

- fluorine- containing organophosphates,” *Analytica Chimica Acta*, vol. 442, pp. 15-23, 2001.
- [468] T. T. Bachmann and R. D. Schmid, “A Disposable Multielectrode Biosensor for Rapid and Simultaneous Detection of the Insecticides Paraoxon and Carbofuran at High Resolution,” *Analytica Chimica Acta*, vol. 401, pp. 95-103, 1999.
- [469] T. T. Bachmann, B. Leca, F. Vilatte, J.-L. Marty, D. Fournier, and R. D. Schmid, “Improved Multianalyte Detection of Organophosphates and Carbamates with Disposable Multielectrode Biosensors Using Recombinant Mutants of *Drosophila* Acetylcholinesterase and Artificial Neural Networks,” *Biosensors and Bioelectronics*, vol. 15, pp. 193-201, 2000.
- [470] O. V. Fedosseeva, H. Uchida, T. Katsube, Y. Ishimaru, and T. Iida, “Cholinesterase-based biosensor using surface photovoltage technique,” *Electrochemistry*, vol. 67, pp. 755-759, 1999.
- [471] P. Mulchandani, W. Chen, A. Mulchandani, J. Wang, and L. Chen, “Amperometric microbial biosensor for direct determination of organophosphate pesticides using recombinant microorganism with surface expressed organophosphorus hydrolase,” *Biosensors & Bioelectronics*, vol. 16, pp. 433-437, 2001.
- [472] A. Mulchandani, P. Mulchandani, I. Kaneva, and W. Chen, “Biosensor for direct determination of organophosphate nerve agents using recombinant *Escherichia coli* with surface- expressed organophosphorus hydrolase. 1. Potentiometric microbial electrode,” *Analytical Chemistry*, vol. 70, pp. 4140-4145, 1998.

- [473] A. Mulchandani, I. Kaneva, and W. Chen, "Biosensor for direct determination of organophosphate nerve agents using recombinant *Escherichia coli* with surface-expressed organophosphorus hydrolase. 2. Fiber optic microbial biosensor," *Analytical Chemistry*, vol. 70, pp. 5042-5046, 1998.
- [474] J. Wang, R. Krause, K. Block, M. Musameh, A. Mulchandani, P. Mulchandani, W. Chen, and M. J. Schoning, "Dual amperometric-potentiometric biosensor detection system for monitoring organophosphorus neurotoxins," *Analytica Chimica Acta*, vol. 469, pp. 197-203, 2002.
- [475] S. H. Chough, A. Mulchandani, P. Mulchandani, W. Chen, J. Wang, and K. R. Rogers, "Organophosphorus hydrolase-based amperometric sensor: Modulation of sensitivity and substrate selectivity," *Electroanalysis*, vol. 14, pp. 273-276, 2002.
- [476] A. Mulchandani, P. Mulchandani, S. Chauhan, I. Kaneva, and W. Chen, "A potentiometric microbial biosensor for direct determination of organophosphate nerve agents," *Electroanalysis*, vol. 10, pp. 733-737, 1998.
- [477] J. Wang, L. Chen, A. Mulchandani, P. Mulchandani, and W. Chen, "Remote biosensor for in-situ monitoring of organophosphate nerve agents," *Electroanalysis*, vol. 11, pp. 866-869, 1999.
- [478] E. I. Rainina, E. N. Efremenco, S. D. Varfolomeyev, A. L. Simonian, and J. R. Wild, "The development of a new biosensor based on recombinant *E. coli* for the direct detection of organophosphorus neurotoxins," *Biosensors & Bioelectronics*, vol. 11, pp. 991-1000, 1996.

- [479] A. L. Jenkins, M. O. Uy, and G. M. Murray, "Polymer-Based Lanthanide Luminescent Sensor for Detection of the Hydrolysis Product of the Nerve Agent Soman in Water," *Anal. Chem.*, vol. 71, pp. 373-378, 1999.
- [480] A. Mulchandani, S. T. Pan, and W. Chen, "Fiber-optic enzyme biosensor for direct determination of organophosphate nerve agents," *Biotechnology Progress*, vol. 15, pp. 130-134, 1999.
- [481] R. Gruss, F. Scheller, M. J. Shao, and C. C. Liu, "Electrochemical Determination of Cholinesterase Activity and Indication of its Inhibitors Using a Thick-Film Platinum Electrode," *Anal. Letters*, vol. 22, pp. 1159, 1989.
- [482] S. Okazaki, H. Nakagawa, S. Asakura, K. Kukuda, H. Kiuchi, S. Takahashi, and T. Shigemori, "A Re-usable Biosensor for Organophosphate Pesticides," *Denki Kagaku*, vol. 66, pp. 615-619, 1998.
- [483] H. Shibata, H. Ochiai, T. Kahashima, T. Okamoto, and I. Inamura, "Preparation and Properties of the Water-Soluble Chlorophyll-Bovine Serum Albumin Complexes," *Biochim. Biophys. Acta*, vol. 852, pp. 175-182, 1986.
- [484] I. E. Borissevitch, T. T. Tominaga, and C. C. Schmitt, "Photophysical Studies on the Interaction of two Water-Soluble Porphyrins with Bovine Serum Albumin. Effects Upon the Porphyrin Triplet State Characteristics," *J. Photochem. Photobiol.*, vol. 114, pp. 201-207, 1998.
- [485] H. J. Harmon, "Spectroscopic Determination of Acetylcholine Esterase-Inhibitor Complex: Determination of Conformational Shifts of Proteins," *Biosensors & Bioelectronics*, vol. 16, pp. 1035-1041, 2001.

- [486] T. B. Amor, L. Bortolotto, and G. Jori, "Porphyrins and Related Compounds as Photoactivatable Insecticides. 3. Laboratory and Field Studies," *Photochemistry and Photobiology*, vol. 71, pp. 124-8, 2000.
- [487] R. Lenigk, E. Lam, A. Lai, H. Wang, Y. Han, P. Carlier, and R. Renneberg, "Enzyme Biosensor for Studying Therapeutics of Alzheimer's Disease," *Biosensors and Bioelectronics*, vol. 15, pp. 541, 2000.
- [488] P. G. Antuono, "Effectiveness and Safety of Velnacrine for the Treatment of Alzheimer's Disease: A Double-blind, Placebo-controlled Study," *Archives of Internal Medicine*, vol. 155, pp. 1766-73, 1995.
- [489] S. J. Griffiths, P. F. Heelis, A. K. Haylett, and J. V. Moore, "Photodynamic Therapy of Ovarian Tumours and Normal Cells Using 5,10,15,20-tetra-(3-carboxymethoxyphenyl)-chlorin," *Cancer Letters*, vol. 125, pp. 177-84, 1998.
- [490] V. Ruddy, B. D. MacCraith, and J. A. Murphy, "Evanescent Wave Absorption Spectroscopy Using Multimode Fibers," *J. Appl. Phys.*, vol. 67, pp. 6070-6074, 1990.
- [491] C. Egami, K. Takeda, M. Isai, and M. Ogita, "Evanescent-Wave Spectroscopic Fiber Optic pH Sensor," *Optics Communications*, vol. 122, pp. 122-126, 1996.
- [492] B. D. MacCraith, "Enhanced Evanescent Wave Sensors Based on Sol-Gel-Derived Porous Glass Coatings," *Sensors and Actuators B*, vol. 11, pp. 29-34, 1993.
- [493] M. H. Sidek, C. Nyquist-Battie, and G. Vanderkooi, "Inhibition of Synaptosomal Enzymes by Local Anesthetics," *Biochimica et Biophysica Acta*, vol. 801, pp. 26-31, 1984.

- [494] F. Perez-Guillermo, M. E. Delgado, and C. J. Vidal, "Inhibition of Human Serum and Rabbit Muscle Cholinesterase by Local Anesthetics," *Pharmacology*, vol. 36, pp. 3593-3596, 1987.
- [495] A. G. Hadd, S. C. Jacobson, and J. M. Ramsey, "Microfluidic assays of acetylcholinesterase inhibitors," *Analytical Chemistry*, vol. 71, pp. 5206-5212, 1999.
- [496] L. J. Scott and K. L. Goa, "Galantamine - A review of its use in Alzheimer's disease," *Drugs*, vol. 60, pp. 1095-1122, 2000.
- [497] J. C. Fernando, K. R. Rogers, N. A. Anis, J. J. Valdes, R. G. Thompson, A. T. Eldefrawi, and M. E. Eldefrawi, "Rapid Detection of Anticholinesterase Insecticides by a Reusable Light Addressable Potentiometric Biosensor," *J. Agric. Food Chem.*, vol. 41, pp. 511-516, 1993.
- [498] V. Marcel, S. Estrada-Mondaca, F. Magne, J. Stojan, A. Kläebe, and D. Fournier, "Exploration of the *Drosophila* acetylcholinesterase substrate activation site using a reversible inhibitor (Triton X-100) and mutated enzymes," *Journal of Biological Chemistry*, vol. 275, pp. 11603-11609, 2000.
- [499] C. Piraud, E. Mwarania, G. Wylangowski, and J. Wilkinson, "Optoelectrochemical Thin-Film Chlorine Sensor Employing Evanescent Fields on Planar Optical Waveguides," *Anal. Chem.*, vol. 64, pp. 651, 1992.
- [500] G. Goodlet and R. Narayanaswamy, "An Optical Fibre Vitamin C Sensor Based on Immobilized 2,5-dichloroindophenol," *Measurement Science and Technology*, vol. 5, pp. 677-670, 1994.

- [501] A. R. Lennie and F. Kvasnik, "Near-Infrared Sensing Utilising the Evanescent Field," *Anal. Chim. Acta*, vol. 281, pp. 265, 1993.
- [502] L. C. Baylor and B. R. Buchanan, "Reflectance Probe for Uranium(VI) Based on Colorimetric Indicator Arsenazo III," *Applied Spectroscopy*, vol. 49, pp. 679, 1995.
- [503] X. Liu and W. Tan, "A Fiber-Optic Evanescent Wave DNA Biosensor Based on Novel Molecular Beacons," *Anal. Chem.*, vol. 71, pp. 5054, 1999.
- [504] S. Christesen, K. Ong, M. E. Womble, R. Clarke, and R. Premasiri, "Detection and Identification of Chemical Agents in Water Using Surface Enhanced Raman Spectroscopy (SERS) on Gold and Silver Doped Sol-Gels," presented at First Joint Conference on Point Detection for Chemical and Biological Defense, Williamsburg, Virginia, 2000.
- [505] A. Chatonnet and O. Lockridge, "Comparison of butyrylcholinesterase and acetylcholinesterase," *Biochem. J.*, vol. 260, pp. 625-634, 1989.
- [506] E. Krejci, N. Duval, A. Chatonnet, P. Vincens, and J. Massoulie, "Cholinesterase-like domains in enzymes and structural proteins: Functional and evolutionary relationships and identification of a catalytically essential aspartic acid," *Proc. Natl. Acad. Sci.*, vol. 88, pp. 6647-6655, 1991.
- [507] L. Austin and W. K. Berry, "Two selective inhibitors of Cholinesterase," *Biochem. J.*, vol. 54, pp. 695-700, 1953.
- [508] O. Lockridge, S. Adkins, and B. N. La Du, "Location of Disulfide Bonds within the Sequence of Human Serum Cholinesterase," *J. Biol. Chem.*, vol. 262, pp. 12945-12952, 1987.

- [509] O. Lockridge, C. F. Bartels, T. A. Vaughan, C. K. Wong, S. E. Norton, and L. L. Johnson, "Complete Amino Acid Sequence of Human Serum Cholinesterase," *J. Biol. Chem.*, vol. 262, pp. 549-557, 1987.
- [510] M. Schumacher, S. Camp, Y. Maulet, M. Newton, K. MacPhee-Quigley, S. S. Taylor, T. Friedmann, and P. Taylor, "Primary structure of *Torpedo californica* acetylcholinesterase deduced from its cDNA sequence," *Nature (London)*, vol. 319, pp. 407-409, 1986.
- [511] A. Ordentlich, D. Barak, C. Kronman, N. Ariel, Y. Segall, B. Velan, and A. Shafferman, "The architecture of human acetylcholinesterase active center probed by interactions with selected organophosphate inhibitors," *Journal of Biological Chemistry*, vol. 271, pp. 11953-11962, 1996.
- [512] C. B. Millard, G. Kryger, A. Ordentlich, H. M. Greenblatt, M. Harel, M. L. Raves, Y. Segall, D. Barak, A. Shafferman, I. Silman, and J. L. Sussman, "Crystal Structures of Aged Phosphonylated Acetylcholinesterase: Nerve Agent Reaction Products at the Atomic Level," *Biochemistry*, vol. 38, pp. 7032-9, 1999.
- [513] W. D. Mallender, T. Szegletes, and T. L. Rosenberry, "Organophosphorylation of acetylcholinesterase in the presence of peripheral site ligands," *J. of Biological Chemistry*, vol. 274, pp. 8491-9, 1999.
- [514] M. C. Quintero, M. Silva, and D. Pérez-Bendito, "Enzymatic determination of *N*-methylcarbamate pesticides at the nanomolar level by the stopped-flow technique," *Talanta*, vol. 38, pp. 1273-1277, 1991.

- [515] F. Villatte, V. Marcel, S. Estrada-Mondaca, and D. Fournier, "Engineering sensitive acetylcholinesterase for detection of organophosphate and carbamate insecticides," *Biosensors & Bioelectronics*, vol. 13, pp. 157-164, 1998.
- [516] E. V. Gogol, G. A. Evtugyn, J.-L. Marty, H. C. Budnikov, and V. G. Winter, "Amperometric Biosensors Based on Nafion Coated Screen-Printed Electrodes for the Determination of Cholinesterase Inhibitors," *Talanta*, vol. 53, pp. 379-389, 2000.
- [517] E. J. Cho and F. V. Bright, "Optical sensor array and integrated light source," *Analytical Chemistry*, vol. 73, pp. 3289-3293, 2001.
- [518] S. Andreescu, V. Magearu, A. Lougarre, D. Fournier, and J. L. Marty, "Immobilization of enzymes on screen-printed sensors via an histidine tail. Application to the detection of pesticides using modified cholinesterase," *Analytical Letters*, vol. 34, pp. 529-540, 2001.
- [519] V. N. Arkhypova, S. V. Dzyadevych, A. P. Soldatkin, A. V. El'skaya, N. Jaffrezic-Renault, H. Jaffrezic, and C. Martelet, "Multibiosensor based on enzyme inhibition analysis for determination of different toxic substances," *Talanta*, vol. 55, pp. 919-927, 2001.
- [520] E. Bodur, A. N. Cokugras, and E. F. Tezcan, "Inhibition effects of benactyzine and drofenine on human serum butyrylcholinesterase," *Archives of Biochemistry and Biophysics*, vol. 386, pp. 25-29, 2001.
- [521] A. N. Cokugras and E. F. Tezcan, "Amitriptyline: A potent inhibitor of butyrylcholinesterase from human serum," *General Pharmacology*, vol. 29, pp. 835-838, 1997.

- [522] C. H. Park, Y. J. Lee, S. H. Lee, S. H. Choi, H. S. Kim, S. J. Jeong, S. S. Kim, and Y. H. Suh, "Dehydroevodiamine center dot HCl prevents impairment of learning and memory and neuronal loss in rat models of cognitive disturbance," *Journal of Neurochemistry*, vol. 74, pp. 244-253, 2000.
- [523] S. J. Gatley, "Activities of the Enantiomers of Cocaine and Some Related-Compounds As Substrates and Inhibitors of Plasma Butyrylcholinesterase," *Biochemical Pharmacology*, vol. 41, pp. 1249-1254, 1991.
- [524] R. Duran, C. Cervenansky, and E. Karlsson, "Effect of fasciculin on hydrolysis of neutral and choline esters by butyrylcholinesterase, cobra venom and chicken acetylcholinesterases," *Toxicon*, vol. 34, pp. 959-963, 1996.
- [525] C. E. Felder, S. A. Botti, S. Lifson, I. Silman, and J. L. Sussman, "External and internal electrostatic potentials of cholinesterase models," *Journal of Molecular Graphics & Modelling*, vol. 15, pp. 318-327, 1997.
- [526] M. Harel, J. L. Sussman, E. Krejci, S. Bon, P. Chanal, J. Massoulie, and I. Silman, "Conversion of Acetylcholinesterase to Butyrylcholinesterase - Modeling and Mutagenesis," *Proceedings of the National Academy of Sciences of the United States of America*, vol. 89, pp. 10827-10831, 1992.
- [527] M. Ekholm and H. Konschin, "Comparative model building of human butyrylcholinesterase," *Journal of Molecular Structure-Theochem*, vol. 467, pp. 161-172, 1999.
- [528] M. Harel, I. Schalk, L. Ehret-Sabatier, F. Bouet, M. Goeldner, C. Hirth, P. H. Axelsen, I. Silman, and J. L. Sussman, "Quaternary ligand binding to aromatic

- residues in the active-site gorge of acetylcholinesterase,” *Proc. Natl. Acad. Sci. USA*, vol. 90, pp. 9031-9035, 1993.
- [529] H. Sun, J. El Yazal, O. Lockridge, L. M. Schopfer, S. Brimijoin, and Y. P. Pang, “Predicted Michaelis-Menten complexes of cocaine- butyrylcholinesterase - Engineering effective butyrylcholinesterase mutants for cocaine detoxication,” *Journal of Biological Chemistry*, vol. 276, pp. 9330-9336, 2001.
- [530] F. Villatte, P. Ziliani, V. Marcel, P. Menozzi, and D. Fournier, “A high number of mutations in insect acetylcholinesterase may provide insecticide resistance,” *Pesticide Biochemistry and Physiology*, vol. 67, pp. 95-102, 2000.
- [531] J. Raba and H. A. Mottola, “Glucose-Oxidase As an Analytical Reagent,” *Critical Reviews in Analytical Chemistry*, vol. 25, pp. 1-42, 1995.
- [532] X. H. Chen, N. Matsumoto, Y. B. Hu, and G. S. Wilson, “Electrochemically mediated electrodeposition/electropolymerization to yield a glucose microbiosensor with improved characteristics,” *Analytical Chemistry*, vol. 74, pp. 368-372, 2002.
- [533] A. S. Prasad, *Biochemistry of Zinc*, vol. 11. New York: Plenum Press, 1993.
- [534] A. Galdes and B. L. Vallee, *Zinc and Its Role in Biology and Nutrition*, vol. 15. New York: Marcel Dekker, Inc, 1983.
- [535] R. G. Khalifah, J. I. Rogers, and J. Mukherjee, “Interaction of the Unique Competitive Inhibitor Imidazole and Related-Compounds With the Active-Site Metal of Carbonic- Anhydrase - Linkage Between Ph Effects On the Inhibitor Binding-Affinity and Ph Effects On the Visible Spectra of Inhibitor Complexes

- With the Cobalt-Substituted Enzyme,” *Biochemistry*, vol. 26, pp. 7057-7063, 1987.
- [536] C. R. Chong and D. S. Auld, “Inhibition of carboxypeptidase A by D-penicillamine: Mechanism and implications for drug design,” *Biochemistry*, vol. 39, pp. 7580-7588, 2000.
- [537] U. Langheinrich, “Plasma Membrane-Associated Aminopeptidase Activities in *Chlamydomonas-Reinhardtii* and Their Biochemical- Characterization,” *Biochimica Et Biophysica Acta-Protein Structure and Molecular Enzymology*, vol. 1249, pp. 45-57, 1995.
- [538] J. M. Wilson, Q. Tanko, M. M. Wendland, J. E. Meany, J. F. Nedved, and Y. Pocker, “The inhibition of bovine carbonic anhydrase by saccharin and 2- and 4-carbobenzoxybenzene sulfonamide,” *Physiological Chemistry and Physics and Medical Nmr*, vol. 30, pp. 149-162, 1998.
- [539] H. J. Vreman, D. A. Cipkala, and D. K. Stevenson, “Characterization of porphyrin heme oxygenase inhibitors,” *Canadian Journal of Physiology and Pharmacology*, vol. 74, pp. 278-285, 1996.
- [540] A. Thorslund and S. Lindskog, “Studies of the Esterase Activity and the Anion Inhibition of Bovine Zinc and Cobalt Carbonic Anhydrases,” *Eur. J. Biochem.*, vol. 3, pp. 117-123, 1967.
- [541] R. B. Thompson and E. R. Jones, “Enzyme-Based Fiber Optic Zinc Biosensor,” *Analytical Chemistry*, vol. 65, pp. 730-734, 1993.
- [542] D. Elbaum, S. K. Nair, M. W. Patchan, R. B. Thompson, and D. W. Christianson, “Structure-Based Design of a Sufonamide Probe for Fluorescence Anisotropy

- Detection of Zinc with a Carbonic Anhydrase-Based Biosensor,” *JACS*, vol. 118, pp. 8381-8387, 1996.
- [543] L. C. Chirica, B. Elleby, and S. Lindskog, “Cloning, expression and some properties of alpha-carbonic anhydrase from *Helicobacter pylori*,” *Biochimica Et Biophysica Acta-Protein Structure and Molecular Enzymology*, vol. 1544, pp. 55-63, 2001.
- [544] B. D. Di Sioudi, C. E. Miller, K. H. Lai, J. K. Grimsley, and J. R. Wild, “Rational design of organophosphorus hydrolase for altered substrate specificities,” *Chemico-Biological Interactions*, vol. 120, pp. 211-223, 1999.
- [545] F. M. Raushel and H. M. Holden, “Phosphotriesterase: An enzyme in search of its natural substrate,” in *Advances in Enzymology, Vol 74*, vol. 74, *Advances in Enzymology and Related Areas of Molecular Biology*, 2000, pp. 51-+.
- [546] G. A. Omburo, J. M. Kuo, L. S. Mullins, and F. M. Raushel, “Characterization of the Zinc-Binding Site of Bacterial Phosphotriesterase,” *Journal of Biological Chemistry*, vol. 267, pp. 13278-13283, 1992.
- [547] D. M. Munnecke, “Hydrolysis of Organophosphate Insecticides by an immobilized-enzyme system,” *Biotechnol. Bioeng.*, vol. 21, pp. 2247-2261, 1979.
- [548] K. I. Dave, L. Phillips, V. A. Luckow, and J. R. Wild, “Expression and Posttranslational Processing of a Broad-Spectrum Organophosphorus-Neurotoxin-Degrading Enzyme in Insect Tissue- Culture,” *Biotechnology and Applied Biochemistry*, vol. 19, pp. 271-284, 1994.

- [549] S. R. Caldwell and F. M. Raushel, "Detoxification of Organophosphate Pesticides Using a Nylon Based Immobilized Phosphotriesterase From *Pseudomonas-Diminuta*," *Applied Biochemistry and Biotechnology*, vol. 31, pp. 59-73, 1991.
- [550] K. I. Dave, C. Lauriano, B. W. Xu, J. R. Wild, and C. M. Kenerley, "Expression of Organophosphate Hydrolase in the Filamentous Fungus *Gliocladium-Virens*," *Applied Microbiology and Biotechnology*, vol. 41, pp. 352-358, 1994.
- [551] U. Ghosh and H. Gangopadhyay, "Enzymatic clarification of bael juice by calcium alginate gel immobilized PME of *Aspergillus oryzae*," *Indian Journal of Chemical Technology*, vol. 9, pp. 504-507, 2002.
- [552] R. D. Richins, I. Kaneva, A. Mulchandani, and W. Chen, "Biodegradation of organophosphorus pesticides by surface- expressed organophosphorus hydrolase," *Nature Biotechnology*, vol. 15, pp. 984-987, 1997.
- [553] E. N. Efremenko and V. S. Sergeeva, "Organophosphate hydrolase - an enzyme catalyzing degradation of phosphorus-containing toxins and pesticides," *Russian Chemical Bulletin*, vol. 50, pp. 1826-1832, 2001.
- [554] J. E. Kolakowski, J. J. DeFrank, S. P. Harvey, L. L. Szafraniec, W. T. Beaudry, K. H. Lai, and J. R. Wild, "Enzymatic hydrolysis of the chemical warfare agent VX and its neurotoxic analogues by organophosphorus hydrolase," *Biocatalysis and Biotransformation*, vol. 15, pp. 297-312, 1997.
- [555] I. Horne, T. D. Sutherland, R. L. Harcourt, R. J. Russell, and J. G. Oakeshott, "Identification of an opd (organophosphate degradation) gene in an *Agrobacterium* isolate," *Applied and Environmental Microbiology*, vol. 68, pp. 3371-3376, 2002.

- [556] J. J. DeFrank and M. A. Guelta, "Biodegradation and Oxidation Approaches for the Demilitarization of VX Hydrolysate," presented at 2002 Joint Service Scientific Conference on Chemical & Biological Defense Research, Hunt Valley, MD, November 2002.
- [557] J. J. DeFrank, T. Cheng, S. P. Harvey, and V. K. Rastogi, "Advanced Catalytic Enzyme System (ACES) - Dual Use Capabilities," presented at 2002 Joint Service Scientific Conference on Chemical & Biological Defense Research, Hunt Valley, MD, November 2002.
- [558] R. J. Russell, M. V. Pishko, A. L. Simonian, and J. R. Wild, "Poly(ethylene glycol) hydrogel-encapsulated fluorophore-enzyme conjugates for direct detection of organophosphorus neurotoxins," *Analytical Chemistry*, vol. 71, pp. 4909-4912, 1999.
- [559] S. Gopal, V. Rastogi, W. Ashman, and W. Mulbry, "Mutagenesis of organophosphorus hydrolase to enhance hydrolysis of the nerve agent VX," *Biochemical and Biophysical Research Communications*, vol. 279, pp. 516-519, 2000.
- [560] J. M. Kuo, M. Y. Chae, and F. M. Raushel, "Perturbations to the active site of phosphotriesterase," *Biochemistry*, vol. 36, pp. 1982-1988, 1997.
- [561] M. Chen-Goodspeed, M. A. Sogorb, F. Y. Wu, S. B. Hong, and F. M. Raushel, "Structural determinants of the substrate and stereochemical specificity of phosphotriesterase," *Biochemistry*, vol. 40, pp. 1325-1331, 2001.
- [562] J. F. Powell, "Isolation of Dipicolinic Acid (Pyridine-2:6-dicarboxylic Acid) from Spores of *Bacillus megatherium*," *Biochem. J.*, vol. 54, pp. 210-211, 1953.

- [563] L. M. F. Herman, M. J. M. Vaerewijck, R. J. B. Moermans, and G. M. A. V. J. Waes, "Identification and Detection of *Bacillus sporothermodurans* Spores in 1, 10, and 100 Milliliters of Raw Milk by PCR," *App. and Envir. Micro.*, vol. 63, pp. 3139-3143, 1997.
- [564] P. Belgrader, W. Benett, D. Hadley, G. Long, R. Mariella, F. Milanovich, S. Nasarabadi, W. Nelson, J. Richards, and P. Stratton, "Rapid Pathogen Detection Using a Microchip PCR Array Instrument," *Clinical Chemistry*, vol. 44, pp. 2191-2194, 1998.
- [565] H. Yu, J. W. Raymonda, T. M. McMahon, and A. A. Campagnari, "Detection of Biological Threat Agents by Immunomagnetic Microsphere-Based Solid Phase Fluorogenic- and Electro-Chemiluminescence," *Biosens and Bioelec.*, vol. 14, pp. 829-940, 2000.
- [566] K. A. Uithoven, J. C. Schmidt, and M. E. Ballman, "Rapid Identification of Biological Warfare Agents Using an Instrument Employing a Light Addressable Potentiometric Sensor and a Flow-Through Immunofiltration -Enzyme Assay System," *Biosens. and Bioelec.*, vol. 14, pp. 761-770, 2000.
- [567] N. Velappan, J. L. Snodgrass, J. R. Hakovirta, B. L. Marrone, and S. Burde, "Rapid Identification of Pathogenic Bacteria by Single-Enzyme Amplified Fragment Length Polymorphism Analysis," *Diagnostic Micro and Infectious Diseaseq*, vol. 39, pp. 77-83, 2001.
- [568] A. Castro and R. T. Okinaka, "Ultrasensitive, Direct Detection of a Specific DNA Sequence of *Bacillus Anthracis* in Solution," *The Analyst*, vol. 125, pp. 9-11, 2000.

- [569] H. Paulus, "Determination of Dipicolinic Acid by High-Pressure Liquid Chromatography," *Anal. Biochem.*, vol. 114, pp. 407-410, 1981.
- [570] D. Helm and D. Naumann, "Identification of Some Bacterial Cell Components by FT-IR Spectroscopy," *FEMS Microbiology Letters*, vol. 126, pp. 75-80, 1995.
- [571] N. Grecz and T. Tang, "Relation of Dipicolinic Acid to Heat Resistance of Bacterail Spores," *J. Gen. Microbiol.*, vol. 63, pp. 303-310, 1970.
- [572] M. W. Tabor, J. MacGee, and J. W. Holland, "Rapid Determination of Dipicolinic Acid in the Spores of *Clostridium* species by Gas-Liquid Chromatography," *Appl. Envir. Microbiol.*, vol. 31, pp. 25-28, 1976.
- [573] A. D. Warth, "Liquid Chromatographic Determination of Dipicolinic Acid from Bacterial Spores," *Appl. Envir. Microbiol.*, vol. 38, pp. 1029-1033, 1979.
- [574] A. D. Warth, "Determination of Dipicolinic Acid in Bacterial Spores by Derivative Spectroscopy," *Anal. Biochem.*, vol. 130, pp. 502-505, 1983.
- [575] L. E. Sacks, "Chemical Germination of Native and Cation-Exchanged Bacterial Spores with Trifluoperazine," *Appl. Envir. Microbiol.*, vol. 56, pp. 1185-1187, 1990.
- [576] D. L. Rosen, C. Sharpless, and L. B. McGown, "Bacterial Spore Detection and Determination by Use of Terbium Dipicolinate Photoluminescence," *Anal. Chem.*, vol. 69, pp. 1082-1085, 1997.
- [577] E. Ghiamati, R. Manoharan, W. H. Nelson, and J. F. Sperry, "UV Reasonance Raman Spectra of Bacillus Spores," *Appl. Spec.*, vol. 46, pp. 357-364, 1992.
- [578] A. A. Hindle and A. H. H. Hall, "Dipicolinic Acid (DPA) Assay Revisited and Appraised for Spore Detection," *Analyst*, vol. 124, pp. 1599-1604, 1999.

- [579] P. M. Pellegrino, N. F. Fell, D. L. Rosen, and J. B. Gillespie, "Bacterial Endospore Detection Using Terbium Dipicolinate Photoluminescence in the Presence of Chemical and Biological Materials," *Anal. Chem.*, vol. 70, pp. 1755-1760, 1998.
- [580] R. Goodacre, B. Shann, R. J. Gilbert, E. M. Timmins, A. C. McGovern, K. B. Alsberg, D. B. Kell, and N. A. Logan, "Detection of the Dipicolinic Acid Biomarker in Bacillus Spores Using Curie-Point Pyrolysis Mass Spectrometry and Fourier Transform Infrared Spectroscopy," *Anal. Chem.*, vol. 72, pp. 119-127, 2000.
- [581] N. F. Fell, P. M. Pellegrino, and J. B. Gillespie, "Mitigating Phosphate Interference in Bacterial Endospore Detection by Tb Dipicolinate Photoluminescence," *Anal. Chim. Acta*, vol. 426, pp. 43-50, 2001.
- [582] R. W. Scheidt and C. A. Reed, "Stereochemistry of the Toluene Sodate of $\alpha,\beta,\gamma,\delta$ -Tetraphenylporphinatochromium(II)," *Inorganic Chemistry*, vol. 17, pp. 710-714, 1978.
- [583] B. J. White and H. J. Harmon, "Interaction of Dipicolinic Acid with Water Soluble and Immobilized Porphyrins," *Sensors and Actuators B*, vol. 97, pp. 277-83, 2004.
- [584] M. Mock and A. Fouet, "Anthrax," *Annual Review of Microbiology*, vol. 55, pp. 647-671, 2001.
- [585] A. Fox, G. C. Stewar, L. N. Waller, K. F. Fox, W. M. Harley, and R. L. Price, "Carbohydrates and glycoproteins of *Bacillus anthracis* and related bacilli: targets for biodetection," *J. Microb. Methods*, vol. 54, pp. 143-152, 2003.

- [586] L. L. Matz, T. C. Beaman, and P. Gerhardt, "Chemical Composition of Exosporium from spores of *Bacillus cereus*," *J. Bacteriol.*, vol. 101, pp. 196-201, 1970.
- [587] M. Garcia-Patrone and J. S. Tandecarz, "A Glycoprotein Multimer from *Bacillus Thuringiensis* Sporangia: Dissociation into Subunits and Sugar Composition," *Molec. and Cell. Bioch.*, vol. 145, pp. 29-37, 1995.
- [588] P. Sylvestre, E. Couture-Tosi, and M. Mock, "A collagen-like surface glycoprotein is a structural component of the *Bacillus anthracis* exosporium," *Molec. Microb.*, vol. 45, pp. 169-178, 2002.
- [589] H. Murakami, T. Nagasaki, I. Hamachi, and S. Shinkai, "Sugar Sensing Utilizing Aggregation Properties of Boronic-Acid-Appended Porphyrins and Metalloporphyrins," *Journal of the Chemical Society-Perkin Transactions 2*, pp. 975-981, 1994.
- [590] H. Suenaga, H. Yamamoto, and S. Shinkai, "Screening of boronic acids for strong inhibition of the hydrolytic activity of alpha-chymotrypsin and for sugar sensing associated with a large fluorescence change," *Pure and Applied Chemistry*, vol. 68, pp. 2179-2186, 1996.
- [591] H. Chou, C. T. Chen, K. F. Stork, P. W. Bohn, and K. S. Suslick, "Langmuir-Blodgett-Films of Amphiphilic Push-Pull Porphyrins," *Journal of Physical Chemistry*, vol. 98, pp. 383-385, 1994.
- [592] K. T. Yue, M. F. Lin, T. A. Gray, and L. G. Marzilli, "Nickel(II) Porphyrin Binding to Anionic Biopolymers Investigated By Resonance Raman and Optical Spectroscopy," *Inorganic Chemistry*, vol. 30, pp. 3214-3222, 1991.

- [593] B. J. White and H. J. Harmon, "Optical Determination of Sugars Using Immobilized Porphyrins," *IEEE Sensors Journal*, vol. Submitted, 2004.
- [594] D. L. Recalde-Ruiz, E. Andres-Garcia, and M. E. Diaz-Garcia, "Fluorimetric flow injection and flow-through sensing systems for cyanide control in waste water," *Analyst*, vol. 125, pp. 2100-2105, 2000.
- [595] J. Z. Lu, W. Qin, Z. J. Zhang, M. L. Feng, and Y. J. Wang, "A Flow-Injection Type Chemiluminescence-Based Sensor For Cyanide," *Analytica Chimica Acta*, vol. 304, pp. 369-373, 1995.
- [596] K. Ikebukuro, M. Shimomura, N. Onuma, A. Watanabe, Y. Nomura, K. Nakanishi, Y. Arikawa, and I. Karube, "A novel biosensor system for cyanide based on a chemiluminescence reaction," *Analytica Chimica Acta*, vol. 329, pp. 111-116, 1996.
- [597] V. K. Rao, S. Suresh, A. Bhattacharya, and N. Rao, "A potentiometric detector for hydrogen cyanide gas using silver dicyano complex," *Talanta*, vol. 49, pp. 367-371, 1999.
- [598] J. I. Lee and I. Karube, "A Novel Microbial Sensor For the Determination of Cyanide," *Analytica Chimica Acta*, vol. 313, pp. 69-74, 1995.
- [599] M. H. Smit and A. E. G. Cass, "Cyanide Detection Using a Substrate-Regenerating, Peroxidase- Based Biosensor," *Analytical Chemistry*, vol. 62, pp. 2429-2436, 1990.
- [600] A. Amine, M. Alafandy, J. M. Kauffmann, and M. N. Pekli, "Cyanide Determination Using an Amperometric Biosensor Based On Cytochrome-Oxidase Inhibition," *Analytical Chemistry*, vol. 67, pp. 2822-2827, 1995.

- [601] M. S. a. R. Frant, J. W. and Riseman, J. H., "Electrode Indicator Technique for Measuring Low Levels of Cyanide," *Analytical Chemistry*, vol. 44, pp. 2227-2230, 1972.
- [602] Z. H. Zhu and Z. L. Fang, "Spectrophotometric Determination of Total Cyanide in Waste- Waters in a Flow-Injection System With Gas-Diffusion Separation and Preconcentration," *Analytica Chimica Acta*, vol. 198, pp. 25-36, 1987.
- [603] T. Toida, T. Togawa, S. Tanabe, and T. Imanari, "Determination of Cyanide and Thiocyanate in Blood-Plasma and Red-Cells By High-Performance Liquid-Chromatography With Fluorometric Detection," *Journal of Chromatography*, vol. 308, pp. 133-141, 1984.
- [604] E. Miralles, D. Prat, R. Compano, and M. Granados, "Assessment of different fluorimetric reactions for cyanide determination in flow systems," *Analyst*, vol. 122, pp. 553-558, 1997.
- [605] E. Miralles, D. Prat, R. Compano, and M. Granados, "On-line gas-diffusion separation and fluorimetric detection for the determination of acid dissociable cyanide," *Analyst*, vol. 123, pp. 217-220, 1998.
- [606] A. Tanaka, K. Deguchi, and T. Deguchi, "Spectrofluorometric Determination of Cyanide and Thiocyanate Based On a Modified Konig Reaction in a Flow-Injection System," *Analytica Chimica Acta*, vol. 261, pp. 281-286, 1992.
- [607] P. a. L. Hambright, Robert, "Cyanide Scavengers: Kinetics of the Reaction of Rhodium(III)-Tetrakis(4-sulfonatophenyl)porphyrin with Cyanide and Hydrogen Cyanide," *Inorganica Chimica Acta*, vol. 137, pp. 209-212, 1987.

- [608] K. Ikebukuro, A. Miyata, S. J. Cho, Y. Nomura, S. M. Chang, Y. Yamauchi, Y. Hasebe, S. Uchiyama, and I. Karube, "Microbial cyanide sensor for monitoring river water," *Journal of Biotechnology*, vol. 48, pp. 73-80, 1996.

BRANDY J. WHITE

Oklahoma State University
Department of Physics
145 Physical Sciences II
Stillwater, OK 74078
Office: (405) 744-9477
Cell: (405) 326-1096
Fax: (405) 744-6811
Email: bj3568@juno.com

Updated: June, 2004

Citizenship: U.S.

Date of Birth: July 14, 1977

EDUCATION

Doctor of Philosophy in Photonics graduation July 2004

Oklahoma State University, Stillwater, OK 74078

Thesis Topic: *Porphyrins as colorimetric indicators for detection and identification of chemical and biological agents.*

Thesis Advisor: H. James Harmon

Master of Science in Physics graduated December 2001

Oklahoma State University, Stillwater, OK 74078

Thesis Topic: *Development of a Reagent-Less Sensor for Inhibitors of Acetylcholinesterase.*

Thesis Advisor: H. James Harmon

Bachelor of Science in Engineering Physics graduated May 1998

Northeastern State University, Tahlequah, OK 74464

Bachelor of Science in Mathematics graduated May 1998

Northeastern State University, Tahlequah, OK 74464

EXPERIENCE

January 2001 – present: **Research assistant for Dr. H. J. Harmon, Department of Physics, Oklahoma State University.** Research on detection and destruction of biological and chemical weapons and environmental pollutants using UV/Vis absorbance and fluorescence techniques. Primary project focus: The development of a unique detection protocol for analytes including organophosphates and CO₂ involving reversible competitive inhibition of enzymes resulting in a system based on a handheld PC and miniature spectrophotometer. Extensive experience in development of immobilization techniques for proteins and porphyrins on surfaces including glass, polystyrene, and cellulose. Experience with characterization of porphyrin-analyte and porphyrin-protein interactions both in solution and on immobilized surfaces including enzyme kinetics and binding constants as well as development of techniques for these characterizations. Major Equipment: Cary 4E (Varian), Gilford single beam spectrophotometer, SDB-3 dual wavelength spectrophotometer (Johnson Research Foundation), OLIS

RSM 1000 rapid scan spectrophotometer, OceanOptics USB2000 and HR2000 spectrophotometers, SPEX Fluoromax 3 spectrofluorometer (JY-Horiba).

May 1999 – December 2000: **Research assistant for Dr. Aihua Xie, Department of Physics, Oklahoma State University.** Research on photoactive yellow protein (PYP) focusing on studies of the conformational changes and charge transfer mechanisms involved in the photocycle using Fourier transformed infrared spectroscopy (FT-IR) and UV/vis absorbance spectroscopy. The publication resulting from this work presented some of the earliest data on step-scan and rapid-scan FT-IR of protein crystals. Experience with bacterial growth and protein purification as well as growth of protein crystals. Vibrational structure calculations for amino acids and other small molecules using Gaussian 98 for Windows. Major Equipment: Cary 5E, Bruker IFS 66v FTIR spectrometer, Continuum Surelite II pumped OPO laser.

August 1998 – May 1999: **Teaching assistant for the Department of Physics, Oklahoma State University** under Dr. Leslie Colyott and Dr. Paul Westhaus. Taught undergraduate labs for introductory physics courses focusing on mechanics, heat, and electromagnetics. Responsibility was for preparing and presenting lectures on basic principles and lab procedures for a standard set of experiments as well as grading reports and maintaining records of student performance.

June 1998 – August 1998: **Research assistant for Dr. George Dixon, Department of Physics, Oklahoma State University.** Research on thermally and optically stimulated conductivity in silicate glass samples. Major Equipment: cw argon laser, assorted power supplies and lock-in amplifiers

August 1995 – May 1998: **Departmental tutor for the departments of Mathematics and Physics, Northeastern State University.** Tutored students in core curriculum mathematics and physics courses ranging from basic algebra to differential equations and including introductory courses in physics as well as electronics.

August 1995 – March 1998: **Teaching assistant for the department of Physics, Northeastern State University.** Responsible for assisting students with completion of laboratory experiments and reports as well as for grading completed reports and homework assignments from lecture sections.

RELEVANT COURSEWORK

Organic Chemistry	Electricity and Magnetism	Advanced Optics
Biochemistry	Statistical Thermodynamics	Optical Electronics
Classical Mechanics	Quantum Mechanics	Ultrafast Optoelectronics
Methods of Theoretical Physics	Statistical Mechanics	Terahertz Time Domain Spectroscopy

HONORS AND AWARDS

Physics Department Graduate Research Excellence 1999-2000 academic year
NSF-sponsored Integrated Graduate Education and Research Training (IGERT) Fellowship June 2002 – July 2004
Sigma Pi Sigma (Physics Honors Society)
Rho Theta Sigma (Honors Society)
Kappa Mu Epsilon (Mathematics Honors Society)

MEMBERSHIPS

Arkansas-Oklahoma Center for Space and Planetary Sciences
Biophysical Society
American Physical Society

Name: Brandy J. White

Date of Degree: July, 2004

Institution: Oklahoma State University

Location: Stillwater, Oklahoma

Title of Study: PORPHYRINS AS COLORIMETRIC INDICATORS FOR DETECTION AND IDENTIFICATION OF CHEMICAL AND BIOLOGICAL AGENTS

Pages in Study: 370

Candidate for the Degree of Doctor of Philosophy

Major Field: Photonics

Scope and Method of Study: The objective of this study was to design sensor surfaces for rapid, real-time, optical detection of chemical/biological warfare agents and/or environmental pollutants that yield a minimum of false readings. Porphyrins were used as colorimetric indicators for transduction in surfaces using biological recognition elements such as enzymes and as combination recognition element/transducer in other surfaces. Immobilization protocols and assaying procedures were developed for each of the sensor surfaces.

Findings and Conclusions: As a reversible, competitive inhibitor of enzymes, porphyrins can be used for identification and quantification of the presence of a substrate or another competitive inhibitor of the enzyme. This technique has been useful for development of glass surfaces for the detection of cholinesterase inhibitors such as organophosphate compounds and nerve agent simulants at parts per trillion levels using acetylcholinesterase, butyrylcholinesterase, and organophosphorous hydrolase as recognition elements. Evanescent wave absorbance spectroscopy with a small CCD array spectrophotometer allowed for measurements to be completed in less than six seconds. The specificity of the enzyme active site insured a minimum of false responses. In addition, the technique has been demonstrated for detection of glucose using glucose oxidase and for detection of carbon dioxide using carbonic anhydrase. Porphyrins immobilized to cellulose films or to glass surfaces can be used for detection of part per billion levels of cyanide in liquid phase and part per million levels in gas phase. Porphyrins immobilized to cellulose tissues can be used to identify and quantify the presence of dipicolinic acid, a constituent of bacterial endospores in the *Bacillus* genus, as well as sugars similar to those found in the exosporium of *Bacillus anthracis*. The tissues may be useful as a wipe test for the indication of the presence of these compounds.

ADVISOR'S APPROVAL: _____ H. James Harmon